The role of the E- to N-cadherin switch in the neural differentiation of embryonic stem cells

Karolina Punovuori

THE UNIVERSITY *of* EDINBURGH

Doctor of Philosophy

MRC Centre for Regenerative Medicine

University of Edinburgh

2018

Declaration

I declare that this thesis is of my own composition. The work presented in this thesis is my own, unless otherwise stated, and has not been presented for any other degree or professional qualification.

A. Karolina Punovuori

Acknowledgements

This work would not have been possible without the support of a number of people. First, I would like to thank my supervisor *Sally Lowell* for her unwavering optimism and guidance from the day that I first set foot at the SCRM for my PhD interview. By complete chance, I stumbled across a supervisor who has been the embodiment of a role model throughout my studies, and I cannot thank her enough for that. I would also like to extend my thanks to my thesis committee: *Val Wilson, Charles ffrench-Constant, Mattias Malaguti* and *Gillian Morrison*, for their constructive input at various stages of the project. I am also very grateful to the UK Medical Research Council for funding this research.

I have been lucky during my project to be supported by a dedicated team of facility staff. Thank you to *Fiona Rossi* and *Claire Cryer* from the flow lab, *Bertrand Vernay* and *Eoghan O'Duibhir* from the imaging facility, and *Helen Henderson* and *Marilyn Thomson* from tissue culture for sharing their specialist expertise, and to *Theresa O'Connor* for her help with cell line karyotyping.

For the last four years, coming to work every day has been a joy thanks to the brilliant team of the Lowell lab: thank you to *Mattias Malaguti* and *Chia-Yi Lin* for being my scientific babysitters in my early days and for patiently answering all my silly questions; *Julia Watson* for being a great friend and comic relief; *Rosa Portero Migueles* for her embryology expertise and stellar mystery baking; *Guillaume Blin* for his computational, statistical and philosophical insights; *Aida Costa* for sharing my love of food; *Chandrika Rao* for enduring vegetarian catering together; *Darren Wisniewski* for the R advice and Scottish banter; *Daina Šadurska* for her help in setting up mutant cell lines; and all the students who have passed through the lab for contributing to a wonderful and supportive working atmosphere. Special thanks also to *Colin Plumb,* for sharing the ups and downs of the PhD journey with me since day one, and *Filip Wymeersch* for the coffees and brilliant lunchtime chats.

Thank you to my friends, both in Edinburgh and around the globe, for being there: to my high school nerd herd, *Natasha Avery, Barbara De Kegel, Tereza Steinhüblová,* and *Niels Cautaerts*, for the reunions and friendship; *Marius Linten* for always being just one message away; *Jillian Levick* and *Antoine Guillaume* for shared laughs and memories along the St Andrews–Edinburgh–London axis; and to all the friends I've made through volleyball, especially at Portobello beach, who have ensured that I get my dose of vitamin D each year and who have kept me physically and mentally fit through a long summer of thesis writing.

I owe a debt of gratitude to my family. Thank you to my parents for equipping me with the education, skills, and life experiences that have enabled me to pursue my dreams with passion and confidence. Thank you to *Kasia* for a lifetime of sisterly advice and encouragement. Most importantly, największe podziękowania go to my mother, *Barbara*, not only for making my conference travel into joint holidays, but also for her love, unwavering support and no-nonsense approach to all aspects of life.

Finally, thank you to *JordOn Williams* for being my personal driver and for his unconditional love over the past five years.

Abstract

During early embryonic development in mammals, the initially uniform cells of the naïve epiblast generate the structurally diverse and functionally specific tissues of the adult organism. The naïve epiblast expresses the cell-cell adhesion molecule epithelial (E-) cadherin, which is essential for early embryonic development. During subsequent neural differentiation in the ectoderm, E-cadherin becomes downregulated, and neuronal (N-) cadherin becomes upregulated in a process known as cadherin switching. Premature loss of E-cadherin activity leads to faster, more synchronous neural differentiation in embryonic stem cells by an unknown mechanism (Malaguti et al., 2013). Cadherins are mainly classed as adhesion molecules, but can also modulate cellular signalling by binding various growth factor receptors. This raises the possibility that cadherin switching may modulate signalling during early neural induction, thus affecting differentiation.

This thesis investigates the mechanisms by which cadherin switching can bias differentiation decisions during neural induction in mouse embryonic stem (ES) cells . First, the spatio-temporal patterns of cadherins were investigated in the post-implantation embryo and during differentiation of pluripotent cells *in vitro*. The results of this analysis suggest that cadherin switching is initiated before the loss of pluripotency and co-occurs with lineage priming, consistent with the hypothesis that this process may bias cell fate decisions.

Next, ES cells in which the N-cadherin gene was knocked in to the E-cadherin locus (NcKI) were studied. These cells displayed elevated levels of neural marker genes during differentiation, suggesting that forced, premature cadherin switching promotes neural differentiation. To determine whether this effect could be ascribed to the loss of E-cadherin or to the gain of N-cadherin, an inducible N-cadherin overexpressing ESC line was generated. Experiments with this cell line confirmed that N-cadherin alone can promote neural fate.

Cadherin switching also occurs at a later developmental stage: during the maturation of bi-potent neuro-mesodermal progenitors (NMPs). Premature induction of N-cadherin was shown to bias immature NMPs towards neural differentiation, similarly to the effect of N-cadherin on pluripotent cells.

To establish whether the pro-neural effect of N-cadherin was due to its adhesive function, a quantitative image analysis method was used to measure adhesion defects. Adhesion phenotypes did not correlate with the pro-neural effect observed in NcKI and N-

cadherin overexpressing cells, suggesting that adhesion may not be the primary cause for the neural bias of these cells.

Finally, the signalling effects of cadherin switching were studied. The loss of E-cadherin in E-cadherin null (EcKO) and NcKI cells was found to correlate with a drop in global and nuclear levels of β-catenin, a central component of the canonical WNT signalling pathway. However, these cells were found to retain WNT responsiveness, suggesting that any neural bias shown during cadherin switching is unlikely to be caused by altered WNT signalling.

An mRNA-based signalling pathway analysis showed that cells overexpressing N-cadherin had reduced levels of FGF signalling cascade components at days three and four of neural differentiation. Subsequent experiments in NcKI cells showed that these cells express lower levels of FGF readouts during neural differentiation than WT cells, and that their pro-neural effect can be erased by adding FGF pathway ligands, or replicated by blocking the FGF pathway. These results suggest that the pro-neural effect observed in NcKI cells is caused by dampened FGF responsiveness.

Taken together, the results presented in this thesis support a model in which N-cadherin promotes neural differentiation by dampening FGF signalling. This mechanism, rather than being an instructive cue for neural induction, is likely to contribute to the robustness of neural differentiation in the developing embryo.

Lay summary

The body of a mammal is made up of trillions of cells, and each of these cells has a highly specialised function. All of the diverse cell types found in an adult body once originated from just one cell: the fertilised egg. During early development of the embryo, the fertilised egg divides, and a subset of its cells will go on to create all the organs in the adult body. These cells are called pluripotent cells, and they can be removed from the embryo and grown in a dish, allowing researchers to study their behaviour. How these cells make decisions about what adult cell type to become is a large field of scientific inquiry.

This thesis explores the question of how pluripotent cells make the decision to become part of the nervous system. Pluripotent cells that have not yet decided on their fate are called “naïve”, and their surface contains large amounts of a protein called E-cadherin, which is an adhesion molecule that allows cells to stick to each other tightly. In the earliest stages of nervous system development, E-cadherin becomes switched off, and the early neural cells switch on a very similar cell-surface protein called N-cadherin. This process is called cadherin switching. Previous studies have shown that turning off E-cadherin makes pluripotent cells become neural cells faster, raising the possibility that cadherin switching may regulate the development of the nervous system in the embryo.

The experiments summarised in this thesis showed that the cadherin switch was initiated before pluripotent cells had made a firm decision on what to become. By using genetic engineering to modify the types and amounts of cadherins that cells had on their surface, it was shown that forced or premature cadherin switching encouraged the cells to commit to the nervous fate faster. Image analysis software was used to show that this neural bias was not a result of changes in the ways the cells adhered to one another. Instead, genetic analysis and additional experiments were used to show that cadherin switching lowered the levels of FGF signalling, a type of chemical messaging taking place in the cells. This signalling prevents the pluripotent cells from making a final decision on what cell type to become. Thus, by lowering these inhibitory FGF signals, cadherin switching encourages pluripotent cells to become part of the nervous system, and may ensure that this organ system develops correctly and robustly in the embryo.

Table of Contents

List of tables

List of figures

List of abbreviations

2D	Two-dimensional
2i-Lif	Double inhibition with the addition of LIF
3D	Three-dimensional
7AAD	7-amino-actinomycin-D
BABB	1 Benzyl Alcohol: 2 Benzyl Benzonate
BMP	Bone morphogenetic protein
BSA	Bovine serum albumin
cDNA	Complementary deoxyribonucleic acid
CLE	Caudal lateral epiblast
CNH	Chordoneural hinge
Cre	“Causes recombination”, referring to Cre-recombinase enzyme
DAPI	4',6-diamidino-2-phenylindole
DMEM	Dulbecco’s modified Eagle’s medium
DMSO	Dimethyl sulphoxide
DNA	Deoxyribonucleic acid
dNTP	Deoxynulcleosidetriphosphate
Dox	Doxycycline hyclate
Ecad	E-cadherin
EcKO	E-cadherin knock-out (*Cdh1*$^{-/-}$)
ECD	Extracellular cadherin domain
ECM	Extracellular matrix
EDTA	Ethylenediaminetetraacetic acid
EGF	Epidermal growth factor
EGFR	Epidermal growth factor receptor
EMT	Epithelial to mesenchymal transition
ERK	Extracellular signal-regulated kinase
ESC	Embryonic stem cell
EpiSC	Epiblast stem cell
FACS	Fluorescence-activated cell sorting
FB	FACS buffer
FCS	Foetal calf serum

FGF	Fibroblast growth factor
FGFR	Fibroblast growth factor receptor
Floxed	Flanked by LoxP sites
FSC-A	Forward scatter – area
FSC-H	Forward scatter – height
GMEM	Glasgow minimum essential medium
GSK3	Glycogen synthase kinase 3
HA	Hemagglutinin
HPRT	Hypoxanthine guanine phosporibosyl transferase
ICC	Immunocytochemistry
ICE	Inducible cassette exchange
ICM	Inner cell mass
IGF	Insulin-like growth factor
IGF1R	Insulin-like growth factor 1 receptor
JAK	Janus kinase
KOSR	KnockOut serum replacement
LB	Lysogeny broth
LRP	Low-density lipoprotein receptor-related protein
LIF	Leukaemia inhibitory factor
LoxP	Locus of crossing over, P1
MAPK	Mitogen activated protein kinase
MEK	MAPK/ERK kinase
MK	MAPK-activated protein kinase
M-MLV RT	Moloney-murine leukaemia virus reverse transcriptase
Ncad	N-cadherin
NcKI	N-cadherin heterozygously knocked-in into the E-cadherin locus ($Cdh1^{Cdh2/\Delta}$)
NDiff	Neural differentiation
NESSys	Nuclear Envelope Segmentation System
NMP	Neuromesodermal progenitor
NSB	Node-streak border
NT	Neural tube
PCM	Pre-cardiac mesoderm
PBS	Phosphate buffered saline

PBST	Phosphate buffered saline with added Triton
PCR	Polymerase chain reaction
PFA	Paraformaldehyde
PI3K	Phosphatidylinositol 3-kinase
PLC-γ	Phosphoinositide phospholipase C-gamma
PS	Primitive streak
qPCR	Quantitative polymerase chain reaction
RNA	Ribonucleic acid
ROCK	Rho-associated protein kinase
RPPA	Reverse phase protein array
RTK	Receptor tyrosine kinase
rtTA	Reverse tetracycline-controlled transactivator
SD	Standard deviation
shRNA	Short hairpin RNA
SSC-A	Side scatter – area
STAT	Signal transducer and activator of transcription
TBE	Tris/Borate/EDTA buffer
TC	Tissue culture
TCF	T-cell factor
TE	Trophectoderm
UPL	Universal Probe Library
UV	Ultraviolet
WNT	Wingless-related integration site
WT	Wild-type

Chapter I – Introduction

1.1 The interface of developmental and stem cell biology

The term "embryonic stem cell" was coined by Gail Martin in the early 1980s, when two independent scientific teams successfully cultured these cells in a dish for the first time (Evans and Kaufman, 1981; Martin, 1981). Since then, embryonic stem cells (ESCs) have captured the imaginations of both scientists and the public alike. ESCs are isolated from an early embryo, and have two defining properties: self-renewal, the ability to give rise to at least one identical copy of themselves, and pluripotency, the ability to become any cell type of the adult organism through the process of differentiation.

In 1998, ESCs were derived from a human blastocyst for the first time (Thomson et al., 1998). Since then, research on ESCs has been surrounded by both hype and controversy. In theory, owing to their ability to generate any cell type, these cells could be used to alleviate or even cure a wide range of injuries and diseases. However, their use for scientific or medical purposes necessitates the destruction of a fertilised embryo, leading to ethical concerns and moratoria on their use in research in several countries. A landmark discovery came in 2006, when a team of Japanese scientists developed a method to generate a pluripotent stem cells from the skin cell of an adult mouse (Takahashi and Yamanaka, 2006). These cells, termed induced pluripotent stem cells (iPSCs), represented a major breakthrough in the field as they eliminated the need for the destruction of a fertilised embryo, paving the way for novel stem cell treatments without potentially unethical origins.

As the field of stem cell biology develops at a great pace, the use of stem cells for biomedical applications requires not only the methods for their generation, isolation, and culture, but also an understanding of how to differentiate them into the cell types required for therapeutic purposes. Protocols exist for the differentiation of ESCs into diverse cell types *in vitro*, but even under standardised culture protocols, individual cells make lineage choices that can often be unpredictable or stochastic. This is in sharp contrast to the *in vivo* context of the developing embryo, where an initially identical population of pluripotent ESCs gives rise to the diverse and complex cell types of an adult organism with astounding efficiency and staggering reproducibility. This leads to a very basic research question: how do pluripotent stem cells make decisions about their commitment to diverse lineages?

To try to answer this question, scientists are studying the events of embryonic development to inform research on *in vitro* differentiation of stem cells. The two systems complement each other: embryos represent the biological blueprint for the differentiation of stem cells into all the lineages of the adult organism, while ESCs cultured *in vitro* provide a platform for diverse experimental manipulations in an easily accessible system that reduces the need for animal experimentation. By using a combination of these systems, researchers hope to gain a fuller understanding of the decision-making process of pluripotent stem cells: both to better understand the events of early embryonic development, and to inform the generation of ESC differentiation protocols for use in further research and to generate potential therapies.

1.2 Early embryonic development in the mouse

1.2.1 Pre- and peri-implantation development

Embryonic development begins at fertilisation, when a single sperm penetrates the membrane of the egg, delivering its haploid genome to that of the oocyte. Sperm penetration triggers the egg to complete its second meiotic division, forming a diploid cell with a peripheral polar body (reviewed in Wennekamp et al., 2013). In the next one to two days following fertilisation, the conceptus divides to reach the two- and four-cell stages. On the most part, these cells are very similar to one another, with small differences in gene expression (Goolam et al., 2016).

During the subsequent days of development, the conceptus does not grow in size but increases in cell number with each mitotic division, resulting in a structure called a morula, which is made up of individual cells called blastomeres. At around 2.5 days after conception (referred to as embryonic day 2.5, or E2.5), cellular adhesion increases, causing the blastomeres to flatten in a process known as compaction (Wennekamp et al., 2013).

Following compaction, and at around E3.0, the morula consists of a layer of outer cells and a cluster of central cells: the outer cells are directed towards the trophectoderm (TE) lineage and express the Cdx2 protein, while the inner cells go on to form the inner cell mass (ICM) and express Oct4 (Boroviak et al., 2015). This division represents the first lineage divergence event in the embryo, as the cells of the TE will go on to develop extraembryonic structures such as the placenta, while the ICM will give rise to all tissues of the developing embryo (Muñoz-Descalzo et al., 2015). Cdx2 and Oct4 reciprocally downregulate one another, resulting in cells with differential gene expression in the outer and inner layers of the morula (Arnold and Robertson, 2009). However, cell fate at this stage remains reversible, as single blastomeres isolated from these early embryos can continue to give rise to both embryonic and extra-embryonic lineages (Gardner, 1998; Hillman et al., 1972).

When the conceptus reaches the 16-to-32-cell stage at around E3.5, its outer cells mature into an epithelium, with tight junctions, gap junctions and desmosomes forming between the cells, enabling the transport of fluids from the outside to the inside of the embryo. This build-up of fluids accumulates in a central cavity which slowly increases in size. While this cavitation is occurring, the pluripotent cells of the ICM remain closely associated with one another (Lanza and Atala, 2014; Wennekamp et al., 2013). The embryo at this stage is referred to as the blastocyst.

Over the next day (E4.0-E4.5), the blastocyst matures, and is composed of four distinct structures: the pluripotent epiblast, the primitive endoderm which will give rise to yolk sac structures, the TE, and the fluid-filled cavity called the blastocoel. At around the same time, the blastocyst implants into the lining of its mother's uterus (Arnold and Robertson, 2009; Lanza and Atala, 2014). At E5.5, a cavity appears in the epiblast, and its cells elongate around this cavity to form a cup-shaped epithelium. At this stage, the embryo is referred to as the egg cylinder. This is also a time when axis specification occurs, driven by morphogen gradients of Nodal and WNT along the proximal-distal and anterior-posterior axes, respectively (reviewed in Arnold and Robertson, 2009).

An important distinction between the pluripotent cells of the blastocyst and those in the egg cylinder lies in their pluripotent state; at E4.5, the pre-implantation epiblast is said to be in a naïve ground state, meaning that these cells are equipotent and have no bias towards any particular embryonic lineage. By contrast, the pluripotent cells of the E5.5 egg cylinder are primed for differentiation towards a certain lineage, however this priming can be reversible. The naïve epiblast appears to be a unique mammalian feature (for a review, see Nichols and Smith, 2009).

1.2.2 Lineage specification

1.2.2.1 Gastrulation

Gastrulation is a crucial event in the development of all animal embryos, and is defined as the migration, differentiation and division of embryonic cells that leads to the formation of the gastrula, an early embryo with three distinct embryonal germ layers: the ectoderm, mesoderm and endoderm (Campbell and Reece, 2004). Gastrulation is driven by a conserved set of transcriptional programmes, leading to the emergence of heterogeneous gene expression in cells that are otherwise phenotypically similar (Tam and Loebel, 2007). The cells of the gastrula are individually fated according to their location within the embryo, but they are not yet fully committed to a certain lineage (Lawson et al., 1991; Peng et al., 2016; Smith, 2017).

Gastrulation begins with the formation of the primitive streak (PS) in the posterior embryo at around E6.25, when cells of the epiblast converge towards a posterior proximal pole (Arnold and Robertson, 2009). Some epiblast cells then ingress through the PS and undergo a process called epithelial-to-mesenchymal transition (EMT) to form mesodermal and endodermal lineages. Those cells that do not encounter the PS become confined to the anterior side of the embryo and give rise to the ectoderm (Li et al., 2013; Tam and Loebel, 2007).

1.2.2.2 Epithelial-to-mesenchymal transition

EMT is a highly conserved cellular program in which polarised, immobile epithelial cells lose their polarity and disassemble their cell-cell junctions to become migratory, motile mesenchymal cells. This process takes place at various stages of embryonic development, and also during cancer metastasis (reviewed in Yang and Weinberg, 2008). Cells undergoing EMT progress through discrete stages (reviewed in Lamouille et al., 2014): the dissolution of epithelial cell-cell junctions (including adherens junctions), loss of apical-basal polarity and acquisition of front-rear polarity, reorganisation of the actin cytoskeleton, changes in gene expression, increased motility, remodelling of the extracellular matrix, and, in the case of metastising cancer cells, the acquisition of resistance to senescence and apoptosis.

EMT is regulated by a set of transcriptional master regulators, such as Snail, Twist and Zeb. They are activated early in EMT, and their expression produces many of the hallmark features of EMT; one of these is the loss of the cell-cell adhesion molecule and early pluripotency marker E-cadherin, which is replaced by an analogous adhesion molecule, N-cadherin, whose expression is characteristic of mesodermal and neural cells (Lamouille et al., 2014; Radice et al., 1997).

1.2.2.3 Neural differentiation

From gastrulation onwards, cells of the anterior epiblast that do not ingress through the primitive streak go on to form ectodermal tissues, giving rise to neurectoderm, which generates the nervous system, and surface ectoderm, which will go on to generate epithelial and dermal structures (Lawson et al., 1991; Quinlan et al., 1995). Neural development begins at around E7.5 with the formation of the anterior neural plate, which is initially a monolayer of thickened neuroepithelial cells opposite the PS. As development progresses, the cells multiply, causing to neuroepithelium to thicken and stratify, and the neural plate gradually folds in on itself to create the neural groove, and, later on in development, the neural tube (Aaku-saraste et al., 1996; Henrique et al., 2015).

The fate and potency of the early neurectoderm has been investigated using fate mapping studies. At E6.5, the anterior epiblast retains pluripotency and can give rise to all three germ layers. Within half a day however, the anterior neurectoderm loses its pluripotency, and is fated to either epidermis of neurectoderm, depending on the presence of absence of bone morphogenetic protein (BMP) 4, respectively (Li et al., 2013). At E7.5, the proximal region of the ectoderm is restricted towards the surface ectodermal fate, while the remaining parts of the anterior neurectoderm have been mapped as progenitor regions for the developing central nervous system: the forebrain, midbrain, hindbrain and spinal cord (Tam, 1989; Tam and Quinlan, 1996).

In vivo, neural fate specification is an autonomous process that occurs in the absence of inhibitory signals, such as BMPs or WNTs (Muñoz-Sanjuán and Brivanlou, 2002; Zhu et al., 2014). This has led researchers to propose a “neural default model”, which argues that pluripotent cells adopt a neurectodermal fate unless specified otherwise by additional morphogens.

1.2.2.4 Neuro-mesodermal progenitors

Gastrulation is traditionally viewed as the stage where the pluripotent cells of the epiblast undergo their first lineage specification, becoming committed to one of three germ layers that give rise to defined organ systems. However, in 2009, a single-cell clonal analysis revealed a distinct population of cells arising during early gastrulation that could give rise to both neural and mesodermal lineages (Tzouanacou et al., 2009). These neuro-mesodermal progenitors (NMPs) are a transient population of cells that emerge at head-fold stage (around E7.5) and persists throughout axis elongation until E13.5 (Gouti et al., 2017; Lawson and Wilson, 2016; Wymeersch et al., 2016), long after other organ systems become specified. The existence of NMPs therefore challenges the paradigm of cell fate assignment from the three germ layers.

In vivo, NMPs are found in three different regions of the developing mouse embryo: at the early stages (E8.5-E9.5), they are located in the node-streak border (NSB), the area where the PS meets the node, and in the caudal lateral epiblast (CLE), the region of epiblast flanking the rostral PS. At later stages (E10.5-13.5), they are also found in the chordoneural hinge (CNH), a region in the tail bud comprising cells of the posterior-most ventral neural tube and underlying notochord (Wilson et al., 2009). NMPs act as a progenitor pool for the elongation of both the neural tube and the paraxial mesoderm during the extension of the body axis (Brown and Storey, 2000; Cambray and Wilson, 2007; Tzouanacou et al., 2009).

In several vertebrates – including mouse, chick, and zebrafish – NMPs can be identified by the co-expression the transcription factors T (Brachyury) and Sox2 (Martin and Kimelman, 2012; Olivera-Martinez et al., 2012; Tsakiridis et al., 2014; Wymeersch et al., 2016). Cells that subsequently differentiate into neural lineages downregulate T but maintain Sox2 expression (Gouti et al., 2014; Gouti et al., 2015; Tsakiridis and Wilson, 2015), while those committing to mesoderm downregulate Sox2 and upregulate Msgn1 and Tbx6 (Chalamalasetty et al., 2014; Gouti et al., 2017). Indeed, gene expression analysis has revealed that T and Sox2 play antagonistic roles in NMP lineage specification, with T being essential for NMP maintenance and promoting mesodermal fate, while Tbx6 commits cells to paraxial fate (Koch et al., 2017)

The induction, maintenance and differentiation of NMPs involves the convergence of predominantly two cellular signalling pathways: the "Wingless-related integration site" (WNT) and the fibroblast growth factor (FGF) pathways. Embryonic regions containing NMPs express ligands for both of these pathways, and interfering with either of these signalling cascades results in the depletion of NMPs and premature truncation of the body axis (Takada et al., 1994; van de Ven et al., 2011; Wilson et al., 2009; Yoshikawa et al., 1997). In the absence of specific components of the WNT or FGF signalling pathways, the embryo becomes truncated and ectopic neural tissue forms in place of posterior paraxial mesoderm, showing that both WNT and FGF signals are required for mesoderm specification and axis elongation, but are dispensable for neural commitment (Boulet and Capecchi, 2012; Chal and Pourquié, 2017; Ciruna and Rossant, 2001; Takada et al., 1994; Wymeersch et al., 2016; Yoshikawa et al., 1997).

WNT signalling has sequential (and sometimes contrasting) roles in the induction and maintenance of NMPs and in the differentiation of their derivatives (Henrique et al., 2015). Premature Wnt3a expression has been found to completely block neural tube formation and inhibit mesoderm formation, with the cells remaining in an early epiblast-like state (Jurberg et al., 2014). However, in NMP-derived neural and mesodermal tissues, WNT signalling blocks the progression of further differentiation (Garriock et al., 2015), while in the established neural tube it promotes cell proliferation (Megason and McMahon, 2002). Similarly, FGF signalling is regulated differently in NMPs and committed neural progenitors (Olivera-Martinez et al., 2014), while downregulation of FGFR1 in the chick embryo results in the premature exit of NMPs from the progenitor pool (Mathis et al., 2001). These studies highlight a complex regulatory signalling network involved in the maintenance and differentiation of NMPs.

Despite a rapidly growing body of work about NMPs, several open questions remain about this unique cell type (Henrique et al., 2015). For example, what, other than FGF and WNT signals, influences their cell fate decisions? How can these two pathways act to both maintain NMP and induce mesodermal fate? Are there any additional factors that modulate the response to these signals? Further research is required to better understand the fate decisions occurring in this cell population.

1.3 Pluripotent stem cells

1.3.1 Historical perspectives in the study of embryonic stem cells

Advances in embryological techniques in the second half of the 20th century set the stage for a series of discoveries that have helped shape the field of stem cell biology. In the sixties, cells from a testicular tumour, or teratocarcinoma, of a strain 129 mouse were used to demonstrate the capacity of single cells to differentiate into multiple lineages for the first time (Kleinsmith and Pierce, 1964). When single teratocarcinoma cells were injected into the peritoneum of recipient mice, the cells developed into tumours that could contain derivatives of all three embryonic germ layers. This experiment was the first demonstration that a single cell could give rise to multiple embryonic lineages, introducing the concept of pluripotency that would become a defining feature of ESCs.

Two decades later, two independent research groups succeeded in the isolation and *in vitro* propagation of pluripotent stem cells from the mouse embryo (Evans and Kaufman, 1981; Martin, 1981), and the term "embryonic stem cell" was coined, opening up a world of possibility for the study of ESCs in a dish. The same year, the epiblast was established as the pluripotent compartment of the early mouse embryo in a series of experiments showing that these cells can give rise to multiple embryonic tissues (Beddington, 1981; Beddington, 1982). A decade later, fate-mapping studies were used to demonstrate that the fate of an epiblast cell in an E6.7 embryo is dependent on its location, demonstrating that during development, epiblast cells lose their pluripotency and become committed to a specific embryonic lineage based on environmental cues (Lawson et al., 1991).

Since these seminal works, the field has continued to expand and garner attention owing to high-profile publications that have generated a buzz in the scientific community and in popular media. In the fifties, a team of researchers in Oxford clones a frog by using the nucleus from a somatic cell of a tadpole, showing that the somatic cell retains all the components required for the development of clonal offspring (Gurdon et al., 1958). In the nineties, Dolly the sheep was born at the Roslin Institute near Edinburgh as a result of somatic nuclear transfer, demonstrating the same principle in a mammal for the first time (Wilmut et al., 1997). Ten years later, the same principle was used by a group of Japanese scientists who were the first to reprogram a mouse fibroblast into a novel type of artificially derived stem cell: the iPS cell (Takahashi and Yamanaka, 2006), and the significance of this discovery was recognised with a Nobel Prize for Physiology or Medicine for the researchers. The finding was reproduced in human cells a year later by two different groups (Takahashi et al., 2007; Yu et al., 2007), ushering in a new age of potential therapeutic uses of stem cells that circumvented their major ethical drawbacks.

1.3.2 Stages of pluripotency

As the field of stem cell research continues to expand, knowledge surrounding the phenomenon of pluripotency has developed in incremental steps. This has led the identification of several distinct stages of pluripotency in early development, and to the establishment of *in vitro* culture conditions for their study in the lab.

1.3.2.1 Naïve pluripotency

Naïve pluripotency is defined as a state of broad developmental plasticity in which cells can go on to develop into any of the three germ layers, and subsequently any cell type of the developing embryo, but not into extraembryonic tissues such as the placenta. *In vivo*, this state is characteristic of the pre-implantation epiblast at around E4.5 (Nichols and Smith, 2009). Both in the embryo and in the dish, naïve pluripotency is characterised by the expression of general pluripotency factors, such as Oct4, Sox2, and Sall4, and distinguished from other pluripotent states by the expression of naïve factors such as Nanog, Klf4, Tfcp2l1, Tbx3, Esrrb and Rex1 (Boroviak et al., 2014; Guo et al., 2010; Kalkan and Smith, 2014; Ohnishi et al., 2014).

In vitro, ESCs are propagated in a naïve state in medium called 2i-Lif, which contains two pharmacological inhibitors of differentiation and the leukaemia inhibitory factor (Lif); this medium is discussed in depth later on in this chapter. Exit from naïve pluripotency occurs shortly after the withdrawal of these inhibitors, when naïve factor expression is lowered within 24h hours and completely eliminated by 48h (reviewed in Kalkan and Smith, 2014).

1.3.2.2 Formative pluripotency

The transitional state of formative pluripotency was first proposed by Kalkan & Smith (2014), and later formalised by Smith (2017). This state is proposed to be devoid of either naïve factors or lineage specifiers. It occurs after the clearance of naïve factors (*in vivo*) or upon withdrawal of 2i-Lif conditions (*in vitro*), and involves formerly naïve cells becoming receptive to differentiation stimuli. Cells in the formative state have therefore exited naïve pluripotency but remain lineage neutral.

There are two underlying assumptions of the hypothesised formative pluripotent state: first, that naïve cells are not prepared to execute lineage decisions and must undergo a process of maturation, and second, that primed cells have initiated a response to inductive cues, and already exhibit a bias towards a certain fate; the formative state is therefore hypothesised to occur in between these two well-defined stages (Smith, 2017). The existence of such a state is supported by several observations: the presence of a 24h interval (both *in vitro* and *in utero*) between the loss of naïve pluripotency and the overt manifestation of lineage priming, a remodelling of gene regulatory newtorks, changes in epigenetic landscape and metabolic state between naïve and primed stages, and the fact that germ cell competence is acquired between these two pluripotent states (Smith, 2017). However, more experimental evidence will be required before the formative state can be recognised as a canonical stage of pluripotency similar to the naïve and primed states.

1.3.3.3 Primed pluripotency

The cells of the post-implantation epiblast exist in a state referred to as primed pluripotency (Nichols and Smith, 2009). These cells can self-renew and have the ability to form all embryonic lineages, but are also biased towards a particular fate. In the embryo, they remain pluripotent until the onset of somitogenesis, or the development of the first somites (Beddington, 1981; Beddington, 1982; Osorno et al., 2012).

Epiblast stem cells (EpiSCs) are the *in vitro* analogue of the primed epiblast (Brons et al., 2007; Nichols and Smith, 2009; Tesar et al., 2007). EpiSCs can generate derivatives of all three germ layers in teratoma assays, but fail to contribute to chimera formation when injected into recipient blastocysts, and cannot contribute to the germline, unlike earlier-stage ESCs (as reviewed in Smith, 2017). EpiSCs can be derived from the embryonic epiblast between E5.5 and E8.0, but the transcriptome of EpiSC lines derived from different stages of development converges to resemble that of late gastrulation-stage epiblast, regardless of the age of the original embryo from which they were derived (Kojima et al., 2014; Osorno et al., 2012).

EpiSCs are defined by the expression of general pluripotency markers, such as Oct4 and Sox2, and early post-implantation markers like Fgf5, Otx2 and Oct6 (Kalkan and Smith, 2014). These cells have been found to exhibit significant levels of heterogeneity on the gene expression level, as they contain at least two large and mutually exclusive subpopulations, which express markers of either the early PS (such as T) or the neural lineage (such as Sox1). The PS-like subpopulation represents a more un-differentiated and dynamic population, while the neural-like subpopulation was found to be less dynamic, with some cells in this subpopulation appearing to have committed to neural differentiation (Tsakiridis et al., 2014).

1.3.4 Pluripotent culture conditions for stem cell culture *in vitro*

Several culture systems exist for the recapitulation of established pluripotent states *in vitro*. While these conditions represent a practical model for the study of development, some features of these conditions, such as the “iterations” of pluripotency that they produce, may be artefacts of the conditions themselves and may not correspond to true developmental events *in vivo* (Morgani et al., 2017).

1.3.4.1 Naive stem cell culture in 2i-Lif

2i-Lif is a serum-free culture medium used for the culture of ESCs in a state of naïve pluripotency. "2i" refers to the use of two pharmacological molecules to inhibit the activity of MEK/ERK1/2 and glycogen synthase kinase 3 (GSK3); these inhibitors allow for the suppression of FGF and activation of WNT signalling, respectively, to maintain pluripotency (discussed in greater detail later in this chapter)(Ying et al., 2008). 2i conditions can be used with or without the addition of the cytokine Lif, which is used to activate the STAT pathway, conferring additional stability to the naïve condition (Dunn et al., 2014). Cells cultured in these conditions are considered to be homogenous, without any obvious subpopulations, with some researchers suggesting that these conditions represent a more natural and self-sustainable pluripotent gene regulatory network than that in cells cultured in Lif-serum (Papatsenko et al., 2015)

1.3.4.2 Mixed stem cell culture in Lif-serum

Lif-serum is the oldest and most widely used pluripotent stem cell medium, and relies on the use of animal-derived serum and the cytokine Lif for the maintenance of a pluripotent state (Smith et al., 1988). This was the standard pluripotency culture medium before the introduction of 2i-Lif, but gene expression studies have shown that cells cultured in Lif-serum consist of two distinct subpopulations, one resembling the pluripotent epiblast equivalent to E3.5, and the other resembling a more mature epiblast at around E5.5. These two subpopulations may exist in a dynamic equilibrium with one another, with some authors suggesting that Lif-serum may therefore represent a state of stalled differentiation (Papatsenko et al., 2015). Others argue that since this dynamic and fluctuating gene expression signature has not been convincingly demonstrated *in vivo*, Lif-serum conditions represent a sub-optimal tool for the study of early development because it does not accurately recapitulate the behaviour of the embryonic epiblast (Kalkan and Smith, 2014).

1.3.4.3 Primed stem cell culture in EpiSC conditions

EpiSCs are derived from post-implantation epiblast at E5.5-E8.0, and are maintained *in vitro* in basal medium supplemented with Activin and FGF, to stimulate Activin/Nodal and FGF signalling, respectively. Optionally, the medium can also be supplemented with KOSR (Brons et al., 2007; Tesar et al., 2007). EpiSCs do not tolerate passage as single cells, and must instead be passaged as small clumps; this effect has been tied to the hyper-activation of Rho-associated protein kinase (ROCK)/myosin signalling which leads to apoptosis in response to changes in cell-cell adhesion (Ohgushi et al., 2010). Additionally, moving EpiSCs to 2i-Lif conditions causes the cells to differentiate into neurons, which is linked to the inhibitory activity of the pharmacological inhibitor PD on the FGF signalling pathway (Yu et al., 2018).

1.3.4.3.1 – Post-implantation epiblast-like cells (EpiLCs)

An alternative to the use of EpiSCs *in vitro* is the use of a closely related cell type known as post-implantation epiblast-like cells (EpiLCs). Unlike EpiSCs, which can be maintained in self-renewing culture, EpiLCs represent a transitional state occurring during differentiation from 2i-Lif. They are formed from naïve ESCs cultured in naïve conditions after around 48h from the withdrawal from 2i-Lif, and upon supplementation with FGF, Activin and KOSR (Hayashi et al., 2011). Transcriptome profiling places EpiLCs close to early post-implantation epiblast, and they can be efficiently differentiated into primordial germ cells and functional gametes: these properties are characteristic of the intermediate pre-gastrulation epiblast but are absent in EpiSCs (Hayashi et al., 2011; Kalkan and Smith, 2014).

1.3.4.4 Neural differentiation culture

In the embryo, the neural lineage is borne out of anterior epiblast cells that do not ingress through the primitive streak (Arnold and Robertson, 2009), and in its early stages does not rely on overt extrinsic signals. This has led to the development of the “neural default” model for neural differentiation, where it is argued that neurectodermal competence is the fate that pluripotent cells are going to adopt unless instructed otherwise (Muñoz-Sanjuán and Brivanlou, 2002; Smith, 2017). Monolayer neural differentiation culture reflects this idea, as neuro-epithelial precursor cells can be derived by culture in basal medium with few additional factors, but with an increased concentration of insulin to enhance the efficiency of neural differentiation (Ying et al., 2003a). This is a widely used neural differentiation culture protocol that has become standard in the field.

1.4 WNT and FGF signalling in early development

Throughout development and in other biological processes, cells are able to transmit information from their environment to their nucleus through chemical cascades known as signalling pathways. Typically, these pathways rely on the binding of an extracellular molecule (such as a hormone or ligand) to a cell-surface signalling receptor. This binding usually then triggers structural or chemical changes (such as phoshorylations) to the receptor, prompting an intracellular cascade of pathway components to chemically transmit the message to the nucleus, where it triggers gene expression. A number of complex and precisely timed signalling events orchestrate embryonic development (reviewed in Arnold and Robertson, 2009). Here, two signalling pathways most relevant to work presented in this thesis are discussed: the WNT and FGF pathways.

1.4.1 WNT signalling

Early research on WNT ("wingless-related integration site") signalling emerged through the convergence of mouse models of cancer and developmental genetics in the fruit fly *Drosophila melanogaster* (Nusse and Varmus, 2012; Nusse et al., 1991). It is now widely acknowledged that WNT signalling plays a crucial role in developmental patterning throughout the animal kingdom (Clevers, 2006).

Upon the activation of a cell-surface WNT receptor, three pathways can be switched on: the canonical WNT/β-catenin cascade, which relies on signal transduction through β-catenin, the non-canonical planar cell polarity pathway, and the Wnt/Ca^{2+} pathway; the two latter signalling cascades do not rely on β-catenin (Clevers, 2006). Of the three pathways, the canonical pathway is the best characterised and most relevant for the current project, and is discussed in greater detail in the following sections.

1.4.1.1 The canonical WNT signalling pathway

The central player of the canonical WNT signalling cascade is an intracellular protein called β-catenin, encoded by the *Ctnnb1* gene. When WNT signalling is inactive, two serine/threonine kinases, CK1 and GSK3, phosphorylate β-catenin. This phosphorylation marks β-catenin for ubiquitination by the ominously named multi-protein "destruction complex", which targets β-catenin for rapid degradation by the proteasome (Stamos and Weis, 2013). In the nucleus, the binding of the protein Groucho blocks the transcriptional activator T-cell factor (TCF) from transcribing WNT target genes. When WNT signalling is activated, Axin2, a scaffold protein of the destruction complex, becomes bound to the cytoplasmic side of the cell membrane, protecting β-catenin from phosphorylation and degradation. This un-phosphorylated form of the protein is then translocated to the nucleus, where it displaces Groucho, binds to TCF and promotes the transcription of WNT target genes (Fig. 1.1) (Clevers, 2006).

Importantly, the activation of the WNT signalling cascade can occur as a result of Wnt-ligand binding to the cell-surface receptor, or independently of receptor binding. This can take place whenever β-catenin from the membrane-bound pool (where it associates with cadherin proteins), is released into the cytoplasm and the nucleus (Kam and Quaranta, 2009). This may explain the lack of an "obligate correlation" between the expression of Wnt ligands and pathway activation in certain contexts (Howard et al., 2011; Maretto et al., 2003).

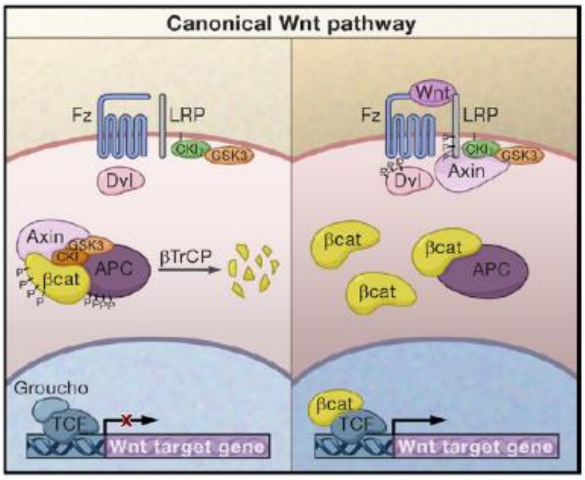

Figure 1.1: The canonical WNT signalling pathway. *Reproduced from Clevers 2006. For pathway details, see text in 1.4.1.1.*

1.4.1.2 Canonical WNTsignalling function

The canonical WNT signalling pathway plays diverse roles in several biological processes, including development and disease (reviewed in Clevers 2006). For the purposes of this thesis, its role in pluripotency and neural differentiation in mammals is discussed below.

1.4.1.2.1 – WNT signalling in pluripotency

WNT signalling is reported to be inactive during pre-implantation development in the mouse (Kemler et al., 2004; Maretto et al., 2003). However, its role in the maintenance of pluripotency, especially in the *in vitro* context, has been widely investigated. Several studies have shown that WNT signalling is required, or at least promotes, the self-renewal of mouse ESCs (Faunes et al., 2013; Miyabayashi et al., 2007; Ogawa et al., 2006; Sato et al., 2004), and inhibits their differentiation into EpiSCs (ten Berge et al., 2011). WNT signalling was found to be dispensable for the maintenance of the primed pluripotent state in EpiSCs, but was found to be necessary for the induction of a PS-like subpopulation in these cells at the expense of an anterior epiblast-like subpopulation (Tsakiridis et al., 2014).

1.4.1.2.2 – WNT signalling in neural differentiation

In vivo, a WNT gradient exists in the pre-gastrulation embryo, with the posterior epiblast expressing high levels of WNT ligands, while the anterior epiblast is negative for them (Arnold and Robertson, 2009; Maretto et al., 2003). This is reflected in the role of WNT signalling in the induction of different lineages: it is implicated in the formation of the PS, a posterior structure, both *in vivo* and *in vitro* (Mohamed et al., 2004; Tsakiridis et al., 2014), and, conversely, inhibits neural differentiation in the anterior of the embryo (Haegele et al., 2003). The addition of Wnt3a into neural differentiation culture is enough to prevent ESCs from adopting the neural fate (Faunes et al., 2013). Taken together, these studies confirm an inhibitory role for WNT signalling in anterior neural induction.

1.4.2 FGF signalling

1.4.2.1 The FGF signalling pathway

Fibroblast growth factor (FGF) signalling refers to a number of intracellular signalling cascades lying downstream of FGF receptors (FGFRs), a class of receptor tyrosine kinases (RTKs). FGF signalling plays a role in diverse cell processes in multiple contexts, including cell proliferation, survival and motility (Goetz and Mohammadi, 2013).

Binding of FGF ligand to its receptor causes autophosphorylation of tyrosine residues in the intracellular domain of the FGFR, and the signal is then transduced through one of four distinct pathways: (i) mitogen-activated protein kinase/extracellular signal-regulated kinase (MAPK/ERK), (ii) phosphoinositide phospholipase C-gamma (PLC-γ), (iii) phosphatidylinositol 3-kinase (PI3K)/Akt and (iv) Janus kinase/signal transducer and activator of transcription (Jak/STAT) (Lanner and Rossant, 2010). The individual branches can have distinct roles in different contexts, but for the purposes of the current project, two will be reviewed in more detail: the MAPK/ERK branch and the PI3K/Akt branch.

1.4.2.1.1 – The MAPK/ERK branch of the FGF pathway

MAPK/ERK refers to one of the branches of the FGF pathway, and all eukaryotes have multiple MAPK pathways with various functions: in mammals, at least five distinct groups have been characterised. “MAPK” refers to a generic kinase of the pathway, with different species having different MAPK orthologues- in mammals, this orthologue is called ERK. The MAPK pathway consists of a set of three evolutionarily conserved, sequentially acting kinases (in the nomenclature, each “K” simply refers to kinase): MAPKKK, which phosphorylates, and thus activates, MAPKK, which dual-phosphorylates MAPK, which in turn phosphorylates target substrates (Roux and Blenis, 2004).

In mammals, the sequence of MAPK activation follows a prescribed order of events: signalling is initiated when an extracellular growth factor, such as an FGF protein, binds to a corresponding transmembrane FGF receptor. This phosphorylates and activates MAPKKKs (for example Raf proteins), which in turn phosphorylate MAPKKs: in mammals, these are MEKs 1 through 7. These proteins then phosphorylate MAPKs, such as ERK1/2, which in turn phosphorylate MAPK-activated protein kinases (MKs), which execute downstream cellular functions. For an exhaustive review of the signalling cascade, see Roux and Blenis, 2004.

1.4.2.1.2 – The PI3K/Akt branch of the FGF pathway

The PI3K/Akt pathway is involved in the regulation of cell cycle and survival, EMT and cancer progression (Larue and Bellacosa, 2005). The pathway is activated by ligand binding to receptor tyrosine kinases (RTKs) such as FGFR, which phosphorylates a chain of successive kinases: the first is PI3K, followed by PDK, followed by Akt, which mediates downstream gene expression (Goetz and Mohammadi, 2013).

1.4.2.2 FGF pathway function

The FGF pathway plays very diverse roles during multiple cellular processes, including development and in disease. Here, two processes will be highlighted: pluripotency and neural differentiation.

1.4.2.2.1 – FGF signalling in development and pluripotency

Different combinations of FGF receptors and cascade components are expressed at various stages of embryonic development, and their knockout causes multiple developmental phenotypes, including embryonic lethality (summarised in Lanner and Rossant, 2010). Cues mediated by the FGF pathway also play important roles at different stages of development. For example, in the pre-implantation blastocyst, FGF/ERK signalling is involved in the segregation of the primitive endoderm lineage from the ICM: blocking the pathway causes all the cells of the ICM to become Nanog-positive epiblast, at the expense of primitive endoderm and hypoblast lineages (Nichols et al., 2009; Yamanaka et al., 2010). During gastrulation, signalling through the FGF1R receptor has been found to be critical for EMT, cell movement through the PS, and consequently for the formation of mesodermal and endodermal lineages (Ciruna and Rossant, 2001; Ciruna et al., 1997).

FGF signalling has been shown to play distinct roles in ESCs depending on their stage of pluripotency. In general, the inhibition of FGF signalling promotes the self-renewal of naïve ESCs, while the addition of FGF2 stimulates conversion of naïve ESCs to primed EpiSCs, and subsequently promotes self-renewal and maintenance of the primed state (Lanner and Rossant, 2010). This is reflected in the ways that these cells are cultured in vitro: naïve ESCs are cultured in 2i-Lif medium containing PD, a MEK/ERK inhibitor (Hamilton et al., 2013; Ying et al., 2008), while the derivation and propagation of EpiSCs involves the addition of FGF2 to the culture medium (Brons et al., 2007; Tesar et al., 2007).

However, the exact role for FGF signalling (and especially the MAPK/ERK branch of the pathway) for pluripotency remains somewhat controversial. Most studies have shown that MAPK/ERK signalling is not required for self-renewal, and that pharmacological inhibition of ERK promotes pluripotency (Burdon et al., 1999; Hamilton and Brickman, 2014; Hamilton et al., 2013). However, Chen et al., (2015) argue that most studies on the topic have either focused on pharmacological inhibition of ERK signalling, or on the knockout of one of two ERK proteins, and point out that this may not be a valid approach since the two proteins have redundant roles and one can rescue the function of the other (Hamilton et al., 2013; Pages et al., 1999; Saba-El-Leil et al., 2003). Instead, these researchers used an ERK1/2 double knockout approach to show that these mutant cells suppress pluripotency genes, display increased rates of apoptosis, and cannot be maintained in pluripotency conditions (Chen et al., 2015a). Therefore, more research may be required to pin down the exact role for FGF/ERK signalling in the maintenance of naïve pluripotency.

By contrast, FGF signalling is required for the derivation and maintenance of EpiSCs in a primed pluripotent state. FGF signalling has been shown to inhibit both the reversion of EpiSCs back into a Lif-serum-like ESC state and their differentiation down the neural lineage (Greber et al., 2010; Sterneckert et al., 2010). It is therefore proposed that FGF signalling, and especially FGF1R, plays a role in stabilising the "metastable" state of primed pluripotency in EpiSCs (Lanner and Rossant, 2010; Takehara et al., 2015).

1.4.2.2.2 – FGF signalling in neural differentiation

The role of FGF signalling in the neural differentiation of pluripotent cells has yielded contrasting findings in the past ten years, leading to some controversy in the literature on the topic. Earlier findings showed that FGF signalling promotes neural induction from Lif-serum (Kunath et al., 2007; Stavridis et al., 2007). However, subsequent reports have shown that blocking FGF signalling in EpiSCs promotes their neural differentiation (Greber et al., 2010; Jaeger et al., 2011), and *in vivo* findings have shown that FGF signalling does not act as a neural inducer in the post-implantation embryo (Di-Gregorio et al., 2007).

While these findings may appear contradictory, they can be explained by viewing neural differentiation as a progression through discrete stages of pluripotency, priming and commitment: naïve ESCs must become primed for the neural lineage, and must subsequently exit primed pluripotency to undergo neural differentiation. In this progression, FGF signalling promotes the conversion of naïve cells into primed cells, while inhibition of the pathway promotes exit from the primed state and entry into the neural lineage (Stavridis et al., 2010; Sterneckert et al., 2010). It appear that FGF signalling therefore has stage-dependent functions during pluripotency, priming and neural commitment.

1.5 Cadherins in early development and pluripotency

1.5.1 The cadherin protein family

The cadherins are a large, evolutionarily conserved superfamily of cell-surface proteins (Hulpiau and van Roy, 2009). Their main function is in facilitating cell-cell adhesion, which is usually accomplished by the proteins preferentially binding to cadherins of their own type on the surface of neighbouring cells, forming adherens junctions (Schäfer et al., 2014). Intracellularly, cadherins bind to cytoskeletal proteins such as catenin and actin; through this function, cadherins are able to bridge the cytoskeletons of neighbouring cells (Stepniak et al., 2009). Different cadherins are dynamically expressed at different times during development and in various adult tissues, and they can also play a role in cell signalling by binding cell-surface receptors or intracellular mediators of various signalling pathways (Hoschuetzky et al., 1994; Williams et al., 1994).

Epithelial (E-) cadherin is highly expressed in the cells of the early embryo, and becomes downregulated in favour of neuronal (N-) cadherin during EMT and neural differentiation; this phenomenon is termed “cadherin switching”. It also occurs when cancer cells undergo metastasis to gain a more motile, aggressive cancer phenotype (Wheelock et al., 2008). Cadherin switching has been widely studied in the context of EMT and cancer biology, though its role during embryonic development, and neural specification in particular, is not fully understood. Here, E- and N-cadherin, and their roles in development, adhesion and signalling, are discussed further in the context of cadherin switching.

1.5.2 E-cadherin

1.5.2.1 E-cadherin structure

E-cadherin (also called uvomorulin in older literature) is encoded by the *Cdh1* gene. It is a single-pass transmembrane protein found at the cytoplasmic membrane (extensively reviewed in van Roy & Berx 2008). The extracellular domains are mainly responsible for forming homotypic interactions with cadherin proteins on neighbouring cells, while the intracellular domains bind different catenin species to anchor the cadherin to the actin cytoskeleton.

The N-terminal extracellular portion of E-cadherin is made up of five repeating cadherin domains, termed "extracellular cadherin structural domains" and labelled EC-1 through EC-5, each being around 110 amino acids in size (reviewed in Kim et al 2000). In between each of the repeating cadherin domains are calcium binding pockets, which are required for calcium-dependent binding to other cadherins on adjacent cells. The C-terminal intracellular domain is about 150 amino acids in size and consists of two subdomains: the juxtamembrane domain that binds p120-catenin, and the catenin binding domain that interacts with the central "armadillo" domain of β-catenin or with γ-catenin (also called plakoglobin). Both of these proteins bind α-catenin, which in turn connects the entire cadherin complex to the actin cytoskeleton. (Anastasiadis and Reynolds, 2000; van Roy and Berx, 2008). E-cadherin and other cadherins lose their adhesive functions if their catenin-binding domains are deleted (Nagafuchi and Takeichi, 1988; Ozawa et al., 1990).

Different cadherin species preferentially bind cadherins of their own type on neighbouring cells, a process known as homophilic binding (van Roy and Berx, 2008). This species specificity is conferred by the N-terminal 113 amino acid region of the extracellular domain (Nose et al., 1990). The classical cadherin family is structurally conserved, with slight differences in structure conferring subtle but functionally important differences in their behaviour.

1.5.2.2 E-cadherin expression in early embryogenesis

E-cadherin protein is present in the unfertilised egg (Kemler et al., 1977; Ohsugi et al., 1997), and significant amounts of E-cadherin are contributed maternally to facilitate compaction and adhesion between blastomeres early in development (Stepniak et al., 2009). The protein is present in high levels in the embryo until gastrulation, when it begin to be downregulated in favour of N-cadherin in cells undergoing EMT and forming mesoderm, allowing the cells to gain a more motile phenotype as they ingress through the primitive streak (Larue et al., 1996; Luo et al., 2001; van Roy and Berx, 2008). The same cadherin switch occurs in neurulation, during the transition of the neural plate into the neural tube (Aaku-saraste et al., 1996). In further development, E-cadherin continues to be expressed in various tissues, most commonly in epithelia.

1.5.2.3 E-cadherin function in adhesion

E-cadherin can homophilically bind to other cadherins of the same species in two ways: through trans-interactions, or binding an E-cadherin protein on an opposing cell, and though cis-interactions, or binding to an E-cadherin protein on the surface of the same cell. The two processes have distinct mechanisms, so a single E-cadherin molecule may be able to participate in both interactions at the same time (summarised in Wu et al 2015).

Trans-interactions of E-cadherin are most commonly mediated by a tryptophan residue on the first cadherin domain (EC-1) of one cadherin, which is inserted into the hydrophobic pocket of another molecule, and vice versa (Harrison, 2005; Shapiro et al., 1995). By contrast, the cis-interactions are mediated by an EC1-EC2 bond between two molecules on the same cell surface. Studies suggest that the cis-interaction is necessary for the formation of trans-dimers, ie. that E-cadherin molecules on one cell surface must cluster together before they can bind other cadherin molecules on the surface of another cell (Tamura et al., 1998; Tomschy et al., 1996).

While the extracellular cadherin domains form the structural links of the adherens junction, the intracellular domains are also involved in E-cadherin mediated adhesion: mutants lacking the intracellular domain exhibit impaired adhesion (Nagafuchi and Takeichi, 1988). E-cadherin can additionally form heterophilic interactions with other cell-surface adhesion molecules, such as integrins or signalling receptors (van Roy and Berx, 2008). While E-cadherin is chiefly regarded as an adhesion molecule, it serves many functions in diverse cellular contexts, and these functions can be both dependent and independent of its role in adhesion.

1.5.2.4 E-cadherin function in pluripotency and development

1.5.2.4.1 – E-cadherin function in early embryogenesis

E-cadherin plays a critical role in pre-implantation development. Embryos lacking E-cadherin die during early embryogenesis: they are able to undergo morula compaction with the aid of maternally contributed E-cadherin, but subsequently fail to produce a blastocyst cavity or a functional TE epithelium (Larue et al., 1994). Embryos with intact E-cadherin but a deletion of the actin-binding domain of αE-catenin display disrupted adhesion in the throphoblast epithelium, phenocopying the E-cadherin null embryos and suggesting that the lethality is due to defects in adhesion (Torres et al., 1997). Knocking in N-cadherin into E-cadherin locus (NcKI) is able to rescue morula compaction in the absence of maternally-contributed E-cadherin, but cannot form a fully polarised TE (Kan et al., 2007). Further studies using hybrid cadherin molecules showed that the extracellular domain of E-cadherin is required to activate integrin growth factor 1 receptor (IGF1R)-mediated signalling, which is indispensable for TE formation (Bedzhov et al., 2012). These studies highlight critical roles for E-cadherin during peri-implantation development that are both dependent and independent of its role in cell-cell adhesion.

E-cadherin is also critical at later stages of development. When the NcKI mutation is induced after implantation, gastrulation progresses as normal and all three germ layers are formed, but the embryos die at around E8.5 due to severe morphological defects in the epiblast, extra-embryonic compartment, amnion, and ectoderm. These defects were ascribed to defects in adhesion, but also in cellular signalling, where E-cadherin is required to facilitate a feedback loop stabilising BMP expression (Basilicata et al., 2016). Taken together, these studies underscore the crucial role of E-cadherin at multiple stages of development in both cell-cell adhesion and signal transduction through various pathways.

1.5.2.4.2 – E-cadherin function in pluripotency

Several studies have implicated E-cadherin as an important pluripotency marker and a key player in the pluripotent gene regulatory network. E-cadherin overexpression allows EpiSCs to have a higher reprogramming efficiency back into naïve ESCs, and can replace Oct4 in the “Yamanaka cocktail” of factors supporting efficient reprogramming of somatic cells (Murayama et al., 2014; Redmer et al., 2011). The repression of E-cadherin using shRNA is enough to cause rapid differentiation of blastocyst-derived stem cells, while the forced overexpression of E-cadherin is enough to induce teratoma-forming ability in EpiLCs that previously lacked this capacity (Chou et al., 2008). One study has suggested that E-cadherin binds Oct4 at the cytoplasmic membrane to titrate the nuclear availability of this transcription factor to an optimal level for the maintenance of pluripotency (Faunes et al., 2013).

E-cadherin appears to play a role in the upregulation of naïve pluripotency genes: E-cadherin-null ESCs have an altered gene expression profile similar to that of EpiSC, including lower levels of naïve pluripotency genes such as Nanog, Esrrb and Klf4 (Hawkins et al., 2012; Soncin et al., 2011), and elevated levels of T/Brachyury (Larue et al., 1996). These results suggest that E-cadherin may inhibit the transition of cells from the naïve to the primed state.

The loss of E-cadherin is also a hallmark of exit from pluripotency. A drop in the levels of E-cadherin was shown to be a limiting requirement for neural differentiation, and the levels of E-cadherin and Oct4 were found to decrease in synchrony upon the onset of differentiation (Malaguti et al., 2013). However, one study using embryoid body aggregates concluded that E-cadherin is necessary for lineage commitment of mESCs, as knock-out cells failed to upregulate lineage markers even after 30 days in differentiation culture conditions (Pieters et al., 2016). The role of E-cadherin in differentiation is therefore not completely understood.

1.5.2.5 E-cadherin function in cellular signalling

1.5.2.5.1 – E-cadherin and WNT signalling

E-cadherin binds β-catenin at adherens junctions, and due to β-catenin's central role in canonical WNT signalling, the effects of E-cadherin on WNT signal transduction have been extensively studied. Cadherins have been generally regarded as negative regulators of the WNT pathway, since they reduce the amount of β-catenin available for signalling by sequestering it at the cytoplasmic membrane. However, this effect can be very context dependent (Howard et al., 2011; Murayama et al., 2014). There has been much speculation, and some contradictory reports, on whether β-catenin molecules can be freely exchanged between the cadherin-bound and transcriptionally-active pools (Gottardi and Gumbiner, 2004; Kam and Quaranta, 2009). In fact, one study showed that binding to E-cadherin at the membrane "primes" β-catenin for transcription, as β-catenin that never bound E-cadherin exhibited significantly reduced transcriptional efficiency (Howard et al., 2011). As discussed above, another study went as far as suggesting that E-cadherin and β-catenin exist in a cytoplasmic membrane-bound complex with Oct4; the authors propose that the complex titrates nuclear Oct4 levels for the optimal maintenance of pluripotency (Faunes et al., 2013).

Knockdown or loss of E-cadherin has been linked to a drop in levels of β-catenin in diverse cell types (Hendriksen et al., 2008; Wetering et al., 2001), including mouse ES cells (Orsulic et al., 1999). However, these studies also report that despite a massive rearrangement of the cellular β-catenin pool in cells lacking E-cadherin, WNT signalling activity remains comparable to that in control cells. These results suggest a lack of correlation between fluctuating β-catenin availability (caused by changes in levels of E-cadherin) and WNT pathway activation.

1.5.2.5.2 – E-cadherin and FGF signalling

E-cadherin can form membrane-bound complexes with diverse RTKs, allowing signal transduction through the FGF/MAPK cascade. Upon the formation of homophilic adherens junctions, E-cadherin can bind to epithelial growth factor receptor (EGFR) (Pece and Gutkind, 2000); this E-cadherin/EGFR interaction has been shown to be mediated through a conserved binding site on β-catenin (Hoschuetzky et al., 1994), but can also occur independently of β-catenin interaction (Qian et al., 2004). Similarly, the extracellular domain of E-cadherin has been shown to bind IGF1R, which was found to be critical for pre-implantation embryonic survival (Bedzhov et al., 2012).

1.5.3 N-cadherin

1.5.3.1 N-cadherin structure

N-cadherin is a single-pass transmembrane protein encoded by the *Cdh2* gene that has a very similar domain architecture to E-cadherin. Its N-terminal extracellular portion is made up of five cadherin-binding domains (EC-1 through EC-5) separated by calcium binding pockets. The protein is embedded in the cytoplasmic membrane through a transmembrane helix, and its C-terminal cytoplasmic domain functions as a scaffold for intracellular binding partners like catenin proteins, similarly to E-cadherin (Shapiro et al., 1995; Tamura et al., 1998).

The classical cadherins share highly conserved residues in their binding pockets (Tamura et al., 1998), but their specificity for their own type maps to the most N-terminal EC-1 domain (Nose et al., 1990; Shan et al., 2000). Additional functional specificity of N-cadherin lies in a unique 69-amino acid portion of the EC-4 domain, which is both necessary and sufficient to confer a motile phenotype in squamous carcinoma epithelial cells (Kim et al., 2000). E- and N-cadherin therefore represent similar molecules with subtle differences in structure, leading to refined differences in their function.

1.5.3.2 N-cadherin expression in embryogenesis

N-cadherin expression begins on the mRNA level during gastrulation in the posterior epiblast of the E6.0 mouse embryo (Peng et al., 2016). Expression of N-cadherin in early embryonic tissues is accompanied by cadherin switching, where E-cadherin is downregulated and N-cadherin is expressed in its place. The first such cadherin switch, and the first expression of N-cadherin protein, is in the primitive streak, allowing EMT and the formation of the migrating mesoderm (Butz and Larue, 1995; Luo et al., 2001; Nagafuchi and Takeichi, 1988; Radice et al., 1997). The next cadherin switch occurs at around E8.0 in the ectoderm during neurulation, when the neural plate invaginates to form the neural tube (Luo et al., 2001; Yang and Weinberg, 2008). At E8.5, N-cadherin is present in the neural plate, the neural tube and in the somites (Lee et al., 2007; Radice et al., 1997). Further on in development, it is present in the neural tube, non-neural ectoderm derivatives, and mesoderm derivatives such as the heart (Luo et al., 2001; Moore and Walsh, 1993; van Raamsdonk and Tilghman, 2000).

1.5.3.3 N-cadherin function in adhesion

E- and N-cadherin have similar functions in mediating homophilic adhesion through the same intracellular binding partners (Bedzhov et al., 2013). Like E-cadherin, N-cadherin forms cis-dimers on the surface of one cell before forming homophilic trans-interactions with cadherins on adjacent cells (Koch et al., 2004). Mutations of certain key residues in the calcium binding pockets, the donor strand, or the acceptor pockets of the extracellular domains of N-cadherin result in the abrogation of adhesion, between both mutant-mutant and mutant-WT cadherin pairings (Martinez-Garay et al., 2016; Tamura et al., 1998). These mutations have been used to study the effects of N-cadherin-based adhesion on cell migration and signalling (Martinez-Garay et al., 2016).

While E- and N-cadherin-mediated adhesion is achieved through similar mechanisms, junctions formed by the two molecules give rise to different strengths of adhesion. Atomic force microscopy studies have shown that E-cadherin has three times the adhesive strength of N-cadherin (Chu et al., 2004; Chu et al., 2006).

1.5.3.3.1 – N-cadherin function in early embryogenesis

N-cadherin is essential for embryonic survival; embryos lacking the protein die by E10.0 due to multiple developmental defects caused by faulty adhesion, most notably in the heart, but also in the somites, neural tube, and yolk sac (Radice et al., 1997). The lethality caused by heart defects can be rescued by knocking-in E-cadherin, suggesting that the phenotype is caused by faulty adhesion, and not a specific role of N-cadherin signalling (Luo et al., 2001). In other developmental contexts, N-cadherin regulates the migration of neuronal progenitor cells and the organisation of internal cortical structures of the brain (Kadowaki et al., 2007; Nguyen and Mège, 2016).

1.5.3.3.2 – N-cadherin and WNT signalling

N-cadherin can also interact with β-catenin, though this interaction has been less studied than that between β-catenin and E-cadherin. In HEK293 cells, siRNA knockdown of N-cadherin was shown to lead to a significant decrease in the transcriptional activity of β-catenin, showing that N-cadherin can promote WNT signalling in certain contexts. In the same study, embryos lacking N-cadherin exhibited an attenuation of WNT signalling in posterior and midline epiblast and laterally migrating mesoderm, showing that N-cadherin may play a role in WNT-driven induction of mesoderm (Howard et al., 2011).

N-cadherin can also interact with β-catenin in a WNT-independent manner. In cortical neural precursor cells, N-cadherin knockdown was shown to cause premature migration and neuronal differentiation. The authors showed that blocking N-cadherin led to a reduction in β-catenin mediated signalling, but that this signalling was likely to take place through a WNT-independent mechanism; indeed, they went on to show that N-cadherin mediates β-catenin signalling through the activation of Akt signalling. The study concluded that cortical neural precursors maintain their own niche by signalling to one another through homotypic adhesion via N-cadherin (Zhang et al., 2010).

1.5.3.3.3 – N-cadherin and FGF signalling

In contrast to E-cadherin, which binds EGFR and IGF1R (Bedzhov et al., 2012; Hoschuetzky et al., 1994), N-cadherin binds FGFR and promotes signal transduction through this receptor (Williams et al., 1994), suggesting the existence of cadherin species-dependent interactions with different members of the RTK family (Fedor-Chaiken et al., 2003). N-cadherin has been shown to bind FGF receptors via a functional motif on its fourth extracellular cadherin domain (EC4) (Williams et al., 2001).

N-cadherin-based stimulation of FGF signalling has been demonstrated in many additional contexts. In EpiSCs, blocking N-cadherin causes a decrease in pluripotency marker expression and promotes differentiation while simultaneously inhibiting phosphorylation or ERK and Akt, a phenotype that could not be rescued by the overexpression of E-cadherin.

The authors concluded that N-cadherin promotes the primed pluripotent state in EpiSCs by stabilising FGF1R and promoting signalling through the MAPK/ERK and Akt pathways (Takehara et al., 2015). Similarly, in breast cancer cell lines, N-cadherin binding to FGFR was found to stabilise the receptor and protect it from ligand-induced internalisation, thus causing sustained activation of the MAPK/ERK pathway and leading to the acquisition of metastatic properties (Suyama et al., 2002). N-cadherin has been shown to play a role in promoting neurite outgrowth independently of its role in adhesion (Doherty et al., 2000; Utton et al., 2001), and ectopically expressed N-cadherin in the epithelial cells of the mammary gland was enough to induce constitutively active FGF signalling in these cells (Kotb et al., 2011). These studies highlight a functional link between N-cadherin and FGF signalling in multiple biological contexts.

1.6 Regulation of cadherin expression

There has been considerable study of the regulatory mechanisms of E- and N-cadherin expression in EMT and cancer metastasis (reviewed in van Roy and Berx, 2008; and Wheelock et al., 2008). In most cellular contexts, E- and N-cadherin are expressed in mutually exclusive patterns, suggesting that the two proteins may co-repress each other. In neural stem cells, for example, E- and N-cadherin have been shown to reciprocally downregulate one another (Chen et al., 2015b).

E-cadherin expression is negatively regulated during EMT by several zinc finger transcription factors, such as *Snail, Slug, Twist*, various E-proteins, *Zeb1* and *Zeb2;* E-cadherin protein is additionally stabilised by p120-catenin (Wheelock et al., 2008). Conversely, some of these transcription factors also function to upregulate N-cadherin expression; for example, *Twist* has been identified as an activator of N-cadherin transcription in prostate carcinoma cells, human breast epithelial cells, and in gastric cancer cells (Alexander et al., 2006; Wheelock et al., 2008). However, it is acknowledged that the negative regulation of the *Cdh1* promoter and the positive regulation of the *Cdh2* promoter are both complex processes, and the details of their function in other contexts, including neural differentiation, remain to be established (Wheelock et al., 2008).

1.6.1 E- and N-cadherin function in cancer metastasis

In addition to EMT, neural differentiation, and other stages of development, another context in which cadherin switching is of great importance is in cancer metastasis. In general, E-cadherin is associated with the suppression of invasiveness, while in contrast, N-cadherin is linked to more aggressive, invasive and motile metastising cancer phenotypes (Hazan et al., 2000; Seidel et al., 2004). The effects of cadherin switching in cancer, and the regulatory mechanisms by which it is driven, appear to be similar to that occurring during EMT, and is therefore not fully relevant to the current project. For reviews on the topic, see Hazan et al., 2004; and Larue and Bellacosa, 2005.

1.7 Aims of the thesis

As discussed in this introduction, E- and N-cadherin play diverse roles during early embryogenesis through their functions in both adhesion and signalling. Previous research in our lab has shown that blocking the function of E-cadherin promotes faster and more synchronous neural differentiation, raising the possibility that cadherin switching may play a role in regulating this process (Malaguti et al., 2013). It is therefore hypothesised that the switch from E- to N-cadherin during early neural induction modulates signalling and differentiation competence, with the WNT and FGF pathways proposed as two candidate pathways through which such an effect may be achieved. Specifically, the research summarised in this thesis aims to answer three broad questions:

1. Is cadherin switching initiated before neural differentiation?
2. If so, does cadherin switching help regulate neural differentiation?
3. If so, is this due to effects on adhesion or effects on signalling?

Answering these questions should shed more light on how neural differentiation proceeds robustly in the embryo, and provide novel insights that can be applied to further studies of cadherin switching in the various biological contexts in which it occurs.

Chapter II – Materials & Methods

2.1 Materials

2.1.1 Instruments

2.1.1.1 – Biosafety cabinets

- Labculture® Class II Type A2 biological safety cabinet - Esco
- UV3 HEPA PCR Workstation – UVP

2.1.1.2 – Centrifuges

- Centrifuge 5702 – Eppendorf
- Fisherbrand™ Standard Mini centrifuge – Fisher Scientific
- Heraeus Biofuge 13 – Sepatech
- Shandon CytoSpin III Cytocentrifuge, 8358-30-0001 – Shandon

2.1.1.3 – Electrophoresis power packs

- PowerPac™ Basic power supply – BioRad

2.1.1.4 – Flow cytometers

- BD Accuri™ C6 – BD Biosciences
- BD FACSAria™ II – BD Biosciences

2.1.1.5 – Specialist Freezers

- Ultra low temperature freezer U725 – New Brunswick Scientific
- Liquid nitrogen storage tank – Statebourne Biostytem 100+

2.1.1.6 – Incubators

- CO_2 UV Incubator, MCO-19AICUV – Sanyo/Panasonic
- Heratherm™ Compact microbiological incubator – Thermo Scientific

2.1.1.7 – Microscopes

- AE2000 inverted microscope – Motic
- Leica SP8 3- and 5-detector confocal microscope – Leica
- Olympus BX61 widefield upright metallurgical microscope – Olympus
- Olympus IX51 inverted microscope – Olympus

- Operetta® High Content Imaging System - PerkinElmer

2.1.1.8 – Nucleofectors

- 4D-Nucleofector™ System – Lonza

2.1.1.9 – Plate readers

- GloMax®-Multi Microplate Multimode Reader, E7061 – BioRad

2.1.1.10 – Spectrophotometers

- NanoDrop™ Lite – Thermo Fisher, ND-LITE

2.1.1.11 – Thermocyclers

- LightCycler® 480 Instrument II – Roche
- TProfessional thermocycler – Biometra

2.1.1.12 – Thermal mixers and shakers

- Incu-Shaker Mini – Benchmark Scientific
- ThermoMixer® F – Eppendorf

2.1.1.13 – Transilluminators

- Dark Reader blue light transilluminator – Clare Chemical Research
- GeneFlash gel documentation system – Syngene

2.1.2 Supplies and Reagents

2.1.2.1 General reagents

Table 2.1: List of general reagents used in the thesis.

Reagent	Manufacturer	Catalogue number
1kb DNA ladder	New England Biolabs	N3232L
2-Mercaptoethanol, 50mM (1000x)	Life Technologies	31350010
7AAD viability staining solution	eBioscience	00-6993-59
Accutase® solution	Sigma-Aldrich	A6964
Activin-A (Human/murine/rat raised in *E. coli*)	Peprotech	120-14E
Ampicillin sodium salt	Calbiochem	171254
Apo-transferrin, human	Sigma-Aldrich	T-1147
B-27® Supplement	Gibco	17504-044

Bacto™ Agar	BD	214010
BamHI-HF® (100,000 U/mL)	New England Biolabs	R3136T
Benzyl alcohol	Sigma-Aldrich	8421
Benzyl benzoate	Sigma-Aldrich	B6630
Boric acid, solid	Fisher Scientific	BP168-1
Bovine serum albumin (7.5%)	Gibco	15260-037
Bovine serum albumin (solid)	Sigma-Aldrich	A3059
Brilliant III Ultra-Fast qPCR Master Mix, 2x	Agilent	600880-51
Chick serum	Sigma	C5405
Chiron / CHIR 99021	Axon	1386
Complete™, EDTA-free Protease Inhibitor Cocktail	Roche	05056489001
CutSmart® Buffer (10x)	New England Biolabs	B7204S
DAPI	Sigma	D9542
Dimethyl sulphoxide, dehydrated	VWR	23500.260
DMEM/F-12	Gibco	21331-020
dNTP Mix (10mM)	Invitrogen	18427-013
Donkey serum	Sigma	D9663
Doxycycline Hyclate	Sigma	D9891
Dulbecco's Phosphate Buffered Saline (PBS)	Sigma-Aldrich	D8537
EDTA	Fisher	BP2482
EDTA (for tissue culture)	VWR	20301.186
Ethanol absolute 100%	VWR Chemicals	20821.330
FGF2, recombinant human basic protein	R&D	233-FB
Fibronectin from bovine plasma	Sigma-Aldrich	F1141
Foetal calf serum	APS	S-001B-BR
Foetal calf serum	Life technologies	10270106
Formaldehyde solution, 37-41%	Fisher Chemical	F/1501/PB08
Gelatin, powder	Sigma	G1890
Geneticin® Selective Antibiotic (G418 Sulfate), powder	Thermo Fisher Scientific	11811031

Giemsa stain	VWR	350864X
Glasgow minimum essential medium	Sigma	G5154
Glycerol	CalBiochem	356350
High QC Enhancer (5x)	New England Biolabs	B9028S
HyClone™ Water, molecular biology grade	Fisher Scientific	SH3053802
Insulin from bovine pancreas	Sigma-Aldrich	I-1882
Kanamycin sulfate	Calbiochem	420311
KaryoMAX™ Colcemid™ Solution in HBSS	Gibco	15210040
KnockOut™ Serum Replacement	Gibco	10828028
Laminin, 1-2mg/mL	Sigma-Aldrich	L2020
LightCycler® 480 Probes Master (2X)	Roche	04887301001
L-glutamine, 200mM	Invitrogen	25030-024
M2 Medium	Sigma	M7167-100mL
MEM non-essential amino acids, 100x	Invitrogen	11140-036
N-2® Supplement	Gibco	17502-048
Neurobasal® Medium	Gibco	21103049
NotI-HF (100,000 U/mL)	New England Biolabs	R3189M
Orange G	Sigma-Aldrich	O3756
Paraformaldehyde (PFA)	Sigma-Aldrich	P6148
PD 0325901	Axon	1408
Penicillin (10,000 U/mL) / streptomycin (10,000 µg/mL)	Invitrogen	15140-122
Pertex®	HistoLab	00801-EX
Phosphate buffered saline tablets	Sigma-Aldrich	P4417-100TAB
PhosSTOP™ tablets	Roche	04906837001
Poly-L-ornithine solution, 0.01%	Sigma-Aldrich	P4957
Progesterone	Sigma-Aldrich	P8783
ProLong™ Gold Antifade Mountant	Thermo Fisher Scientific	P36930
Protein assay dye reagent concentrate	BioRad	500-0006
Putrescine dihydrochloride	Sigma-Aldrich	P5780

Q5® DNA Polymerase (2000 U/mL)	New England Biolabs	M0493S
Quick Start™ bovine serum albumin standard	BioRad	500-0206
Random Primers	Invitrogen	48190-011
rAPid Alkaline Phosphatase (1000U)	Roche	04-898-133-001
RNAseOUT™ Recombinant Ribonuclease Inhibitor (40 U/μL)	Invitrogen	10777019
RNAse*Zap*® RNAse decontamination solution	Ambion	AM9780
Sodium pyruvate, 100mM	Invitrogen	11360-039
Sodium selenite	Sigma-Aldrich	S5261
Subcloning Efficiency™ DH5α™ Competent Cells	Invitrogen	18265017
SYBR® Safe DNA gel stain	Thermo Fisher Scientific	S33102
T4 DNA Ligase (400,000 U/mL)	New England Biolabs	M0202S
T4 DNA Ligase reaction buffer (10x)	New England Biolabs	B0202S
Tris Base, solid	Fisher Scientific	BP152
Triton™ X-100	Sigma	X100-100ML
Trypsin 2.5%, 100x	Invitrogen	15090-046
Tryptose phosphate broth solution	Sigma	T8159
UltraPure™ Agarose	Invitrogen	16500-500
Universal Probe Library probes	Roche	Variable
X-Gal (50mg/mL)	Promega	V394A
XhoI (20,000 U/mL)	New England Biolabs	R0146

2.1.2.2 Plastics, glassware and supplies

Table 2.2: List of standard plastics, glassware and supplies.

Name	Supplier	Catalogue number
Borosilicate thin wall capillaries, 1.0mm x 0.78mm	Harvard Apparatus	30-0036
Cell scrapers, small	Corning	3010
Centrifuge tubes, 15mL clear polypropylene	Corning	430790
Costar® multiple well plates, 6-well	Corning	3516
Costar® multiple well plates, 12-well	Corning	3513
Costar® multiple well plates, 24-well	Corning	3524
Costar® multiple well plates, 96-well	Corning	3595
Cover glasses, 12 mm diameter	Marienfeld-Superior	0111520
CryoTube™ Vials, 1.0mL	Thermo Scientific	377224
Falcon® 5mL round bottom polystyrene test tube with cell strainer snap cap	Corning	352235
Fast Read 102® hemocytometer system	Kova International	BVS100H
ImmEdge Hydrophobic Barrier PAP Pen	Vector Laboratories	H-4000
LightCycler® 480 Multiwell Plate 384, white	Roche	04729749001
Microscope slides	VWR	ECN 631-1553
Micro tubes with screw cap, 1.5mL	Sarstedt	72692005
Multiply® µStrip Pro PCR tubes	Sarstedt	72.991.002
Polysine® adhesion slides, white	VWR	631-0107
Round bottom polypropylene test tube with snap cap, 14mL	Falcon	352059
Shandon™ Single Cytofunnel™	Thermo Fisher Scientific	5991040
Sterilin™ Polystyrene 30mL Universal Containers	Thermo Fisher Scientific	128A/FS

Sterilin™ standard 90mm petri dish	Thermo Fisher Scientific	101VR20
Syringe filter unit, 0.22µm, Millex-GP	Millipore	SLGP033RS
TC-treated culture dish, 100mm	Corning	430167
Transfer pipettes, 3.5mL	Sarstedt	86.1172.001
U-shaped canted neck cell culture flask, 75cm²	Corning	430720U
White filter cards	Thermo Fisher Scientific	5991022

2.1.2.3 Kits

Table 2.3: List of standard kits used in thesis.

Name	**Supplier**	**Catalogue number**
Absolutely RNA Miniprep Kit	Agilent	400800
M-MLV Reverse Transcriptase Kit	Invitrogen	28025
P3 Primary Cell Nucleofector™ Kit L (12 RCT)	Lonza	V4XP-3012
QIAprep Spin Miniprep Kit	Qiagen	27104
QiaQuick Gel Extraction Kit	Qiagen	28704
Zero Blunt® TOPO® PCR Cloning Kit	Invitrogen	K2800-20SC

2.1.3 Compositions of standard solutions

Table 2.4: Standard solution compositions. *All solutions made up in Milli-Q filtered and deionised water unless otherwise stated.*

Solution	**Components**
Activin A solution, 20µg/mL	100µg/mL Activin A (Peprotech) diluted to 20µg/mL in sterile-filtered 0.1% BSA (Sigma-Aldrich) in PBS
BABB	1:2 solution of benzyl alcohol : benzyl benzoate
Blocking solution (for ICC)	3.33% Donkey serum (Sigma), 0.1% Triton™ X-100 (Sigma), 0.001% sodium azide in PBS
DNA loading dye, 6x	0.25% Orange G (Sigma), 30% glycerol (CalBiochem)
FACS buffer (FB), 2%	2% FCS (Life technologies) in Dulbecco's PBS (Sigma)

FACS collection buffer, 50%	50% FCS (Life technologies) in Lif-serum medium
FGF2 solution, 10µg/mL	Lyophilised FGF2 powder (R&D) reconstituted to 10µg/mL in sterile-filtered 0.1% BSA (Sigma-Aldrich) in PBS
Formaldehyde fixative solution, 4%	1:10 dilution of 40% Formaldehyde solution (Fisher chemical, as supplied) in PBS
Gelatin, 0.1%	1% gelatin (Sigma) in water and autoclaved, then diluted to 0.1% in PBS (Sigma)
Glutamine/Pyruvate	100mM L-glutamine (Invitrogen), 50mM sodium pyruvate (Invitrogen)
Laminin coating solution, 5µg/mL	Laminin (Sigma) diluted to 5µg/mL in PBS
Leukaemia inhibitory factor, human, 100,000 units/mL	Prepared in-house by TC staff by transfecting Cos7 cells with plasmid to make them produce LIF. The concentration was then assayed by using indicator cells, diluted in PBS to final concentration.
PBS, non-TC	One PBS tablet (Sigma-Aldrich) dissolved in 200mL water yields 0.01M phosphate buffer, 0.0027M KCl and 0.137M NaCl, pH7.4 at 25°C
PBST	PBS (Sigma-Aldrich) with 0.1% Triton X-100 (Sigma)
TBE Buffer, 10x	40mM Tris Base (Fisher) 450mM boric acid (Fisher), 10mM EDTA, pH 8.0
Trypsin (1:5)	0.186g of EDTA (VWR) added to 500mL PBS (Sigma) and filter-sterilised. 5mL chick serum (Sigma) and 20mL 100x Trypsin (Invitrogen) added. Prepared by TC service. This solution was diluted 1:5 in PBS prior to use.

2.1.4 Antibodies

2.1.4.1 Primary antibodies

Table 2.5: Primary antibodies used for ICC and flow cytometry. *All primary antibodies were diluted in blocking solution prior to ICC staining or in FACS buffer prior to staining for flow cytometry.*

Epitope recognised	Clone	Host species	Dilution factor	Company	Cat. number
β-catenin (total)	Polyclonal	Rabbit	1:1000	Sigma	C2206
β-catenin (active), dephosphorylated on Ser37 or Thr41	8E7	Mouse	1:1000	Millipore	05-665
Brachyury	Polyclonal	Goat	1:200	R&D	AF2085
E-cadherin	DECMA-1	Rat	1:200	Sigma	U3254
E-cadherin, eFluor660-conjugated	DECMA-1	Rat	1:300	eBioscience	50-3249-82
GFP	Polyclonal	Chicken	1:1000	Abcam	13970
HA	HA-7	Mouse	1:1000	Sigma	H3663
Laminβ1	Polyclonal	Chicken	1:1000	Abcam	Ab90169
Laminβ1	Polyclonal	Rabbit	1:1000	Abcam	Ab16048
N-cadherin	32	Mouse	1:200	BD	610920
N-cadherin, AlexaFluor488-conjugated	Polyclonal	Sheep	1:50	R&D	FAB6426G
Oct4	N-19	Goat	1:200	Santa Cruz	SC-8628
Sox1	N23-844	Mouse	1:200	Pharmigen	560749
Sox2	EPR3131	Rabbit	1:200	Abcam	Ab92494

2.1.4.2 Secondary antibodies

Table 2.6: Secondary antibodies for ICC. *All secondary antibodies were diluted at 1:1000 in blocking solution prior to ICC staining unless stated otherwise.*

Host species	**Species recognised**	**Alexa Fluor excitation wavelength (nm)**	**Company**	**Cat. number**
Donkey	Chicken	488	Jackson Labs	703-545-155
		647	Merck	AP194SA6
	Goat	488	Invitrogen	A11055
		568	Invitrogen	A11057
		647	Invitrogen	A21447
	Mouse	488	Invitrogen	A21202
		568	Invitrogen	A10037
		647	Invitrogen	A31571
	Rabbit	405	Abcam	AB175651
		488	Invitrogen	A21206
		555	Invitrogen	A31572
		647	Invitrogen	A31573
	Rat	488	Invitrogen	A21208
		568	Abcan	AB175475
	Sheep	488	Invitrogen	A11015
Goat	Rat	405	Biolegend	405412
		488	Invitrogen	A-11006

2.1.5 Plasmids

Table 2.7: Plasmids used in the thesis.

Plasmid name	**Generated by**
p2Lox-eGFP	Iacovino et al., 2009
p2Lox-Ncad-HA	Karolina Punovuori
pCR^{TM}-BluntII-TOPO®	Thermo Fisher Scientific, Cat. No. K28002
pCR-BluntII-Topo-Ncad-HA	Karolina Punovuori
pPYCAG-3xFlag-eGFP-IP	Ian Chambers lab
pPYCAG-Ncad-HA-IRES	Karolina Punovuori

2.1.6 PCR primer sequences

2.1.6.1 qPCR primer sequences

Table 2.8: qPCR primer sequences. *Forward (F) and reverse (R) primers used to recognise each gene shown together with UPL probe they were used with.*

Target	**Names (F, R)**	**Forward sequence**	**Reverse sequence**	**UPL probe number**
Ap2a	SL297, SL298	CCGGGTATTAACATCCCAGAT	CCGAAGAGGTTGTCCTTGTTA	94
Axin2	SL149, SL150	TGGGGAGCAGTTTTGTGC	CGGCTGACTCGTTCTCCT	96
Cdh1	SL161, SL162	ATCCTCGCCCTGCTGATT	ACCACCGTTCTCCTCCGTA	18
Cdh2	SL233, SL234	GCCATCATCGCTATCCTTCT	CCGTTTCATCCATACCACAAA	18
Dlx5	SL133, SL134	AGCCCCTACCACCAGTACG	GCTCCGCCACTTCTTTCTC	20
Dusp4	SL476, SL477	GCCTGGCCTACCTGATGAT	GCTGCTTGACGAACTCAAAA	25
Egr1	SL717, SL718	CCTATGAGCACCTGACCACA	TCGTTTGGCTGGGATAACTC	22
Etv4	SL559, SL560	GGGTACCTTGGTGAGCACAG	CCCTGAGGAGATGTGAAGGA	66
JunB	SL689, SL690	CGAGCACTGGGGACTTTG	CGTCGCTTCCCTCAGTTC	18
Klf4	SL359, SL360	CGGGAAGGGAGAAGACACT	GAGTTCCTCACGCCAACG	62
Nanog	SL543, SL544	CCTCCAGCAGATGCAAGAA	GCTTGCACTTCATCCTTTGG	25
Pax6	SL131, SL132	GTTCCCTGTCCTGTGGACTC	ACCGCCCTTGGTTAAAGTCT	78
Pou3f1 (Oct6)	SL619, SL620	CTCAAGCCGCTGCTCAAC	CGCGATCTTGTCCAGGTT	25

Pou5f1 (Oct4)	SL274, SL275	GTTGGAGAAGGTGG AACCAA	CTCCTTCTGCAGGGC TTTC	95
SDHA	SL759, SL760	CAGTTCCACCCCACA GGTA	TCTCCACGACACCCTT CTGT	71
Sox1	SL547, SL548	GTGACATCTGCCCCC ATC	GAGGCCAGTCTGGTG TCAG	60
Sox17	SL583, SL584	CACAACGCAGAGCTA AGCAA	CGCTTCTCTGCCAAG GTC	97
T (Brachyury)	SL463, SL464	ACTGGTCTAGCCTCG GAGTG	TTGCTCACAGACCAG AGACTG	27
TBP	SL117, SL118	GGGGAGCTGTGATG TGAAGT	CCAGGAAATAATTCT GGCTCA	97
Ywhaz	SL761, SL762	TTACTTGGCCGAGGT TGCT	TGCTGTGACTGGTCC ACAAT	9

2.1.6.2 Cloning primer sequences

Table 2.9: Cloning primer sequences. *"F" and "R" refer to forward and reverse primer orientation, respectively.*

Name	**Target**	**Additional features**	**Sequence**
KP01	N-cadherin (F)	-	ATGTGCCGGATAGCGGGAGC
KP02	N-cadherin (R)	-	TCAGTCGTCACCACCGCCGT
KP03	N-cadherin-HA (F)	Flanked by a XhoI restriction site	CTAGCTCGAGGCCGCCACC ATGTGCCGGATAGCGGGAGC
KP04	N-cadherin-HA (R)	Flanked by a NotI restriction site, contains C-terminal HA tag	CATGGCGGCCGCTCAAGCGTA ATCTGGAACATCGTATGGGTAA CTACCTGTGTCGTCACCACCGC CGTACA

2.1.6.3 Sequencing primer sequences

Table 2.10: Sequencing primer sequences. *"F" and "R" refer to forward and reverse primer orientation, respectively.*

Name	**Target**	**Sequence**
CAGF	CAG vector (F)	TGCTGGTTGTTGTGCTGT
CAGR	CAG vector (R)	CGCACACCGGCCTTATTCCA
KP05	N-cadherin (F)	GCCTTTCAAACACAGCCACAG
KP06	N-cadherin (F)	TCATCCTGCTGATCCTTGTTCTC
KP07	N-cadherin (F)	CCAGCTCCAGCAACCAGATAC
KP08	N-cadherin (F)	AGTCTTTGACTACGAGGGCAGC
M13F	Blunt II Topo vector (F)	GTAAAACGACGGCCAG
M13R	Blunt II Topo vector (R)	CAGGAAACAGCTATGAC
p2LoxF	p2Lox vector (F)	GCTGTTCTCCTCTTCCTCATCTC
p2LoxR	p2Lox vector (R)	TCCCCCTGAACCTGAAACAT

2.1.7 Software packages & databases

2.1.7.1 – Cloning and sequencing

- ApE, A plasmid Editor – M. Wayne Davis, University of Utah

2.1.7.2 – Data processing and statistical analysis

- GraphPad Prism 6 – GraphPad Software Inc.
- Microsoft Excel 2013 – Microsoft Corporation
- R version 3.4.1 – R Foundation for Statistical Computing (R Core Team, 2017)

2.1.7.3 – Flow cytometry

- FlowJo – LLC

2.1.7.4 – Image analysis

- Columbus^{TM} image data storage and analysis system – PerkinElmer
- ImageJ/Fiji – (Schindelin et al., 2012)
- PickCells – Guillaume Blin, University of Edinburgh

2.1.7.5 – Nanostring RNA expression analysis

- nSolver™ 4.0 – NanoString Technologies, Inc

2.1.7.6 – qPCR analysis

- LightCycler® 480 – Roche Life Sciences

2.1.7.7 – qPCR primer design

- UPL assay design centre – Roche Life Sciences

2.1.7.8 – Referencing

- Mendeley – Elsevier

2.2 Methods

2.2.1 DNA methods

2.2.1.1 DNA cloning methods

2.2.1.1.1 – Restriction enzyme digestion

DNA digestions were performed with 0.2-100µg DNA with 2-100 units of selected restriction enzymes, using digestion conditions and buffers recommended by the manufacturer (New England Biolabs). Digestions were typically performed for 1-3 hours at 37°C, with heat inactivation performed (where appropriate) according to the manufacturer's recommendations.

2.2.1.1.2 – DNA fragment ligation

Linear DNA fragments were ligated using T4 DNA Ligase (New England Biolabs). Reactions were prepared with 50ng of vector backbone and a 1:1 vector:insert molar ratio. Ligation reactions were performed in a 10µL total reaction volume with 400U of T4 DNA ligase and T4 Buffer (New England Biolabs) at a final concentration of 1x. For each vector/insert combination, a no-insert control was prepared as a ligation control for subsequent transformations into bacteria. Ligation reactions were performed for 1h at 37°C or overnight at 4°C.

For problematic ligation reactions where a re-ligation of the vector backbone was suspected, the backbone was treated with rAPid Alkaline Phosphatese (Roche) following the manufacturer's protocol. Briefly, 100ng of vector backbone was incubated in a 10µL reaction with 1µL each of supplied buffer and enzyme. The reaction was incubated at 37°C for 30min and heat-inactivated at 75°C for 15min. The alkaline phosphatase-digested backbone was then used in a ligation reaction as usual.

2.2.1.1.3 – Preparation of agarose gels

Gels were prepared by mixing UltraPure^{TM} agarose powder (Invitrogen) into 1x TBE to a final concentration of 0.5-2% (mass/volume), dependent on application. The solution was heated in a standard microwave at full power until the agarose was fully dissolved. After briefly cooling the solution, SYBR® Safe DNA Gel Stain (Invitrogen) was added at 1:10,000 dilution. The solution was then poured into a gel mould with a well comb of desired size and allowed to set at room temperature.

2.2.1.1.4 – Gel electrophoresis

Before loading onto gels, DNA samples were mixed with DNA loading dye at 1:6 dilution. An agarose gel was covered in 1x TBE in a gel mould, with the well comb removed. The samples were then loaded into individual wells alongside a well of 1kb DNA ladder (New England Biolabs). The gel mould was then connected to a PowerPac^{TM} Basic power supply (BioRad), and gels were electrophoresed at 80V for 40-90 minutes depending on the size of the DNA samples. After the run was complete, gels were visualised under a blue-light transilluminator (Clare Chemical Research), or visualised and photographed under a UV transilluminator (SynGene) to verify band sizes.

2.2.1.1.5 – DNA extraction from agarose gels

DNA that was to be used in further applications was visualised under a blue-light transilluminator (Clare Chemical Research) only to protect it from degradation. DNA bands of interest were cut out from the gel using a scalpel. The DNA was subsequently extracted using the QiaQuick Gel Extraction Kit (Qiagen). Following gel extraction, DNA concentration was quantified using a NanoDrop^{TM} Lite scectrophotometer (Thermo Fisher).

2.2.1.1.6 – DNA sub-cloning into pCR^{TM}-Blunt II-TOPO® vector

After DNA purification from agarose gels, blunt-ended PCR products were sub-cloned into a pCR^{TM}-Blunt II-TOPO® vector by using a Zero Blunt® TOPO® PCR Cloning Kit (Invitrogen). This method allows the insertion of a PCR product into the TOPO vector without the need for a separate ligation reaction. The resulting DNA mix was transformed directly into competent bacteria, with addition of X-Gal (Promega) for blue-white screening.

2.2.1.1.7 – Preparation of antibiotic selection plates

Lysogeny broth (LB) agar was prepared by the institute's wash staff by dissolving 1.5% Bacto^{TM} Agar (BD) in LB. The solid stock was microwaved at full power until it liquefied, and the solution was allowed to cool before addition of antibiotics.

Stocks of 1000x ampicillin and kanamycin were prepared by dissolving 100mg or 50mg of ampicillin sodium salt powder or kanamycin sulfate powder (respectively, both Calbiochem) in 1mL of nuclease free water (Gibco) and filtering the solution through a 0.22µm syringe filter unit (Millipore). The appropriate antibiotic was then added at 1:1000 dilution to the cooled LB-agar solution. In a microbiological UV hood, 15mL LB-agar-antibiotic solution was pipetted into 90mm Standard Petri dishes (Sterilin), and allowed to set at room temperature.

2.2.1.1.8 – Plasmid transformation into competent bacteria

Plasmids were transformed into chemically competent DH5α *Escherichia coli* (Invitrogen) following manufacturer's instructions. Briefly, less than 200ng of plasmid DNA was added to a tube of 50µl of DH5α cells and incubated on ice for 30 minutes. The mixture was then heat-shocked by holding the tube in a water bath at 42°C for 45s. The tube was then returned to ice for 2min, after which 950µL of LB was added. The solution was then incubated in a shaker set to 800rpm at 37°C for one hour to allow the bacteria to start expressing antibiotic resistance genes. The solution was then centrifuged at 8000rpm for 3mins, 800µL of supernatant was removed, and the pellet was resuspended in the remaining solution, and 100µL of the resulting bacterial solution was spread onto antibiotic selection agar plates. For transformations requiring blue-white screening, 10µL (500µg) X-gal (Promega) was added to each plate. Plates were incubated at 37°C overnight.

2.2.1.1.9 – Preparation and use of bacterial glycerol stocks

Following overnight incubation, bacterial colonies were picked from selection plates using a yellow (200µL) pipette tip, which was used to inoculate 5mL LB supplemented 1:1000 with appropriate antibiotics in a 14mL Falcon Snap Cap tube (Falcon). The tubes were incubated overnight at 37°C, shaking at 225rpm. For long-term storage of bacteria containing constructs, glycerol stocks were prepared by mixing 500µL of the bacterial suspension with 500µL of 50% glycerol (Calbiochem) in a screw-cap 1.5mL micro tube (Sarstedt). The glycerol stocks were stored long-term at -80°C.

To grow bacterial cultures from glycerol stocks, the tube containing the stock was removed from -80°C and kept on dry ice. In a microbiology UV hood, a 200uL pipette tip was used to scrape off a small amount of frozen suspension and used to inoculate 5mL of LB supplemented with appropriate antibiotic. The culture was incubated overnight at 37°C, shaking at 225rpm. The glycerol stock was returned to -80°C for long-term storage.

2.2.1.1.10 – DNA purification from bacterial cultures

DNA was purified from the overnight cultures by using a QIAprep spin miniprep kit (Qiagen), and DNA concentration was quantified using a NanoDrop™ spectrophotometer (Thermo Scientific). The resulting DNA stocks were stored at -20°C until further use.

2.2.1.1.11 – Plasmid sequencing

Sequencing of DNA plasmids was performed by Edinburgh Genomics at the University of Edinburgh via BigDye® Terminator Cycle Sequencing technology (Invitrogen). For each construct/primer pair to be used for sequencing, Edinburgh Genomics were supplied with a reaction containing 500ng DNA, 1uL primer solution at 3.2µM, with nuclease-free water (Fisher Scientific) supplemented to 6µL. Returned sequencing reads were analysed using ApE software.

2.2.1.2 PCR methods

2.2.1.2.1 – Q5® Hot Start PCR

Q5® Hot Start High-Fidelity DNA Polymerase (NEB) was used to amplify genes of interest from cDNA in which the given gene was shown to be expressed by qPCR. PCR reactions were performed according to manufacturer's recommendations in a final reaction volume of 50µL.

Table 2.11: Q5® Hot Start PCR reaction components.

Component	Volume per reaction	Final concentration
5x Q5 Reaction Buffer	10 µL	1x
10 mM dNTPs	1 µL	0.2 mM
10 µM forward primer	2.5 µL	0.5 µM
10 µM reverse primer	2.5 µL	0.5 µM
Template cDNA	4 µL	0.2 ng/µL

Q5® Hot Start High Fidelity DNA Polymerase	0.5 µL	1 U/reaction
5x High QC Enhancer (optional)	10 µL	1x
Nuclease-free water	To 50µL	-

PCR reactions were performed in a TProfessional thermocycler (Biometra) using cycling conditions listed below:

Table 2.12: Q5® Hot Start PCR reaction conditions.

Step	**Temperature (°C)**	**Duration (min:s)**	**Number of cycles**
1. First denaturation	98	0:30	1
2. Denaturation	98	0:10	35
3. Annealing	58	0:30	
4. Extension	72	2:30	
5. Final extension	72	2:00	1

2.2.1.3 qPCR methods

Quantitative PCR (qPCR) was used to quantify relative gene expression levels of cell populations. To this end, mRNA was isolated from cell lysates and was then reverse-transcribed into cDNA as described in "2.2.2 RNA methods". The Roche LightCycler® 480 Real-Time PCR system, coupled with the Universal Probe Library (UPL) from Roche, was used for all qPCR measurements. Primers used for qPCR were designed using the online UPL Assay Design Centre facility from Roche.

qPCR reactions were carried out in a 384-well plate (Roche) with a total reaction volume of 8µL. Two commercially available qPCR master-mixes were used, depending on their availability in the lab. For the two master-mixes, reaction components remained unchanged but slight changes were made to the reaction conditions.

Table 2.13: qPCR reaction components

Component	**Volume per reaction**	**Final concentration**
Mastermix; either: • LightCycler® 480 Probes Master (Roche)	4 µL	1X

or • 2× Brilliant III Ultra-FastqPCR Master Mix (Agilent)		
Nuclease-free water	1.2 µL	-
Forward primer (10µM)	0.36 µL	450 nM
Reverse primer (10µM)	0.36 µL	450 nM
UPL probe (10µM)	0.08 µL	100 nM
Template cDNA	2 µL	-

Table 2.14: qPCR reaction conditions for Roche master-mix.

Step	**Temperature (°C)**	**Duration (min:s)**	**Ramp rate (°C/s)**	**Number of cycles**
1. Pre-incubation	95	5:00	4.8	1
2. Denaturation	95	0:05	4.8	45
3. Annealing	60	0:10	2.5	
4. Extension	72	0:01	4.8	
5. Fluorescence measurement	-	-		
6. Cooling	40	2:00	2.5	1

Table 2.15: qPCR reaction conditions for Agilent master-mix.

Step	**Temperature (°C)**	**Duration (min:s)**	**Ramp rate (°C/s)**	**Number of cycles**
1. Pre-incubation	95	3:00	4.4	1
2. Denaturation	95	0:05	4.4	45
3. Annealing	60	0:10	2.2	
5. Fluorescence measurement	-	-		
6. Cooling	40	0:30	2.2	1

For each gene tested, a 10:1 dilution series of a DNA plasmid or PCR amplicon was prepared containing the gene of interest. This was used in the LightCycler® 480 software (Roche) to determine primer efficiency for each primer pair used. For each experiment, one or two housekeeping genes (*TBP*, *SDHA* or *Ywhaz*) were assayed, and the levels of the housekeeping gene were used to normalise readings for other genes within each sample. For each gene tested, three technical replicates were set up on the qPCR plate to account for small-volume pipetting error.

qPCR data were analysed in Microsoft Excel. The mean concentration and standard deviation were calculated for each sample from three technical replicates, with any obvious outliers removed manually. Readings were then normalised to the geometric mean of the housekeeping gene concentrations. Where primer efficiency calculations could not be performed by LightCycler® 480 software, sample concentration was calculated from the crossing point (Cp) value using the formula:

$$Concentration = 2^{(-Cp)}$$

All qPCR data, unless otherwise stated, are presented either as raw relative expression values, or normalised to the mean expression of the first condition of the dataset, which is denoted as having an expression value of 1.

2.2.2 RNA methods

2.2.2.1 RNA isolation

RNA isolation was performed using an Absolutely RNA Miniprep Kit (Agilent) according to the manufacturer's instructions. Briefly, cells were plated at least one day before lysis for RNA isolation, cells were washed once with PBS (Sigma-Aldrich), and 350µL of RNA lysis buffer (containing 2.5µL β-Mercaptoethanol) was added per well – this amount was scaled up or down depending on plate confluence and culture volume. When performing the spin steps, lab bench surfaces, tube racks and gloves were wiped with RNAse-Zap (Ambion) to prevent RNAse contamination. RNA concentration was quantified using a NanoDrop™ Lite spectrophotometer (Thermo Fisher).

2.2.2.2 cDNA synthesis from RNA

cDNA was synthesised from RNA by using Moloney-Murine Leukaemia Virus Reverse Transcriptase (M-MLV RT, Invitrogen) according to manufacturer's instructions. Briefly, 300-500ng of RNA, 50ng of random primers (Invitrogen), and 1µL of 10mM dNTP mix (Invitrogen) were combined in a nuclease-free PCR tube (Sarstedt), and nuclease-free water (Fisher

Scientific) was supplemented to a total reaction volume of 12µL. In a thermocycler (Biometra), samples were heated to 65°C for 5mins, and then cooled at 4°C for 5min. Next, the following components were added: 4uL First-strand buffer (5x), 2µL DTT (0.1M) (both Invitrogen) and 1µL RNaseOUT™ recombinant ribonuclease inhibitor (40U/µL, Invitrogen). The reactions were incubated at 37°C for 2min. Next, 1µL (200U) of M-MLV RT was added, and the reaction was incubated at 25°C for 10min, then 37° for 50min for the reverse transcription, and finally at 70°C for 15min for heat inactivation of the enzymes. The reaction was then diluted in 180µL of nuclease-free water and stored at -20°C.

2.2.2.3 Nanostring analysis

Nanostring analysis was used to study the expression levels of genes involved in various signalling pathways. RNA samples were generated using the Absolutely RNA Miniprep Kit (Agilent), and 8µL of each sample was diluted to 20ng/µL in RNAse-free water. The samples were then shipped on dry ice to the Edinburgh Cancer Research Centre at the Institute of Genetics and Molecular Medicine at the University of Edinburgh, where Nanostring analysis was performed by Alison Munro.

Briefly, Nanostring is an RNA microarray platform that uses molecular barcoding to detect and count hundreds of unique transcripts in one RNA hybridisation reaction (Geiss et al., 2008). Each color-coded barcode is attached to a single target-specific probe corresponding to a gene of interest. The first step of the process is hybridisation, where two small probes per mRNA hybridise in solution: a reporter probe carrying a detectable signal, and a capture probe allowing the mRNA/probe complex to be immobilised for data collection. Following hybridisation, excess probes are removed and the probe/target complexes are aligned and immobilised in an nCounter cartridge. These cartridges are then read using an analyser, where the colour codes on the cartridge surface are quantified for each target molecule.

The system works by using pre-prepared panels containing a set of hundreds of genes of interest for a certain application. For this study, a mouse PanCancer Pathways Panel containing 770 genes from 13 cancer-associated pathways was used, due to the fact that it measures levels of genes involved in diverse cellular signalling pathways. Once the samples were analysed, the raw expression values were processed using Nanostring’s associated quantitiative analysis software, nSolver4.0. By using the software’s analysis wizard, the data were quality controlled and normalised to housekeeping genes before being exported as an MS Excel file for downstream data processing.

2.2.3 Protein methods

2.2.3.1 Immunocytochemistry

2.2.3.1.1 – Adherent cell culture on glass coverslips

For imaging applications requiring sample mounting onto glass slides, cells were grown on glass coverslips in 6- or 12-well plates (Corning). Prior to use, the coverslips (Marienfeld Superior) were stored in 100% ethanol (VWR). In a sterile biosafety cabinet (Esco), the relevant coating solution was added to the cell culture plate. Glass coverslips were then removed from ethanol using sterile forceps and the ethanol was rapidly evaporated by passing it through the flame of a lighter. The coverslip was aired for 2-3 seconds and immediately dropped into a cell culture well, ensuring that it was completely covered in the coating medium. The coverslip-containing wells were then coated for the correct amount of time for the coating medium used, and cells were seeded into the well following standard protocol.

2.2.3.1.2 – Fixation of adherent cells

When cultured cells were ready to be fixed for imaging, the supernatant was removed, the cells were washed once in PBS (Sigma), and overlaid with 4% Formaldehyde fixative solution for 10-15 minutes at room temperature. The fixative was then removed and cells were washed three times in PBS.

2.2.3.1.3 – Fixation of cells in suspension by Cytospin

For applications where cells were to be fixed and stained as single cells without adhesions to each other or an ECM, cells were prepared for fixation by using a Cytospin centrifugation protocol.

Adherent cells were washed once in PBS and detached by incubation in Accutase® (Sigma) for 2-3 minutes at 37°C. Cells were then quenched in ice-cold FACS buffer (FB), centrifuged to remove Accutase solution, resuspended in FB and counted. 5×10^4 cells were aliquoted into 1.5mL tubes and centrifuged. The cells were then resuspended in 200µL FB and stored on ice.

To assemble the Cytospin clamp units, Polysine® adhesion slides (VWR) were labelled and placed onto a metal Cytospin clamp. A white filter card (Thermo Fisher) was placed on top of the clamp, and a Shandon™ single cytofunnel™ (Thermo Fisher) was placed on top, making sure that the hole in the card was aligned with the end of the funnel. The whole assembled units were locked securely in place and loaded into a Shandon Cytospin III cytocentrifuge (Shandon). 200µL of cell suspension were added into each corresponding funnel. Programme 2 (7 mins at 1000rpm) was used.

Following centrifugation, the clamps were quickly disassembled, the spots corresponding to cells were circled with an ImmEdge Hydrophobic Barrier PAP pen (Vector Laboratories), the glass slides were moved to a humidified chamber in a fume hood, and a 50µL drop of formaldehyde fixative solution was placed on the cells. The cells were fixed at room temperature for 10-20 minutes, after which time the formaldehyde was removed and the cell spots were washed three times in PBS. The cells were immediately blocked for antibody staining.

2.2.3.1.4 – Antibody staining for immunocytochemistry

Prior to antibody staining, fixed cells were incubated in blocking solution for at least one hour at room temperature to block any non-specific sites that antibodies may bind to. Primary antibodies were diluted in blocking solution to a concentration recommended by the manufacturer, with up to four antibodies used simultaneously. Once the blocking step was complete, the blocking solution was removed and the cells were overlaid with diluted primary antibody solution for at least one hour at room temperature. The antibody solution was then removed and stored at 4°C to be re-used. Cells were washed three times in PBS and overlaid with diluted secondary antibody solution. Secondary antibodies were diluted 1:1000 in blocking solution unless otherwise stated. Where applicable, DAPI was added to the secondary antibody mixture at a concentration between 1:3000 – 1:10,000. Cells were stained with secondary antibody for 1 hour at room temperature and washed three times in PBS. Secondary antibodies were not routinely re-used. For cells stained in plastic culture plates, the cells were overlaid with PBS for imaging.

For cells cultured on glass coverslips, all staining steps were performed in a humidified chamber. Once staining was complete, the coverslips were mounted onto glass slides (VWR) with ProLong Gold Antifade Mountant (Thermo Fisher Scientific). When the mounting medium solidified, the coverslips were sealed using clear nail varnish.

2.2.3.1.5 – Sample imaging on bright-field and fluorescent microscopes

Mounted and stained samples were imaged using various fluorescent and bright-field systems (See "Microscopes" under instruments). The most appropriate visualisation parameters (including microscope type, magnification, exposure, gain, bit-depth, etc) were determined by the intended outcomes of each experiment. Where applicable, negative and positive fluorescence controls were used to set exposure and gain levels. Images were stored as .tiff files or as .lif databases and processed in ImageJ/Fiji image analysis software for optimal visualisation of pertinent features. For all experiments where fluorescence intensity was to be compared between samples, samples were stained simultaneously using the same antibody solution and then imaged in one session, using the same imaging and visualisation parameters across the whole dataset.

2.2.3.1.6 – Imaging of stained samples on the Operetta® high content imaging system

The Operetta® high content imaging system (referred to as "Operetta" from now on) from PerkinElmer® is an automated fluorescence microscopy system compatible with imaging samples both mounted on slides or those fixed in multi-well plates – these were overlaid with and imaged in PBS.

For 2D imaging, the height of acquisition and exposure time were individually optimised for each channel to achieve the best focal plane and highest quality fluorescent signal. For all analyses in this thesis, samples were imaged using the 20x wide-angle objective.

2.2.3.1.7 – Quantitative image analysis in Columbus®

Images acquired on the Operetta system were analysed using the Columbus® software supplied with the system by PerkinElmer®. Using the "Image Analysis" tool, individual image analysis pipelines were generated for each experiment. First, flat-field correction was set to "Basic" using the Input Image building block. Next, nuclear segmentation was performed on the DAPI channel using the Find Nuclei building block and selecting the most appropriate segmentation method for the sample. Quality control measures were applied to reject incorrectly segmented nuclei using the Select Population building block: these included filtering out incorrectly assigned nuclei by size and shape (using the Nucleus Area and Nucleus Roundness filters), and rejecting nuclei that were too bright (using the Instensity DAPI filter), as these usually represented areas where multiple nuclei were found on top of each other, resulting in unreliable segmentation and fluorescence intensity calculations.

Once nuclear segmentation was satisfactory, nuclear intensities in the “Nucleus” population were calculated using a Calculate Intensity Properties building block for each channel to be quantified. Where necessary, positive and negative populations for a given marker were selected using the Select Population building block by empirically studying the scatter plots generated to determine positive/negative thresholds.

After all desired populations were selected, the Define Results building block was used to select all the parameters to be reported for each population. The analysis pipeline was then saved and run on the appropriate image files, with results exported and analysed further in Microsoft Excel.

2.2.3.1.8 – Imaging of stained samples by confocal fluorescent microscopy for single-cell image analysis

For downstream image analysis of stained samples, mounted coverslips were imaged using a Leica SP8 confocal microscope, and all images were acquired as 12-bit files using a 40x oil immersion objective. A sample with the highest expected expression level of a stained protein of interest for a given dataset was used to determine optimal laser power, gain and exposure parameters: for each fluorophore, laser power was gradually increased until a few pixels in the image were saturated, resulting in the optimal dynamic range of pixel intensities for a given dataset. Once optimal image parameters were set for all channels, they were kept constant for the full dataset. Z-stacks were then set up independently for each sample using a 0.5µm step size.

2.2.3.1.9 – Quantitative single-cell image analysis in PickCells

PickCells is a bespoke quantitative image analysis software developed in our lab by postdoc Guillaume Blin, and it allows nuclear segmentation – using an inbuilt Nuclear Envelope Segmentation System (NESSys) – and subsequent deep analysis of cellular properties based on imaging data.

To analyse properties of cellular nuclei in PickCells, confocal 3D images were first segmented using the NESSys ridge-based segmentation system, which requires nuclei to be stained with either a nuclear envelope marker, such as Laminβ1, or with a nuclear content marker, such as DAPI. Optimal segmentation parameters were selected empirically for each experiment, and a linear classifier was trained to distinguish between correctly and incorrectly identified nuclei. Sample segmentation parameters are shown in the table below.

Table 2.16: Sample nuclear segmentation parameters in NESSys

Pipeline stage	Parameter	Value
Initial parameters	Segmentation method	Nuclear envelope
	Scale	2
	Maxima threshold	2.5
2D linear classifier	Search radius	4
	Delta	0.3
	Minimum radius	10
	Maximum radius	40
3D segmentation	Minimum volume	2000
	Maximum volume	20,000
	Search radius	60
	Minimum overlap	0.7
Advanced 3D segmentation settings	Allowed slice jumps	4
	Split tolerance	4

Following nuclear segmentation, PickCells was used to analyse nuclear properties in 3D images. These included nuclear fluorescence intensities in different channels and distance between nuclear edges to quantify changes in clustering or adhesion.

2.2.3.2 Flow cytometry

2.2.3.2.1 – Antibody staining for flow cytometry

In the days leading up to flow cytometry analysis or fluorescence-activated cell sorting (FACS), cells were cultured to reach 50-90% confluence in an appropriately sized culture vessel. FACS buffer (FB) was prepared by adding 2% FCS (Life technologies) to (Sigma) and was maintained at 4°C for all flow cytometry applications.

To prepare cells for flow cytometry, adherent cells were washed once with PBS (Sigma) and detached from the culture dish by incubation in Accutase® solution (Sigma) for 2-3 minutes at 37°C. The Accutase was then quenched in FB, and cells were pelleted by centrifugation at 300g (1300rpm) for 3 minutes. The pellet was resuspended in FB and cells were counted using a FastRead 102® hemocytometer (Kova International). The required number of cells was transferred to a Sterilin™ universal tube (Thermo Fisher scientific) and centrifuged. The supernatant was aspirated and the pellet was resuspended in 100µL flow-cytometry compatible antibody solution (made up in PBS) per 5 x 10^5 cells. The cells were incubated in antibody solution on ice in the dark for 15 minutes. After incubation, 10mL of FB was added to the universal tube to dilute the antibody, and the sample was centrifuged. The supernatant was aspirated and the cells were washed three times by resuspension and centrigugation in 5mL FB. Finally, the cells were resuspended in 0.5-1mL FB, and filtered into Falcon® 5mL round bottom polystyrene test tubes (Corning) through a filter cap. Samples were stored on ice until analysis or sorting.

2.2.3.2.2 – Flow cytometric analysis

Antibody-stained and/or fluorescent cells were analysed using a BD Accuri™ C6 flow cytometer (BD Biosciences) and accompanying acquisition software. 0.5-1 x 10^6 cells were prepared and stained per sample. Prior to analysis, 5µL of 7AAD cell viability solution (eBioscience) was added per 1 x 10^6 cells directly into the tube and incubated on ice for 5 minutes. Cells were sequentially gated using the following axes to yield reliable populations:

- FSC-A v SSC-A: gating for cells based on size and shape
- FSC-A v FSC-H: gating for single cells
- FSC-A v FL-3: gating for live cells. The live/dead marker 7AAD emits in the FL-3 laser channel, and 7AAd-negative cells were gated.

Following gating, 1-2 x 10^4 events in the final gate were recorded per sample.

2.2.3.2.3 – Single cell sorting

To generate clonal cell lines for karyotyping, cloning and other purposes, cultured cells were sorted as single cells into 96-well plates (Corning) using a BD FACS Aria™ II flow cytometer (BD Biosciences). 96-well plates were pre-coated with 50uL of 0.1% gelatin solution per well for 15 minutes. The gelatin was then removed and 180µL of Lif-serum medium supplemented 1:100 with penicillin-streptomycin solution (Invitrogen) was added per well.

Adherent cells were washed once in PBS (Sigma) and detached using 1:5 trypsin solution and incubated for 2-5 minutes at 37°C. The trypsin solution was then quenched using 2% FB. The cells were then centrifuged, resuspended in FB, counted, diluted to a concentration of 2 x 10^6 cells/mL and stored on ice until analysis. DAPI (Sigma) was added to a concentration of 1µL/mL to be used as a live-dead marker. The population was gated for live cells only and one cell was sorted into each well. The cells were returned to TC and allowed to proliferate. The cells were then serially expanded to generate a working stock of each clonal cell line and validated for further applications.

2.2.3.2.4 – Fluorescence-activated cell sorting for gene expression analysis

Antibody-stained and/or fluorescent cells were sorted using a BD FACS Aria^{TM} II flow cytometer (BD Biosciences). In the days leading up to sorting, cells were cultured to 50-90% confluence in 75cm^2 flasks (Corning). Cells were washed in PBS (Sigma) and dissociated by culturing in Accutase solution (Sigma) for 2-3 minutes at 37°C and quenched in 2% FB. Cells were centrifuged and counted, and 5 x 10^5 cells were resuspended for all control populations (including unstained and DAPI-only controls), with the remaining millions of cells left for sorting. Where applicable, cells were then stained with FACS-compatible antibodies.

Immediately prior to sorting, the control populations were used to compensate the cytometer for all fluorescent channels used. Cells were then sequentially gated to yield a population of live single cells for sorting, and additional gates were made that were relevant to the fractions to be sorted. Desired cells were then sorted into 15mL polypropylene centrifuge tubes (Corning) containing 3mL of FACS collection buffer (50% FCS in Lif-serum medium). Upon completion of sorting, the cells were centrifuged and the pellet was lysed in RNA lysis buffer (from Absolutely RNA Miniprep Kit, Agilent) for RNA extraction.

2.2.3.3 Reverse-phase protein array (RPPA)

Reverse-phase protein array (RPPA) was used to quantify protein expression and phosphorylation levels, and was performed in collaboration with the RPPA facility at the Institute of Genetics and Molecular Medicine at the University of Edinburgh, managed by Kenneth MacLeod. The facility provided the reagents and performed most of the analysis once samples were cultured, lysed and delivered to the facility.

2.2.3.3.1 – RPPA sample collection

Cells were cultured in 100mm TC-Treated culture dishes (Corning) under experimental conditions. Before lysis, media were removed from the culture plates and the cells were washed twice in PBS (Sigma). Next, 400µL of RPPA lysis buffer was added and the plates were incubated at 4°C for 20 minutes with shaking every five minutes to evenly distribute the lysis buffer.

Table 2.17: RPPA lysis buffer composition. *The 2x buffer and remaining components (excluding glycerol and sterile water) were pre-supplied by the RPPA facility.*

Component	**Volume**	**Final concentration**	**Supplier**
2x Buffer	5mL	1x Buffer: • Triton X-100, 1% • HEPES, 50mM, pH 7.4 • NaCl, 150mM • $MgCl_2$, 1.5 mM • EGTA, 1mM	RPPA facility
Glycerol	1mL	10%	CalBiochem
NaF	1mL	100mM	RPPA facility
Tetrasodium pyrophosphate (TSPP)	1mL	10mM	RPPA facility
Na_3VO_4	0.1mL	1mM	RPPA facility
H_2O, molecular biology-grade	1.9mL	-	Fisher Scientific
PhosSTOP™ tablet	-	-	Roche
cOmplete™ tablet	-	-	Roche

Following incubation, cells were scraped off the plates using a cell scraper (Corning) and pipettor into 1.5mL centrifuge tubes. The lysates were centrifuged at 14,000 rpm for 10min at 4°C. The supernatant was collected and stored on ice. The protein level in the supernatant was then quantified using a Bradford assay (see below). The protein concentration was then adjusted to 1mg/ml with remaining lysis buffer. The samples were stored at -80°C and shipped on dry ice to the RPPA facility where all the remaining analysis was performed.

2.2.3.3.2 – Quantification of protein concentration by Bradford assay

A Bradford assay was used to measure protein concentrations in RPPA lysate supernatants. Briefly, a set of dilutions was generated containing between 0-0.6 mg/mL Quick Start™ BSA standard (BioRad) diluted in PBS (Sigma) with 5% RPPA lysis buffer. The protein supernatant samples were then diluted 1:20 in PBS.

Next, 10µL of the diluted standards and diluted samples were loaded into duplicate plates on a 96-well plate (Corning). Protein assay dye reagent concentrate was diluted 1:4 in water and 240µL of this diluted dye reagent was added to each well. The plate was incubated in the dark at room temperature for 10min. The absorbance at 600nm was then determined using a GloMax®-Multi Microplate reader (Promega).

The resulting data were imported into Microsoft Excel, and a standard curve of concentration against Abs_{600} was plotted. The "linear regression" function was used to generate a standard linear equation in the form:

$$Abs_{600} = (m \times Concentration) + b$$

where *m* represents the slope of the line and *b* represents the x-intercept of the function. To determine protein concentration (in mg/mL) in the protein samples, the above equation was transformed to:

$$Concentration = \left(\frac{Abs_{600} - b}{m}\right) \times 20$$

The above equation was used to determine the concentration of all unknown samples, which were then diluted to 1mg/mL in leftover RPPA lysis buffer.

2.2.3.3.3 – RPPA microarray layout

The remaining RPPA analysis steps were performed by Kenneth MacLeod at the Proteomics and Metabolomics unit of the MRC Institute of Genetics and Molecular Medicine at the University of Edinburgh. The following protocols were provided by this facility.

Samples were denatured by the addition of 4X sample buffer (40% Glycerol, 8% SDS, 0.25M Tris-HCl, pH6.8; 2-mercaptoethanol was added to the buffer at 1/10 of the volume before use) and heated to 95°C for five minutes prior to processing.

Following denaturation, a dilution series was prepared for each sample in PBS with 10% glycerol. The samples were printed as a dilution series of 1.5, 0.75, 0.375 and 0.1875 mg/mL. Samples were printed as arrays consisting of 36 x 12 spots at a 500µm spot-to-spot distance. Array spotting was carried out with an Aushon 1740 Arrayer Patform using 8 x 185µM pins. Two deposition rounds were performed per feature.

Sample dilution series were spotted in triplicate on each array, with eight arrays per slide, on single pad Avid Nitrocellulose slides (Grace Biolabs). Three side-by-side technical replicates were also set up.

2.2.3.3.4 – RPPA assay procedure

RPPA slides were washed in deionised water and incubated for 15mins in 1x Antigen Retrieval Reagent. This was followed by two 5min submerged washes in deionised water. The slides were then places in a ProPlate chamber and the wells were filled with deionised water. The wells were then washed twice with 1x TBST and incubated for 10mins in Superblock T20 blocking buffer (Pierce/Thermo Scientific, cat. no. 37536). The slides were again washed twice in TBST before a 1h incubation in primary antibody at 1:250 dilution in blocking buffer. After incubation, slides were washed twice in PBS and blocked for 10mins in blocking buffer as before. Following two more washes, the slides were incubated for 30mins in secondary antibody solutions: Dylight-800-labelled anti-species antibodies diluted 1:2500 in blocking buffer. This was followed by two more washes in TBST and rinsed with fresh deionised water. The slides were allowed to dry at room temperature for 10mins prior to data acquisition; they were then imaged using an Innopsys 710 slide scanner.

Non-specific signals were determined for each slide by omitting the first incubation step with primary antibody on one array per secondary antibody type. Sample loading on arrays (for normalisation purposes) was determined by staining with fast-green dye and scanning at 800nm.

2.2.3.3.5 – RPPA data analysis

Microarray images were analysed using Mapix software (Innopsys). The spot diameter of the grid was set to 270 µm. Background signal intensity was determined for each spot individually and subtracted from the sample spot signal leading to a net signal for each spot.

Data analysis was performed in a standard way: fluorescence intensity for each feature (spot) on the array was measured. A test was performed for linear fit through the four-point dilution series for all samples on all arrays using a flag system where $R^2 > 0.9$ was deemed good, >0.8 was deemed acceptable and <0.8 was poor (and may be excluded from data analysis). Median values from the four-point dilution series were calculated and used as a measure of fluorescence intensity. Raw relative fluorescence intensity (RFI) values relating to the abundance of total phosphorylated proteins across the sample set were calculated, and the expression data was normalised to total protein (as determined by a fast-green stained slide). These data were then provided to the end user as MS Excel spreadsheets.

2.2.4 Cell culture methods

2.2.4.1 Cell lines

2.2.4.1.1 – Wild-type cell lines

Two wild-type (WT) mouse embryonic stem cell lines were used in this study. The first, E14TG2a, is a male clonal stem cell line derived from ES cells generated from 129/Ola mouse blastocysts. They are deficient for hypoxanthine guanine phosphoribosyl transferase (HPRT) (Hooper et al., 1987). The second cell line, E14Ju09, is a clonal stem cell line derived by the transgenics service at our institute from ES cells generated from chimaeric embryos derived from E14TG2a ES cells. They have the same genetic background as E14TG2a cells and have a high propensity for germline colonisation, an observation made by the staff at the transgenics unit (Malaguti, 2014).

2.2.4.1.2 – Sox1-GFP (46C) cells

Sox1 is a marker gene of the early neural lineage. The Sox1-GFP ($Sox1^{+/eGFP}$) cell line has a heterozygous knock-in of *eGFP* into the *Sox1* locus on an E14TG2a background. These cells are also referred to as 46C, corresponding to the clone number that was injected into blastocysts and passaged through the germline to generate a Sox1-GFP mouse line (Aubert et al., 2003).

2.2.4.1.3 – E-cadherin knockout (EcKO) cells

E-cadherin knockout ($Cdh1^{-/-}$) cells are negative for E-cadherin protein expression. They are derived from blastocysts of an E-cadherin-floxed ($Cdh1^{fl/fl}$) mouse line in which exons 4 to 15 of the *Cdh1* gene were floxed (Derksen et al., 2006). The floxed alleles were then Cre-excised *in vitro* (Pieters et al., 2016). These cells are referred to as “EcKO” throughout the thesis.

2.2.4.1.4 – N-cadherin knock-in (NcKI) cells

N-cadherin knock-in ($Cdh1^{Cdh2/Cdh2}$) cells contain a *Cdh2* gene knocked in to the *Cdh1* locus; the cells are negative for E-cadherin protein expression and express N-cadherin under the control of the E-cadherin promoter (Kan et al., 2007). These cells are referred to as “NcKI” throughout the thesis. The *Cdh1* gene sequence is not translated but is still present in these cells on the *Cdh2*-containing allele, leading to Ecad occasionally being detected on the mRNA level in the cell line by qPCR.

2.2.4.1.5 – A2Lox.Cre cells

A2Lox.Cre cells are the parental cell line of the Inducible Cassette Exchange (ICE) system for generating inducible murine ES cell lines (Iacovino et al., 2011). They contain an ICE locus targeted into the HPRT gene on the X chromosome of A17 mouse ES cells, which are a derivative of the E14TG2a cell line and where the reverse tetracycline-controlled transactivator (rtTA) has been inserted into the constitutively active Rosa26 locus. The ICE locus contains a Cre-recombinase site flanked by two LoxP (Locus of crossing over, P1) sites (a "floxed *Cre"*), and downstream of this is a G418 resistance gene lacking a start codon and promoter, which is referred to as *Δneo*. At this site, recombination is very high because it is embedded in constitutively active chromatin. Recombinant clones can be selected in G418, because upon recombination the *Δneo* gene is repaired (Iacovino et al., 2014).

2.2.4.1.6 – Generation of the pCR Blunt II Topo-Ncad-HA plasmid

To test the effect of N-cadherin overexpression in various cellular contexts, Doxycycline (Dox)-inducible mouse ES cell lines were generated using an inducible cassette exchange protocol developed by the Michael Kyba lab (Iacovino et al., 2009; Iacovino et al., 2011; Iacovino et al., 2014). Primers KP03 and KP04 were designed to allow for the PCR-amplification of a DNA fragment containing the N-cadherin gene C-terminally tagged with an influenza virus hemagglutinin (HA) tag, with the whole construct being flanked by XhoI and NotI restriction sites. This DNA fragment was generated by Q5® HotStart PCR (NEB) from template cDNA (reverse-transcribed from mRNA) originating from E14-JUO9 cells cultured in neural differentiation conditions for five days.

The PCR product was electrophoresed in a 1% agarose gel and the band of the correct size (2721bp) was excised from the gel and purified using a QIAQuick Gel Extraction kit (Qiagen). The purified DNA was ligated into a pCR Blunt II Topo Vector (Thermo Fisher Scientific) using the kit provided, and the construct was then transformed into competent DH5α *Escherichia coli* cells. The transformed cells were plated onto kanamycin (Calbiochem) selection plates, with 0.5mg of X-gal (Promega) added per plate for blue/white screening. Following overnight incubation, white colonies were picked into kanamycin selection media and the cultures were expanded overnight. DNA was purified from the resulting cultures using a QIAprep Spin Miniprep Kit (Qiagen) and test-digested using EcoRI-HF restriction enzyme (NEB). Once the expected band size (2.8kbp) was confirmed by electrophoresis, the DNA sequenced using sequencing primers M13F, M13R, SL773F, SL774R, SL233F and SL234R.

2.2.4.1.7 – Generation of the p2Lox-Ncad-HA plasmid

After the construct was confirmed correct by sequencing, this newly generated pCR-BluntII-Topo-Ncad-HA plasmid and a p2Lox-eGFP plasmid (Iacovino et al., 2009) were digested using XhoI and NotI-HF restriction endonucleases (NEB) to generate DNA fragments with sticky ends. The reactions were electrophoresed, and the bands for the p2Lox backbone (3547bp) and Ncad-HA insert (2773bp) were excised and gel purified. The Ncad-HA insert was then ligated into the p2Lox backbone using T4 Ligase (NEB), treated with rAPid Alkaline Phosphatase (Roche) to prevent re-ligation of the backbone, and transformed into competent DH5α *E. coli* cells. The cells were plated onto ampicillin selection plates and cultured overnight, after which colonies were picked and expanded, and DNA was extracted as before. The resulting DNA was test-digested using XhoI and NotI-HF restriction endonucleases to confirm presence of two bands: one for the Ncad-HA insert (2772bp) and one for the p2Lox backbone (3548bp). Once a correct clone was identified, the DNA was confirmed correct by sequencing using sequencing primers SL773F, SL774R, SL233F, SL234R, KP05, p2LoxF and p2LoxR.

2.2.4.1.8 – Generation of A2Lox-Ncad-HA inducible ES cell lines

Nucleofection was performed using the P3 Primary Cell 4D-Nucleofector™ Kit (Lonza) as described in "ES cell transgenesis", with 1.7µg (10µL) of p2lox-Ncad-HA plasmid nucleofected into $5x10^5$ A2LoxCre cells. After 10 days of selection in G418, the surviving clonal colonies were picked into 96-well plates (Costar) and gradually expanded in G418 (PAA)-supplemented medium until frozen stocks of each clone were prepared. Surviving clones were screened for Ncad-HA expression by ICC. Cells were fixed 24 or 48 hours after addition of 1µg/mL Dox and stained for N-cadherin and HA. Clones #4, #5, and #7 were selected for further tests.

2.2.4.2 Cell culture conditions

Mammalian cell lines were maintained and passaged according to the standard conditions described below. All work with live cells was performed in a biological safety cabinet (Esco) observing sterile practice methods and using tissue culture compatible sterile plastic ware (Corning). Cells were incubated in a humidified incubator (Sanyo/Panasonic) at 37°C in 5% CO_2. All centrifugation steps were performed for 2.5-3 minutes at 300g (1,300rpm) in a table-top centrifuge (Eppendorf) unless otherwise stated. Where required, reagents and media were pre-warmed to 37°C in a 26L unstirred water bath (Grant).

2.2.4.2.1 – Standard (mixed) pluripotent stem cell culture (Lif-serum)

Mouse ES cells were cultured in Lif-serum media as standard, unless otherwise stated. The medium composition is based on that published by Smith *et al*. (1988), below.

Table 2.18: Lif-serum medium composition.

Component	Volume	Final Concentration
Glasgow minimum essential medium (Sigma)	500 mL	-
Foetal calf serum (Life technologies)	51 mL	10%
L-glutamine/sodium pyruvate solution	11 mL	2mM L-glutamine 1mM sodium pyruvate
MEM non-essential amino acids, 100x (Invitrogen)	5.5 mL	1x
2-mercaptoethanol, 50mM (Life technologies)	1140 µL	100nM
Human leukaemia inhibitory factor (LIF)	550 µL	100 U/mL

To passage ES cells cultured in Lif-serum, sterile cell culture dishes were coated with 0.1% gelatin solution for at least 10 minutes before passage. Media were aspirated from cells, the cells were washed once in PBS (Sigma) before the addition of 1:5 trypsin solution. The cells were incubated at 37°C until they detached from each other and the plate (usually around 2-5 minutes). Next, 5-10 volumes of Lif-FCS medium were added to quench the trypsin. The cells were transferred to a 20mL universal tube (Sterilin) and centrifuged at 300g for three minutes. The supernatant was then aspirated, and the cells were resuspended in fresh Lif-serum medium until they formed a single-cell suspension. The cells were then overlaid at desired density into dishes pre-coated with gelatin solution.

2.2.4.2.2 – Serum-free stem cell culture (N2B27)

N2B27, named after the two growth factors added to this medium, was used for serum-free cell culture and differentiation assays as previously described (Pollard et al., 2006; Ying et al., 2003b).

Table 2.19: N2B27 medium composition.

Component	**Volume**	**Final concentration**
DMEM/F12 (Gibco)	25 mL	50%
Neurobasal (Gibco)	25 mL	50%
L-Glutamine, 200mM (Invitrogen)	500 µL	2mM
2-Mercaptoethanol, 50mM (Life Technologies)	100 µL	100nM
N2 (Gibco)	250 µL	0.5x
B27 (Gibco)	500 µL	0.5x

2.2.4.2.3 – Naïve stem cell culture (2i-Lif)

"2i" is an N2B27-based medium used to culture ES cells in a naïve pluripotent state (Ying et al., 2008), where 2i refers to the addition of small molecules to achieve double inhibition of the MEK/ERK1/2 and GSK3 pathways. The addition of Lif activates the STAT pathway, and this combination of pathway activation and inhibition gives rise to a stable naïve ES cell state that can be maintained indefinitely *in vitro* and that broadly corresponds to the E3.5 naïve epiblast (Kalkan and Smith, 2014; Ying et al., 2008).

The composition of the medium is the same as N2B27, with three additional factors: 1µM PD0325901 (Axon), 3µM Chiron 99021 (Axon) and 100 U/mL of human Lif (prepared in-house). Before cell passage, dishes were treated for two hours with 0.01% poly-L-ornithine solution (Sigma) at room temperature, which was then replaced for two hours with 5µg/mL laminin coating solution at room temperature. To passage cells cultured in 2i-Lif conditions, the medium was removed, the cells were washed once in PBS, and then overlaid with Accutase solution (Sigma) and incubated at 37°C until the cells dissociated from the plate (about 3-5 minutes). The Accutase was then quenched in fresh medium, the cells moved to a universal tube (Sterilin) and centrifuged. Cells were then re-plated at a concentration between 1.5 – 2.0 x 10^4/cm^2.

To convert cells cultured in Lif-serum conditions to a more uniform and naïve-like state, the cells were plated as described above into 2i-Lif conditions and maintained in these conditions for at least three passages before further use in experimental assays.

2.2.4.2.4 – Epiblast stem cell culture

Epiblast stem cells (EpiSCs) were cultured in an N2B27-based medium as previously described (Brons et al., 2007; Tesar et al., 2007). Minor modifications were applied in-house following optimisation for improved viability and proliferation; the final conditions are summarised below.

Table 2.20: Epiblast stem cell culture medium composition.

Component	**Volume**	**Final concentration**
DMEM/F12 (Gibco)	25 mL	50%
Neurobasal (Gibco)	25 mL	50%
L-Glutamine, 200mM (Invitrogen)	500 µL	2mM
2-Mercaptoethanol, 50mM (Life Technologies)	100 µL	100nM
MEM non-essential amino acids, 100x (Invitrogen)	500 µL	1x
N2 (Gibco)	250 µL	0.5x
B27 (Gibco)	500 µL	0.5x
Activin A solution, 20µg/mL	50 µL	20ng/mL
FGF2 solution, 10µg/mL	50 µL	10ng/mL

The medium was prepared without the addition of Activin A and FGF2; these components were added to the media immediately prior to use.

Before passage, plates were coated with 7.5µg/mL fibronectin (Sigma) in PBS for at least 15 minutes. Adherent EpiSCs were washed once in PBS, detached using accutase solution, quenched in N2B27, centrifuged, and gently resuspended in EpiSC medium to create a suspension of cell clumps. The fibronectin coating was removed from dishes, and EpiSCs were seeded at a 1:8 dilution.

EpiSCs were derived from ES cells cultured in Lif-serum as previously described (Guo et al., 2009). ES cells were seeded at a density of 3×10^4 onto fibronectin-coated plates in Lif-serum medium. After 24h, the medium was changed to EpiSC medium. The cells were cultured until they reached high density, when they were passaged at high density in 1:2-1:4 dilutions. Following three passages, the cells were gradually passaged at lower-density (1:6-1:8) dilutions.

2.2.4.2.5 – Neural differentiation culture (NDiff)

For neural differentiation experiments, neural differentiation medium (NDiff) was used (Ying et al., 2003a). NDiff has the same composition as N2B27, but the N2 (Gibco) is substituted for an equal volume of home-made N2, which contains additional insulin to enhance the efficiency of neural differentiation.

Figure 2.21: Home-made N2 composition. *40mL total volume. All component solutions sterile filtered (40nm).*

Component	**Volume**	**Concentration**
Insulin (Sigma)	4 mL	25 mg/mL in HCl
Apo-transferrin (Sigma)	4 mL	100 mg/mL in water
BSA (Gibco)	4 mL	75 mg/mL
Progesterone (Sigma)	132 µL	600 µg/mL in ethanol
Putrescine (Sigma)	400 µL	60 mg/mL
Sodium selenite (Sigma)	40 µL	3mM
DMEM:F12 (Gibco)	27.5 mL	-

2.2.4.2.6 – NMP maturation and differentiation culture

A protocol for the generation of putative NMPs from a 2i-Lif starting population using an Epiblast-like cell (EpiLC) intermediate was recently developed in our lab (Watson, 2018). This five-day protocol was used in this thesis to study effects of cadherin switching on the maturation of NMPs.

On day zero of the protocol, cells cultured in 2i-Lif were seeded in a single-cell suspension at a density of 4750 cells per well into plastic 12-well tissue culture plates (Corning) coated with fibronectin solution into EpiLC medium. This medium is identical to EpiSC culture medium, with the addition of 10µL/mL of KOSR (Thermo Scientific). On day two of the protocol (48h after seeding), the medium was changed to NMP medium. This medium is identical to N2B27 medium, with the addition of 0.3µl/mL Chiron (Axon, final concentration 3µM) and 2µL/mL FGF2 (R&D, final concentration 20ng/mL) – this is double the FGF2 concentration used for EpiSC and EpiLC culture. After 48h in this culture, the cells have been shown to represent putative immature NMPs, while after 72h in this culture, the cells are comparable to mature NMPs (Watson, 2018). On day five of the protocol (72h after the media change to NMP conditions), the cells are fixed for ICC.

2.2.4.3 ES cell transgenesis

2.2.4.3.1 – Nucleofection

Nucleofection was performed using the P3 Primary Cell 4D-Nucleofector™ Kit (Lonza). The day before nucleofection, mouse A2LoxCre targeting ES cells were induced to express *Cre* by adding 0.5µg/mL Doxycycline Hyclate (Sigma), rendering them competent for recombination (Iacovino et al., 2011; Iacovino et al., 2014). 24h after addition of Dox, the cells were treated according to kit instructions: $5x10^5$ A2LoxCre cells were resuspended in 82µL P3 Nucleofector Solution, and 18µL of Nucleofector supplement was added. Finally, 4µg (to a maximum volume of 10µL) of circular plasmid was mixed into the solution. The cell solution was transferred to a 100µL nucleofection cuvette (Lonza) and nucleofected in a 4D-Nucleofector (Lonza) using the CG-104 programme. Following nucleofection, the cells were transferred to pre-warmed Lif-serum media in 9cm dishes pre-coated with gelatin. $5x10^5$ non-nucleofected cells were plated in parallel as a negative control for antibiotic selection.

24h after nucleofection, the medium in the dishes was replaced with fresh Lif-serum supplemented with 400µg/mL G418 (PAA). Selection was allowed to progress for 10 days, with media changed every two days. After 10 days, the surviving clonal colonies were picked into 96-well plates (Costar) and gradually expanded in G418-supplemented medium until frozen stocks of each clone could be prepared.

2.2.4.4 Cell cryopreservation

2.2.4.4.1 – Cell freezing

For long-term storage of cell lines, cultured cells were dissociated from their culture dish with trypsin or Accutase treatment and centrifuged following routine passage protocol. The pellet was then resuspended in 0.5-1mL of appropriate culture medium, shown below, supplemented with 10% dimethyl sulphoxide (DMSO, VWR):

- Lif-serum cultures: Lif-serum medium or FCS
- Serum-free cultures: corresponding culture medium or KnockOut™ Serum Replacement (KOSR)(Thermo Scientific).

The cell suspension was transferred to a 1.0mL CryoTube™ vial (Thermo Scientific) and immediately moved to dry ice. Frozen cells were stored short-term (up to 3 months) at -80°C and long-term in liquid nitrogen at 180°C.

2.2.4.4.2 – Cell thawing

Before defrosting, cells were removed from the storage freezer and transferred to the tissue culture facility on dry ice. The cryovials were thawed at room temperature and immediately transferred to 2-5mL of appropriate medium, pre-warmed to 37°C. The cells were centrifuged, supernatant removed and the pellet resuspended in relevant medium and plated into pre-coated culture vessels.

2.2.4.5 Cell line karyotyping

The day before karyotyping, cells were passaged at high density into a T25 flask in standard Lif-serum conditions. The hypotonic 0.075M KCl solution and Carnoys fixative (3:1 methanol:glacial acetic acid) were prepared fresh on the day of karyotyping. To arrest cells in metaphase, 100µL of KaryoMAX™ Colcemid™ Solution (Gibco) was added per 10mL of culture medium (final concentration 100ng/mL) 18 hours after cell splitting and the cells were cultured for a further 2-2.5 hours.

The remainder of the protocol was carried out outside the tissue culture hood. Culture medium was decanted into a 15mL centrifuge tube (Corning), the cells were washed in PBS, 500uL trypsin solution was added and the flask was incubated at 37°C for five minutes or until the cells lifted off. The trypsin solution was then quenched using the leftover culture medium and the resulting single-cell suspension was centrifuged – all the remaining centrifugation steps were performed at 60rcf for eight minutes at room temperature. Supernatant was decanted and the pellet was resuspended in the residual medium by gently tapping the tube.

To gently promote cell swelling, 9mL of hypotonic 0.075M KCl solution was added while slowly mixing on a vortex mixer. The hypotonic cell suspension was incubated at 37°C for 20-25 minutes. After this time, three drops of Carnoys fixative were added using a 3.5mL transfer pipette (Sarstedt) while slowly mixing on a vortex mixer to gently introduce the cells to fixative. The cells were centrifuged, the supernatant was decanted and the pellet was gently resuspended in the residual medium. To fix the cells, 9mL of Carnoys fixative was slowly added drop-by-drop down the side of the tube while gently mixing on a vortex mixer. The cells were then centrifuged. The fixation step was repeated two more times with 6mL and 3mL of fixative. After the final centrifugation step, the cell pellet was resuspended in a few drops of fresh fixative.

A clean microscope glass slide (VWR) was polished with 100% ethanol (VWR Chemicals). The slide was moistened by breathing on it, and several drops (around 50µL) of cell suspension were dropped from a height directly onto the slide to break the cell membranes. After the slides had air-dried, the slides were placed in a slide chamber filled with Giemsa (VWR) solution diluted following manufacturer's recommendations for 8-10 minutes. The slides were then rinsed under running tap water and gently blotted dry with tissue paper. Following drying, a cover-glass (Marienfeld Superior) was mounted onto the slides using Pertex® mountant (HistoLab).

The chromosome spreads were visualised under an Olympus BX61 widefield microscope. The number of individual chromosomes was counted at 40x magnification. A mouse cell line was considered to be karyotypically normal when at least 60% of 20 chromosome spreads counted were found to contain exactly 40 chromosomes.

2.2.5 Embryology

2.2.5.1 Maintenance of mice

WT mice were housed and bred in the Animal Unit of the MRC Centre for Regenerative Medicine, in accordance to the provisions of the Animals (Scientific Procedures) Act 1986. All work with live mice was performed by the Animal Unit staff.

2.2.5.2 Embryo dissections

Pregnant female mice were culled by cervical dislocation by Animal Unit staff. All subsequent embryo work was performed by Rosa Portero Migueles.

The uterus was dissected out of the abdominal cavity, and the deciduae were placed in M2 Medium (Sigma) at room temperature. Embryos were then isolated from the deciduae and the Reichert's membrane was removed. Embryos were fixed for 30mins at room temperature in 4% PFA/PBST, and then incubated in 100mM glycine solution in PBS for 5mins at room temperature. Embryos were incubated overnight at 4°C in blocking solution (PBST with 5% donkey serum).

2.2.5.3 Immunostaining and imaging of embryos

For embryo immunostaining, the embryos were incubated overnight at room temperature in primary antibody diluted in blocking solution. The following day, embryos were washed three times for 5mins at room temperature in PBST, followed by overnight incubation in secondary antibody diluted in blocking solution. The following day, embryos were again washed three times for 5mins in PBST at room temperature.

After staining, the embryos were dehydrated in methanol series in PBST, as described previously (Becker et al., 2013). Embryos were clarified in 50/50 methanol/BABB and transferred into 100% BABB, and stored in borosilicate thin wall capillaries, 1.0mm x 0.78mm (Harvard Apparatus) for imaging. Embryos were imaged using 40x magnification on a Leica SP8 confocal microscope.

2.2.6 Statistical analysis

Data processing and statistical analysis was performed in Microsoft Excel, R, and GraphPad. A student's T-test was used to compare levels of significance between experimental groups, with an unpaired or paired test used depending on the experimental set-up. A significance threshold of $p \leq 0.05$ was used for all studies, with a result of $p \leq 0.01$ considered highly significant. In figures, these two results are denoted with a single or double asterisk (* and **), respectively.

Chapter III – The dynamics of cadherin switching in early development and in pluripotent stem cells

3.1 Introduction & aims

Expression patterns of individual cadherin species during early development are well characterised. E-cadherin is present in the unfertilised egg (Kemler et al., 1977; Ohsugi et al., 1997), and continues to be expressed from the 2-cell stage through to gastrulation. E-cadherin is essential for cell adhesion in the morula and for the formation of trophectoderm (Kan et al., 2007; Larue et al., 1994). At gastrulation, cells of the developing mesoderm are the first to lose E-cadherin expression at around the same time that they upregulate mesodermal markers (Larue et al., 1996). During neurulation, E-cadherin expression is switched off in the ectoderm, though it remains upregulated at the ectoderm-neurectoderm border, where studies in Xenopus have shown it to contribute to the closure of the neural tube (Fujimori et al., 1990).

N-cadherin is first detected in the posterior gastrula on the mRNA level (Peng et al., 2016), and is subsequently expressed in mesodermal and neural tissues at around E7.5 (Kimura et al., 1995; Luo et al., 2001; Radice et al., 1997). In neurulation, during the transition from the neural plate stage to the neural tube, neuroepithelial cells downregulate E-cadherin, which is then replaced by N-cadherin (Aaku-saraste et al., 1996). By E9.5, N-cadherin is expressed in the notochord, optic vesicles and heart tubes (Radice et al., 1997).

The co-expression of E-cadherin and N-cadherin has been less extensively studied. In particular, the dynamics of the cadherin switch in relation to pluripotency and lineage markers are not well characterised. The timing of cadherin switching with respect to commitment and differentiation effects is not well understood, leaving it unclear whether the switch is initiated prior to, during, or after lineage commitment. This leads to the question of whether cadherin switching is a passive read-out of differentiation, or whether it happens early enough to play an active role in directing pluripotent cells towards certain fates. In addition, it is unclear to what extent current *in vitro* systems recapitulate the order of events of cadherin switching as they occur during development *in vivo*.

The address these questions, the aims of this chapter are to:

a) Characterise the co-expression patterns of E-cadherin, N-cadherin and neural lineage markers at various early developmental time-points *in vivo.*
b) Compare expression patterns and timings of these proteins between *in vivo* embryogenesis and *in vitro* culture systems.
c) Assess whether cadherin switching occurs before, during, or after loss of pluripotency and lineage commitment.

3.2 Cadherin expression patterns during early embryonic development in the mouse

3.2.1 Cadherin switching is initiated at E7.0-7.5 in the mouse embryo

To assess when and in which tissues cadherin switching is occurring, mouse embryos of various stages of development were co-stained for E- and N-cadherin (Fig. 3.1). Staging of the embryos was determined according to Lawson & Wilson 2016.

At the pre-streak stage (E6.5), E-cadherin is highly expressed in the epiblast, and is most strongly expressed apically around the proamniotic cavity. No specific membrane staining was detected with the N-cadherin antibody (Fig. 3.1 A); some nuclear staining was observed at this stage, but this is likely due to background signal from the antibody, as observed in cultured cells where *Cdh2* expression was not detected by qPCR (Appendix 1A,B). At the late streak stage (E7.0), E-cadherin continues to be strongly expressed in all parts of the embryo. For the first time, membrane-localised N-cadherin signal can be observed, which is the strongest at the posterior of the embryo, at the site of formation of the PS. The epiblast and the anterior embryo do not appear to be positive for N-cadherin at this stage (Fig. 3.1 B).

The pre-headfold stage (E7.5) was the first stage studied where E- to N-cadherin switching could be clearly observed (Fig. 3.1 C). Here, the anterior pre-cardiac mesoderm was clearly negative for E-cadherin, and expressing high levels of N-cadherin. At the same stage, mesodermal tissues also express N-cadherin, while the anterior epiblast remains uniformly positive for E-cadherin expression. By E8.5, the neural groove is formed and clearly visible (Fig. 3.1 D). In a transverse section through this structure, E-cadherin and N-cadherin are both present at the apical edge of the neural groove, though N-cadherin appears to be the more dominant of the two. Cadherin switching is also noticeable in the paraxial mesoderm surrounding the neural groove.

These results confirm that cadherin switching occurs at protein level in the embryo at around the pre-headfold stage (E7.5), and that it first takes place in mesoderm tissues, followed by ectoderm tissues. Co-expression of E- and N-cadherin was detected in the neural groove by E8.5.

3.2.2 Sox1 is highly expressed in the anterior neural ectoderm at E7.5.

Next, E7.5 embryos were co-stained for E-cadherin, N-cadherin, and the early neural marker Sox1 (Fig3.2A). This time-point was chosen because it represents the first stage where an E- to N-cadherin switch was clearly observed in the early embryo. The anterior neural ectoderm was found to co-express high levels of Sox1 and E-cadherin; Sox1 was also detected in the extra-embryonic ectoderm. Some N-cadherin staining was visible in this $Ecad^+/Sox1^+$ tissue, though it appears more nuclear than membrane-bound and may therefore represent background signal.

To quantify the amount of signal in each tissue, and to determine whether the $Sox1^+$ tissue also co-expressed N-cadherin, four images of E7.5 embryos were quantified using the image analysis software Fiji (Schindelin et al., 2012). An area of equal size was drawn in three embryonic tissues: the epiblast, the precardiac mesoderm and the neurectoderm, and the brightness of each channel was quantified in this area using the “Measure” function in the software. The process was repeated in four Z-planes for four E7.5 embryos in which clear Sox1 staining was observed in the neurectoderm. The intensity of E-cadherin, N-cadherin and Sox1 was then normalised to the DAPI signal in the same tissue and the same Z-plane to control for differences in relative brightness of different parts of the embryo. The intensity for each protein was calculated, and the resulting values for each tissue were normalised to the epiblast (which was assigned a baseline value of 1) to obtain a measure for the expression of each protein in various tissues relative to the epiblast. The results of this analysis are summarised in Fig. 3.2 B.

The analysis showed that E-cadherin was expressed at the highest level in the posterior epiblast. N-cadherin expression was highest in the precardiac mesoderm, while Sox1 was most expressed in the neurectoderm. These readings correspond to signal intensities observed in the embryos by eye. Importantly, the analysis showed that the intensity of N-cadherin did not differ between the epiblast (where this protein is assumed to be absent) and the neurectoderm. This result shows that *in vivo*, neural differentiation is initiated before overt cadherin switching.

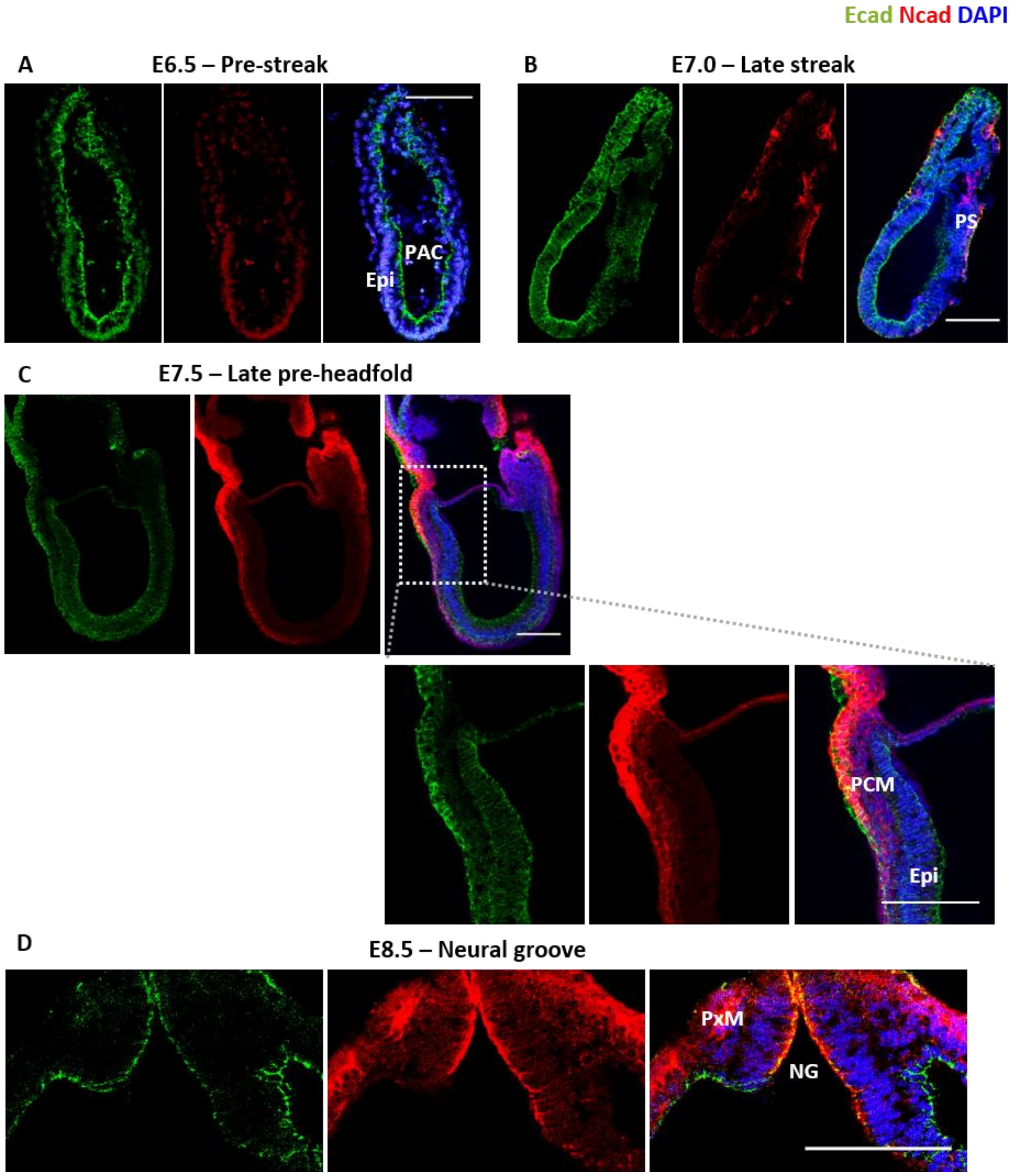

Figure 3.1: E-cadherin and N-cadherin expression in the early mouse embryo. *Embryos were stained and imaged separately, therefore expression levels are not directly comparable between images. Embryo dissection, staining and imaging performed by Rosa Portero Migueles.* ***A-C.*** *Sagittal views of embryos at different stages, left: anterior, right:posterior. Epi: epiblast; PAC: pro-amniotic cavity; PS: primitive streak; PCM: pre-cardiac mesoderm.* ***D.*** *Transverse section section through the E8.5 neural groove. NG: neural groove; PxM: paraxial mesoderm. All scalebars=50µm.*

3.3 Cadherin expression patterns in pluripotent cultures *in vitro*

3.3.1 Heterogeneity of cadherin expression varies by culture condition

To compare cadherin expression between embryonic development *in vivo* and embryonic stem cell culture *in vitro*, three widely used pluripotent culture conditions were used: 2i-Lif, representing naïve pluripotency comparable to the pre-implantation epiblast (Ying et al., 2008); Lif-serum, a mixed pluripotent condition roughly analogous to the peri-implantation epiblast (Smith et al., 1988); and epiblast stem cell (EpiSC) culture containing Activin and FGF, similar to the post-implantation primed epiblast (Brons et al., 2007; Tesar et al., 2007). Figure 3.3 A and B shows ICC staining for Oct4, E- and N-cadherin, and the nuclear envelope marker LaminB1 in these cells.

Cells in each of these culture conditions express high levels of *Pou5f1* (Oct4) and *Cdh1* (E-cadherin) on both the mRNA and protein levels, though qPCR analysis at the population level showed that the mRNA expression of both of these genes is highest in naïve pluripotency (2i-Lif) and decreases progressively in Lif-serum and EpiSC cultures (Fig3.3 B). Flow cytometric analysis of E-cadherin protein expression at the single-cell level confirmed this observation, and additionally showed that cells cultured in 2i-Lif and Lif-serum express high, uniform levels of E-cadherin, while EpiSCs display much more heterogeneous expression of this protein (Fig. 3.3 C).

EpiSCs were the only pluripotent cells in which N-cadherin was detectable on the mRNA or protein levels. They were also the only cells of the three populations expressing Sox1. This could indicate that the EpiSC culture may contain cells that are primed for neural differentiation, or alternatively, that some of the cells have differentiated, and are committed to the neural lineage. Taken together, these observations suggest that EpiSCs represent the earliest pluripotent cell type where cadherin switching occurs *in vitro*.

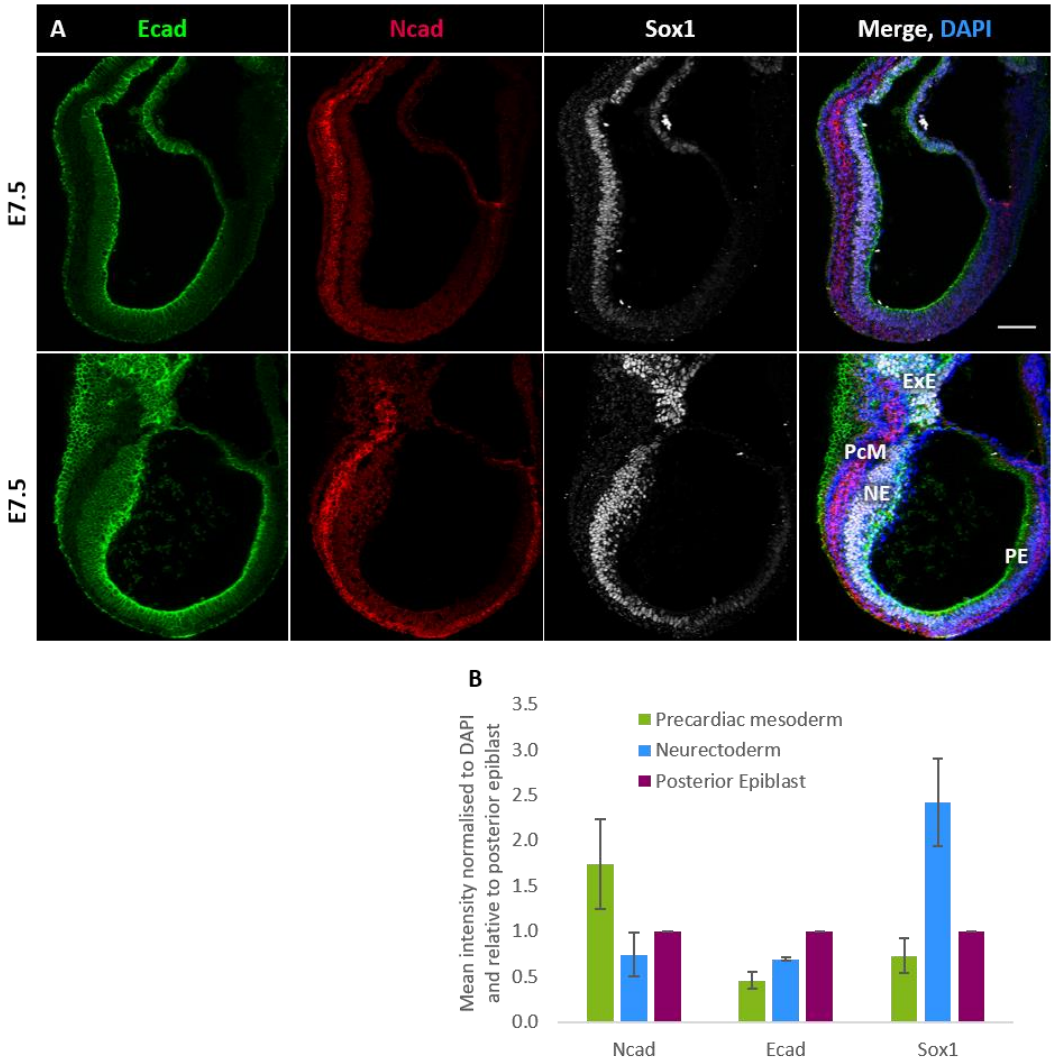

Figure 3.2: E-cadherin, N-cadherin and Sox1 co-expression patterns in the E7.5 mouse embryo. A. *Sagittal sections through two E7.5 embryos. Embryo dissection, staining and imaging performed by Rosa Portero Migueles. ExE: extraembryonic ectoderm; NE: neural ectoderm; PcM: pre-cardiac mesoderm. PE: posterior epiblast. Scale bar = 50µm.* ***B.*** *Quantification of signal intensity of each protein in three embryonic tissues. Error bars=SD. N=4 embryos.*

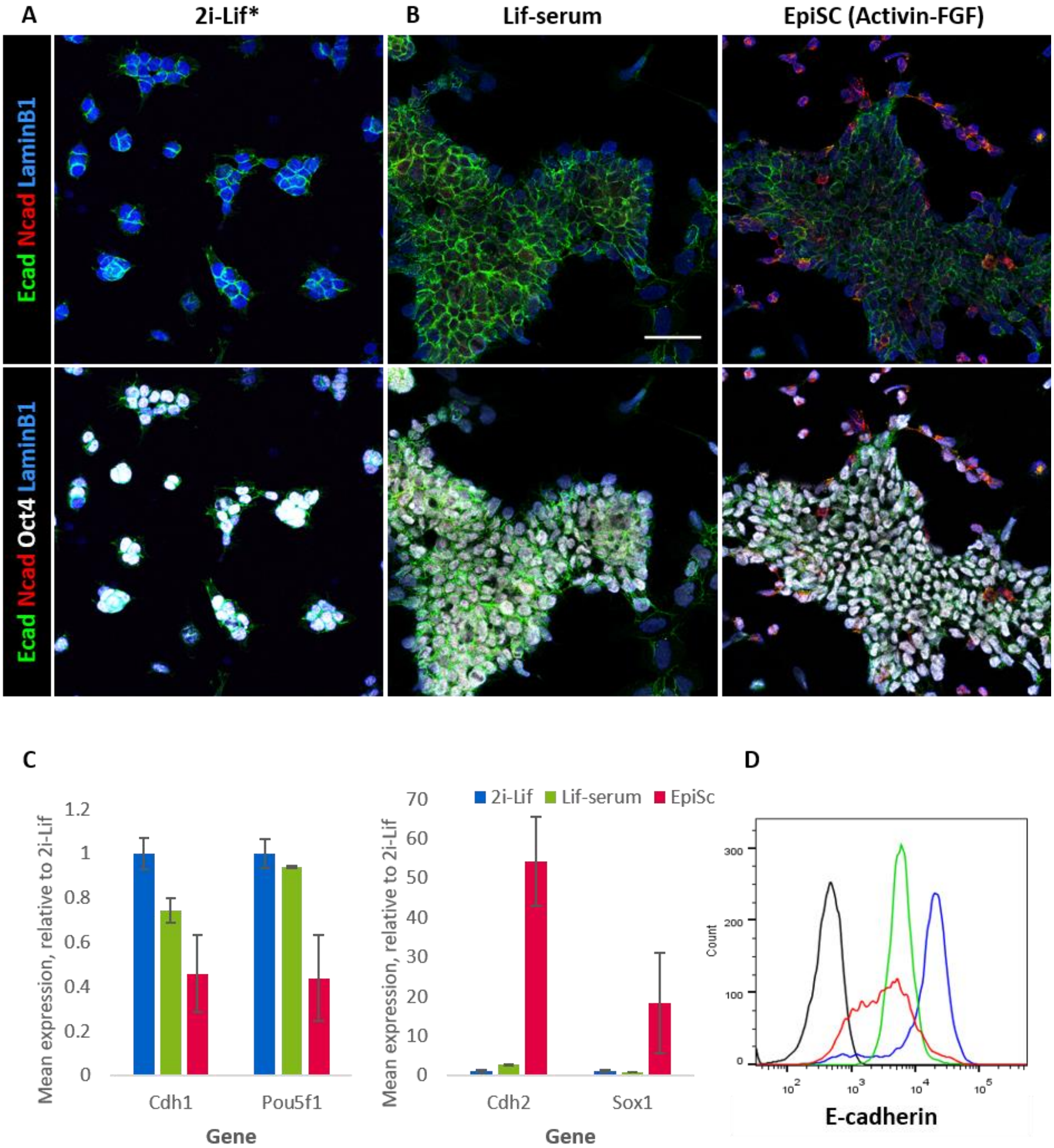

Figure 3.3: E- and N-cadherin expression patterns in three pluripotent cultures **in vitro.** ***A-B.*** *ICC of E-cadherin, N-cadherin, the pluripotency marker Oct4 and the nuclear envelope marker LaminB1. Scale-bar = 50µm. *2i-Lif image (**A**) comes from separate experiment imaged at a different time, so expression levels are not directly comparable to remaining images.* ***C.*** *Gene expression at the mRNA level by qPCR. Values normalised to 2i-Lif condition. Error bar = SD, N=3 biological replicates.* ***D.*** *Representative plot of E-cadherin protein expression at the single cell level by flow cytometry. Black line depicts unstained control cells. N=3 biological replicates.*

3.3.2 Cadherin switching is initiated prior to the loss of pluripotency marker expression and correlates with lineage priming in EpiSCs

EpiSCs were the most heterogeneous of the pluripotent populations studied with regards to E- and N-cadherin expression. They were also the only pluripotent state in which N-cadherin was detectable. To confirm that the EpiSCs expressing N-cadherin were still pluripotent, and not simply differentiated cell types, EpiSCs were stained for E-cadherin, N-cadherin and Oct4, and the proportion of cells co-expressing various combinations of these markers were quantified on the single cell level by eye. Three biological replicates of EpiSCs were cultured and stained, and three fields of view were imaged in 3D by confocal microscopy for each replicate (Fig. 3.4 B). All cells in the images were then classified based on their expression of E-cadherin, N-cadherin and Oct4 by eye. This method of quantification was chosen because the image resolution is generally high enough for there to be a clear distinction between cells that are positive and negative for the proteins analysed. This makes it relatively straightforward to assess the cells' protein expression profile without computational help. A total of 2596 cells were included in the analysis.

Figure 3.5 shows examples of various EpiSC identities co-expressing E-cadherin, N-cadherin and/or Oct4, and figure 3.6 is a summary of the quantification of these identities. The analysis confirmed that over 90% of cells analysed expressed Oct4 and were therefore assumed to be undifferentiated. Within this population, the majority (81.3%) only co-expressed E-cadherin, with the next largest population (12.4%) co-expressing both of the cadherins and Oct4. The four remaining populations combined made up 6.1% of the cells observed. These results show that in pluripotent EpiSCs cultured in FGF and Activin, E-cadherin is the predominantly expressed cadherin, and that some of these cells additionally switch on N-cadherin while remaining in an undifferentiated state, as determined by the presence of Oct4.

To determine whether E- and N-cadherin expression may denote subpopulations of EpiSCs with distinct gene expression profiles, a sorting experiment was set up. EpiSCs were cultured to near-confluence, stained for E-cadherin, and sorted into the top, middle and 20% of cells based on E-cadherin protein expression. The three sorted populations were then lysed for mRNA analysis by qPCR in order to study differential gene expression. The FACS sorting strategy is summarised in figure 3.7.

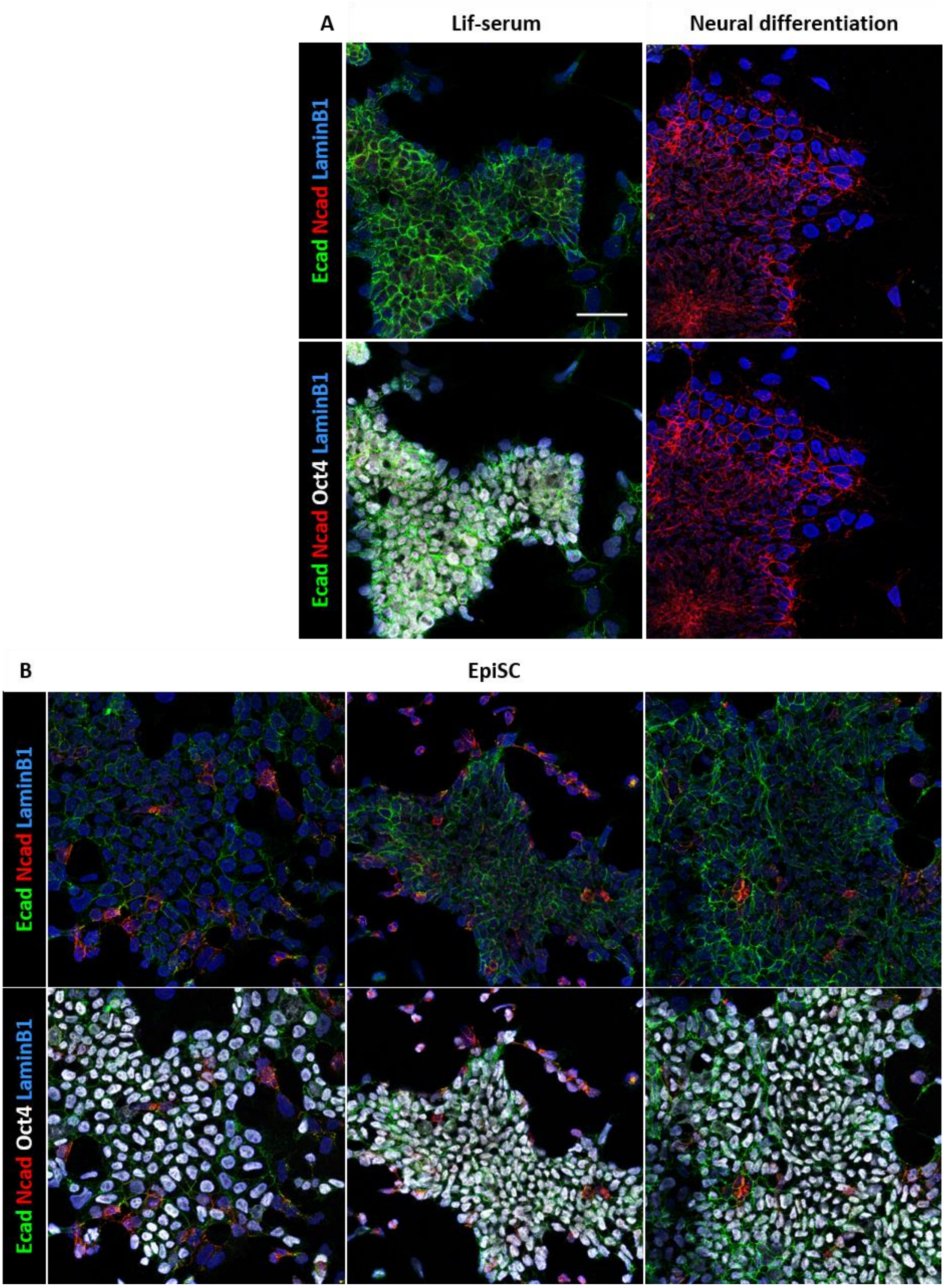

Figure 3.4: Cadherin and Oct4 co-expression in EpiSCs. A. *Control cell populations expressing only one type of cadherin.* ***B.*** *Example EpiSCs from three biological replicates. Scale bar = 50µm.*

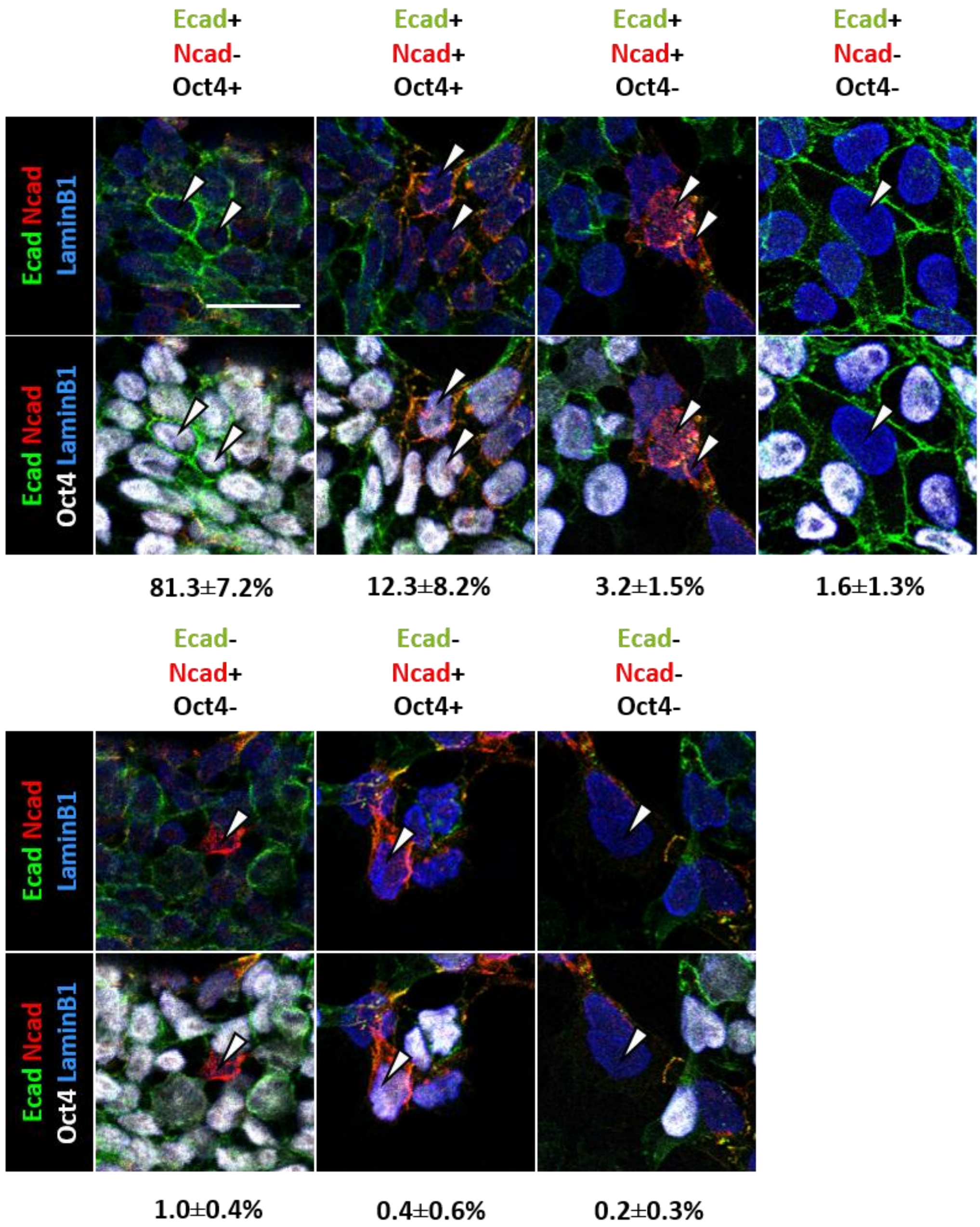

Figure 3.5: EpiSC identities of cadherin and Oct4 co-expression. *Example cells indicated by white arrowheads. Percentages underneath images indicate the mean±SD proportion of cells observed of that identity by manual quantification. N=3 biological replicates, three fields of view per replicate, 2596 total cells counted.*

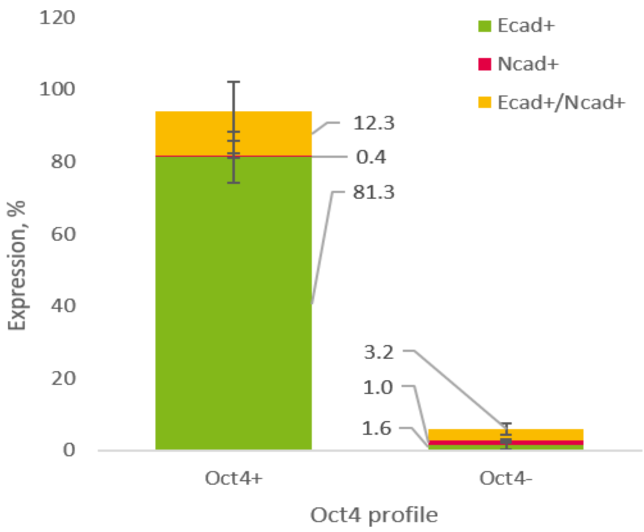

Figure 3.6: Percentages of EpiSCs co-expressing E-cadherin, N-cadherin and/or Oct4. *Summary graph of data from previous page. N= 3 fields of view each for 3 biological replicates. Manual quantification.*

Following sorting, the three subpopulations were analysed by qPCR for differences in gene expression of the mRNA level. The subpopulation expressing "medium" levels of E-cadherin was used as a baseline measurement (with an assigned expression value of 1), and the gene expression readings for the top and bottom subpopulations were normalised to this value. Three independent biological replicates were performed, and a paired T-test was used to assess significance between the E-cadherin low and high subpopulations. The results are summarised in figure 3.8.

Analysis of *Cdh1* expression confirmed that the sorting had been successful, as there was a highly significant difference between the E-cadherin-high and -low populations. A reciprocal expression pattern was observed for *Cdh2*: the E-cadherin^{High} population had significantly lower levels of *Cdh2* than the E-cadherin^{Low} population, and vice versa. This result shows that cadherin switching is taking place and is detectable at the mRNA level in EpiSCs.

Next, pluripotency marker expression was compared between the two populations. There was no significant difference in the levels of the naïve marker *Klf4*, general pluripotency markers *Nanog* and *Pou5f1* (Oct4), and primed marker *Pou3f1* (Oct6) between the E-cadherin^{High} and E-cadherin^{Low} populations, suggesting that cadherin switching occurs before the loss of pluripotency marker expression in EpiSCs.

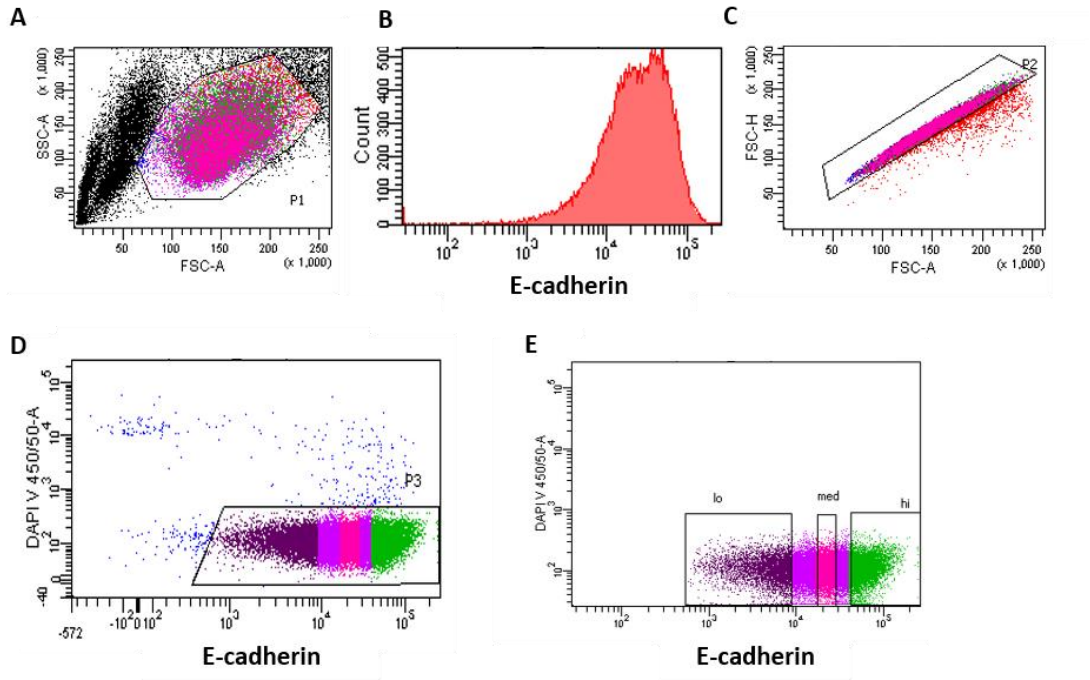

***Figure 3.7: Gating strategy for sorting EpiSCs based on E-cadherin expression**. A: Gating total events for cells (gate P1). **B:** E-cadherin intensity of cells in population P1. **C:** Gating population P1 for single cells (gate P2). **D:** Gating population P2 for live cells based on DAPI staining (gate P3). **E:** Gating population P3 for top (green), middle (pink) and bottom (purple) 20% of cells for sorting based on levels E-cadherin expression. N=3, representative plots shown for one experiment.*

To determine whether cadherin switching correlates with a bias towards a certain embryonic lineage, the expression of various lineage markers was studied. The E-cadherin^{Low} population was found to express significantly higher levels the neural marker gene *Sox1* and mesoderm marker gene *T* (Brachyury) than the E-cadherin^{High} population, while markers of endoderm (*Sox17)* and surface ectoderm *(Ap2a)* were expressed at comparable levels in the two populations. This suggests that cadherin switching correlates with priming towards the neural and mesodermal lineages in EpiSCs. This finding is not surprising since these are the two tissues where N-cadherin is first expressed in the embryo (Radice et al., 1997).

Finally, levels of signalling pathway readout genes were compared between the two sorted populations. There were no significant differences observed in the expression of the Wnt target Axin2 or the FGF targets Dusp4, Egr1 and JunB between the two populations.

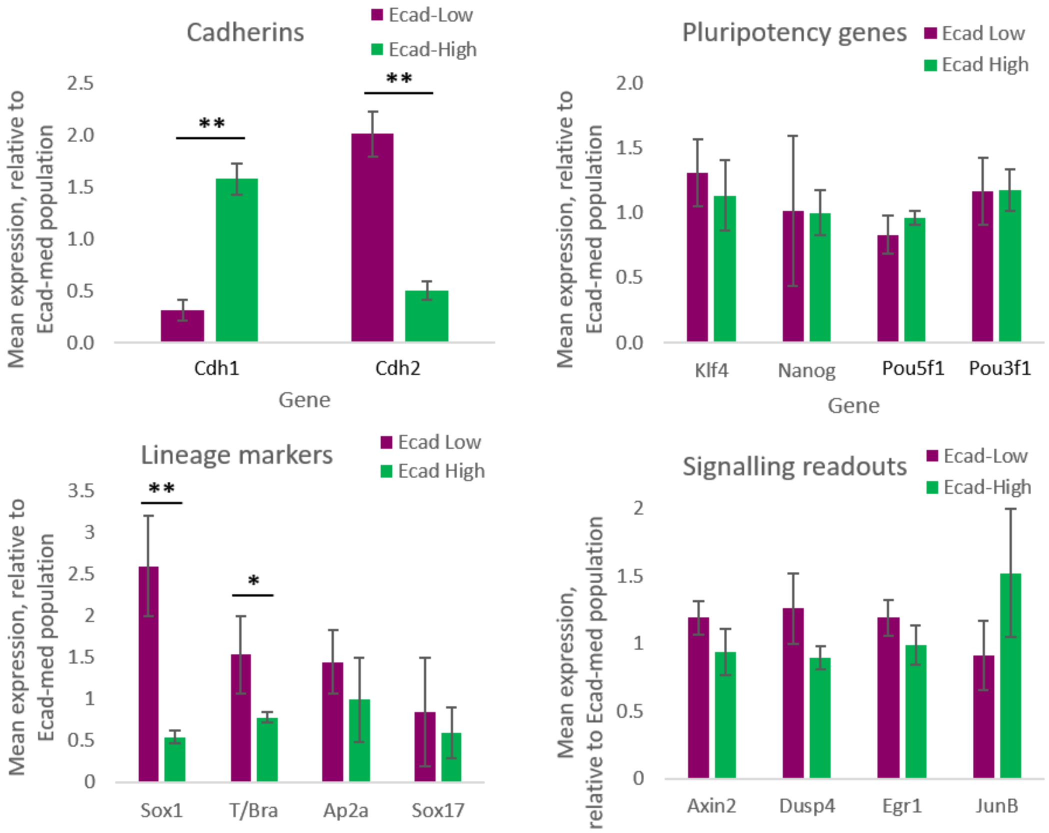

Figure 3.8: mRNA gene expression in EpiSCs sorted into the top and bottom 20% of cells by level of E-cadherin protein expression. *E-cadherin- high and -low populations were normalised to the expression level of an E-cadherin medium population. N= three independent sorts of three biological replicates. Error bars = SD. *p≤0.05, paired T-test.*

3.4 Dynamics of cadherin switching during neural differentiation *in vitro*

Cadherin switching was found to take place in EpiSCs. Next, to determine how this compares with cells exiting pluripotency, the patterns of cadherin expression were studied during *in vitro* neural differentiation. The starting population for this differentiation was a naïve pluripotent culture of ESCs cultured in 2i-Lif. This population was chosen as the starting point to produce as "clean" and reproducible of a differentiation experiment as possible.

Sox1-GFP cells cultured in 2i-Lif conditions were seeded onto glass coverslips on plastic 12-well tissue culture plates coated in poly-L-ornithine and laminin (both Sigma) at a density of 3000 cells per well. The cells were allowed to adhere to the matrix for 24h in 2i-Lif conditions, and after this period the media were changed from 2i-Lif to neural differentiation medium (day 0); for full details of the protocol, see Methods. Whenever the culture medium turned yellow, the old media were aspirated and fresh media were added.

Sample wells were fixed on days two-to-five of the differentiation, and the process was repeated thrice to produce three biological replicates. Coverslips for each time point were then co-stained for E-cadherin, N-cadherin, the nuclear envelope marker Laminβ1, and either Oct4 or Sox1-GFP. The cells were then imaged in 2D on an Olympus BX61 fluorescent microscope. Figures 3.9-3.11 summarise the expression patterns of the different staining combinations.

E-cadherin was found to be highly expressed in tightly packed 2i-Lif-cultured cells, as expected. At day two of neural differentiation, the cells were visibly spread apart from one another in a more flattened colony structure, and E-cadherin staining in the cells was much weaker. Days three-to-four were the first time points where N-cadherin and Sox1-GFP were detected, depending on the biological replicate (Figs. 3.9 and 3.11). Throughout the time-course, E-cadherin and N-cadherin were observed in mutually exclusive regions, and Oct4 was mostly present in cells expressing E-cadherin, while Sox1-GFP was mostly observed in patches of cells expressing N-cadherin. However, at the time points where cadherin switching was first observed, some Oct4 could be detected in cells expressing N-cadherin, and Sox1 was also weakly expressed in cells positive for E-cadherin.

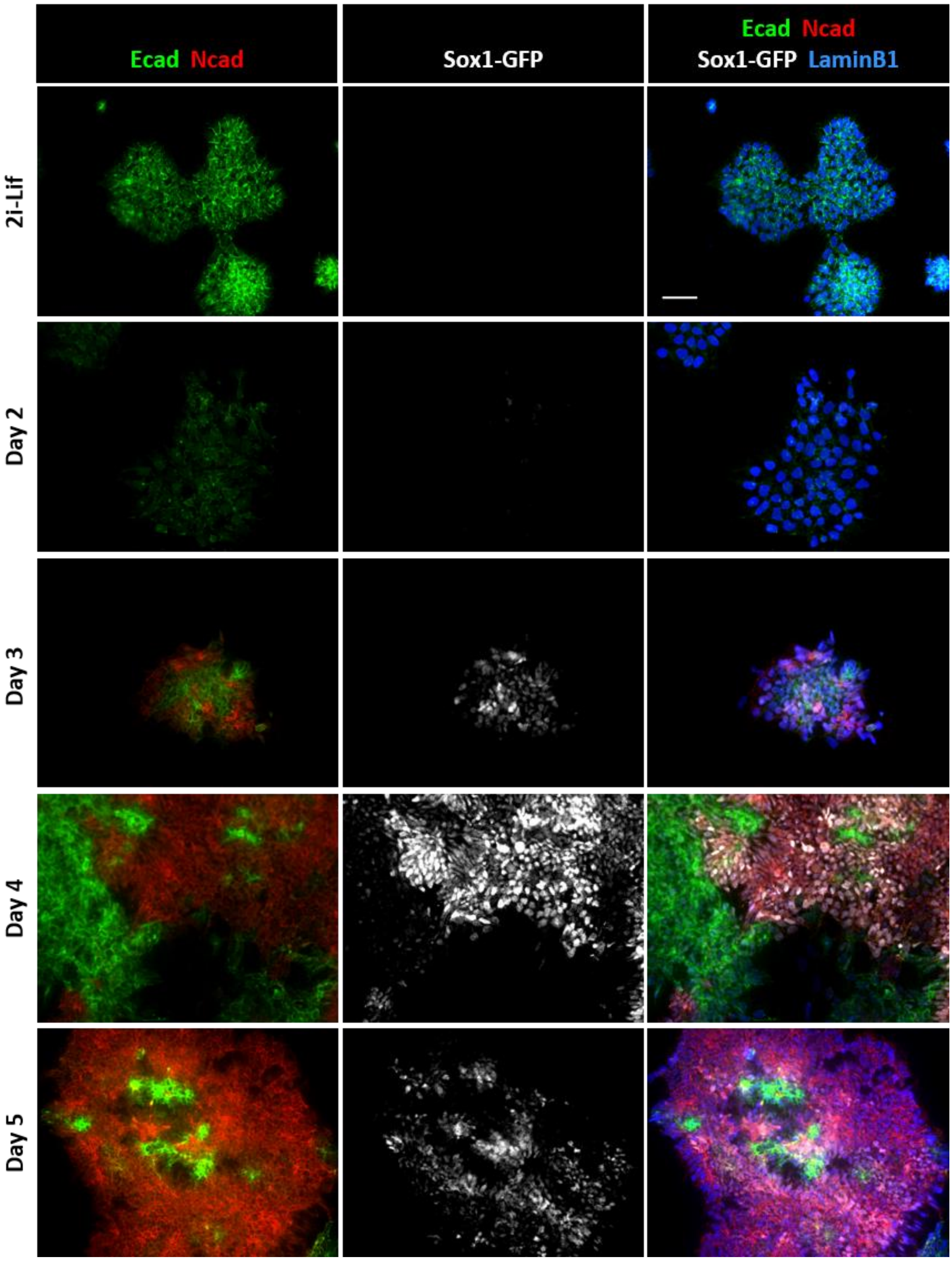

Figure 3.9: Co-expression of E-cadherin, N-cadherin and Sox1-GFP during neural differentiation from 2i-Lif. *Sox1-GFP cells cultured in 2i-Lif were seeded onto glass coverslips in 12-well tissue culture plates at a seeding density of 3,000 cells per well. The cells were cultured in 2i-Lif for 24h hours before a media change to neural differentiation medium (Day 0). Scale bar = 50µm.*

To further study the identity of the cells co-expressing both Oct4 and N-cadherin, cells undergoing neural differentiation were co-stained for N-cadherin, Oct4 and Sox1-GFP. In this biological replicate, cadherin switching was first observed at Day four. At this time point, a cluster of cells positive for all three markers is clearly visible (Figure 3.11, dotted outline): the nuclei express low levels of Oct4 and high levels Sox1 relative to the surrounding cells, and are surrounded by N-cadherin positive membranes. These results suggest that N-cadherin is switched on during neural differentiation at a time point that corresponds to neural priming, when cells remain undifferentiated (and express Oct4) but are becoming biased for the neural lineage (marked by expression of Sox1).

It is important to note that at the later time points, Sox1-GFP expression was high, but in all cases some E-cadherin was still highly expressed in patches of cells, and the extent of E-cadherin or N-cadherin staining at each time point varied greatly between biological replicates. This suggests that *in vitro* neural differentiation is not 100% efficient and that small pockets of pluripotent cells persist even up to day 5 of the differentiation protocol.

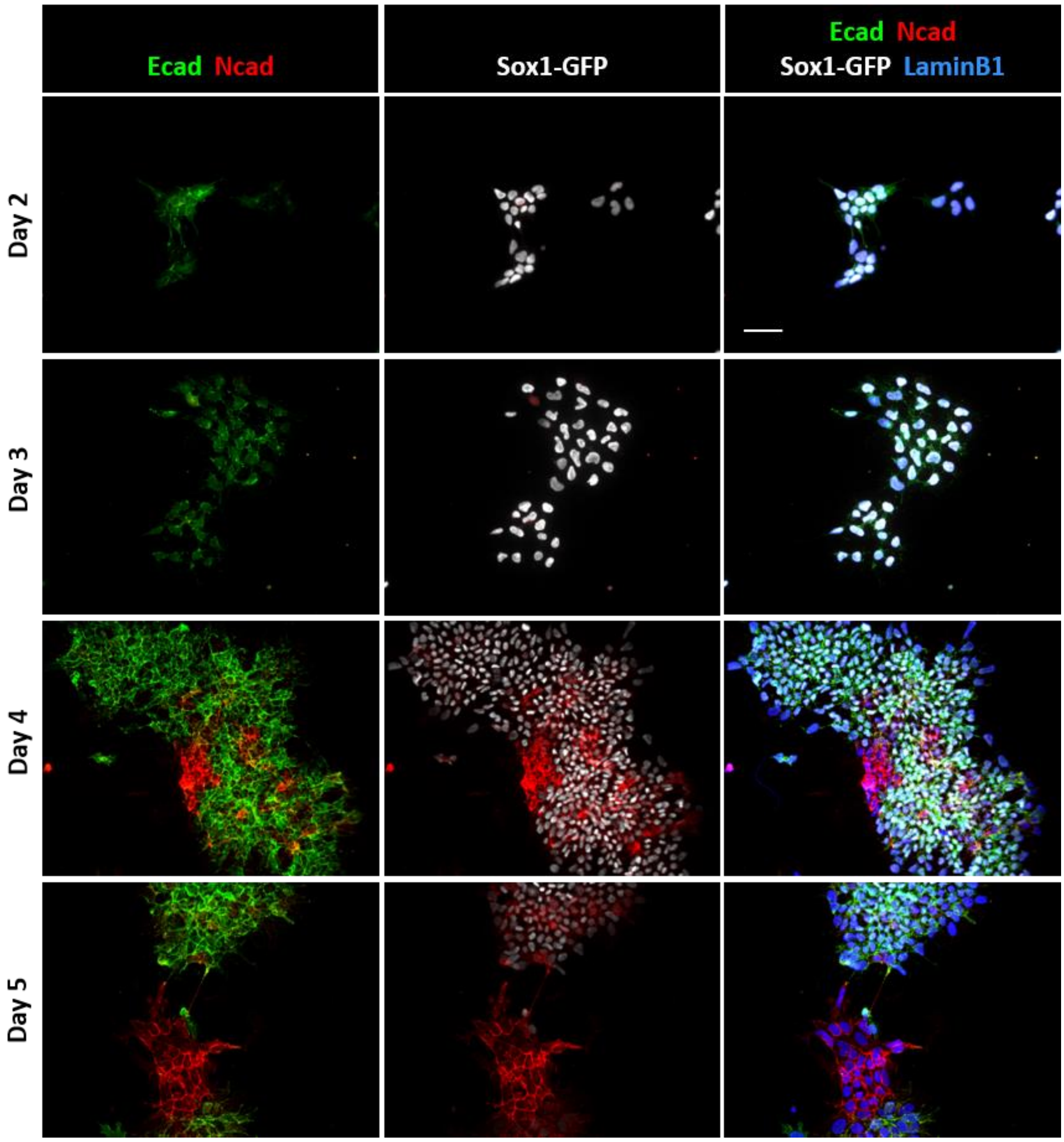

Figure 3.10: Co-expression of E-cadherin, N-cadherin and Oct4 during neural differentiation from 2i-Lif. *Sox1-GFP cells cultured in 2i-Lif were seeded onto glass coverslips in 12-well tissue culture plates at a seeding density of 3,000 cells per well. The cells were cultured in 2i-Lif for 24h hours before a media change to neural differentiation medium (Day 0). Scale bar = 50µm.*

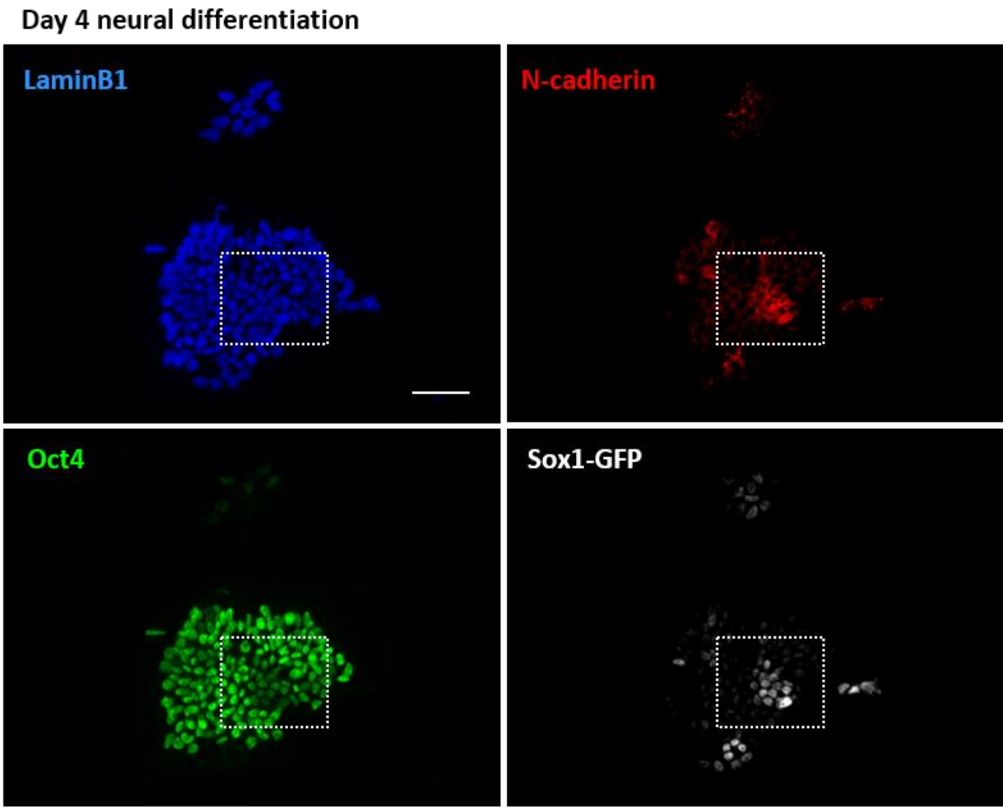

Figure 3.11: *Co-expression of N-cadherin, Oct4 and Sox1-GFP on Day 4 of neural differentiation from 2i-Lif*. *Sox1-GFP cells cultured in 2i-Lif were seeded onto glass coverslips in 12-well tissue culture plates at a seeding density of 3,000 cells per well. The cells were cultured in 2i-Lif for 24h hours before a media change to neural differentiation medium (Day 0). White dashed outline highlights an area where all three of these proteins are at least weakly expressed. Scale bar = 50µm.*

3.5 Discussion

3.5.1 Differences between cadherin switching *in vivo* and *in vitro*

Staining early embryos for E- and N-cadherin showed that cadherin switching is initiated on the protein level between E7.0 and E7.5, first in mesodermal tissues and followed by ectodermal tissues about 24h later, as previously reported (Radice et al., 1997). The first full cadherin switch, consisting of strong N-cadherin staining in a tissue absent for E-cadherin, is seen in the pre-cardiac mesoderm. Transcriptional studies have shown that *Cdh2* transcriptional upregulation is initiated in the E6.5 gastrula (Peng et al., 2016), though N-cadherin protein was not observed at this stage in the current study.

EpiSCs are a cultured stem cell population analogous to the primed epiblast at E5.5, which can be either derived from the post-implantation embryo or produced in culture from ESCs (Nichols and Smith, 2009). N-cadherin has been identified as one of the defining cell-surface markers of this pluripotent state (Rugg-Gunn et al., 2012). EpiSCs therefore exhibit an earlier cadherin switching event than that observed *in vivo*, and highlights an important difference in this *in vitro* model of early development. However, EpiSCs are known to be a highly heterogeneous population consisting of several sub-populations (Tsakiridis et al., 2014). Additionally, previous reports have shown that while EpiSCs can be derived from the embryonic epiblast from E5.5 up to E8.0, their transcriptomes tend to converge *in vitro*, regardless of the age of the embryo from which they were derived (Kojima et al., 2014; Osorno et al., 2012).This suggests that, while EpiSCs can be a useful tool for studying early developmental events, they may not serve as an accurate model of a specific developmental time point due to their heterogeneous and dynamic gene expression resulting from *in vitro* culture.

It has previously been reported that N-cadherin is the predominant cadherin expressed by EpiSCs (Takehara et al., 2015). In the analysis shown here, only around 17% of all EpiSCs studied expressed N-cadherin. However, in contrast to the published EpiSC protocols (Brons et al., 2007; Tesar et al., 2007) the EpiSC culture used in the Takehara et al. (2015) study did not include the addition of Activin, therefore their findings may not be directly comparable to those presented in the current study.

3.5.2 Cadherin switching is initiated prior to the loss of pluripotency

Co-staining for the two cadherins and the early neural marker Sox1 in the E7.5 embryo showed that Sox1 was expressed in the anterior ectoderm by E7.5, before overt cadherin switching was observed in this tissue. Another study has also documented Sox1 protein expression restricted to the neural plate of an E7.5 mouse embryo (Pevny et al., 1998). Expression of the pluripotency marker Oct4 has been reported in the same tissue at this stage (Downs, 2008; Hart et al., 2004), suggesting that the tissue may still be pluripotent and that the Sox1 expression pattern marks an area primed for ectodermal fate.

Fate mapping studies on the differentiation potential of anterior ectodermal tissue have found that E6.5 ectoderm retains full pluripotency (Li et al., 2013). At E7.0, the anterior ectoderm is no longer pluripotent but is instead restricted to either epidermis or neurectoderm, depending on the presence or absence of BMP4, respectively. By E7.5, the ectoderm was found to no longer be responsive to BMP4, and is restricted either to neural or epidermal fate depending on the position within the embryo (Li et al., 2013). The *in vivo* data in the present study are insufficient to conclusively determine whether cadherin switching is initiated before, during or after the specification of the neural lineage in the embryo, but the two events do seem to be occurring at very similar timescales.

However, the *in vitro* data are much clearer on the matter. Analyses of EpiSCs show that cadherin switching can be observed both at the population and single-cell level in these cultures, and that this switch takes place before the loss of pluripotency markers such as Oct4. Likewise, single cells could be identified during *in vitro* neural differentiation that co-expressed Oct4, Sox1 and N-cadherin. This suggests that *in vitro*, cadherin switching is initiated prior to the loss of pluripotency markers, and coincides with neural priming. To our knowledge this study represents the first attempt to identify the exact temporal timeframe in which cadherin switching occurs in the contexts of pluripotency, priming, and differentiation *in vitro*.

These observations prompt the question: could cadherin switching also help modulate this priming and subsequent differentiation? The experiments used to address this question are described in Chapter 4.

Chapter IV – Cadherin switching promotes neural differentiation

4.1 Introduction & aims

Fundamentally, cadherin switching requires two separate molecular events: the loss of E-cadherin, and the concomitant gain of N-cadherin. The loss of E-cadherin has been extensively studied in several contexts, both in the developing embryo and in ESC cultures.

In vivo, E-cadherin knock-out mice die prior to implantation due to a failure in morula compaction and the inability to form functional trophectoderm caused by defective adhesion (Larue et al., 1994). A gene replacement knocking in *Cdh2* into the *Cdh1* locus (N-cadherin knock-in; NcKI) rescued the adhesion defect but was not enough to rescue the trophectoderm lethality phenotype (Kan et al., 2007). Inducing the same replacement after trophectoderm formation, but prior to the onset of gastrulation, allowed embryos to undergo gastrulation but subsequently resulted in gross morphological abnormalities and embryonic lethality at around E8.5 (Basilicata et al., 2016).

Similar experiments using cells expressing a hybrid cadherin with an extracellular E-cadherin domain and an intracellular N-cadherin domain showed that a signalling function involving IGF1R activation was critical for correct pre-implantation development, and was independent of the adhesive function of E-cadherin (Bedzhov et al., 2012). These studies demonstrate that E-cadherin plays important roles in both adhesion and signalling, and that both are critical for early embryonic development.

E-cadherin also plays a major role in pluripotency and lineage commitment of ES cells. E-cadherin-null ES cells are unable to form organised structures in teratoma assays. Re-expression of E-cadherin in these cells allows for the formation of epithelia but not other structures, and transfecting the E-cadherin mutants with N-cadherin resulted in the formation of neuroepithelium and cartilage (Larue et al., 1996). These results suggest that different cadherin species can promote different lineage fates. E-cadherin-null cells are also able to remain in an undifferentiated, proliferative state in the absence of Lif (Soncin et al., 2009), and they can maintain Oct4 expression even after 30 days culture in embryoid body differentiation conditions (Pieters et al., 2016). In addition, blocking E-cadherin expression compromises formation of EBs and teratomas while accelerating differentiation (Chou et al., 2008), and forced expression of E-cadherin can also replace Oct4 in the "Yamanaka cocktail" of factors supporting efficient reprogramming of cells into iPSCs (Redmer et al., 2011). These studies show that E-cadherin is closely linked to ES cell pluripotency.

Transcriptome analyses have found the gene expression profile of E-cadherin-null ESCs to be abnormal. The cells have a similar, though not identical, transcription profile to EpiSCs, suggesting that E-cadherin may prevent the transition from ICM to epiblast (Soncin et al., 2011). They have lower levels of pluripotency markers such as *Nanog* and *Klf4*, and displayed a compensatory upregulation of N-cadherin in Lif/BMP conditions (Hawkins et al., 2012).

Gain of N-cadherin has also been studied, but to a lesser extent. The forced expression of N-cadherin in human squamous carcinoma cells results in a downregulation of endogenous E-cadherin by accelerating its degradation (Islam et al., 1996), and may be driven by competition for binding to p120-catenin (Maeda, 2005; Wheelock et al., 2008). However, this effect appears to be context-dependent: in human breast cancer cell lines the over-expression of N-cadherin does not result in the downregulation of E-cadherin (Nieman et al., 1999).

The role of cadherin switching in neural differentiation has been studied to a limited extent. Studies from our lab have shown that blocking E-cadherin results in faster and more synchronous neural differentiation (Malaguti et al., 2013). N-cadherin was also found to promote neuronal outgrowth in foetal neural stem cells through its interaction with FGF-R1 and through mechanical coupling of adhesion sites with acto-myosin treadmilling (Nguyen and Mège, 2016; Williams et al., 1994; Williams et al., 2001).

To build on existing knowledge, this chapter explores the effects of experimentally controlled E- to N-cadherin switching on the neural differentiation of embryonic stem cells *in vitro*. The aim of this chapter is to answer the following questions:

a) How does the loss of E-cadherin alone affect neural differentiation?
b) Does forced, premature cadherin switching affect neural differentiation?
c) How does gain of N-cadherin alone affect neural differentiation?

4.2 Cadherin switching promotes neural differentiation

4.2.1 Validation of E-cadherin knock-out cells (EcKO) and N-cadherin knock-in (NcKI) cells

To study the behaviour of cells lacking E-cadherin, knock-out (*Cdh1*$^{-/-}$, referred to as EcKO) cells were used, which were supplied by a collaborating lab (Pieters et al., 2016). To complement these cells, N-cadherin knock-in cells (*Cdh1*$^{Cdh2/Cdh2}$, referred to as NcKI) were supplied by a different collaborating lab (Basilicata et al., 2016; Kan et al., 2007). The NcKI cells have the *Cdh2* gene knocked in to the *Cdh1* locus, and are therefore negative for E-cadherin protein expression. Instead, they express N-cadherin mRNA and protein in its place, under the control of the *Cdh1* promoter. These cells therefore represent a premature and forced cadherin switch.

To validate the knock-out and knock-in modifications, $5x10^4$ cells per well were seeded into 2i-Lif conditions in a 12-well plate and allowed to adhere for 24h, before a media change to neural differentiation medium. Another 24h later the cells were fixed, co-stained for E- and N-cadherin, and imaged on a Leica SP8 confocal microscope (Figure 4.1). This time-point was chosen because it represents a stage where E-cadherin, but not N-cadherin, is expressed during the differentiation protocol, based on previous experiments.

Both E14-Juo9 (WT) cells and the parental control cell line for the EcKO cells (Cdh1$^{fl/fl}$, referred to as Flox/Flox)(Derksen et al., 2006) were found to express high levels of E-cadherin at their cytoplasmic membranes. By contrast, both EcKO and NcKI cells were completely negative for E-cadherin staining. The control cell lines were found to express negligible levels of N-cadherin, while NcKI cells expressed high levels of N-cadherin at the membrane. Interestingly, EcKO cells also expressed visibly higher levels of N-cadherin than their parental cell line, suggesting that the loss of E-cadherin leads to a compensatory upregulation of N-cadherin in these cells. All four cell lines robustly expressed high levels of Oct4, suggesting that they remained undifferentiated at the time-point used.

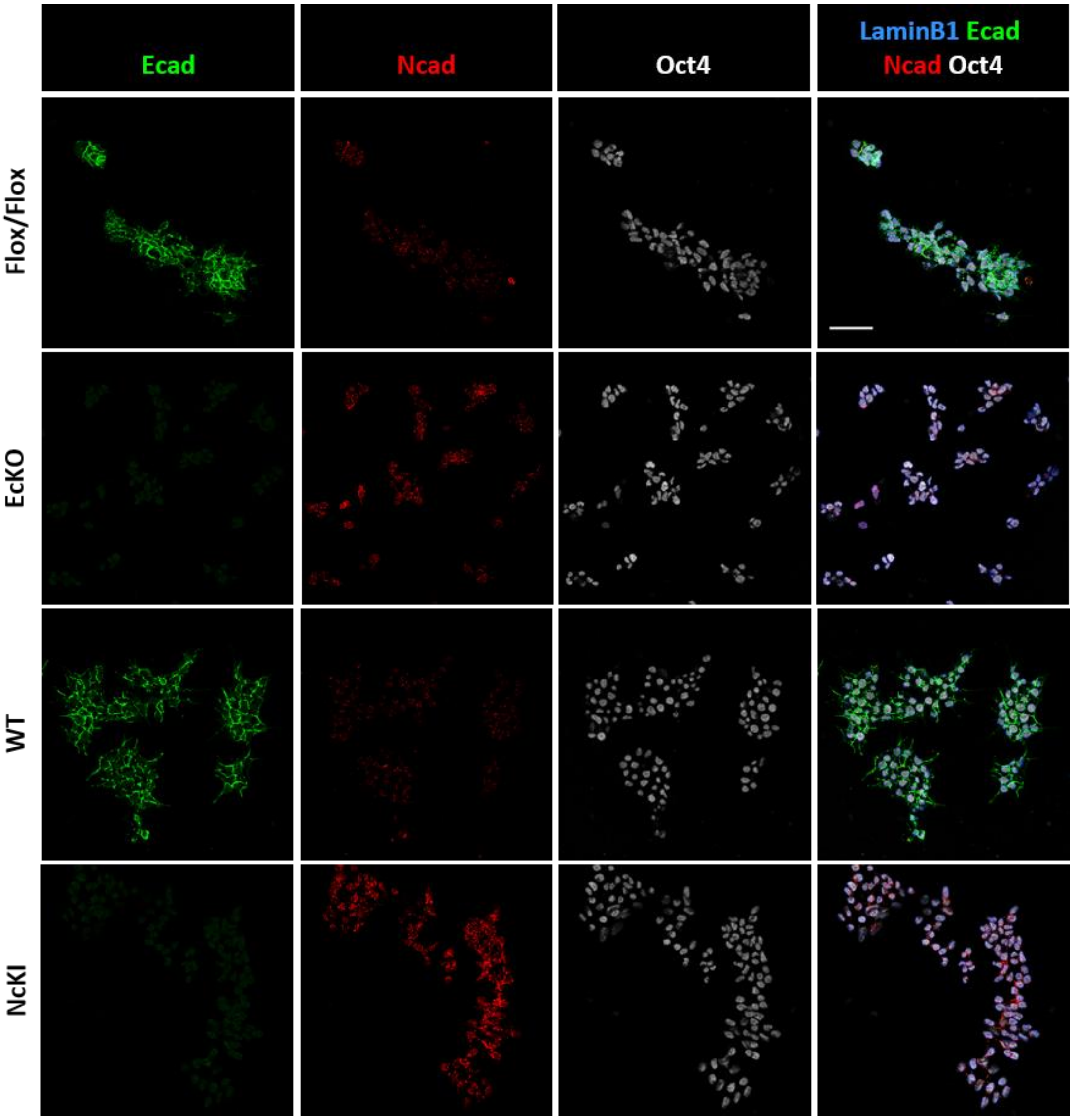

Figure 4.1: Validation of cadherin knock-out and knock-in cell lines. *EcKO and NcKI cells and their corresponding control cell lines were seeded into 2i-Lif conditions for 24h and cultured in neural differentiation conditions for a further 24h. Cells were co-stained for E-cadherin (Ecad), N-cadherin (Ncad), Oct4 and Laminβ1. Scale bar=50µm.*

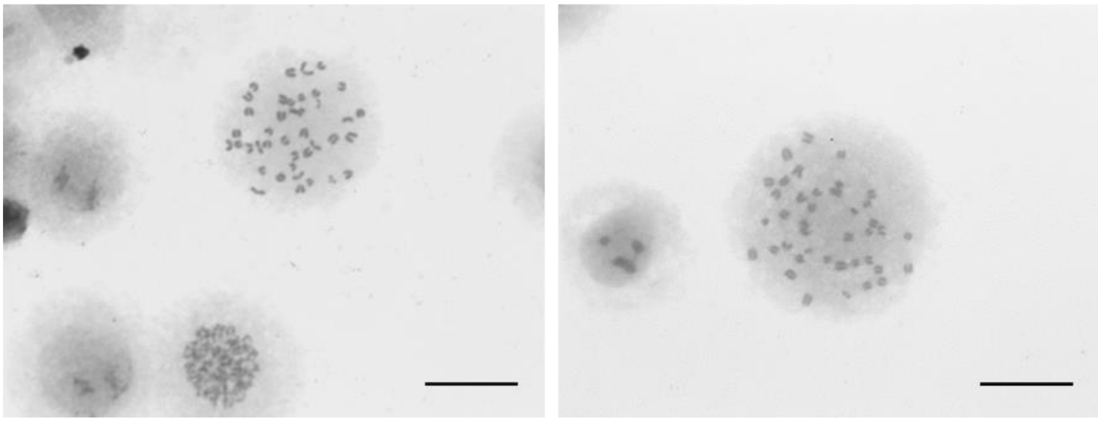

Figure 4.2: Kayotyping WT and NcKI cells. *Chromosome spreads showing a representative number (mode) of 40 chromosome in clonal E14-Juo9 (WT) and NcKI cells lines cultured in Lif-serum. Scale bar=20µm.*

The Flox/Flox and EcKO cell lines were karyotyped in their lab of origin prior to shipping. E14-Juo9 (WT) and NcKI cells were karyotyped in-house. WT cells were found to have a normal karyotype, as represented by a mode of 40 chromosomes per nucleus (Fig. 4.2), but the NcKI cells were found to have an abnormal chromosome counts in a routine karyotyping screen. To overcome this issue, these cells were single-cell sorted by flow cytometry and the resulting clones were serially passaged. These clonal cell lines were then karyotyped until a cell line with a chromosomal mode of 40 was identified (Fig. 4.2). This line was treated as karyotypically normal and was used for all experiments presented in this thesis.

4.2.2 EcKO cells are unstable during neural differentiation

Previous reports from our lab showed that using a function-blocking antibody for E-cadherin caused faster and more synchronous neural differentiation (Malaguti et al., 2013). To test whether this was also the case in cells null for E-cadherin, the EcKO cells were cultured through a six-day neural differentiation protocol, with a 24h incubation period in 2i-Lif, and lysed for qPCR analysis. Cells were initially seeded into 12-well plates at a density of 4,000 cells per well. However, from day four onwards, significant cell death of the EcKO cells was observed (Fig 4.3), leading to insufficient mRNA yield for downstream analysis. To overcome this issue, the experiment was scaled up: both the parental and EcKO were seeded into 6-

well plates (instead of 12-well plates) and seeded at a density from $2x10^4$ to $5x10^4$ cells per well into 2i-Lif conditions, and after 24h media were changed to NDiff. Out of six biological replicates performed, three produced sufficient RNA yield for the EcKO cells up to day four, and only two produced sufficient yield for days five to six. These three replicates were used for qPCR analysis (Fig. 4.4).

qPCR analysis confirmed the deletion of E-cadherin in the mutant cells, as they expressed negligible levels of *Cdh1* transcript compared to the parental cell line. On the transcript level, they did not have significantly different levels of *Cdh2* compared to the control cells at any stage, suggesting that there was no compensatory upregulation of *Cdh2* in *Cdh1*-null cells: this is in contrast to the protein-level staining of EcKO cells, which displayed detectable N-cadherin staining after 24h in NDiff conditions, unlike WT cells (Fig. 4.1). In addition, levels of *Pou5f1, Sox1* and *Pax6* transcript did not differ significantly between the control and EcKO cell lines, with the exception of the day two time-point for *Pax6*, which was significantly lower in the EcKO cells. These results suggest that the deletion of *Cdh1* gene does not affect neural differentiation ability – the cells continue to upregulate neural markers to similar levels as those observed in control cells, and downregulate *Pou5f1* (Oct4) at similar rates.

A major drawback of these results is that it is difficult to assess how representative they are of the complete cell population, as the EcKO cells displayed extensive cell death during neural differentiation, with few adherent cells surviving the media change and wash steps that occur prior to lysis for mRNA extraction, especially at later time points. This limitation must be taken into account when interpreting these results.

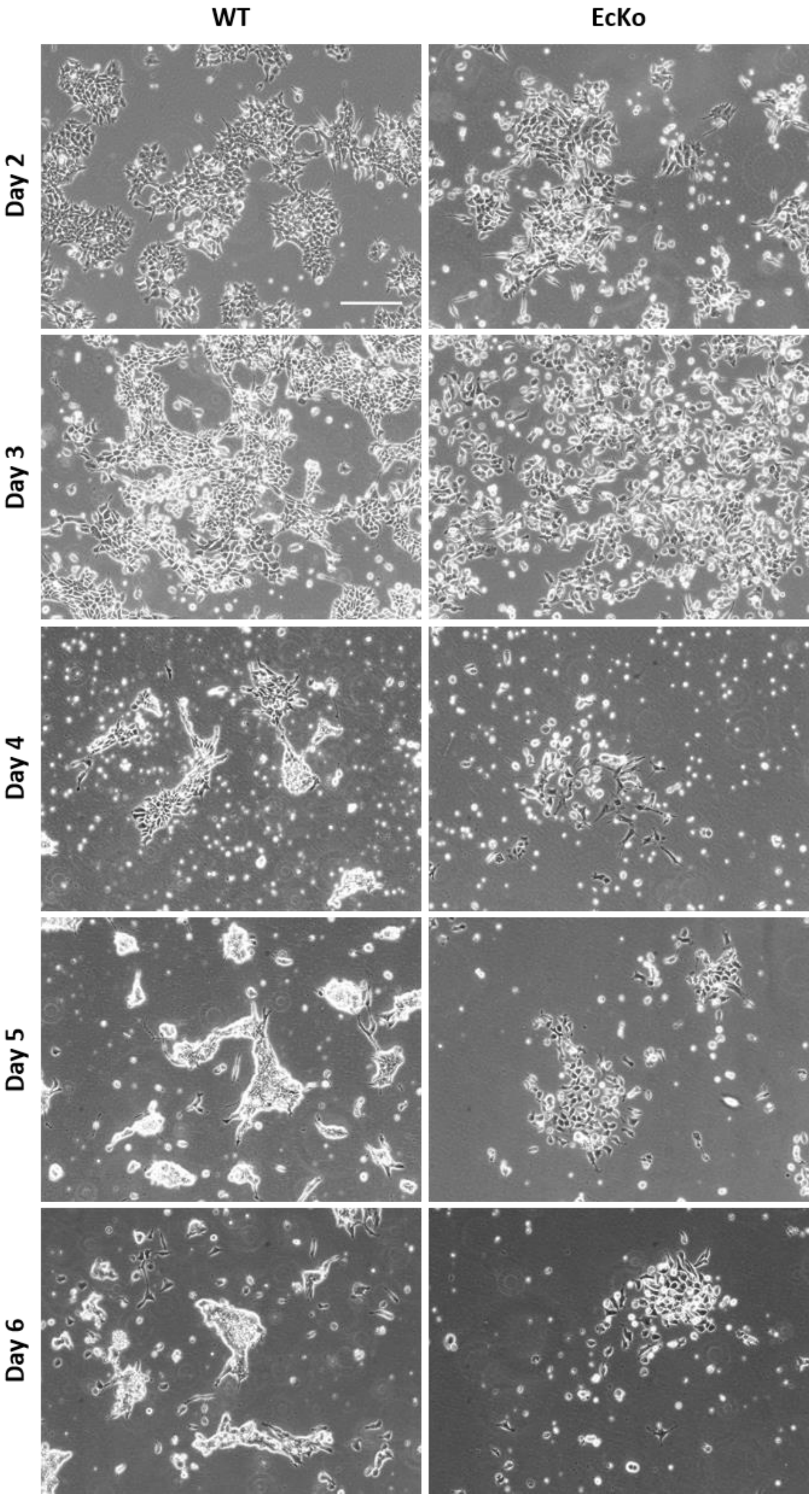

Figure 4.3: EcKO cells have poor survival during neural differentiation. *Cells were seeded into 2i-Lif conditions. After 24h, media were changed to neural differentiation medium. Extensive cell death in EcKO cells compared to control cells is apparent from day 4 onward. Scale bar=100µm*

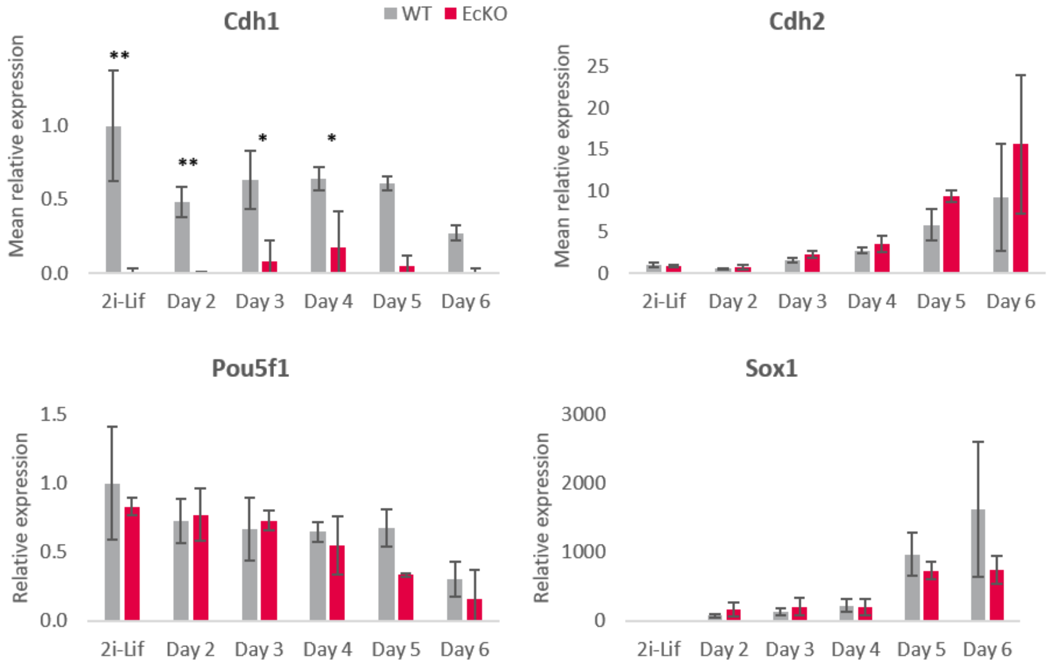

Figure 4.4: Gene expression during neural differentiation of EcKO cells. *Flox/flox (parental) and EcKO cell lines were plated at a density of 2x10^4 to 5x10^4 cells into 2i-Lif conditions in 6-well plates. The cells were incubated in 2i-Lif for 24h before a media change to neural differentiation medium (Day zero). Of six biological replicates attempted, only three produced sufficient RNA yield up to day 4, and only two had sufficient yield on days 5-6. No statistical analysis was undertaken for days 5-6. N=3 up to day 4, and N=2 or days 5-6. Error bars show standard deviation. *p≤0.05, **p≤0.01, unpaired T-test.*

4.2.3 Forced cadherin switching promotes neural differentiation

EcKO cells displayed extensive cell death during neural differentiation, suggesting that E-cadherin is required for cell stability during this process. Next, NcKI cells were used to investigate whether replacing E-cadherin with N-cadherin could make the cells more stable, and whether this forced and premature cadherin switch would have an effect on the efficiency of neural differentiation.

NcKI and WT (E14-Juo9) cells were seeded into 12-well plates at a density of 4,000 cells per well. As before, the cells were pre-incubated in 2i-Lif conditions for 24h to allow time for the cells to adhere to the plate, and media were then changed to NDiff (day 0), and dying cells were washed off and old media supplemented throughout the six-day differentiation.Lysates were collected for qPCR analysis on days two to six. While all cell lines displayed significant cell death during the differentiation protocol, substantially more NcKI cells survived until the later stages of neural differentiation than EcKO cells. Both NcKI and the WT control cell lines yielded enough mRNA for qPCR analysis on all days analysed and in all three biological replicates.

qPCR analysis found significantly lower levels of *Cdh1* transcript in the NcKI cells compared to WT (Fig. 4.5). However, some *Cdh1* expression was still detected in the NcKI cells. Since the *Cdh1* gene is still present behind a transcriptional termination sequence and not deleted from the genomic sequence of this cell line, the presence of some *Cdh1* transcript may reflect leaky termination of transcription, or alternatively, that the qPCR primers used are not completely specific. NcKI cells showed significantly higher levels of *Cdh2* expression than WT cells, as expected, though the levels of *Cdh2* detected may not be as high as expected given that expression of this gene is driven by the *Cdh1* promoter, and *Cdh1* is highly expressed in ESCs. However, on the protein level (Fig. 4.1) these cells were found to be completely negative for E-cadherin protein and showed extensive N-cadherin protein expression, as expected.

NcKI cells express significantly higher levels of the early neural markers *Sox1* and *Pax6* on days two to four of neural differentiation compared to WT cells. By days five and six, the WT cells appear to "catch up" in their levels of expression of these genes, suggesting that forced cadherin switching may accelerate the process of neural induction rather than increasing its eventual efficiency. However, *Pou5f1* (Oct4) levels were lower in NcKI cells at four time points, including 2i-Lif. This raises the alternative possibility that NcKI cells cultured in 2i-Lif may exist in a developmentally more advanced pluripotent state than WT cells, allowing them to differentiate more efficiently in permissive conditions.

To check whether the differentiation phenotype was specific to a particular lineage, the mesoderm marker *T* and endoderm marker *Sox17* were assayed. The only significant difference observed in either of these markers was at Day three for *Sox17*, where NcKI cells showed slightly but significantly higher expression of this gene compared to WT. Since no other time-point was found to have significantly different levels of these two transcripts, the results were taken to indicate that the pro-differentiation effect of NcKI is specific to the neural lineage.

Taken together, the results show that NcKI cells represent a forced, premature cadherin switch, and that this mutation promotes neural differentiation, an effect which was found to be specific for the neural lineage.

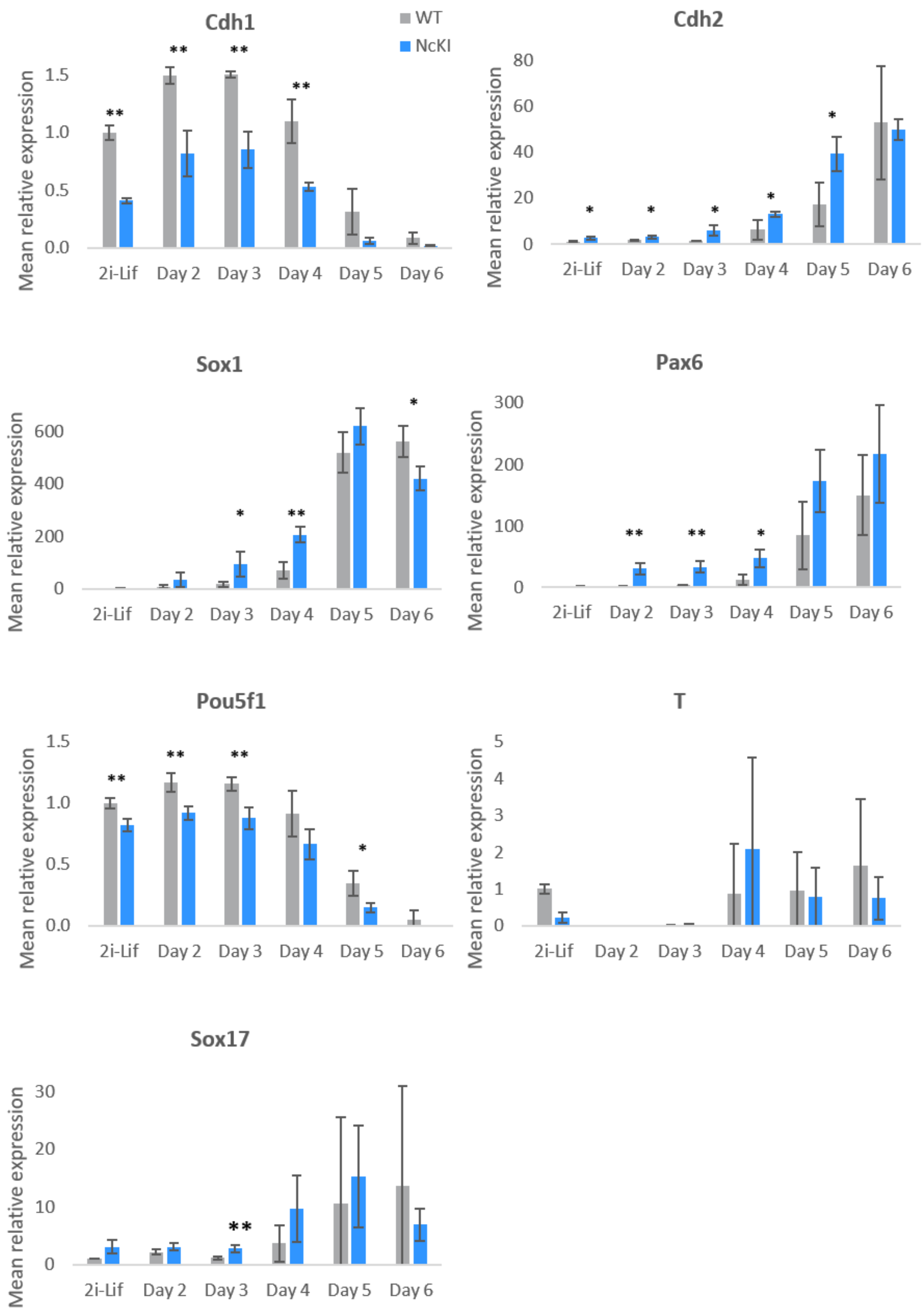

Figure 4.5: Gene expression during neural differentiation of NcKI cells. *WT (E14-Juo9) and NcKI cell lines were plated at a density of 4,000 cells into 2i-Lif conditions in 12-well plates. The cells were incubated in 2i-Lif for 24h before a media change to neural differentiation medium (Day 0). N=3 biological replicates. Error bars show standard deviation. *p≤0.05, **p≤0.01, unpaired T-test.*

4.3 Overexpression of N-cadherin promotes neural fate

4.3.1 Generation of inducible N-cadherin overexpression ES cells

The previous results in EcKO and NcKI cells indicated that while the deletion of E-cadherin led to extensive cell death, the replacement of E-cadherin with N-cadherin rescued the cell death phenotype and additionally promoted neural differentiation. This raises the question of whether the pro-neural phenotype is a result of full cadherin switching, or whether N-cadherin alone is able to promote neural differentiation. To further investigate this question, an inducible N-cadherin overexpression system was developed.

4.3.1.1 A2Lox-Ncad-HA cloning strategy

To study the effect of the gain of N-cadherin independently of any effects of E-cadherin, an inducible ES cell line for N-cadherin overexpression was generated. An Inducible Cassette Exchange (ICE) system was chosen as this system has been developed to rapidly generate ES cell lines with inducible transgenes (Iacovino et al., 2011; Iacovino et al., 2014), and has already been successfully used by other members of the lab.

Briefly, the ICE system makes use of an A2Lox mES cell line. This cell line contains an ICE locus which encodes a doxycycline (Dox)-inducible Cre ("causes recombination")-recombinase flanked by two LoxP (Locus of crossing [x] over, P1) sites (the *Cre* is flanked by LoxP sites, or "floxed")(Sternberg, 1981). Upon Dox induction, the Cre replaces itself with a targeted incoming gene of interest and repairs a downstream *Δneo* gene, rendering the recombinants resistant to G418 selection. The system can therefore be used to create transgenic cell lines that will conditionally express a gene of interest upon Dox treatment (Iacovino et al., 2014). This strategy was used to generate the A2Lox-Ncad-HA mES cell line.

For a detailed description of the cloning strategy, see Methods section 2.2.4.1. The map for the p2Lox-Ncad-HA plasmid is shown in Figure 4.6.

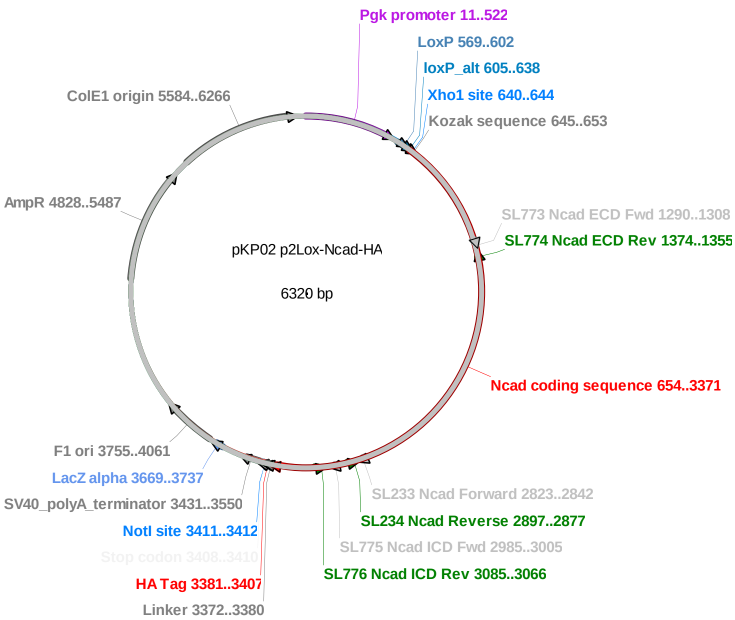

Figure 4.6: Plasmid map of the p2Lox-Ncad-HA plasmid. Cdh2 and HA coding sequences labelled in red. Sequencing primer sites labelled in light grey (forward primers) and green (reverse primers).

Upon addition of Dox to the culture media, these cells overexpress an N-cadherin protein with a C-terminal influenza virus hemagglutinin (HA) tag. The tag was inserted at the intracellular terminus of the protein to prevent it from interfering with the adhesive function of N-cadherin. The drawback of this location was that the tag could not be easily used to sort the cells by flow cytometry for further analysis. The HA tag was chosen over a larger fluorescent reporter for two reasons: the small size of the tag means that it is less likely to interfere with the intracellular functions of the tagged protein, and the use of a non-fluorescent tag allows for the simultaneous use of four fluorescent channels during ICC to visualise other proteins of interest.

A diagram of the inducible transgene locus in the A2Lox-Ncad-HA cells is presented in Figure 4.7.

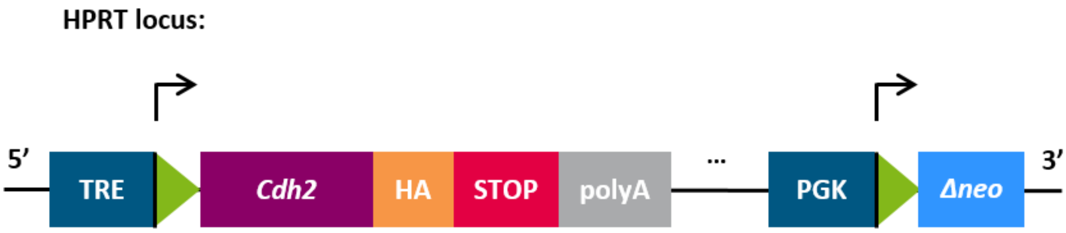

Figure 4.7: Inducible Ncad-HA transgene in A2Lox-Ncad-HA cells following ICE recombination. *The recombination site lies 5' of the HPRT locus on the x chromosome. A doxycycline-inducible promoter (*TRE*) drives the expression of the* Cdh2 *transgene with a C-terminal* HA *tag, STOP codon and polyA sequence. Addition of doxycycline induces expression of the transgene. Downstream of the HPRT site, a PGK promoter is introduced that lies upstream of a neomycin resistance gene (*Δneo*) which renders all recombinants G418-resistant.*

4.3.1.2 Validation of inducible Ncad-HA cell lines

After cloning, electroporation, selection and expansion of recombinants was completed, seven surviving clonal lines were screened for Ncad-HA expression. The clones were cultured in Lif-serum conditions with or without 1µg/mL Dox for 24-48h, stained for HA expression, and imaged on an Operetta High Content Imaging System (Perkin Elmer). The three clones with highest HA expression (numbers 4, 5 and 7) were expanded and used in all subsequent experiments (Fig. 4.8).

To confirm that the HA-tag co-localised with the expressed N-cadherin transgene, a sample of A2Lox-Ncad-HA cells were stained for both N-cadherin and HA and imaged on a Leica SP8 confocal microscope in high resolution (Fig. 4.9). The images show that un-induced cells are negative for both N-cadherin and HA staining, and that induced cells co-express both of these proteins at their cytoplasmic membranes. The 24h time point of NDiff was chosen because it is a stage where N-cadherin is not usually detected during this protocol.

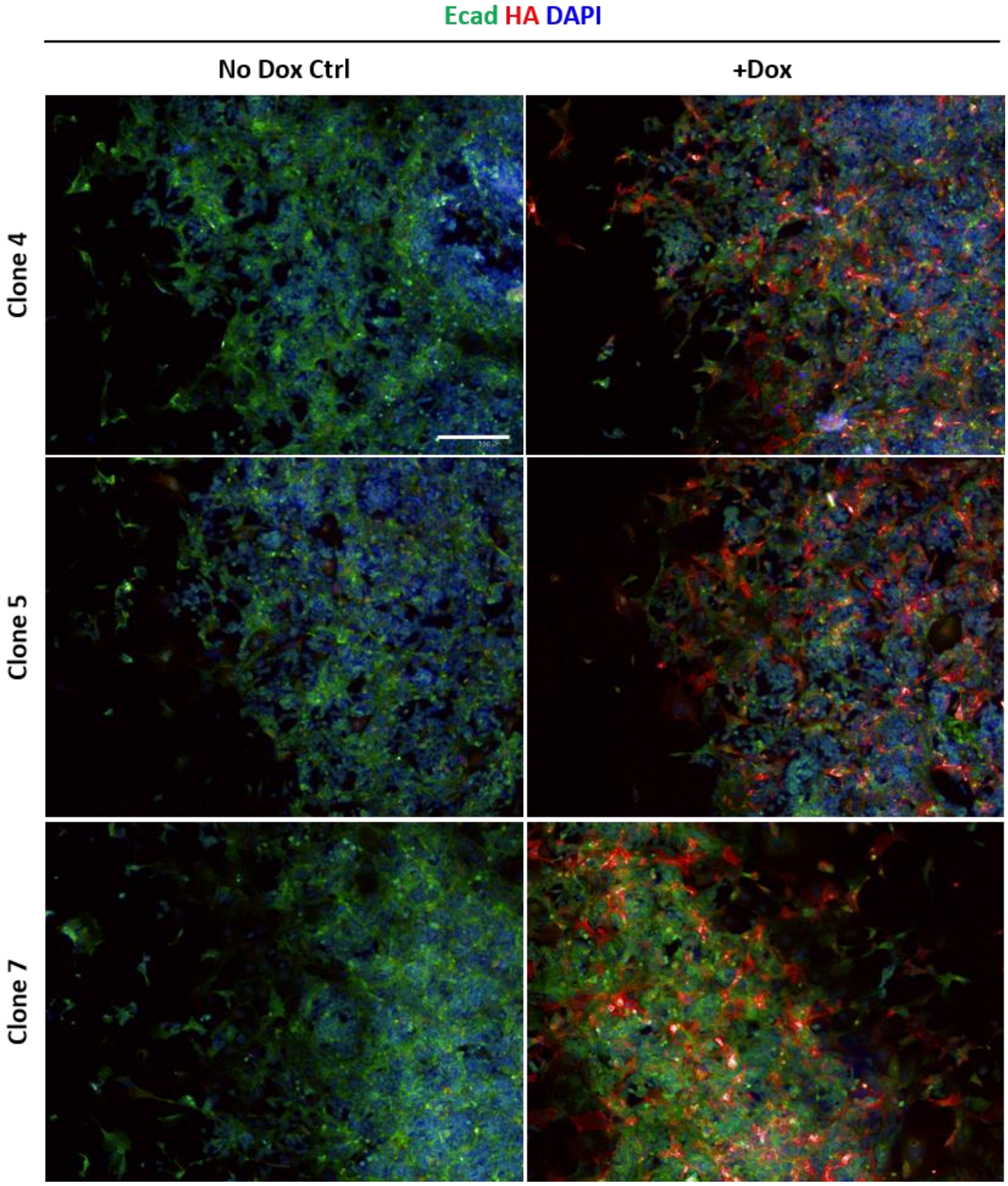

Figure 4.8: A2Lox-Ncad HA clonal cell line validation. *Cells were cultured in Lif-serum with or without a 24h pulse of1µg/mL Dox immediately before staining, and imaged on an Operetta High Content Imaging System (Perkin Elmer). Images show three clones used for all remaining experiments. Scale bar = 200µm.*

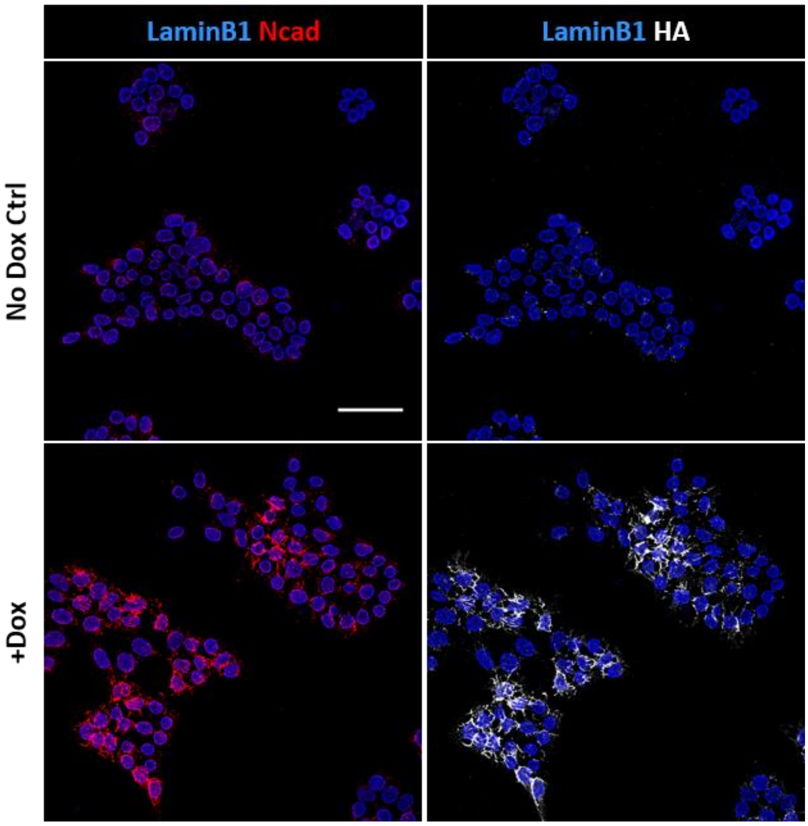

Figure 4.9: The HA-tag co-localises with N-cadherin at the membrane of A2Lox-Ncad-HA cells. *A2Lox-Ncad-HA (clone 4) cells from 2i-Lif cultured in neural differentiation medium for 24h with or without 1µg/mL Dox. Images taken on a Leica SP8 confocal microscope. Scale bar = 50µm.*

Next, the induction efficiency of the inducible overexpression cell lines was quantified. Cells were seeded into Lif-serum conditions in a 12-well plate at a density of $5x10^4$ cells per well with or without Dox. The cells were analysed for gene expression by qPCR and for HA protein expression by cytospin-staining 24 or 48h after induction (for protocol details, see Methods). qPCR analysis showed that in Lif-serum conditions, the induced cells had 2-4-fold higher *Cdh*2 mRNA levels than un-induced control cells when cultured in Dox for 24-48h (Fig. 4.10 A). Levels of *Cdh1*, *Oct4*, and *Sox1* were unaffected by Ncad-HA induction at either time point. When the cells were fixed and stained following a cytospinning protocol and manually counted for Ncad-HA expression, the three clones showed between 10-20% induction of HA protein after 24h of induction in Lif-serum (Fig. 4.10 B).

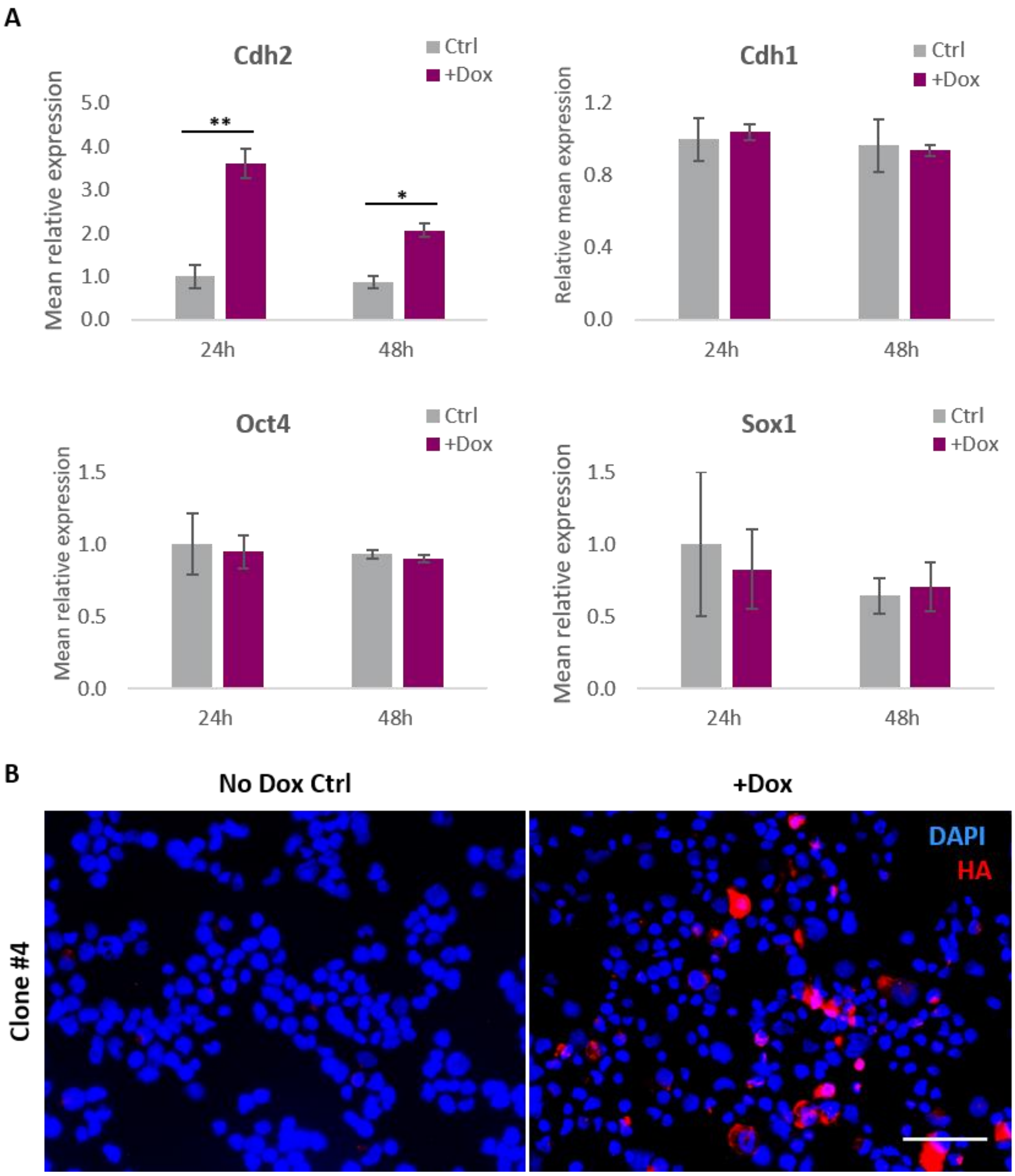

Figure 4.10: Quantification of Ncad-HA induction efficiency in Lif-serum conditions. A. *mRNA expression of A2Lox-Ncad-HA cells after 24 and 48h of induction in Lif-serum. Data normalised to ctrl 24h condition. Bars show mean relative expression for three independent clones. Error bars = SD. **p<0.01, *p<0.05, paired T-test.* ***B.*** *Example image of quantification of Ncad-HA induction efficiency in Lif-serum by cytospin. Image shows A2Lox-Ncad-HA clone 4. Cells were cultured in Lif-serum with or without 1µg/mL Dox or 24h before fixing and staining following a cytospinning protocol. Samples imaged on an Olympus IX51 fluorescent microscope. Manual quantification found 20% induction in this sample. Scale bar = 50µm.*

4.3.2 N-cadherin overexpression promotes anterior neural differentiation *in vitro*

4.3.2.1 Optimisation of Ncad-HA induction for neural differentiation

To test whether induction of Ncad-HA could be improved over the levels observed in Lif-serum, the induction protocol was further optimised for neural differentiation conditions. It was hypothesised that NDiff conditions may be more permissive for N-cadherin induction since endogenous N-cadherin is not observed in Lif-serum (Fig. 3.3 A).

Cells expanded in 2i-Lif were plated at a density of $2x10^5$ cells per well in 6-well plates and cultured in 2i-Lif conditions overnight to allow cells to adhere to the plate, before a media change to NDiff (corresponding to day zero of the protocol). Ncad-HA was induced by the addition of Dox on days two or three of the protocol, and the cells were fixed for imaging 24h after addition of Dox. Manual quantification of membrane HA staining by cytospinning found ~40% and ~20% Ncad-HA induction at the protein level when the cells were induced on days two and three, respectively (Figs. 4.11, 4.12). Induction at day two of NDiff therefore resulted in over two-fold increase in Ncad-HA expression compared to induction in Lif-serum conditions, confirming that NDiff conditions are more permissive for Ncad-HA expression (Fig. 4.12).

Finally, the timing of Ncad-HA induction was optimised with the aim of yielding the highest level of transgene expression during neural differentiation. Three clones of A2Lox-Ncad-HA cells were plated at a density of 3,000 cells per 12-well plate into 2i-Lif conditions. The cells were pre-incubated in 2i-Lif for 24h before a change to neural differentiation conditions (day zero), and Dox was added either at day zero or day two, and mRNA samples were collected on days two to six of NDiff. The day zero time point was chosen as a standard baseline, while day two was chosen because it represents a later time point where N-cadherin is not yet detectable at the protein level (Figs. 3.9 and 3.10).

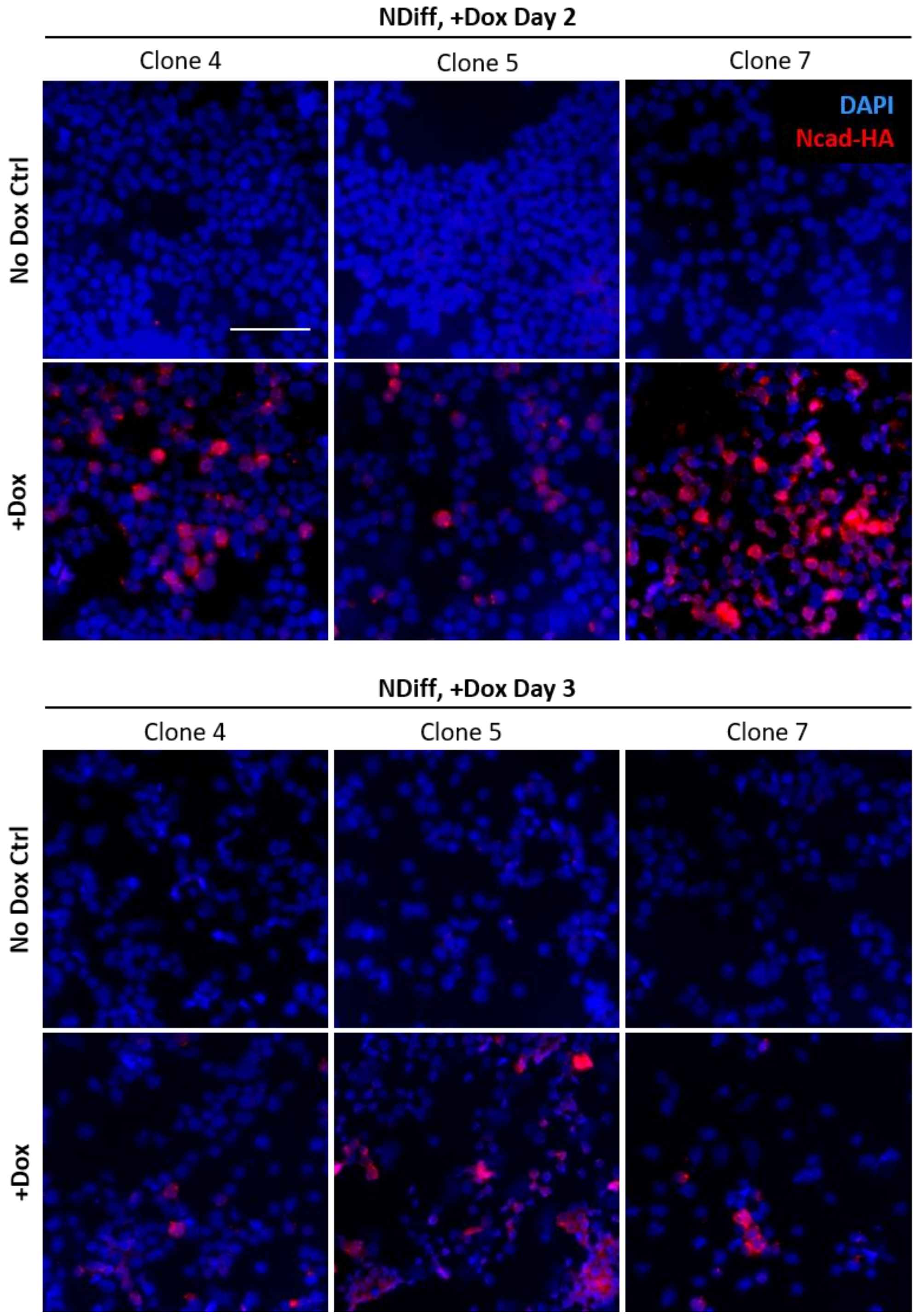

Figure 4.11: Ncad-HA induction during neural differentiation. *Cells were pre-incubated in 2i-Lif for 24h before a media change do NDiff (day 0 of the protocol). 1 µg/mL Dox was added on days 2 (upper panels) or 3 (lower panels), and cells were fixed using a cytospinning protocol 24h after addition of Dox. Stained samples were imaged on an Olympus IX51 fluorescent miscroscope. Scale bar = 50µm.*

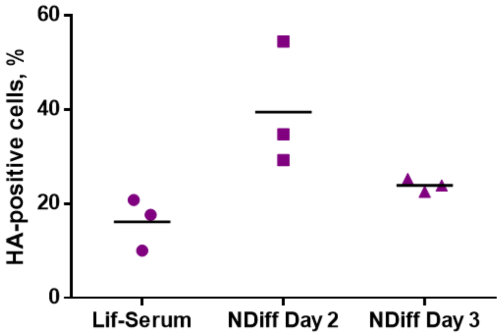

Figure 4.12: Manual quantification of Ncad-HA induction efficiency in three conditions. *Ncad-HA induction was manually quantified from images of cells fixed by cytospinning. Each point represents a single clone, lines show mean. Fixing and quantification was performed 24h after addition of Dox for each condition. N = 3 independent clones.*

qPCR analysis showed that Ncad-HA was robustly induced in both conditions following Dox treatment (Fig 4.13). When Dox was added at the beginning of the NDiff protocol (day zero), *Cdh2* expression increased 60-fold relative to 2i-Lif. By contrast, when Ncad-HA was induced on day two of NDiff, *Cdh2* expression increased over 120-fold relative to 2i-Lif, and the induced cells had between two and five-fold higher *Cdh2* expression compared to un-induced controls throughout the time-course (Fig. 4.13). The day 2 induction time-point was chosen for subsequent triplicate experiments due to higher *Cdh2* expression throughout the time-course relative to un-induced controls. The optimised experimental protocol is summarised in Figure 4.14.

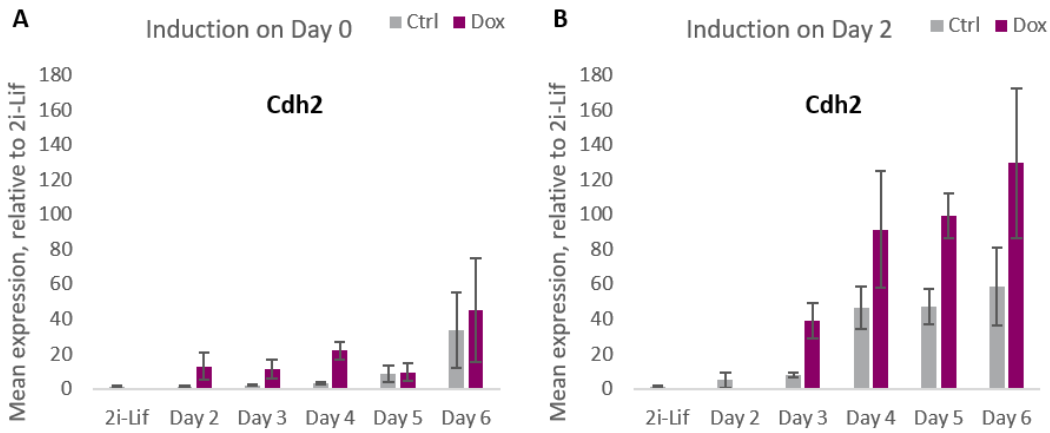

Figure 4.13: Optimisation of Ncad-HA induction during neural differentiation. *A2Lox-Ncad-HA cells were pre-incubated for 24h in 2i-Lif before change to neural differentiation medium (day 0). 1µg/mL of dox was added on either day zero (**A**) or day two (**B**), and samples were collected for qPCR analysis on days two to six. Data normalised to Ctrl 2i-Lif condition. N=3 independent clones, error bars = SD.*

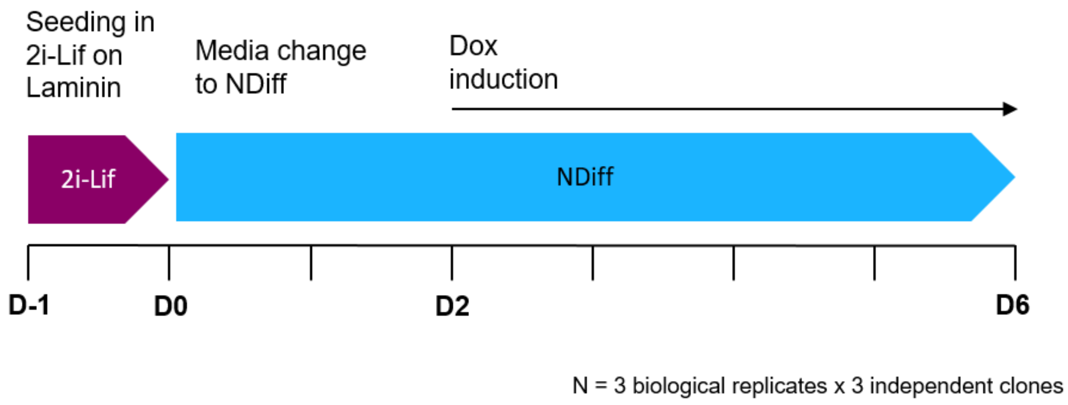

Figure 4.14: Optimised neural differentiation protocol for inducible N-cadherin overexpression cells. *A2Lox-Ncad-HA cells are seeded into 2i-Lif conditions at a density of 3,000 cells per well in a 12-well plate into 2i-Lif conditions on a laminin coating. The cells are pre-incubated for 24h in 2i-Lif to allow proper attachment to the matrix. After 24h, media are changed to neural differentiation media. Doxycycline is added at 1µg/mL on day two, and continues to be replenished every time that media are changed. Cells are lysed for qPCR analysis on days three to six. Uninduced cells are lysed in a 2i-Lif control population and on days two to six. N = 3 biological replicates x 3 independent clones.*

4.3.2.2 N-cadherin overexpression promotes neural fate during anterior neural differentiation

Once the neural differentiation protocol for the inducible N-cadherin overexpression cell lines was optimised, a triplicate experiment was set up. Three independent A2Lox-Ncad-HA clonal cell lines were used in three side-by-side biological replicates. All nine replicates were then analysed in a single qPCR analysis, and the resulting readings were normalised to the geometric mean of two housekeeping genes (*SDHA* and *TBP*). To factor in the variation between different replicates of neural differentiation (as discussed in Chapter 3), a mean of the three normalised expression values for each clone was calculated. Following this, a mean and standard deviation were calculated for the average expression of each clone. Finally, the 2i-Lif reading for each gene was set as 1, and all other readings were set relative to the 2i-Lif expression value.

To assess significance between control and experimental conditions, an unpaired T-test was performed on the mean expression values of the three clones used. Therefore, while the data are representative of a total of nine samples (three biological replicates of three independent clones), the sample size for the significance calculations, and for the mRNA expression data summarised in Figure 4.15, is formally three.

The qPCR analysis showed that inducing the expression of Ncad-HA on day two of the protocol produced a significant and robust upregulation of *Cdh2* within 24h in the induced cells compared to uninduced cells, and this overexpression lasted for the remaining duration of the time course. Next, the effect of *Cdh2* overexpression on the levels of other genes of interest was investigated.

Levels of both *Cdh1* and *Pou5f1* decreased in response to *Cdh2* overexpression. Within 48h of Ncad-HA induction this decrease was significant, and remained so until the end of the experiment on day six. The drop in levels of *Pou5f1* suggests that the induced cells are exiting pluripotency faster or more efficiently than the un-induced controls. The drop in levels of *Cdh1* occurred in synchrony with that of *Pou5f1*, as previously observed (Malaguti et al., 2013).

Next, two early neural markers, *Sox1* and *Pax6*, were assayed to investigate the role of N-cadherin overexpression on neural differentiation. Both of these markers were significantly upregulated within 24h of N-cadherin induction compared to un-induced controls, and remained that way up to day five of the time-course. These results show that the overexpression of N-cadherin either promotes or accelerates the expression of early neural markers during anterior neural differentiation, suggesting that N-cadherin may play a role in promoting neural fate during this process.

To investigate whether this effect was specific to the neural lineage, marker genes for other germ layers were assayed – *T* for mesoderm, *Dlx5* for surface ectoderm, and *Sox17* for endoderm. No significant differences were observed in the levels of these genes in the induced cells compared to their un-induced controls, suggesting that the effect of N-cadherin is specific to the neural lineage in this experimental system.

Finally, the expression levels of marker genes of two signalling pathways were assayed to investigate whether these pathways may play a mechanistic role in the pro-neural effect of N-cadherin. Levels of *Axin2*, a key readout gene of the canonical WNT pathway, were not found to differ significantly between induced and un-induced cells. Next, levels of *Egr1* and *Dusp4*, early and late targets of the FGF pathway, respectively (according to unpublished data from Tilo Kunath), were assayed. On day three, levels of *Egr1* were slightly but significantly higher in induced cells, while on day four the levels of this gene were significantly lower in these cells, suggesting fluctuations in FGF signalling as a result of N-cadherin overexpression. Levels of *Dusp4* were reduced in induced cells on days four to six, and this downregulation was statistically significant on days four and six, suggesting that N-cadherin may cause a dampening of FGF responsiveness.

Taken together, the results of the triplicate qPCR analysis of N-cadherin overexpression during monolayer neural differentiation suggest that N-cadherin alone is able to promote neural induction, and that this effect is specific to the neural lineage. Analysis of signalling readout genes showed that overexpression of N-cadherin may lead to changes in FGF signalling.

4.3.3 N-cadherin overexpression promotes neural specification in neuro-mesodermal progenitors (NMPs)

4.3.3.1 Protocol for generation and analysis of NMPs from ES cells cultured in 2i-Lif

Previous results suggested that the overexpression of N-cadherin promotes induction into the neural lineage during anterior neural differentiation. Next, the ability of N-cadherin to influence lineage choice during another developmental process was investigated. A system for the generation and maturation of putative neuro-mesodermal progenitors (NMPs) was recently developed in the lab (Watson, 2018), and this system was used to investigate whether the overexpression of N-cadherin could also promote neural fate in this developmental context.

NMPs are bipotent progenitor cells that can give rise to either neural or mesodermal cells (Gouti et al., 2014; Tzouanacou et al., 2009). *In vivo*, they are a transient population emerging between E8.5-E13.5 that enables the elongation of axial tissues (Cambray and Wilson, 2002; Cambray and Wilson, 2007; Gouti et al., 2017; Wymeersch et al., 2016). Importantly for this study, the maturation of NMPs (occurring between E8.5 and E9.5) is accompanied by an E- to N-cadherin switch (Gouti et al., 2017). This led to the question of whether cadherin switching can bias lineage choice in maturing or differentiating NMPs.

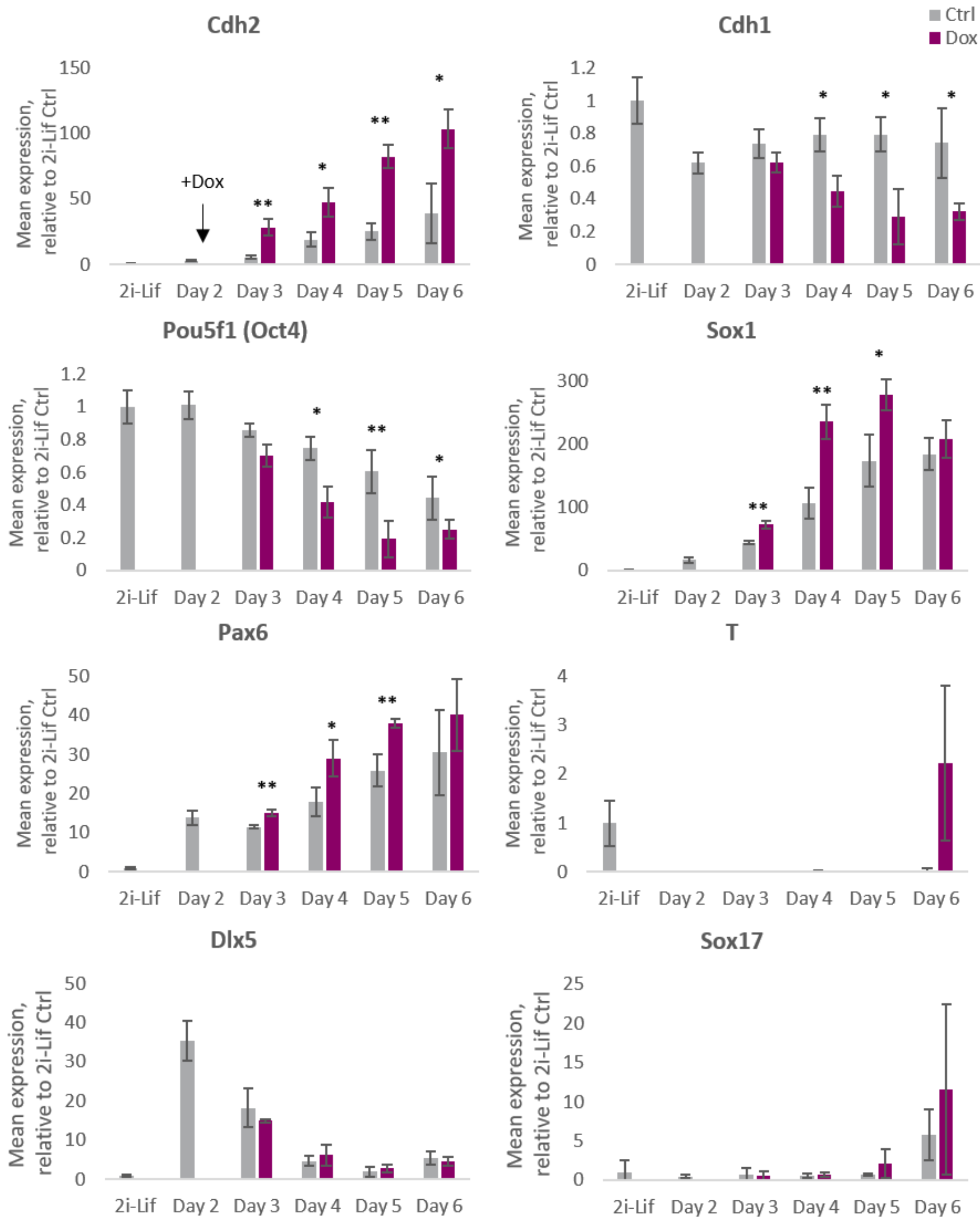
Cdh2
Cdh1
Ctrl
Dox
+Dox
Mean expression, relative to 2i-Lif Ctrl
2i-Lif
Day 2
Day 3
Day 4
Day 5
Day 6
Pou5f1 (Oct4)
Sox1
Pax6
T
Dlx5
Sox17

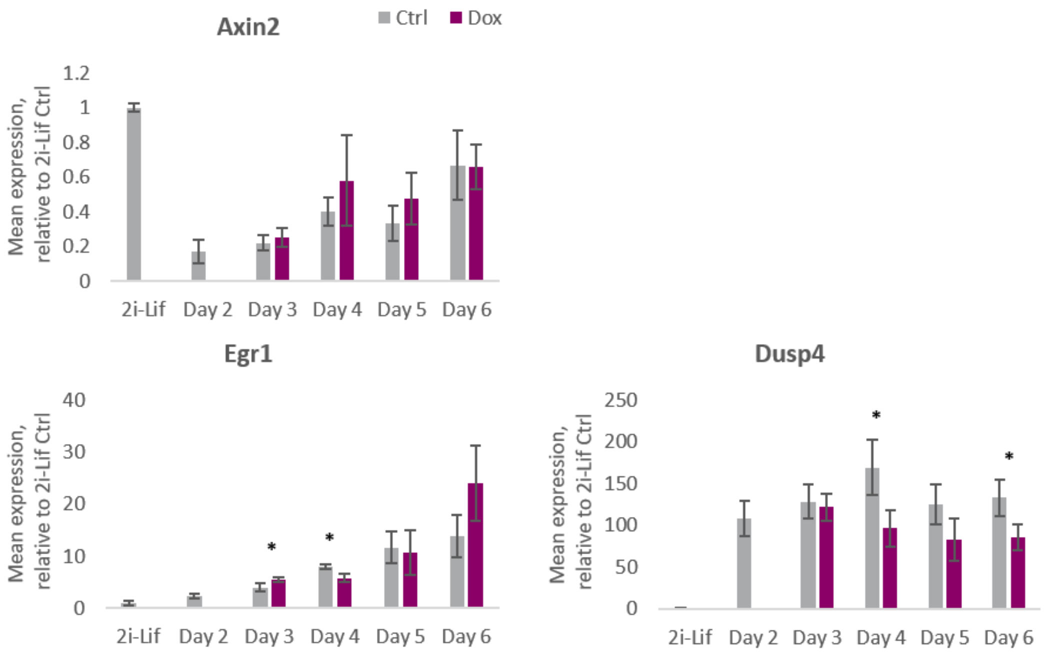

Figure 4.15 (pages 137-138): Changes in gene expression during neural differentiation in response to N-cadherin overexpression. *A2Lox-Ncad-HA cells were used to induce N-cadherin overexpression according to an optimised neural differentiation protocol. Dox was added at 1µg/mL on day two. N=3 mean readings covering biological replicates of three independent clones. Data normalised to Ctrl 2i-Lif condition. Error bars = SD, **p<0.01, *p<0.05, unpaired T-test.*

Several *in vitro* protocols have been developed to study the maturation and differentiation of NMPs for both mouse and human systems (Gouti et al., 2014; Tsakiridis and Wilson, 2015; Turner et al., 2014). They involve the use of an EpiSC population as a “proxy” for the embryonic epiblast, followed by exposure to FGF2 and Chiron (a GSK3B inhibitor) to generate NMPs (Gouti et al., 2014; Henrique et al., 2015). More recently, a protocol for generating putative NMPs has been developed in our lab by Julia Watson which uses an Epi-like stem-cell (EpiLSC) population generated from 2i-Lif cells as the epiblast-like starting population (Watson, 2018). I adapted this protocol for use with A2Lox-Ncad-HA cells to investigate how N-cadherin overexpression in early NMPs affects their maturation and commitment to the two daughter lineages. It was hypothesised that N-cadherin overexpression may promote the bi-potent NMP state, since cadherin switching accompanies the maturation on NMPs *in vivo* (Gouti et al., 2017). Alternatively, N-cadherin overexpression could promote the neural lineage, as observed in anterior neural differentiation.

Briefly, A2Lox-Ncad-HA cells cultured in 2i-Lif are seeded onto fibronectin at a density of 4,750 cells per well of a 12-well plate into EpiLC medium containing KOSR, FGF2 and Activin. After 48h, the cells have matured into EpiLCs, and the medium is change to NMP medium containing double the amount of FGF2 and additional Chiron. Culture for 48h in this medium generate immature NMPs- at this point, Dox is added to induce the overexpression of N-cadherin. After 24h of induction, the cells correspond to mature NMPs, and are fixed and stained for two markers of NMP lineage fate: *T* and *Sox2*. Double-positive cells correspond to bi-potent putative NMPs, while cells that are single-positive for *T* and *Sox2* are assumed to have committed to mesoderm or neural fate, respectively. The protocol is summarised in Figure 4.16.

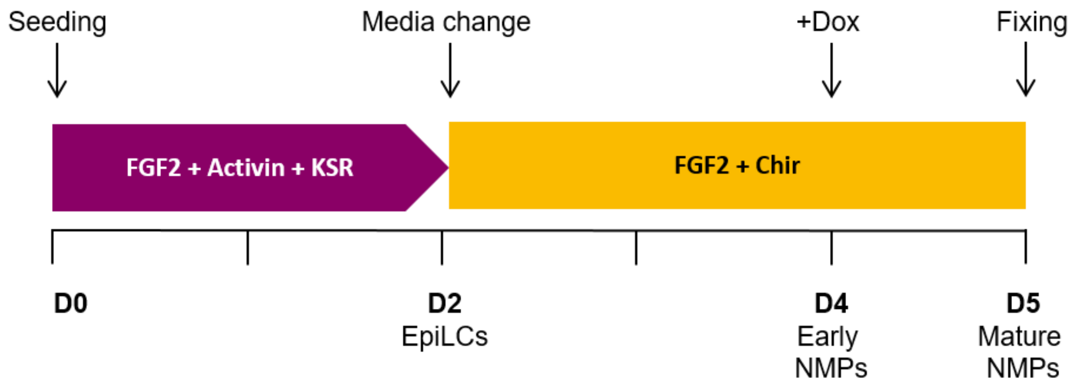

Figure 4.16: Protocol for generation and maturation of NMPs. *A2Lox-NCad-HA cells cultured in 2i-Lif were seeded onto fibronectin in EpiLC conditions containing FGF2, Activin and KOSR. On day two, media are changed to NMP medium containing double the dose of FGF2 and Chiron. On day four, Dox is added at 1µg/mL to induce the expression of Ncad-HA. Cells are fixed on day five and stained for ICC analysis.*

Following fixation, the cells were stained for T, Sox2, HA and DAPI, and were analysed using an Operetta high content imaging system and analysed using the corresponding Columbus® image analysis software (Perkin Elmer). Twelve fields of view were imaged and analysed per well. The design of the nuclear intensity analysis pipeline is described in Methods. The pipeline includes a nuclear segmentation module that assigns individual DAPI-stained nuclei and is designed to filter out regions where segmentation quality is poor (Fig. 4.18). After segmentation, Brachyury and Sox2 intensity thresholds were set empirically for each experiment by using internal controls in the stained samples- these were cells that were visibly and clearly either positive or negative for the given protein.

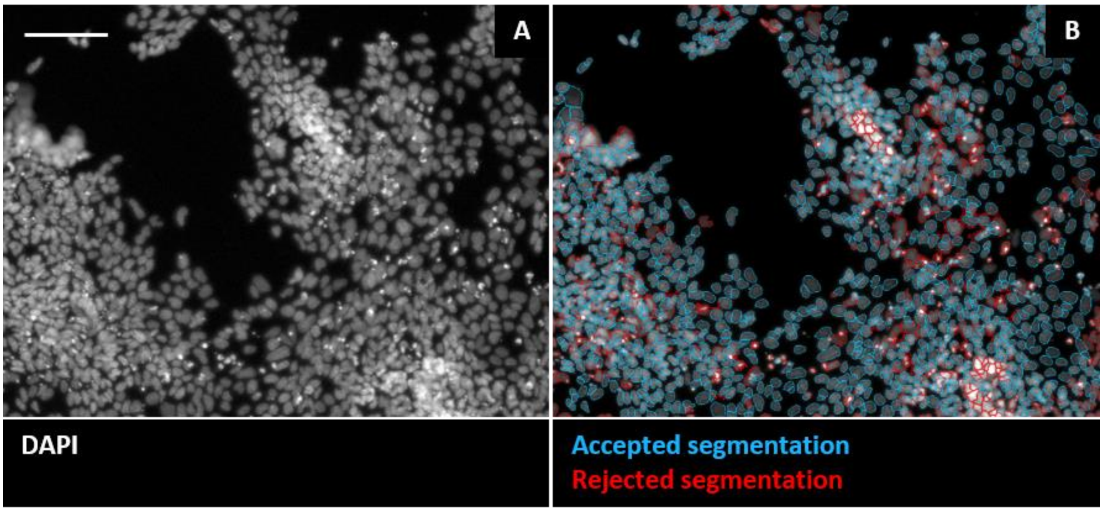

Figure 4.17: Example nuclear segmentation on Columbus® software. A. *DAPI staining of A2Lox-Ncad-HA cells cultured following the optimised NMP protocol.* ***B.*** *Segmentation performed by Columbus software. Incorrectly segmented nuclei were rejected based on size, roundness, and DAPI intensity. Scale bar = 100µm.*

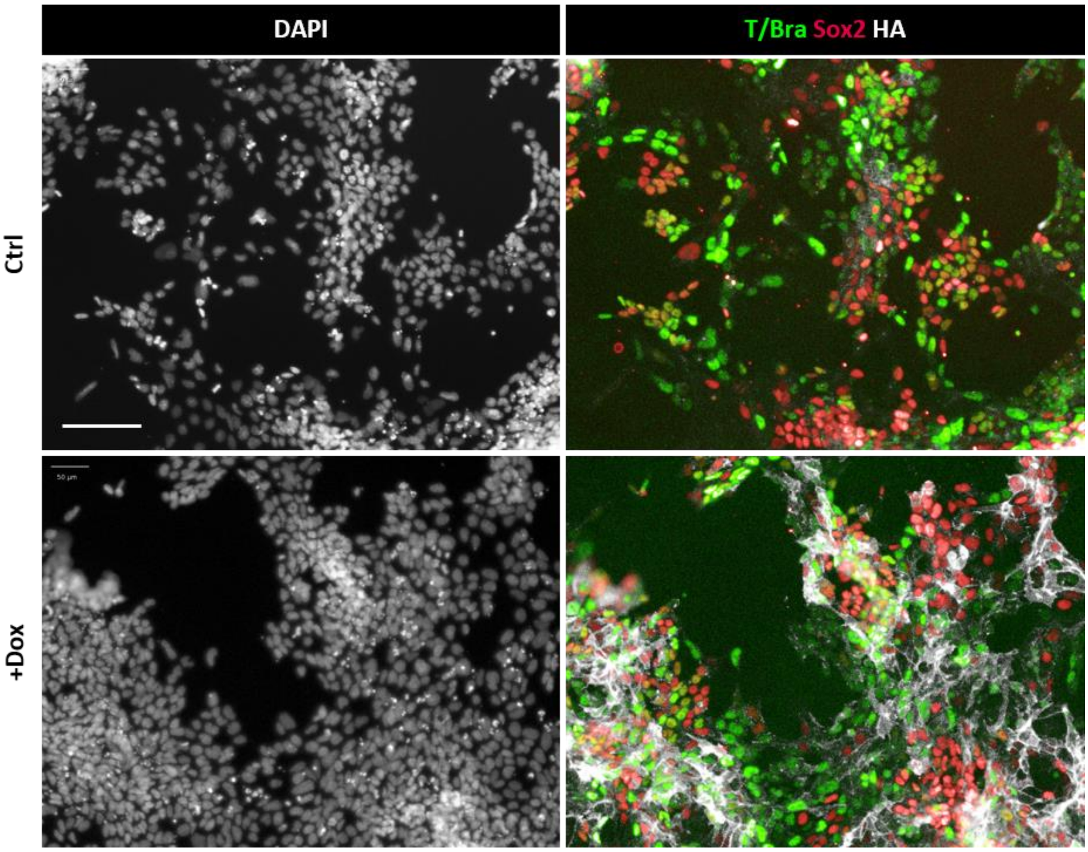

Figure 4.18: Mature NMPs generated from A2Lox-Ncad-HA cells co-stained for T, Sox2 and HA. *Images show cells from clone 5 with or without Dox induction (top and bottom panels, respectively). Scale bar = 100µm.*

Brachyury, Sox2, and HA co-staining showed that at day five of the NMP protocol, cells heterogeneously expressed Brachyury and Sox2 (Fig. 4.18, top right panel). Many cells also co-expressed these two proteins, suggesting that they had a bi-potent NMP identity. Induced cells were found to express high levels of HA at their membranes within 24h of addition of Dox (Fig. 4.18, bottom right panel).

Next, to investigate whether N-cadherin overexpression led to lineage bias in maturing NMPs, single and double expression of Brachyury and Sox2 was quantified in Columbus and compared between induced and un-induced samples. Three A2Lox-Ncad-HA clones were used in each biological replicate. A total of seven independent biological replicates were performed and analysed, yielding 21 independent data points for each condition. These data are summarised in Figure 4.19.

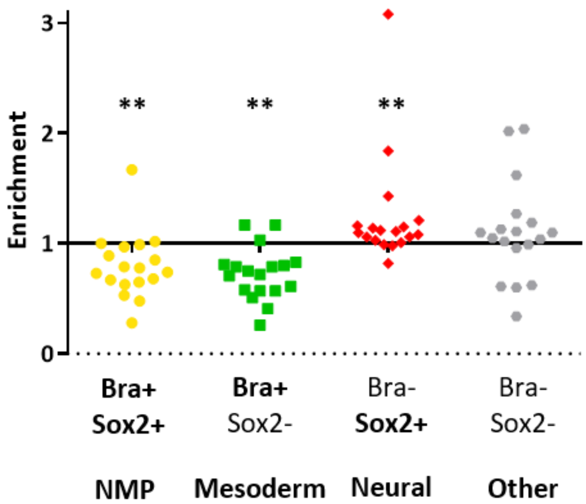

Figure 4.19: Change in Bra and Sox2 co-expression in response to N-cadherin over-expression during maturation of NMPs. *Points show enrichment of the given Bra/Sox2 identity in N-cadherin over-expressing condition compared to un-induced control. Data show seven biological replicates of three independent clones. N=21, **p≤0.01, unpaired T-test.*

The results showed that there was no significant change in the number of double positive or double negative cells following the N-cadherin overexpression. However, the induced cell populations were found to contain significantly fewer Brachyury single-positive cells and significantly more Sox2 single-positive cells than the un-induced wells. These results suggest that overexpression of N-cadherin during the maturation of NMPs biases cell fate towards the neural lineage, at the expense of the mesodermal lineage.

However, it should be noted that a significant amount of variability in protein expression was observed between individual biological replicates. Additionally, some of the un-induced samples had very low levels of double-positive cells, suggesting that there may have been a problem with the NMP induction protocol, or the thresholds used for analyses, in these replicates. Additionally, the number of cells expressing Brachyury appears to be low compared to previously optimised protocols (Gouti et al., 2014). In general, a trend for fewer double-positive cells in the induced samples can be observed, however this negative trend is non-significant due to a few large outliers. Overall, the results suggest that overexpression of N-cadherin leads to a bias in the neural lineage over the mesodermal lineage, though a different or more optimised system may have to be used to generate a more reliable and reproducible dataset in order to confirm these findings.

4.4 Discussion

4.4.1 Loss of E-cadherin leads to instability during neural differentiation

Previous studies in our lab have showed that blocking E-cadherin leads to faster, more synchronous neural differentiation from a Lif-serum starting population (Malaguti et al., 2013). This led us to hypothesise that deleting E-cadherin in ES cells would also promote neural differentiation.

The EcKO cells generated by collaborators (Pieters et al., 2016) were found to be stable in pluripotent cultures, both in Lif-serum and 2i-Lif conditions and could self-renew over several passages. In ICC validation of the cells, the EcKO cells appear to upregulate endogenous N-cadherin to a higher level than their parental cell line- this is an effect previously reported in ES cells lacking E-cadherin (Hawkins et al., 2012).

When the EcKO cells were cultured from 2i-Lif through a neural differentiation protocol, they showed very poor survival (Fig. 4.3), and the protocol had to be scaled up and repeated multiple times to yield enough mRNA for robust qPCR analysis. The analysis found that the surviving cells could upregulate *Cdh2* and the neural marker *Sox1,* and downregulate the pluripotency marker *Pou5f1*, but these changes occurred at similar levels to parental control cells (Fig. 4.4). These results showed that in the experimental system used, while loss of E-cadherin caused cells to become extremely unstable during neural differentiation, the mutation did not appear to either promote or inhibit commitment to the neural lineage.

Similarly, studies *in vivo* have also shown that a loss of E-cadherin leads to instability at several stages during early development, from the pre-implantation stages and beyond gastrulation; these phenotypes appear to involve both adhesive and signalling functions, as rescuing adhesion by knocking in other cadherin species rescues some adhesive functionality but ultimately still leads to embryonic lethality at several stages in early development (Basilicata et al., 2016; Bedzhov et al., 2012; Bedzhov et al., 2013; Kan et al., 2007; Larue et al., 1994; Larue et al., 1996). These reports support the view that E-cadherin is necessary for tissue stability, and the current results suggest that loss of E-cadherin leads to poor cell survival during neural differentiation.

However, *in vitro* studies of the role of E-cadherin in the maintenance of and exit from pluripotency offer contradictory results. In particular, one study found that the same E-cadherin-null cells used here can retain *Pou5f1* expression even after 30 days of culture as EBs in differentiation conditions, and fail to upregulate lineage markers (Pieters et al., 2016). In contrast, our findings show that under certain conditions, these cells are able to downregulate *Pou5f1* and upregulate neural markers at a similar rate to control cells. However in the present study, cellular survival was the limiting factor for this differentiation.

Taken together, the findings of the current study and previous reports paint a muddled picture for the role of E-cadherin during neural differentiation, with some identifying it as an inhibitor, and others, as a promotor of the process. Since the survival issue presented an obstacle for neural differentiation of these cells, we shifted our focus to studying the NcKI cells. The cell death phenotype observed in EcKO cells is rescued in NcKI cells, allowing for the investigation of any differentiation bias in these cells in the absence of the confounding effect of the apoptosis phenotype.

4.4.2 Cadherin replacement rescues cell stability and promotes neural differentiation

NcKI cells have been previously studied at pre-implantation and post-gastrulation stages *in vivo*, and were used to show that E-cadherin is critical for trophectoderm formation and necessary for germ layer maturation at E8.5 (Basilicata et al., 2016; Kan et al., 2007). However, they have not previously been used in the context of *in vitr*o neural differentiation, and they were an attractive model for the current study as they represent a forced, premature cadherin switch, similar to that observed in neural differentiation and the E8.5 neural tube (Chapter 3).

During neural differentiation, NcKI cells expressed significantly higher mRNA levels of early neural markers at the earliest time-points of the differentiation protocol, without a major effect on markers of other lineages. They also expressed consistently lower levels of

Pou5f1 throughout the time-course, from 2i-Lif up to day five of the protocol. There are two mechanistic explanations for this observation: first, that the NcKI mutation may accelerate the process of lineage priming and subsequent differentiation; and second, that the NcKI mutation causes cells to exist in developmentally later stage than WT cells cultured in the same pluripotent condition. A combination of these causes may also be plausible.

Indeed, it has been reported that cells lacking E-cadherin have a more EpiSC-like gene expression profile (Soncin et al., 2011), supporting the second mechanism. This explanation is additionally supported by the fact that NcKI cells already express significantly lower levels of *Pou5f1* in 2i-Lif conditions (Fig. 4.5), suggesting that they may be more "poised" for differentiation than WT cells.

The fact that EcKO cells did not display an overt differentiation bias while NcKI cells did suggests that the gain of N-cadherin is the main contributing factor for the observed phenotype. However, it is also plausible that knock-in N-cadherin may be rescuing cell stability during differentiation, while the loss of E-cadherin may be a contributing factor to a pro-neural effect, as seen in Malaguti et al. 2013. Indeed, numerous studies have shown that N-cadherin plays an important role in the suppression of apoptosis in various cancer cells (Wheelock et al., 2008). To attempt to uncouple these two possible mechanisms, the N-cadherin overexpression cell line was generated to examine the effects of N-cadherin gain-of-function without changing endogenous levels of E-cadherin.

4.4.3 N-cadherin overexpression biases differentiation towards the neural lineage in two developmental contexts

The development of the A2Lox-Ncad-HA cell line allowed for the study of the effects of N-cadherin overexpression at a precise experimental time-point. In Lif-serum conditions, a minority of induced cells expressed N-cadherin at the protein level, which corresponded to a roughly four-fold increase in mRNA expression (Figs. 4.10-12). This overexpression did not give rise to changes the expression of other genes, including *Pou5f1* and *Cdh1*, as reported previously (Takehara et al., 2015). This result suggests that any pro-differentiation effect of N-cadherin is not strong enough to affect the pluripotent gene regulatory network in ES cells cultured in Lif-serum.

By contrast, within 48h of N-cadherin induction in neural differentiation conditons, *Cdh1* and *Pou5f1* expression was significantly reduced in the induced cells (Fig. 4.15). It is unclear whether the downregulation of *Cdh1* is a direct effect of N-cadherin, as observed in human squamous carcinoma cells (Islam et al., 1996), or whether it simply accompanies the loss of *Pou5f1* as the cells exit pluripotency (Malaguti et al., 2013). In other contexts, such as human breast cancer cell lines, overexpression of N-cadherin does not always lead to downregulation of E-cadherin (Hazan et al., 2000; Nieman et al., 1999).

In addition to the downregulation of pluripotency markers, N-cadherin induction was also found to cause the upregulation of early neural markers, but not markers of other lineages, showing that N-cadherin alone can promote neural fate in permissive conditions. N-cadherin is known to play an important role in the development of the nervous system by promoting the growth of neurons, a mechanism that has been linked to N-cadherin coupling with FGF receptors (Doherty et al., 2000; Nguyen and Mège, 2016; Williams et al., 2001). Indeed, significant changes were observed in two FGF pathway readout genes in the N-cadherin overexpression time-course, suggesting that FGF signalling may play a role in this context. In the following chapter, the mechanism behind the pro-neural effect of N-cadherin during monolayer neural differentiation is investigated in greater detail.

In addition to EMT and early neural differentiation, cadherin switching is also reported to occur in embryonic development during the maturation of NMPs (Gouti et al., 2017). Since a system for the studying NMP maturation in vitro had been recently optimised by a current lab member (Watson, 2018), N-cadherin overexpression was additionally investigated in this context. The analysis found that induction of N-cadherin during NMP maturation caused a significant drop in the numbers of cells single-positive for Brachyury, and a significant increase in the proportion of cells single-positive for Sox2 (Fig 4.19). The trends in the data imply that fewer cells express Brachyury as a result of N-cadherin induction, either alone or in combination with Sox2. This result suggests that N-cadherin promotes induction into the neural lineage during NMP maturation and differentiation.

The mechanism for this NMP fate bias remains was not further investigated. The fate decisions of NMPs are delicately balanced *in vivo* by complex gene regulatory network (Gouti et al., 2017), and it is possible that an overexpression of N-cadherin may tip this balance in favour of the neural lineage, or perhaps accelerate neural differentiation at the expense of mesodermal differentiation. A study in chick embryos found that FGFR1 promoted the elongation of the anterior nervous system (Mathis et al., 2001); since N-cadherin is known to interact with FGFR1 in other contexts relating to pluripotency and nervous development

(Takehara et al., 2015; Williams et al., 2001), it is plausible that an interaction between N-cadherin and this receptor may be driving the neural bias in NMPs observed in the current study.

However, there were some caveats in the experimental set-up that would have to be addressed to further analyse the mechanism behind this phenotype. Specifically, the number of cells expressing Brachyury is lower than expected in the NMPs, either on its own or in combination with Sox2. The published protocol for in vitro derivation of NMPs from EpiSCs yields a very high proportion (nearly 100%) of double-positive cells (Gouti et al., 2014), while the protocol used here gave rise to fewer Brachyury-expressing cells: in some experimental replicates, the total percentage of cells expressing Brachyury, either alone or in combination with Sox2, was below 10%. Furthermore, the extent of variation in the proportion of cellular identities between experiments suggests that the experiment could be optimised further to yield more consistent cell populations. In addition, the putative NMPs generated from an EpiLC intermediate through this protocol have not been validated *in vivo*, and therefore cannot be confidently deemed to be true bipotent progenitors.

In conclusion, the overexpression of N-cadherin was found to have significant pro-neural effects *in vitro*, both during anterior neural differentiation and during the maturation of putative NMPs generated from an EpiLC intermediate. These results show that in permissive conditions, N-cadherin alone is able to promote neural fate in two developmental contexts. However, due to the combination of experimental shortcomings around the NMP protocol used here, the mechanisms behind the pro-neural effect of N-cadherin in NMPs were not studied further. In the following chapter, the signalling effects of N-cadherin during neural differentiation will be investigated.

Chapter V – Effects of cadherin switching on signalling

5.1 Introduction & aims

In the previous chapter, it was established that both full cadherin switching, and the gain of N-cadherin on its own, are able to promote induction into the neural lineage during neural differentiation *in vitro.* Cadherins are traditionally regarded as cell-cell adhesion molecules, but a growing body of evidence is showing that they can also perform signalling functions in addition to – and independently of – their role in adhesion. Is the pro-neural effect of cadherin switching therefore a result of changes in adhesion or signalling?

Both the adhesive and signalling functions of E-cadherin have been shown to be critical for early embryonic development, as mutations targeting either function result in gross morphological disruption, developmental defects, and embryonic lethality (Basilicata et al., 2016; Bedzhov et al., 2012; Larue et al., 1994; Larue et al., 1996). E-cadherin has been linked to signalling through the IGF and EGF pathways by forming complexes with their receptors (Bedzhov et al., 2012; Pece and Gutkind, 2000). E-cadherin has also been linked to the WNT pathway through its association with and release of β-catenin at the cytoplasmic membrane, allowing this protein to perform nuclear signalling functions (Gottardi et al., 2001; Howard et al., 2011).

However, since both NcKI cells and N-cadherin overexpressing cells display a pro-neural effect, the focus shifts to the role of N-cadherin in producing this phenotype. Embryos lacking N-cadherin die by E10 due to developmental defects of the heart, but also display malformed somites and yolk sac deformities. The lethality is mostly ascribed to adhesion defects in the heart, where cardiac myocytes dissociate from one another and the heart tube fails to develop normally (Radice et al., 1997). This lethality can be rescued by knocking in E-cadherin, supporting the view that impaired adhesion, and not an N-cadherin specific signalling function, is responsible for the phenotype (Luo et al., 2001).

Nevertheless, N-cadherin also has functions in signalling. N-cadherin has been shown to interact with the FGF receptor and promote signal transduction through it, in contrast to E-cadherin which signals through the EGF receptor (Fedor-Chaiken et al., 2003; Hazan and Norton, 1998; Hoschuetzky et al., 1994; Williams et al., 1994). N-cadherin can also regulate

WNT/β-catenin signalling in neural precursor cells through an Akt-dependent mechanism (Zhang et al., 2010). These signalling interactions have been linked to several physiological processes, including neuronal growth and differentiation (Nguyen and Mège, 2016; Williams et al., 2001; Zhang et al., 2010). Additionally, N-cadherin activation and use of N-cadherin-coated surfaces has been linked to reduction in Rho/ROCK signalling, leading to reduced apoptosis and increased neurite outgrowth in neural precursor cells (Haque et al., 2015).

In summary, there are several putative mechanisms that may be causing the pro-neural effect observed in cells undergoing cadherin switching. This raises several questions: is the neural bias mainly caused by the adhesive or signalling functions of the cadherins, or are these two mechanisms acting co-operatively? If the phenotype is caused by changes in signalling, what are the pathways involved? To answer these questions, the aims of this chapter are to:

a) Assess and quantify changes in adhesion caused by cadherin switching;
b) Investigate changes in signalling pathways caused by cadherin switching;
c) Determine whether the pro-neural effect of cadherin switching can be rescued by manipulating these signalling pathways.

5.2 Quantification of clustering in cells with cadherin manipulations

5.2.1 Nuclear segmentation of confocal images using NESSys

In order to determine whether the pro-neural phenotype caused by cadherin switching was caused by changes in the way cells adhere to one another, a quantitative image analysis strategy was developed to assess differences in cellular adhesion between different cell populations. The strategy involved the nuclear segmentation of 3D confocal images and measurement of distances between the nuclear edges in the different cell types used. These values were used as a measure of cellular clustering, which would serve as an indirect readout of changes in cellular adhesion.

The quantitative image analysis software PickCells, developed in our lab by postdoc Guillaume Blin, was used for this quantification. The software includes a nuclear segmentation module (Nuclear Envelope Segmentation System – NESSys) which was used for the analysis. The system segments nuclei based on nuclear envelope staining and makes use of a combination of manual and machine learning systems to generate an automated nuclear segmentation pipeline. For a detailed description of the workflow pipeline, see Methods, (section 2.2.3.1.9).

Examples of high and lower-quality segmentations based on nuclear envelope staining are shown in Figure 5.1. Panel C shows a high quality segmentation where nearly 100% or nuclei are accurately segmented. The bottom-left corner of panel D shows an example of a high-density area where segmentation is more inaccurate, with some omissions and merges of individual nuclei. In general, certain conditions, such as culture with Wnt3a (pictured) or later-stage neural differentiation led to areas of higher cellular density, which were more challenging for the segmentation software. To improve on this, the software uses 3D Z-stacks of the samples to match individual nuclei between Z-planes, improving segmentation quality for the sample in general. Samples for quantification were therefore always imaged as 3D Z-stacks and the analysis pipeline was empirically optimised for each dataset to yield the highest quality segmentation possible. It was deemed that this segmentation quality was accurate enough for downstream applications.

5.2.2 Loss of E-cadherin leads to clustering defects

Cells with E-cadherin knock-out and N-cadherin knock-in mutations were cultured in 2i-Lif, and then seeded at a density of $5x10^4$ cell per well in 12-well plates onto glass coverslips into 2i-Lif conditions. After a 24h pre-incubation to allow better adhesion to the culture surface, media were changed to NDiff for a further 24h. For A2Lox-Ncad-HA cells, Dox was added at the time of the media change. After one day of culture in neural conditions, all cells were fixed and stained for the nuclear envelope marker Laminβ1. The 24h time point was chosen since many, but not all, of the cell lines formed tight, compact dome-shape colonies in 2i-Lif conditions, and 24h of culture in NDiff conditions cause them to flatten out with surprising consistency. It was therefore hypothesised that 24h NDiff conditions would allow for the most consistent comparison of cellular clustering, and an accurate quantification of adhesive differences between cell lines, at a time point when the cells retained Oct4 expression and before any differentiation effects would substantially alter their morphology.

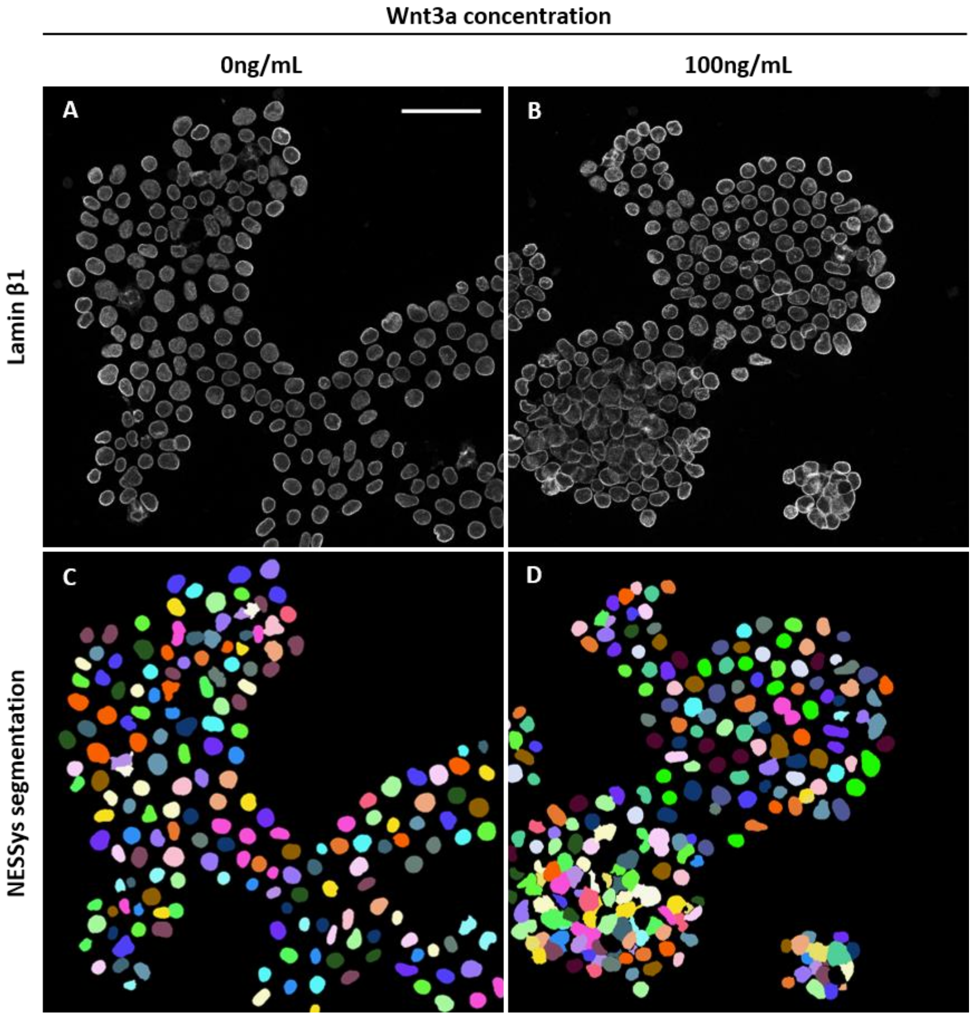

Figure 5.1: Example nuclear segmentation in NESSys. *Cells were seeded at a density 5x10^4 cells per well in a 12-well plate onto glass coverslips into 2i-Lif conditions. After 24h, media were changed to NDiff for a further 24h. Cells were then stained for the nuclear envelope marker Laminβ1.* ***A-B:*** *Nuclear envelope staining for cells cultured with or without Wnt3a.* ***C-D:*** *Corresponding nuclear segmentation. Images show one Z-plane of a larger 3D Z-stack. Scale bar = 50µm.*

Once the cells were stained, imaged, and segmented in NESSys, the PickCells software was used to calculate the distances between nuclear edges of neighbouring cells up to a 40µm radius. The analysis module employs Delaunay triangulation to identify the nearest neighbours of each individual nucleus, and these were the nuclei for which edge distances were calculated. In practice, this method results in the calculation of edge distances only between the nearest neighbours of individual nuclei, up to a distance of 40µm. A graphical summary of this method is illustrated in Figure 5.2.

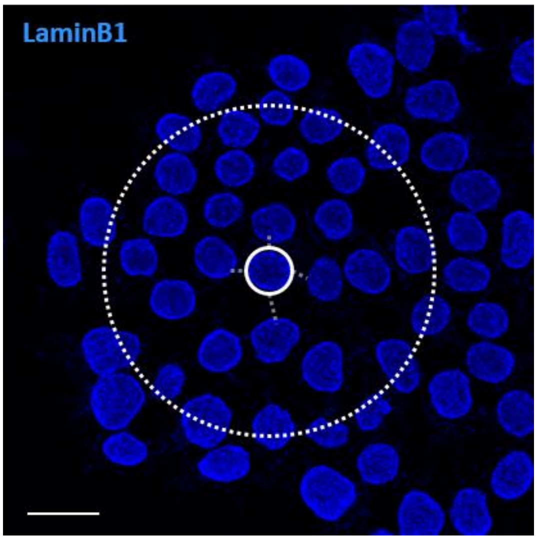

Figure 5.2: Methodology for measuring inter-nuclear edge distances in stained and segmented nuclei. *Delaunay triangulation was used to identify the nearest neighbours for each nucleus (solid white line), and the inter-nuclear distances were calculated for these cells (grey dotted lines). The maximum radius for neighbour detection was set at 40µm (white dotted outline). Scale bar = 20µm, diagram to scale.*

This analysis resulted in several edge distance measurements for each nucleus analysed per image, corresponding to the number of immediate neighbours that each nucleus had. To illustrate the spread of these data, density plots for one biological replicate are displayed in Figure 5.3, where each curve represents 1054 individual distance measurements from a single stained sample. The trends in these density plots show that parental control cells and WT cells tend to mostly have inter-nuclear edge distances below 10 microns. By contrast, both the EcKO cells and NcKI cells display a much larger spread of inter-nuclear edge distance measurements, showing that these cells are spread further apart from one another than the control cells.

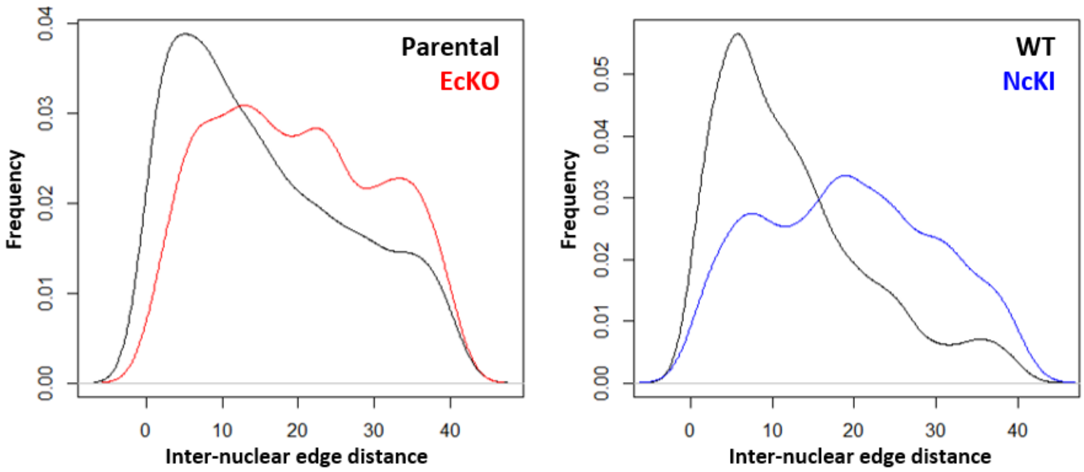

Figure 5.3: Example density plots of inter-nuclear edge distances in cadherin mutant cells. *N=1054 individual edge-distance measurements.*

In total, three biological replicates were plated and analysed for each condition studied, and a minimum of three fields of view were imaged for each replicate. For the A2Lox-Ncad-HA cells, one biological replicate and three independent clones were used for bot the un-induced and induced conditions. The outcomes of the analysis are summarised in Figure 5.4. By eye, the nuclei of cells lacking E-cadherin (EcKO and NcKI) appear to be spread further apart from one another than their control cell lines (Fig. 5.4 A). The inter-nuclear edge distance analysis confirms that these cadherin mutant cells have significantly greater inter-nuclear edge distances than their control cell lines, suggesting that loss of E-cadherin leads to defective adhesion (Fig. 5.4 B). In addition, the EcKO and NcKI cells have nearly identical mean inter-nuclear edge distance values, showing that knocking-in N-cadherin is not enough to rescue the defective clustering of E-cadherin null cells. A2Lox-Ncad-HA cell nuclei are shown to spread slightly but significantly further apart from one another following Dox treatment, suggesting that overexpression of N-cadherin may loosen cell-cell contacts or push cells further apart.

To ensure that the differences observed in cell clustering were not simply an outcome of differences in cell number or survival, the total number of cells per analysis was also recorded (Fig. 5.4 C). Cell numbers between comparable replicates did not differ significantly, supporting the idea that the differences in inter-nuclear edge distances are a result of the cadherin mutations.

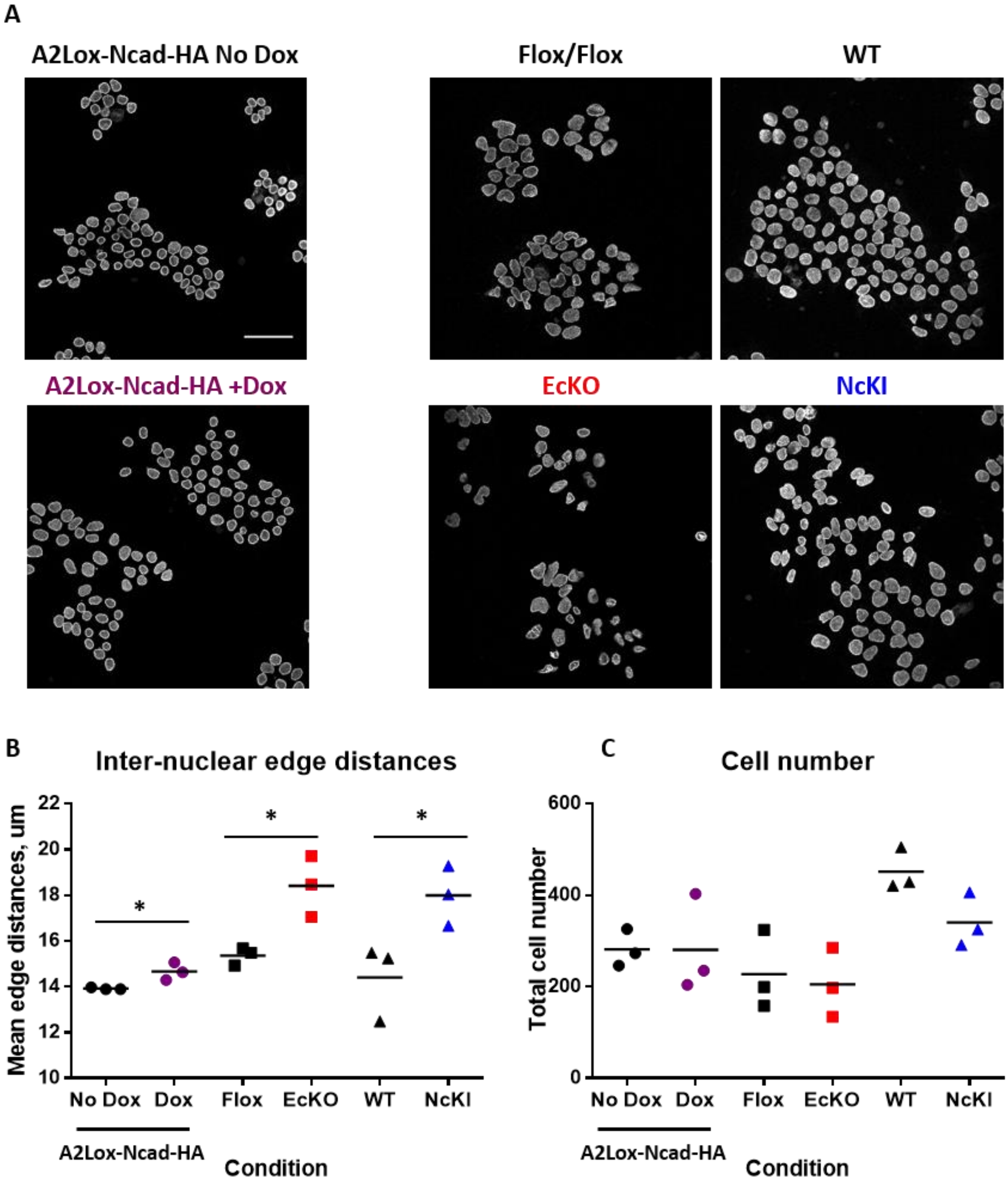

Figure 5.4: Clustering analysis of E-cadherin knock-out and N-cadherin knock-in cell lines. A. *Example images used in the analysis. All images show Laminβ1 nuclear envelope staining. Scale bar = 50µm.* ***B.*** *Summary of inter-nuclear edge distance analysis.* ***C.*** *Total cell number analysed in each biological replicate. For B and C, each point represents a mean of all cells from three fields of view of each biological replicate. *p≤0.05, unpaired T-test, N=3 biological replicates.*

Taken together, the results show that the loss of E-cadherin leads to significant changes in cell clustering which cannot be rescued by knocking-in N-cadherin. Additionally, N-cadherin overexpression caused a slight but significant increase in inter-nuclear distances compared to control cells. These results were interpreted as showing that cadherin switching causes changes in cellular adhesion, with loss of E-cadherin especially resulting in a failure of cells to properly adhere to one another.

It should be noted that this approach for measuring cellular clustering has a few significant limitations. While the changes in inter-nuclear distance are presumed to be due to defective adhesion, they could also be explained by other cellular processes, such as differences in migration, survival, or changes in cell morphology or cytoplasmic volume. Additionally, the data uses distances between nuclei because this was the cellular compartment for which a robust segmentation and analysis pipeline was available; membrane segmentation and analysis could give a more informative view of changes in cellular adhesion. However, the tools for such an analysis were not available for the current study.

Interestingly, the cells in which a pro-neural effect was observed (NcKI and Dox-induced A2Lox-Ncad-HA cells) show very different clustering profiles to one another. Additionally, the populations with the most disrupted clustering (EcKO and NcKI) displayed different behaviours in neural differentiation assays, with EcKO cells behaving similarly to control cells while NcKI cells underwent more efficient neural differentiation. This suggests adhesion may not be the main driver behind the pro-neural phenotype observed, raising the possibility that cadherin switching may influence differentiation via some other mechanism, for example by modulating cellular signalling.

5.3 The relationship between E-cadherin, β-catenin and canonical Wnt signalling

5.3.1 Loss of E-cadherin leads to a global loss of β-catenin

In the previous section, it was proposed that changes in adhesion cannot fully explain the pro-neural effect of cadherin switching, since levels of nuclear clustering did not correlate with the cell lines and conditions exhibiting a neural bias. As such, it was hypothesised that cadherin switching may modulate cellular signalling.

To test this hypothesis, a reverse-phase protein array (RPPA) was used to measure the strength of various signalling pathways. In this method, cellular lysates are prepared at a fixed concentration and printed onto a microarray slide in a dilution series, incubated with specific fluorescent antibodies, and imaged in an analyser. The fluorescence of each sample is then quantified to determine the relative expression of a specific protein or phospho-protein species in a given sample (Spurrier et al., 2008). In this project, RPPA was used to quantify levels of protein and phosphor-protein species involved in signal transduction in various pathways.

For the RPPA, EcKO and NcKI cells, their respective control cell lines, and A2Lox-Ncad-HA cells were used. The cells were plated at a density of 1.5×10^6 cells into 10cm dishes into 2i-Lif conditions and incubated for 24h to allow for proper adhesion to the dish. Media were then changed to neural differentiation medium. For A2Lox-Ncad-HA cells, Dox was added at the time of this medium change. After 24h of culture in neural differentiation conditions, the cells were lysed for protein content, normalised to a standard concentration and shipped to an external facility where RPPA analysis was performed. The 24h time-point was chosen because it was hypothesised that any signalling changes occurring due to cadherin switching would be occurring early on, as differences in gene expression can already be observed within 48h of neural differentiation in the cadherin mutant cells. Three independent biological replicates were performed. For A2Lox-Ncad-HA cells, a different clone was used in each biological replicate.

Figure 5.5 shows the full results of the RPPA experiment, with each value corresponding to mean enrichment relative to the relevant control cell line. Each (phospo-) protein species was manually classified into the signalling pathway that it is most commonly associated with based on entries in the GeneCards.org online database.

Overall, EcKO cells tended to have lower levels of most proteins compared to the parental cell line, but only three protein species were significantly lower: E-cadherin, β-catenin and Tsc2 phosphorylated at Thr1462. By contrast, NcKI cells were found upregulate many proteins compared to WT cells across various signalling pathways, many of them significantly. Finally, no significant change in protein levels was observed in the induced A2Lox-Ncad-HA cells compared to un-induced cells. Interestingly, EcKO cells also displayed higher levels of cleaved caspase-3, suggesting an elevated rate of apoptosis in these cells (Walters et al., 2009), and lending additional support to the idea that loss of E-cadherin causes cellular instability and increased cell death.

After E-cadherin, the protein with the greatest magnitude of change in expression was un-phosphorylated β-catenin, which was highly downregulated in both EcKO and NcKI cells, similarly to previous reports (Soncin et al., 2011). This result shows that the loss of E-cadherin leads to a significant drop in levels of β-catenin, which cannot be rescued by knocking-in N-cadherin. Two phosphorylated forms of β-catenin were also assayed, but no significant difference was detected in their levels compared to control cells (Fig. 5.6). Since β-catenin is an important player in WNT signalling, the results raised the possibility that cadherin switching may be modulating signal transduction through this pathway.

0.5 0 2

Antibody	Pathway/Function	EcKO	NcKI	A2Lox-Ncad-HA
Beta-actin	Housekeeping	1.01	0.95	0.97
Prohibitin		0.78	1.13	1.04
Ecad	Adhesion	0.04*	0.07**	0.94
Zyxin		0.99	1.27	1.07
Akt P Ser473	PI3K/Akt branch of FGF	0.61	1.15	0.88
Akt P Thr308		0.68	1.18	0.90
Akt		1.16	1.48*	1.05
PDK-1 P Ser241		1.00	1.61*	1.00
PDK-1		1.05	1.32	0.88
B-catenin	WNT pathway	0.26*	0.25*	0.95
beta-Catenin P Ser33,Ser37,Thr41		0.92	1.17	0.99
beta-Catenin P Thr41,Ser45		0.78	0.86	1.11
GSK-3-alpha.beta P Ser21.Ser9		0.85	1.24*	1.06
GSK-3-beta P Ser9		0.93	1.21	0.97
GSK-3-beta		0.91	1.17	0.98
C-Jun N-term	MAPK branch of FGF pathway	0.94	1.11	1.00
c-Jun P Ser73		1.10	1.62	1.00
MAPKAPK-2 P Thr334		0.96	1.26	0.99
MAPKAPK-2		0.92	1.14	1.02
MEK1/2		1.04	0.81*	0.98
MEK1/2 P Ser217.221		1.08	2.57*	1.01
MEK6 EP558Y		0.73	1.10	1.04
p38 MAPK PThr180,Tyr182		1.01	1.58**	0.96
p38 MAPK		0.92	1.17	1.01
p44.42 MAPK (ERK1.2) P Thr202.Thr185,Tyr204.Tyr187		0.99	1.66	0.77
p44.42 MAPK (ERK1.2)		1.00	0.72	0.98
p90 S6 kinase (Rsk1-3)		0.95	0.97	0.99
Raf P Ser338		0.83	1.61*	0.88
Rsk2 Pser 227		1.00	1.22**	0.98

Antibody	Pathway/Function	EcKO	NcKI	A2Lox-Ncad-HA
Smad1.5 P Ser463.Ser465	BMP4 pathway	0.96	1.21	1.09
Smad2 P Ser465,Ser467		0.96	1.08	1.02
Smad2.3 P Ser465.Ser423,Ser467.Ser425		1.03	1.09	1.00
Smad3 P Ser423,Ser425		0.95	1.38*	0.98
Caspase-3 cleaved	Apoptosis	1.28	1.14	0.99
Caspase-3		0.88	1.08	0.97
IGF-1R beta	IGF pathway	0.96	1.16	1.03
IRS-1		1.06	1.25	0.94
Tsc-2 P Thr1462		0.72*	0.86	0.94
Tsc-2		0.92	1.13*	1.00
ILK1 (4G9)	ECM adhesion	0.98	1.23	1.02
Integrin a3		0.98	1.10	0.91
Integrin B1		1.05	0.92	0.86
Integrin B3		1.03	1.16	0.96
Integrin B4		1.01	1.20	0.94
JAK1 P Tyr1022,Thr1023	Jak/Stat pathway	0.97	1.13	0.96
JAK1		0.93	1.33	0.88
mTOR P Ser2448	EGF pathway	1.05	1.31*	1.07
mTOR		1.10	1.13*	1.03
NFkB P 65 Ser536		1.00	1.18*	1.03
NFkB P 105/P 50		1.09	1.12	1.02
PKA	NFkB pathway	0.66	1.61	0.96
Slug C19G7	Transcription factor	0.88	1.31	1.08
Stat3 P Y705	Jak/Stat pathway	0.96	1.18*	0.91
Stat3		0.96	0.88	1.02
Stat5 P Tyr694		0.96	1.11	1.00
Stat5		0.95	1.13	1.04
Stat6 P Tyr641		0.91	1.17	0.93
Stat6		1.00	1.01	1.08
YAP P Ser127	YAP/TAZ signalling	0.87	1.18*	1.06
YAP1 P 1674Y		1.00	1.15	1.14

Figure 5.5 (pages 157-158): RPPA protein expression heat-map for 24h in neural differentiation conditions. *Values correspond to mean relative enrichment compared to the relevant control: EcKO/Parental, NcKI/WT, A2Lox-Ncad-HA induced/un-induced. Approximate signalling pathway identity selected manually from GeneCards.org online database. N=3 biological replicates, *p≤0.05, **p≤0.01, paired T-test.*

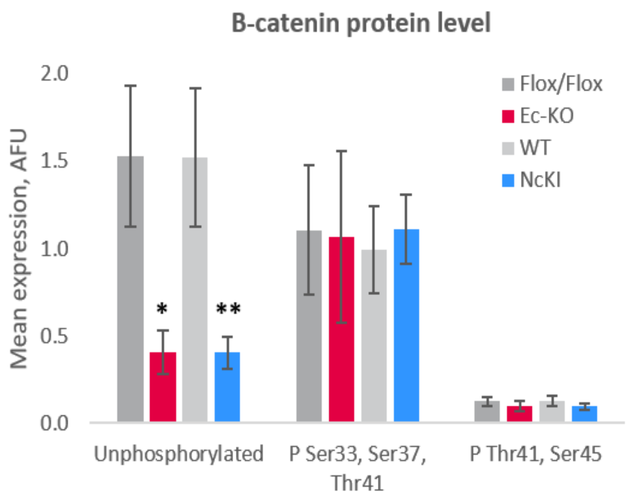

Figure 5.6: Mean expression values for three phosphorylation states of β-catenin in cadherin mutant cell lines. *Values obtained from RPPA analysis. N=3 biological replicates, *p≤0.05, **p≤0.01, paired T-test.*

5.3.2 Quantification of nuclear β-catenin in cadherin mutant cells

β-catenin is a central component of the canonical WNT signalling pathway; when the pathway is activated, translation of β-catenin protein is activated, and its un-phosphorylated form translocates to the nucleus where it activates transcription of WNT target genes (Clevers, 2006). Studies in ESCs have shown that activation of WNT signalling promotes self-renewal (Sato et al., 2004; ten Berge et al., 2011) and inhibits neural differentiation (Faunes et al., 2013; Haegele et al., 2003). In the previous section, the loss of E-cadherin was linked to a significant drop in global levels of β-catenin. This raised the possibility that the pro-neural effect observed in NcKI cells may be due to reduced WNT signalling in these cells, assuming that the drop in β-catenin levels also occurs in the nucleus. To further explore this possibility, the nuclear levels of β-catenin were studied in the cadherin mutant cells, and the cells' responsiveness to external WNT signals was explored.

EcKO, NcKI and their relevant control cell lines were plated onto glass coverslips at a density of $5x10^4$ cells per well in a 12-well plate in 2i-Lif conditions. After a 24h-incubation in 2i-Lif, media were changed to NDiff, and parallel wells were set up with three concentrations of Wnt3a: 0, 25 and 100ng/mL. After 24h of neural differentiation with or without supplemented Wnt3a, the cells were fixed and stained for Laminβ1, E-cadherin, Oct4, and an active (dephosphorylated) form of β-catenin. The samples were then imaged as 3D Z-stacks on a Leica SP8 confocal microscope, with at least three fields of view imaged per sample. Figures 5.7 and 5.8 show example images of representative samples.

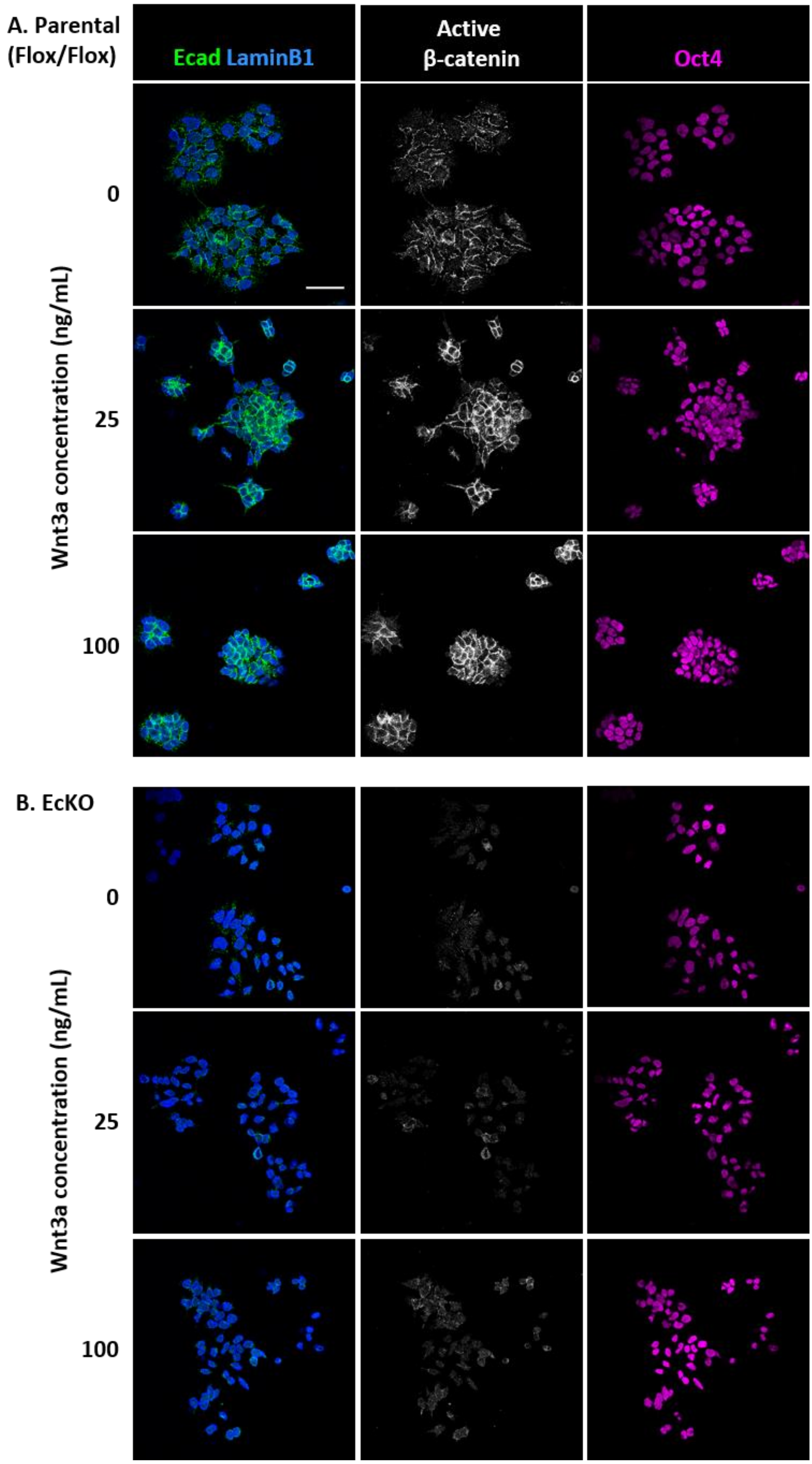
A. Parental
(Flox/Flox)
Ecad LaminB1
Active
β-catenin
Oct4
Wnt3a concentration (ng/mL)
0
25
100
B. EcKO
Wnt3a concentration (ng/mL)
0
25
100

Figure 5.7

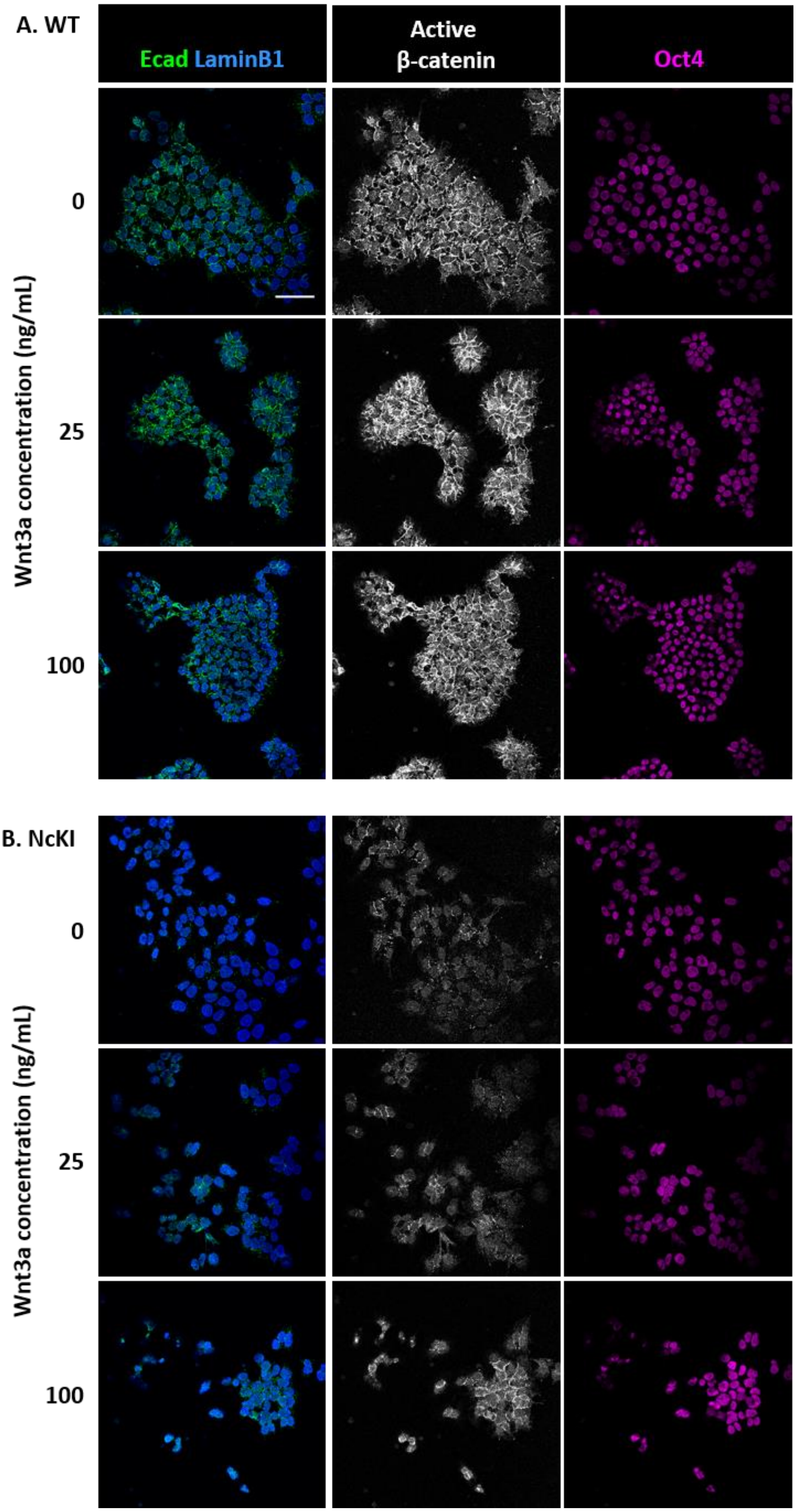
A. WT
Ecad LaminB1
Active
β-catenin
Oct4
0
25
100
Wnt3a concentration (ng/mL)
B. NcKI
0
25
100
Wnt3a concentration (ng/mL)

Figure 5.8

Figure 5.7 (page 160): Example ICC of parental (A) and EcKO (B) cells after 24h of neural differentiation in increasing concentrations of Wnt3a. *Samples images on a Leica SP8 confocal microscope. Scale bar =50µm.*

Figure 5.8 (page 161): Example ICC of WT (A) and NcKI (B) cells after 24h of neural differentiation in increasing concentrations of Wnt3a. *Samples images on a Leica SP8 confocal microscope. Scale bar =50µm.*

By eye, it is evident that both cell lines lacking E-cadherin display substantially lower levels of β-catenin, both at their cytoplasmic membrane and within the nucleus, confirming observations from the RPPA data. Increasing concentrations of Wnt3a appear to yield higher nuclear β-catenin staining, which is most evident in the Flox/Flox cells (Fig. 5.7 A). By eye, nuclear Oct4 intensity appears comparable between the different mutants and varying concentrations of Wnt3a.

5.3.2.1 Optimisation of β-catenin nuclear quantification

Next, the nuclear intensity of β-catenin in the samples was quantified using PickCells. Nuclear segmentation was performed on Laminβ1 signal using the NESSys module as before. The "Intrinsic Features" module in PickCells quantifies several nuclear properties. Here, this module was used to quantify mean intensity of the β-catenin staining in the nuclei, which produced a mean value for each nucleus based on all Z-planes of the 3D Z-stack in which a given nucleus was detected. A visual representation of this quantification is presented in Figure 5.9, showing that the loss of E-cadherin leads to lower nuclear β-catenin signal, and that exposure to a high dose of Wnt3a causes this signal to increase.

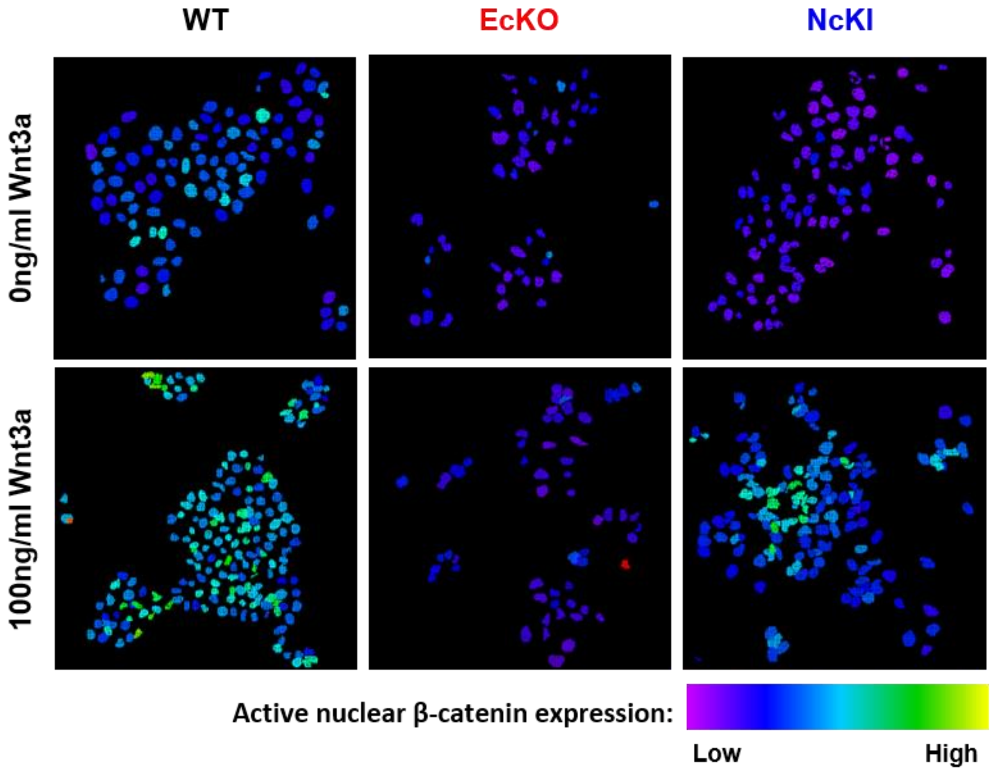

Figure 5.9: PickCells quantification of nuclear signal intensity in cells stained for active β-catenin. *Cells cultured for 24h in neural differentiation conditions with or without a high dose of Wnt3a.*

The nuclear β-catenin quantification experiment was optimised by using two different β-catenin antibodies: one, raised in rabbit, which detects all β-catenin; and a second, raised in mouse, which detects the active form of the protein that is dephosphorylated at both Ser37 and Thr41. Samples of EcKO, NcKI and the relevant control cell lines (cultured as before) were stained with both of these antibodies, and the intensity profiles of their nuclei were investigated using PickCells analysis. Figures 5.10 and 5.11 compare density plots produced by these two antibodies at different concentrations of Wnt3a. It was concluded that the two antibodies produced very similar quantitative results, and in following experiments, the β-catenin antibody was selected that would better match a given panel of other antibodies based on the animal species they were raised in.

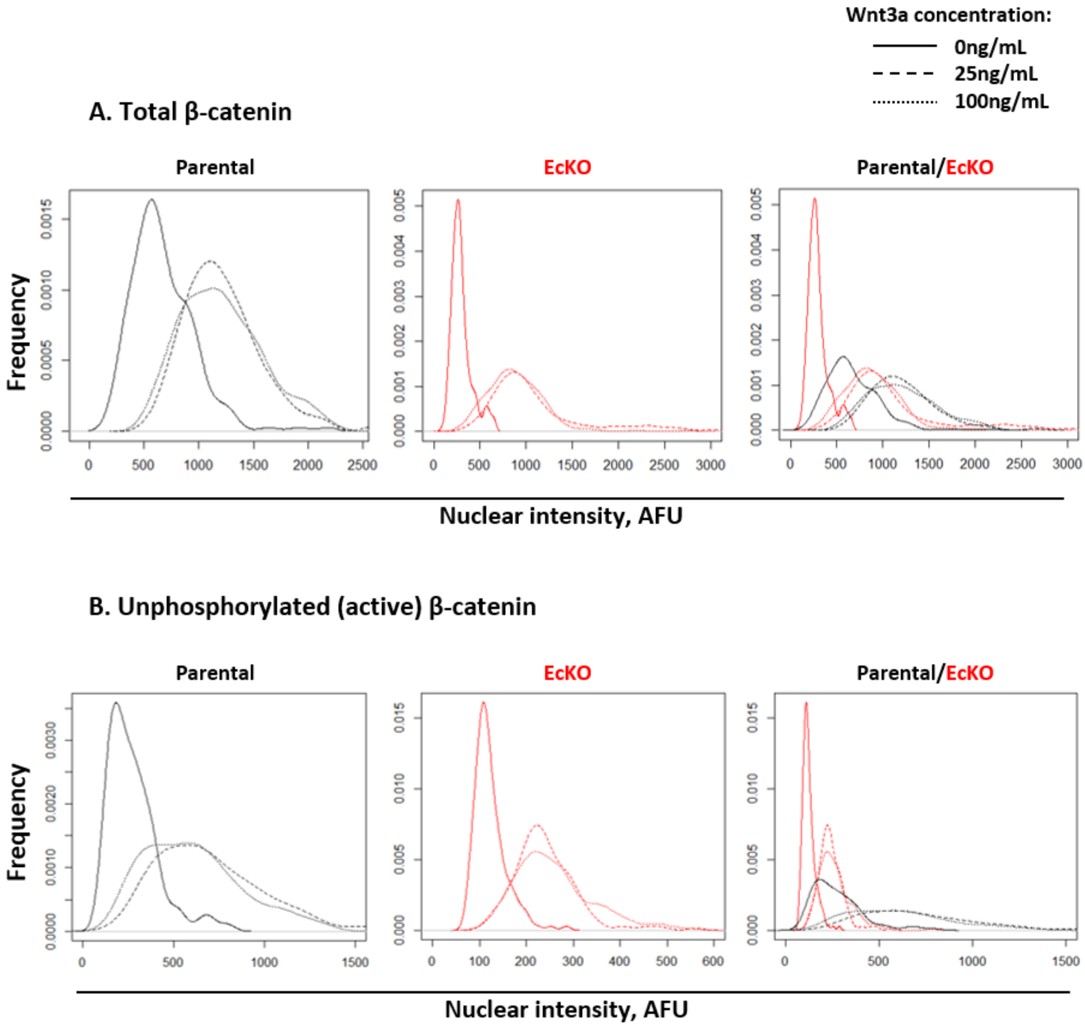

Figure 5.10: Comparison of nuclear β-catenin intensity by two antibodies in EcKO cells. *Flox/Flox (parental) and EcKO cells were cultured for 24h in neural differentiation conditions in varying concentrations of Wnt3a, fixed, and stained with one of two β-catenin antibodies, specific for total (**A**) and unphosphorylated (**B**) β-catenin. Samples were imaged on a Leica SP8 confocal microscope. Nuclear intensity of the antibody signal was quantified using PickCells software. Each curve represents one biological replicate including at least three fields of view. N=162 nuclei per sample.*

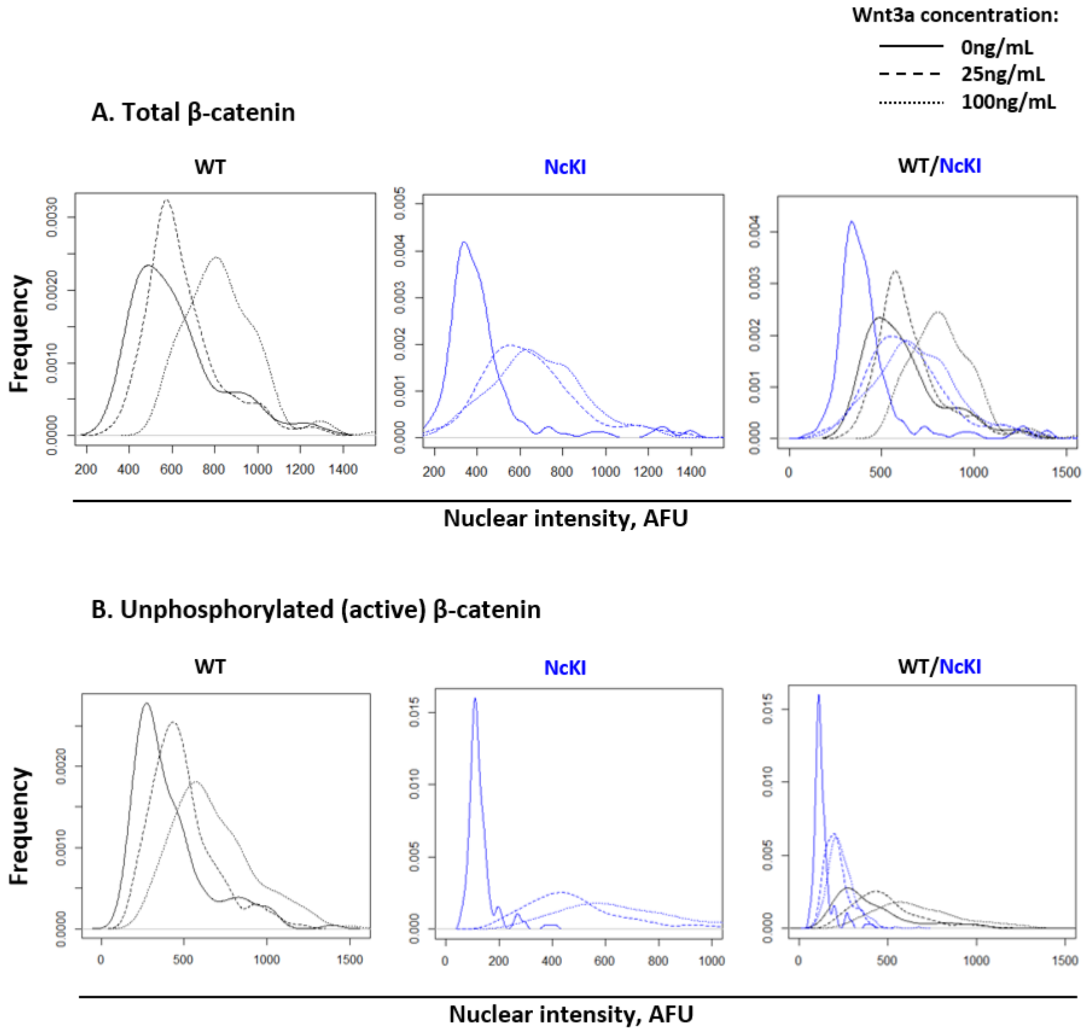

Figure 5.11: Comparison of nuclear β-catenin intensity by two antibodies in NcKI cells. *WT and NcKI cells were cultured for 24h in neural differentiation conditions in varying concentrations of Wnt3a, fixed, and stained with one of two β-catenin antibodies, specific for total (**A**) and unphosphorylated (**B**) β-catenin. Samples were imaged on a Leica SP8 confocal microscope. Nuclear intensity of the antibody signal was quantified using PickCells software. Each curve represents one biological replicate including at least three fields of view. N=162 nuclei per sample.*

5.3.2.2 Loss of E-cadherin leads to a loss of nuclear β-catenin

A previous study showed that E-cadherin and Oct4 are downregulated in synchrony during neural differentiation (Malaguti et al., 2013), while another study has proposed the existence of a membrane-bound E-cadherin/β-catenin/Oct4 complex that is involved in regulating pluripotency (Faunes et al., 2013). To investigate the relationship between E-cadherin, β-catenin and Oct4, the cells in the current experiment were additionally stained for Oct4, and the nuclear levels of this transcription factor were quantified in PickCells. Example density of Oct4 intensity distributions in the different cell lines and at various concentrations of Wnt3a are shown in Figure 5.12.

Once the staining protocol and analysis pipeline for the experiment were optimised, four biological replicates were performed, and samples were collected for both ICC and qPCR for protein and mRNA-level analysis, respectively. The results for nuclear active β-catenin and Oct4 are summarised in figure 5.13. These results show that the loss of E-cadherin leads to a significant drop in levels of nuclear un-phosphorylated β-catenin, and that this effect cannot be rescued by knocking in N-cadherin. In addition, increased concentrations of Wnt3a led to higher levels of nuclear β-catenin staining in all cell lines studied, but these increases were much less pronounced in the two cell lines lacking E-cadherin. This result suggests that E-cadherin is required for the maintenance of global and nuclear levels of β-catenin in the earliest stages of *in vitro* neural differentiation. In the absence of E-cadherin, even high doses of Wnt ligand are unable to rescue WT levels of nuclear β-catenin.

By contrast, analysis of Oct4 levels in the cadherin mutants showed that neither the loss of E-cadherin nor the compensatory knock-in of N-cadherin had an effect on the levels of Oct4 protein in the cells studied at this time point. However, higher concentrations of Wnt3a correlated with higher levels of Oct4, supporting previous reports that in neural differentiation conditions, Wnt3a promotes, and is sufficient to maintain, a pluripotent state (Faunes et al., 2013). This effect was observed to some extent in all the cell lines studied, suggesting that while the cadherin mutant cells exhibit lower levels of nuclear β-catenin, they may still retain WNT-responsiveness. This possibility is investigated further in the next section during later stages of neural differentiation.

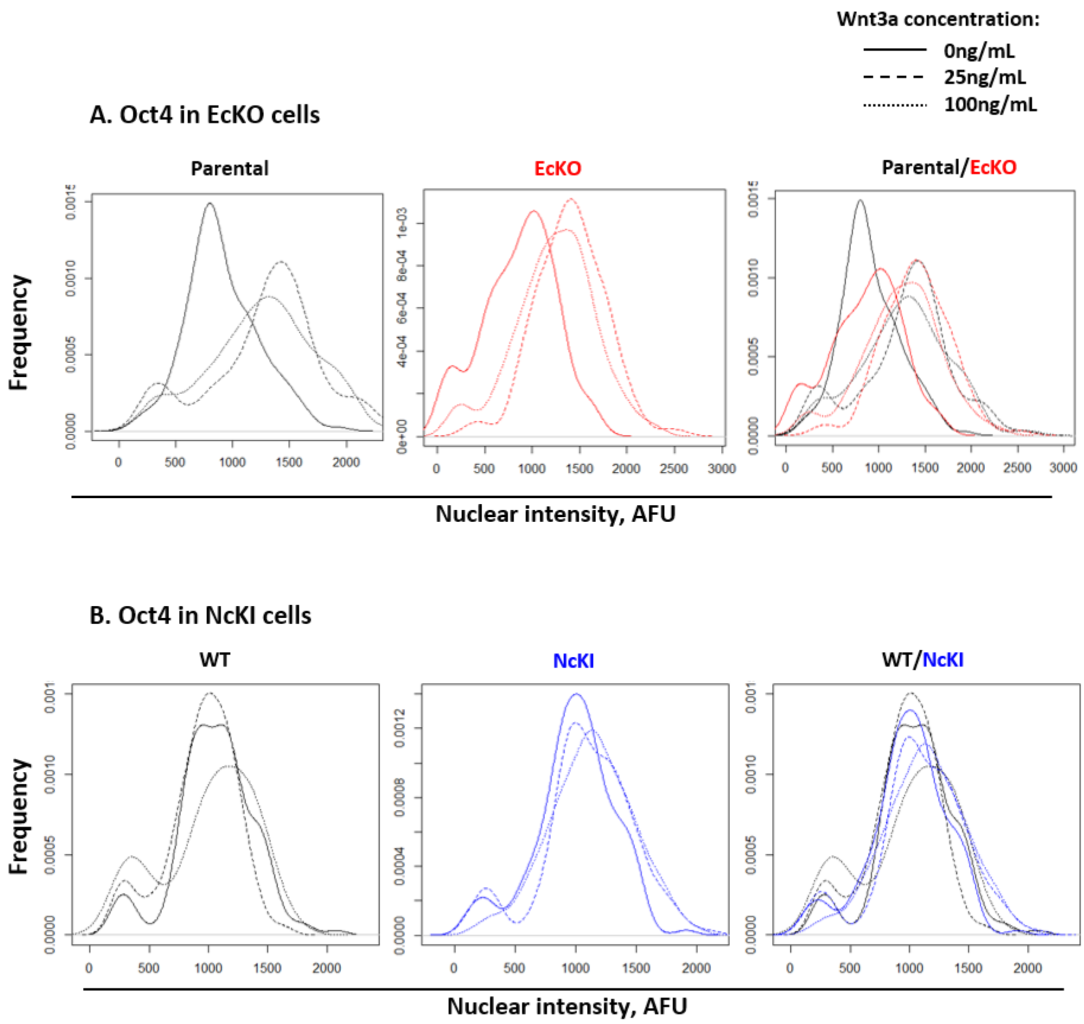

Figure 5.12: Example quantification of nuclear Oct4 intensity in cadherin mutant cells. *Cadherin mutant cells and their relevant control cell lines were cultured for 24h in neural differentiation conditions in varying concentrations of Wnt3a, fixed, and stained for Oct4. Samples were imaged on a Leica SP8 confocal microscope. Nuclear intensity of the antibody signal was quantified using PickCells software. Each curve represents one biological replicate including at least three fields of view. N=162 nuclei per sample.*

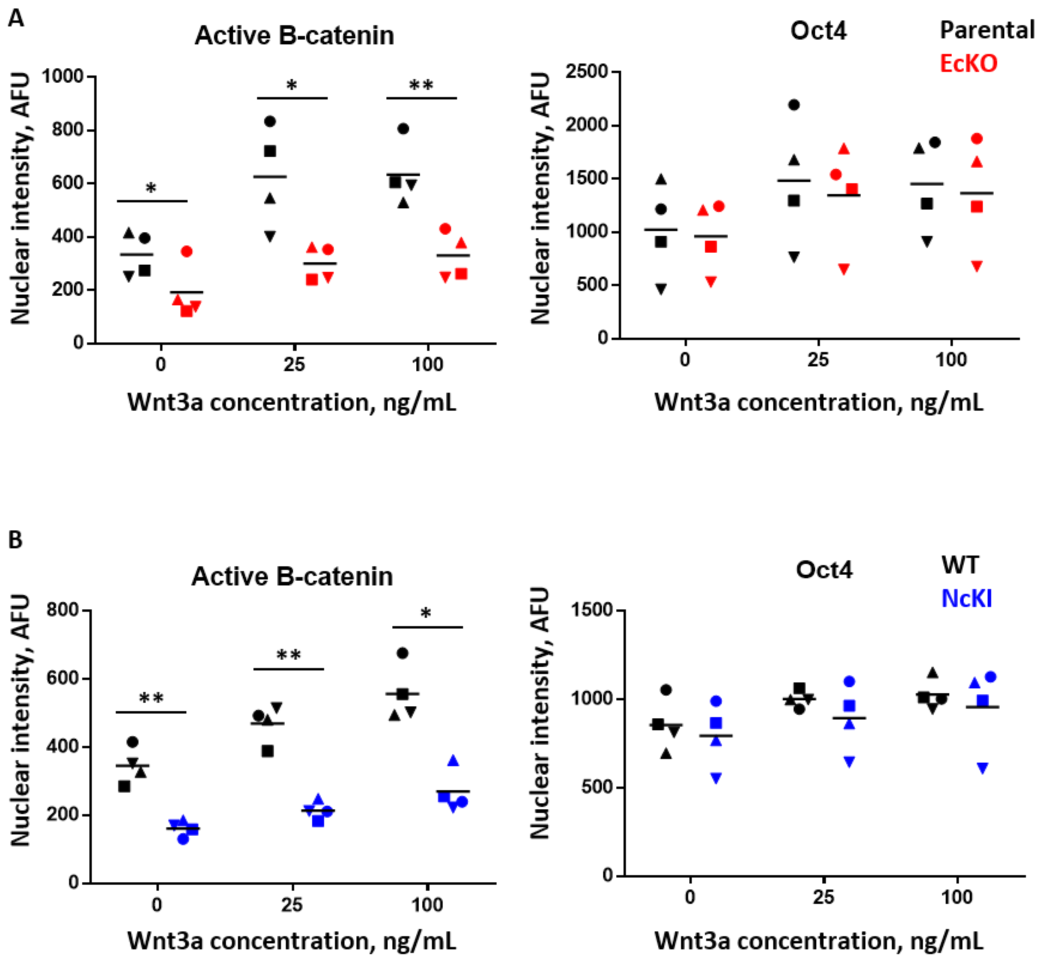

Figure 5.13: Nuclear levels of active β-catenin and Oct4 in cadherin mutant cells. *EcKO and NcKI cells, and their relevant control cell lines, were cultured in neural differentiation conditions for 24h in varying concentrations of Wnt3a, stained for active β-catenin and Oct4, and imaged on a Leica SP8 confocal microscope. The nuclear intensity of these proteins was quantified using PickCells software. Each point represents the mean of hundreds of cells from one biological replicate and at least three fields of view. N=4 biological replicates. *p≤0.05, **p≤0.01, paired T-test.*

5.3.3 Forced cadherin switching allows cells to overcome the inhibitory effects of Wnt on neural differentiation

In the last section, cells lacking E-cadherin were shown to have reduced nuclear β-catenin levels, but the impact of this phenotype on WNT signalling remained unclear. WNT signalling is generally regarded as an inhibitor of neural differentiation (Haegele et al., 2003), and it represses anterior epiblast and early neural features in EpiSCs (Tsakiridis et al., 2014). Therefore, the next step of this study was to investigate whether changes in WNT signalling played a role in the pro-neural effect of cells undergoing cadherin switching.

The previous experiment was repeated, but the cells were plated into 2i-Lif conditions at a lower density ($5x10^3$ cells per well in a 12-well plate) and were subsequently cultured in neural differentiation conditions for three to four days, with Wnt3a added on day zero at the same doses as before. Cells were then either lysed for qPCR analysis or fixed for ICC and PickCells quantification. The fixed cells were stained for Laminβ1, E-cadherin, Sox1 and β-catenin; since the Sox1 antibody was raised in mouse, an antibody for total β-catenin was used as this was raised in rabbit, and therefore was a more practical option for the selected antibody panel. Three biological replicates were analysed for each condition. Example samples stained and imaged by confocal microscopy are shown in figures 5.14 and 5.15.

The confocal images show a varying amount of E-cadherin expression in WT and Flox/Flox cells at different concentrations of Wnt3a, and no staining in the EcKO and NcKI cells, as expected. Nuclear β-catenin staining at varying intensities is visible in all samples. Sox1 staining is visible in all cell lines in the samples cultured without Wnt3a, but is mostly absent in cells cultured with Wnt3a, with the exception of NcKI cells, especially at day four. To further investigate the relationship between cadherin switching, WNT signalling and neural differentiation, the nuclear intensities of Sox1 total β-catenin were quantified using PickCells analysis. The results of this analysis are shown in Figure 5.16.

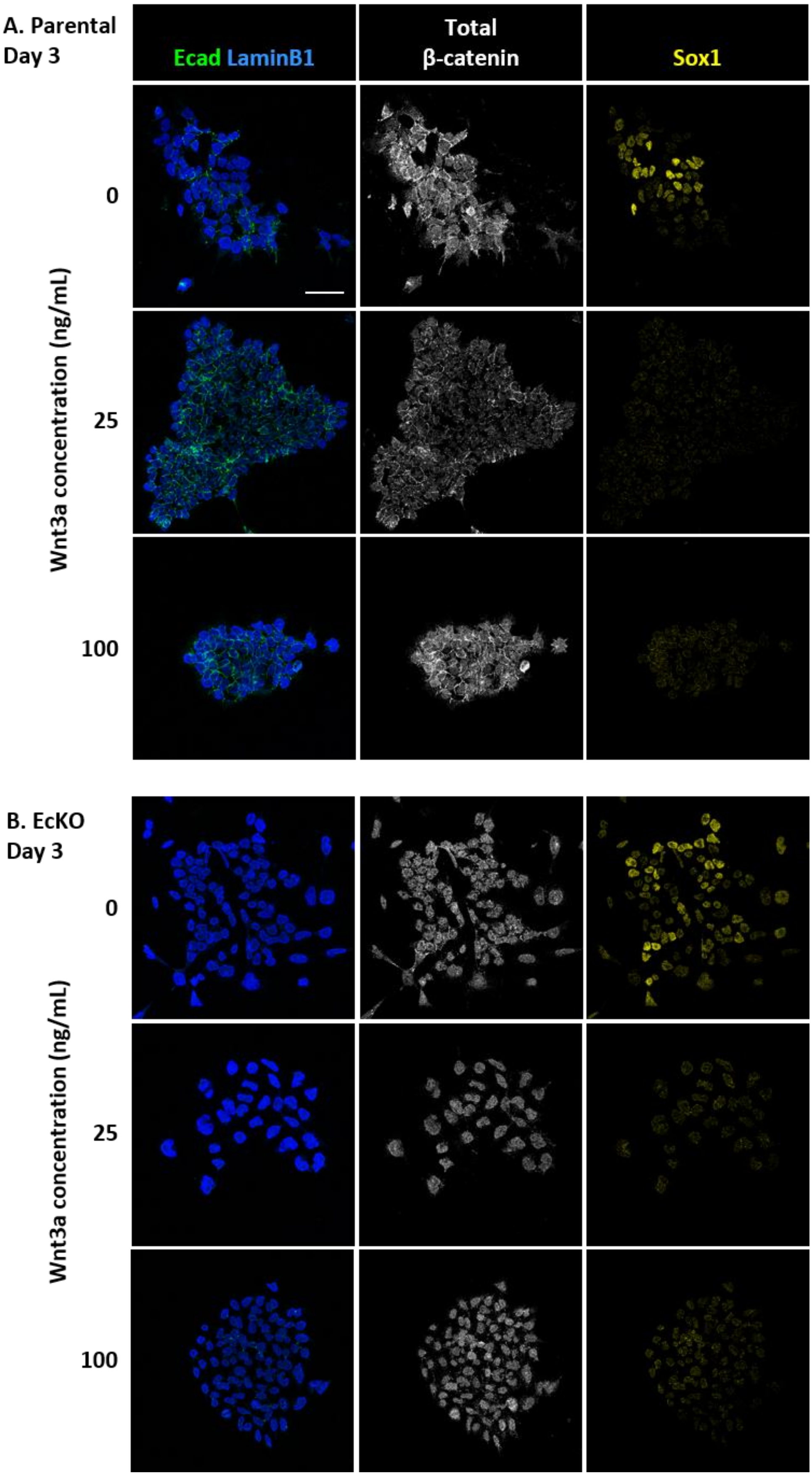
A. Parental
Day 3
Ecad LaminB1
Total
β-catenin
Sox1
0
25
100
Wnt3a concentration (ng/mL)
B. EcKO
Day 3
0
25
100
Wnt3a concentration (ng/mL)

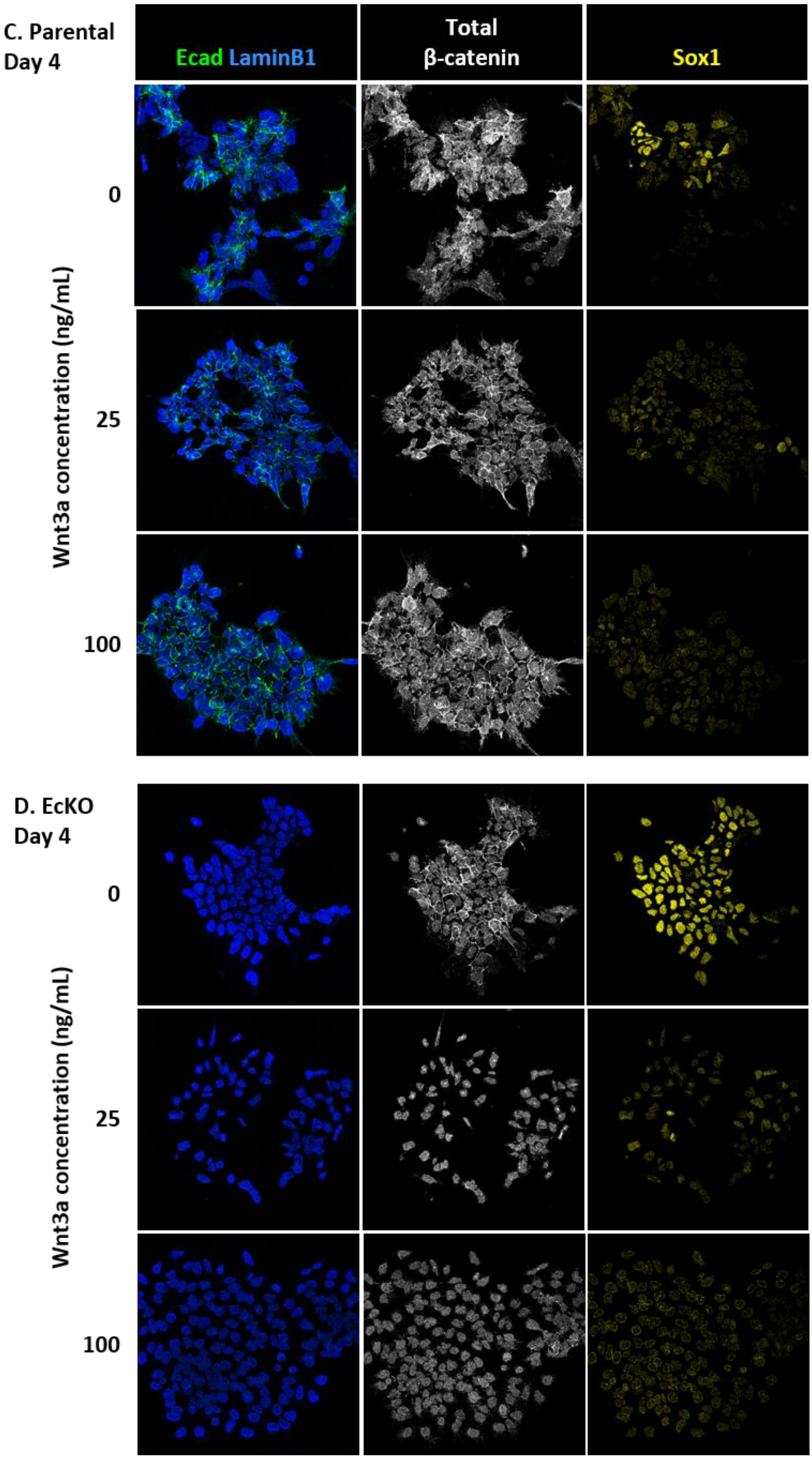
C. Parental
Day 4
Ecad LaminB1
Total
β-catenin
Sox1
0
25
100
Wnt3a concentration (ng/mL)
D. EcKO
Day 4
0
25
100
Wnt3a concentration (ng/mL)

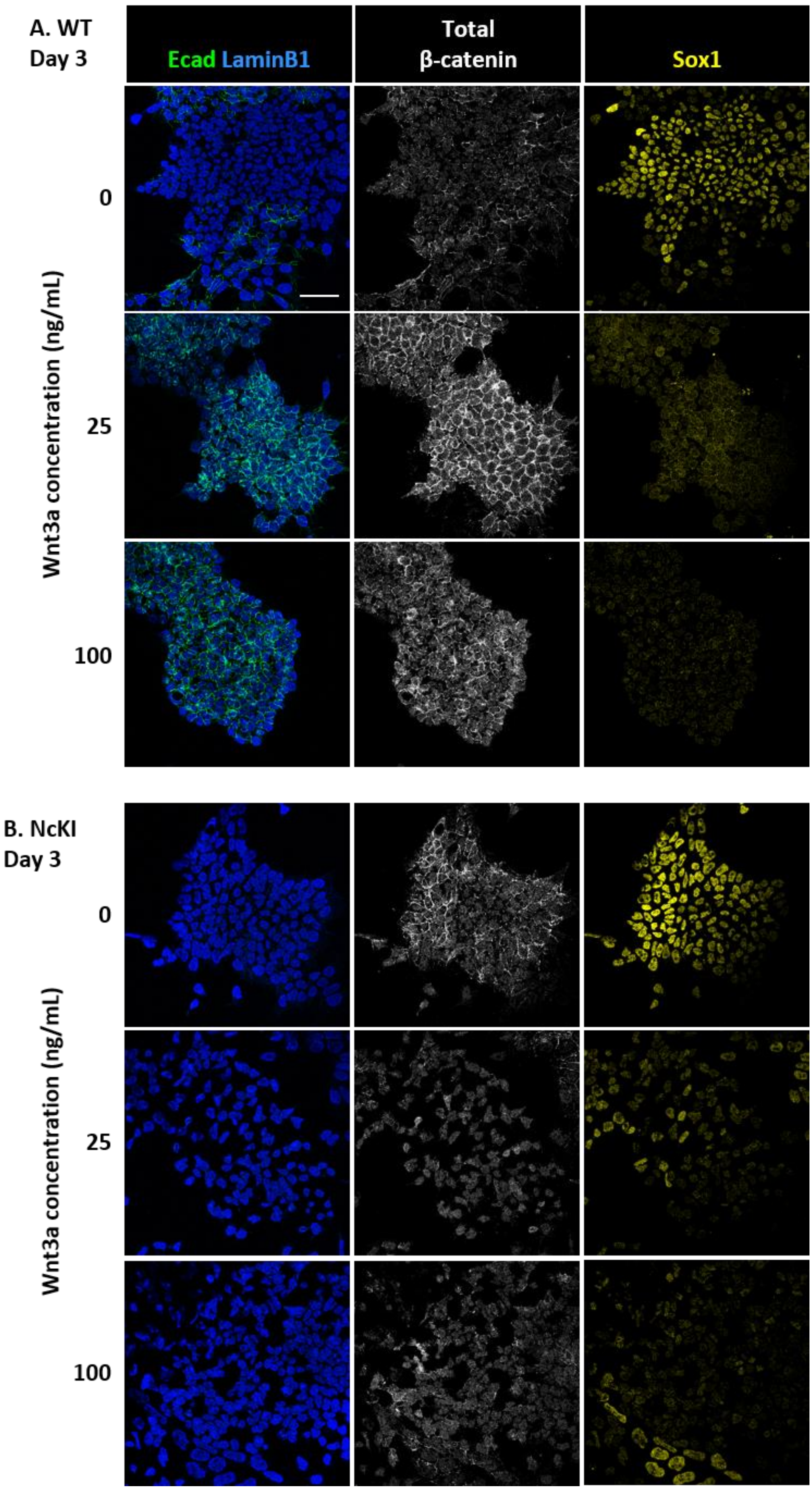
A. WT
Day 3
Ecad LaminB1
Total
β-catenin
Sox1
Wnt3a concentration (ng/mL)
0
25
100
B. NcKI
Day 3
Wnt3a concentration (ng/mL)
0
25
100

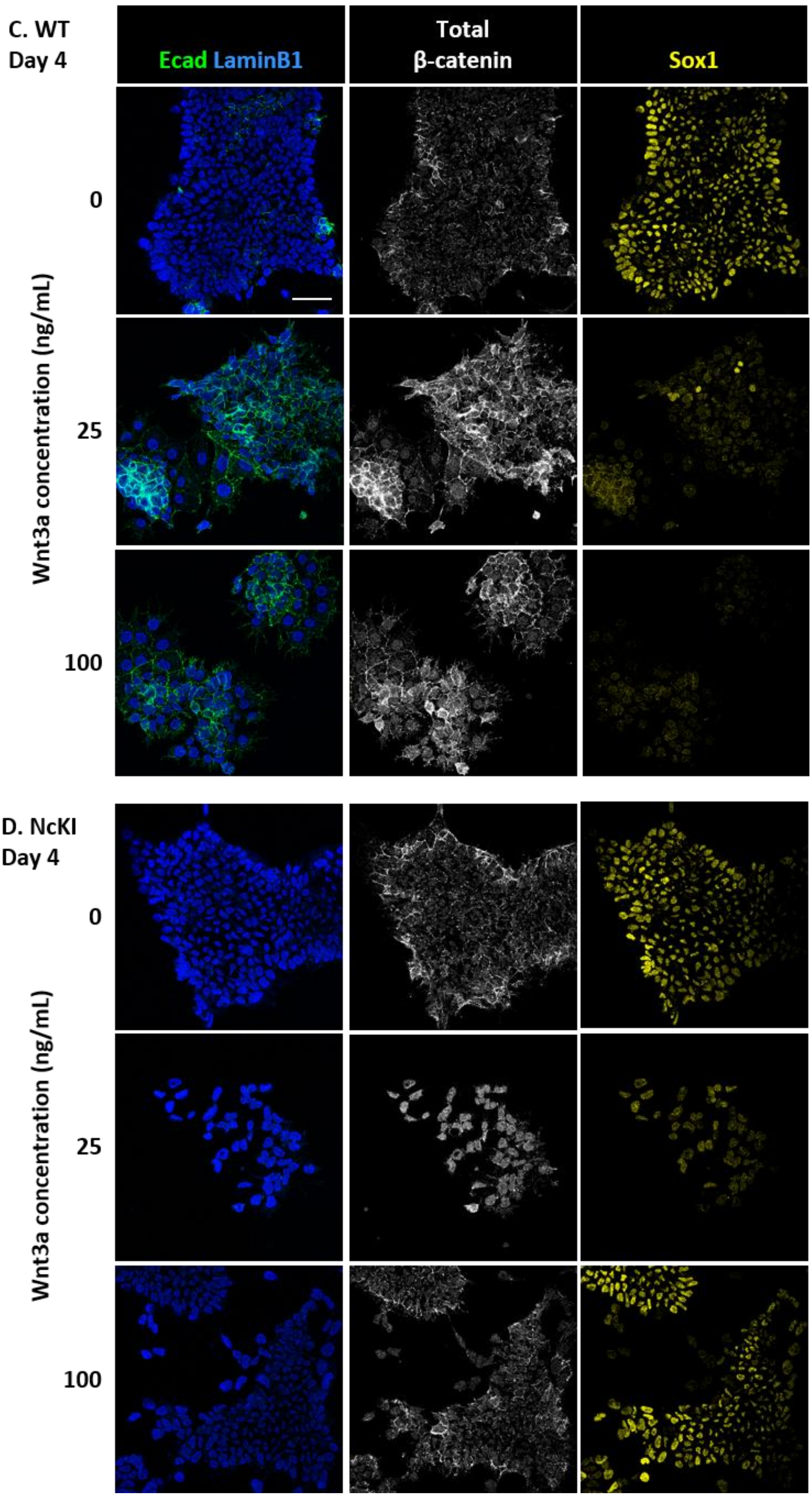
C. WT
Day 4
Ecad LaminB1
Total
β-catenin
Sox1
Wnt3a concentration (ng/mL)
0
25
100
D. NcKI
Day 4
Wnt3a concentration (ng/mL)
0
25
100

Figure 5.14 (pages 170-171): Example ICC of parental (Flox/flox) and EcKO cells after three (A,B) and four (C,D) days of neural differentiation in increasing concentrations of Wnt3a. *Samples imaged on a Leica SP8 confocal microscope. Scale bar =50µm.*

Figure 5.15 (pages 172-173): Example ICC of WT and NcKI cells after three (A,B) and four (C,D) days of neural differentiation in increasing concentrations of Wnt3a. *Samples imaged on a Leica SP8 confocal microscope. Scale bar =50µm.*

Nuclear intensity of β-catenin at days three and four of neural differentiation showed considerable variability between experiments. In general, nuclear β-catenin signal was reduced in EcKO and NcKI cells compared to control cells, with this reduction found to be significant between WT and NcKI cells on day four in cultures with added Wnt3a. In EcKO cells, a spike in Sox1 intensity was observed at day four in the absence of Wnt3a; all other conditions were found to have similar Sox1 levels between EcKO and Flox/Flox cells. Some replicates of NcKI cells showed a very high increase in Sox1 levels compared to WT cells, especially at day 4, and even in high concentrations of Wnt3a. However, due to extensive variability of the data, none of the results for Sox1 were found to be statistically significant.

To try to get a better understanding of the effect of cadherin switching and WNT signalling on neural differentiation, the day one, day three and day four time-points were also analysed by qPCR. It should be noted that cells used for the day one analysis were plated at a 10x greater seeding density than those analysed at days three to four in order to produce high enough RNA yield for downstream qPCR analysis. The results of the qPCR gene expression analysis are presented in Figure 5.17.

Gene expression analysis by qPCR found negligible levels of *Cdh1* transcript in both cadherin mutant cell lines, as expected. Levels of *Cdh2* were significantly elevated in both cell lines at various time-points, and in all cases displayed a negative correlation with Wnt3a concentration.

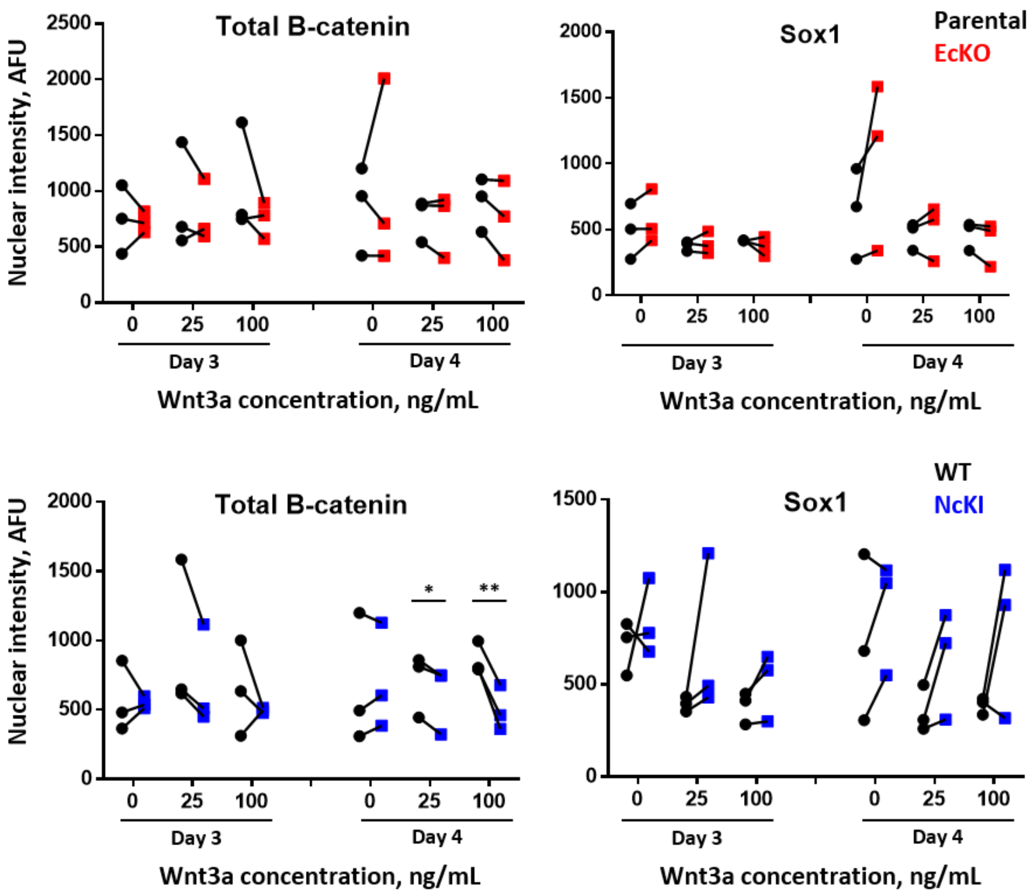

Figure 5.16: Nuclear levels of β-catenin and Sox1 in cadherin mutant cells during neural differentiation. *EcKO and NcKI cells, and their relevant control cell lines, were cultured in neural differentiation conditions for 3-4 days in varying concentrations of Wnt3a, stained for total β-catenin and Sox1, and imaged on a Leica SP8 confocal microscope. The nuclear intensity of these proteins was quantified using PickCells software. Each point represents the mean of hundreds of cells from one biological replicate and at least three fields of view. N=3 biological replicates. *p≤0.05, **p≤0.01, paired T-test.*

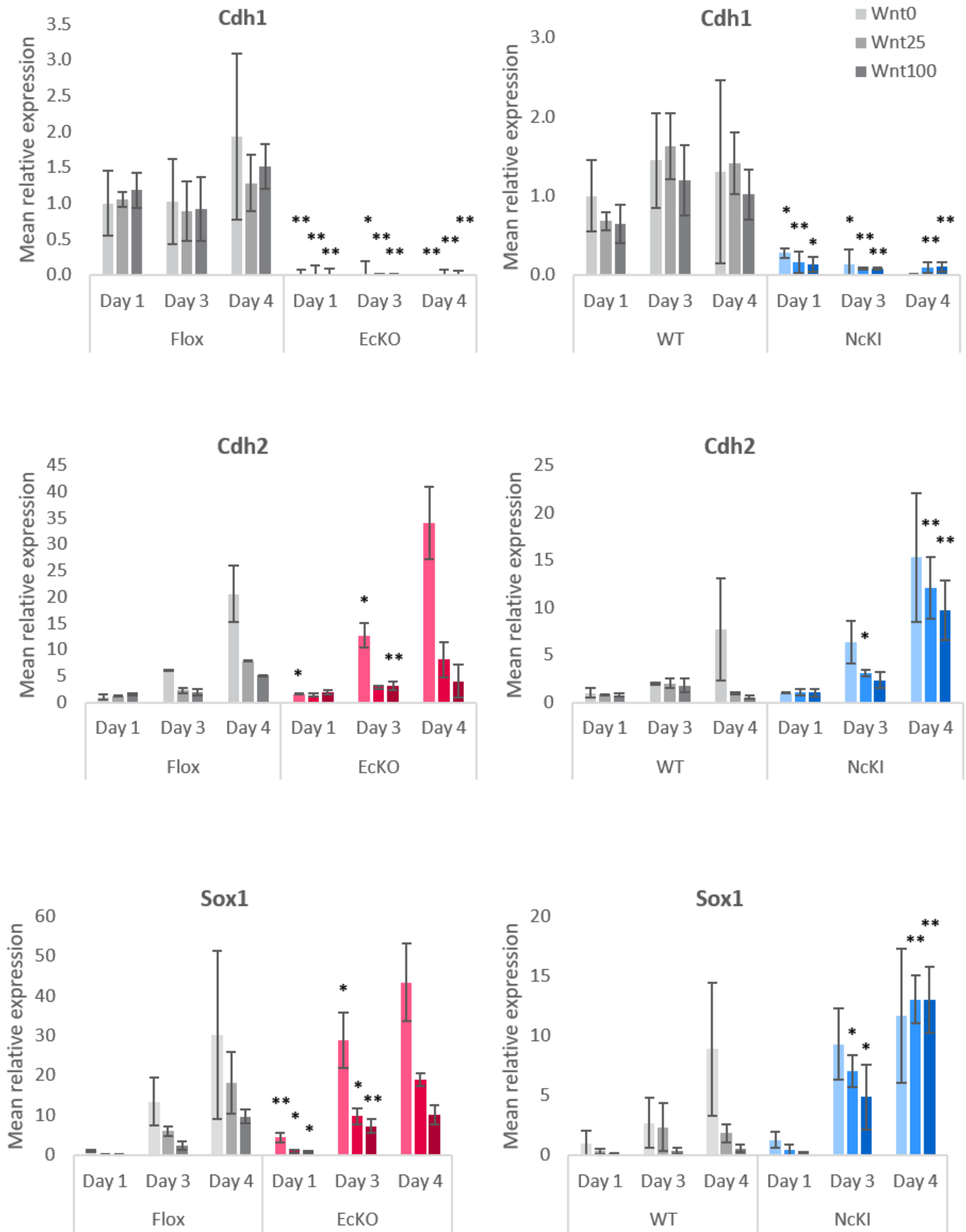
Cdh1
Mean relative expression
Day 1
Day 3
Day 4
Flox
EcKO
Cdh1
Wnt0
Wnt25
Wnt100
WT
NcKI
Cdh2
Cdh2
Sox1
Sox1

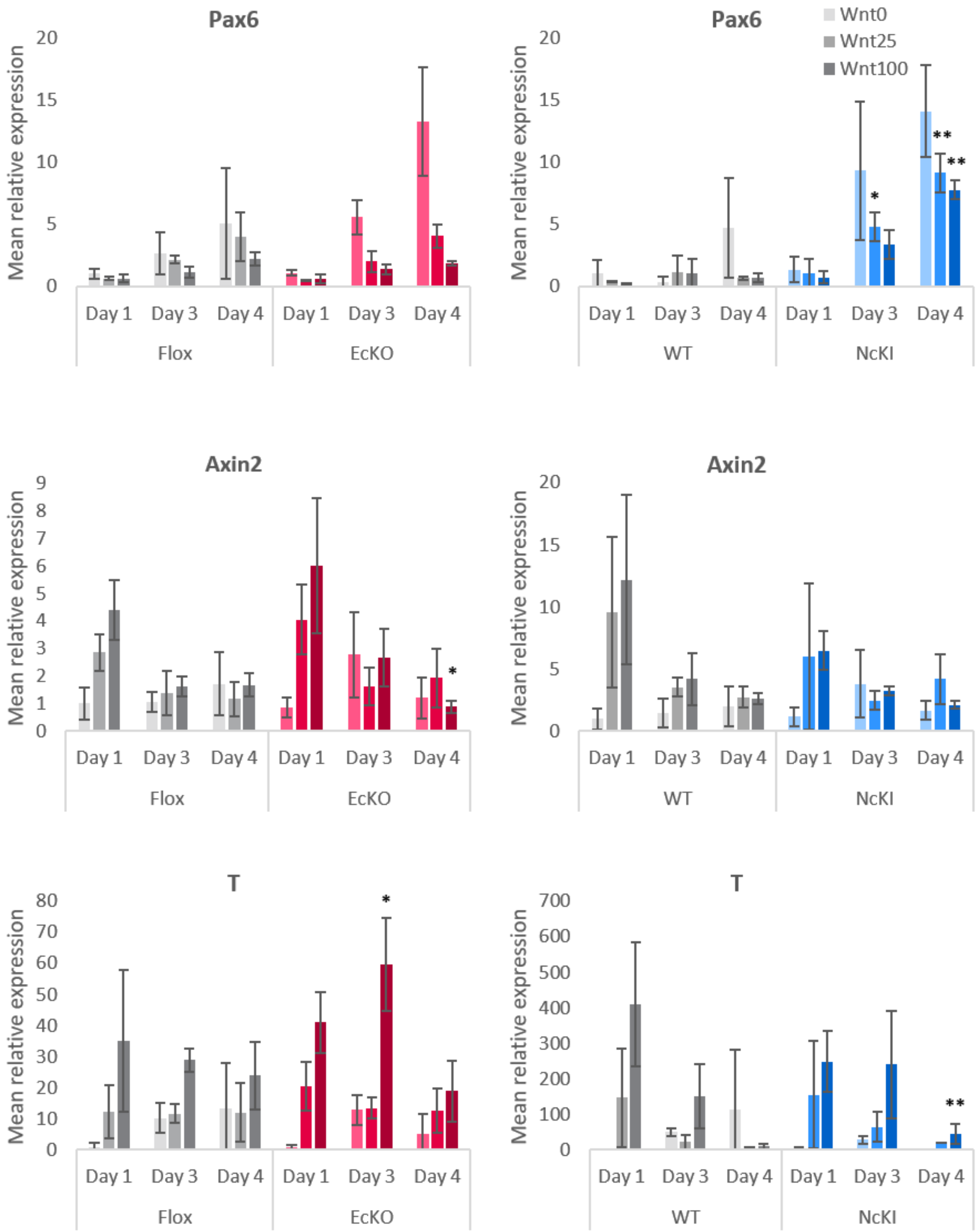
Pax6
Mean relative expression
20
15
10
5
0
Day 1
Day 3
Day 4
Flox
EcKO
Pax6
Wnt0
Wnt25
Wnt100
*
**
**
WT
NcKI
Axin2
9
8
7
6
5
4
3
2
1
0
*
Axin2
T
80
70
60
50
40
30
20
10
*
T
700
600
500
400
300
200
100
**

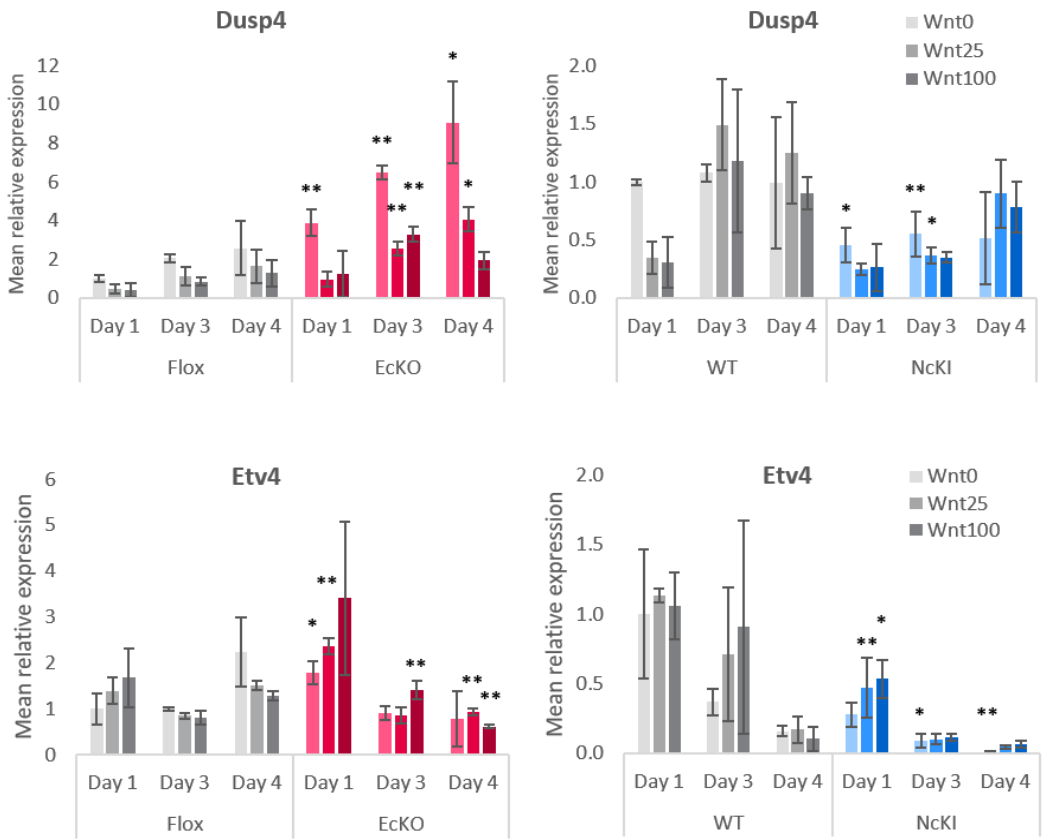

Figure 5.17 (pages 176-178): Gene expression in cadherin mutant cell lines during neural differentiation in varying concentrations of Wnt3a. *EcKO, NcKI and relevant control cell lines were cultured from 2i-Lif in neural differentiation conditions for one, three or four in varying concentrations of Wnt3a. Mean gene expression values were normalised to day one expression in the relevant control cell line. N=3, error bars = SD. Asterisks refer to significant difference compared to control cell line in the same condition, *p≤0.05, **p≤0.01, unpaired T-test.*

Next, the expression of neural marker genes was studied. In the control cell lines, the later time-points had high levels of *Sox1* and *Pax6* transcript in the absence of Wnt3a, but these levels dropped severely with the addition of Wnt3a. This result shows that Wnt3a is a potent inhibitor of neural differentiation, as reported previously (Faunes et al., 2013).

In EcKO cells, *Sox1* was significantly elevated in all Wnt3a concentrations on days one and three compared to the parental cell line, though levels of a second neural marker, *Pax6*, were not found to be significantly different. In NcKI cells however, both of these genes were highly upregulated at days three and four of the protocol, even in high doses of Wnt3a. This result suggests that forced cadherin switching, and specifically the gain of N-cadherin, promotes neural differentiation even in the presence of the anti-neural factor Wnt3a.

Next, the levels of WNT pathway target genes were investigated. Given that both of the cell lines lacking E-cadherin displayed lower levels of nuclear β-catenin during early neural differentiation, it was expected that these cells would have reduced levels of WNT signal responsiveness. In the control cell lines, there was a dose-response relationship between Wnt3a concentration and the levels of activation of *Axin2* and *T* within 24h after the addition of the ligand, as expected. This relationship was much less pronounced at later time-points, suggesting that the Wnt3a was degraded, metabolised or otherwise lost its activity after 72-96h in culture.

Surprisingly, the cadherin mutations seemed to have a minimal effect on WNT responsiveness: at day one, the EcKO and NcKI cells displayed no significant change in their levels of *Axin2* or *T* compared to control cell lines. A few differences in the levels of these genes were observed at later time points, but they did not correlate with one another, suggesting that the changes may not be functionally significant. Taken together, these results show that despite a significant drop in global and nuclear levels of β-catenin in cells lacking E-cadherin, these cells appear to maintain comparable levels of WNT responsiveness to control cells. Additionally, since the NcKI cells did not display an obvious WNT signalling phenotype, this result also suggests that this signalling pathway is not responsible for the pro-neural effect previously observed in these cells.

This raises the question of whether another pathway may be responsible for the pro-neural effect of cadherin switching. The FGF pathway has previously been associated with N-cadherin and is known to modulate neural differentiation (Williams et al., 2001). Two readouts of this pathway were assayed in the current analysis: the later FGF target gene *Dusp4*, and the early target *Etv4* (based on unpublished microarray data from Tilo Kunath). In EcKO cells, the levels of these genes differed significantly from parental cells at various time-points and concentrations of Wtn3a, suggesting that loss of E-cadherin has an effect on FGF signalling. The direction of this change was also variable in EcKO cells, perhaps implying that any effect of E-cadherin deletion on FGF signalling may be very time-dependent. In NcKI cells, several significant differences in transcript levels were also observed, and in these cells, the levels of the FGF readout genes were always found to be lower than in WT cells.

Taken together, the results of the WNT experiments showed that WNT signalling inhibits neural differentiation, and that this effect is retained even when levels of global and nuclear β-catenin are significantly reduced. The analyses also showed that forced, premature cadherin switching allows cells to overcome this WNT-based inhibition, as these cells are able to upregulate neural genes even in high concentrations of Wnt3a. The gene expression analysis also revealed an effect of cadherin switching on FGF signalling. This effect is investigated further in the next section.

5.4 N-cadherin promotes neural differentiation by dampening FGF signalling

5.4.1 Nanostring analysis implicates N-cadherin in the dampening of FGF signalling

In the previous section, NcKI cells were shown to upregulate neural genes even in the presence of high levels of Wnt3a, in contrast to WT or EcKO cells. In addition, the NcKI cells displayed lower levels of FGF readouts than control cells. This raised the possibility that N-cadherin may play a role in modulating FGF signalling, allowing the cells to switch on neural genes even in suboptimal conditions. Additionally, the neural differentiation experiments using the N-cadherin overexpression cell line showed that N-cadherin alone was able to have a pro-neural effect, but the mechanism behind this phenotype remained elusive.

To study the effect of N-cadherin alone on signalling during neural differentiation, A2Lox-Ncad-HA cells were cultured through the same neural differentiation protocol as in Chapter 4, with Dox added to induce N-cadherin overexpression at day two of the protocol. RNA samples were collected 24h and 48h after Dox induction, and the samples were then shipped to an external facility for Nanostring analysis. These time-points were chosen because N-cadherin overexpression was previously shown to cause a significant upregulation of neural markers at these times (Fig. 4.15).

Nanostring analysis tests a given RNA sample against a panel of 770 genes selected for their involvement in key cellular signalling pathways. The output is a microarray showing changes in gene expression between control and experimental samples, giving information on which signalling pathways are up- or downregulated in response to the experimental treatment. The standard sample number for one Nanostring analysis is 12 samples. Therefore, one biological replicate of three A2Lox-Ncad-HA clones was performed. The samples were analysed using a mouse nCounter® PanCancer Immune Profiling Panel containing 770 genes. Enrichment calculations and clustering were performed using the associated nSolver 4.0 software.

A dendrogram for the relationships in gene expression in the analysed samples is shown in Figure 5.18. The clustering shows that the greatest changes in gene expression are between days three and four of neural differentiation. On day three, further clustering is specific to the clone analysed, irrespective of N-cadherin overexpression. On day four however, the cells clearly cluster by presence or absence of Dox, suggesting that the overexpression of N-cadherin has a significant effect on gene expression.

Next, the enrichment of each Dox-induced sample relative to the relevant un-induced control was calculated for each day, and a mean of these relative enrichment scores was obtained based on the three clones. Statistical significance was then calculated using a paired T-test. These mean enrichment scores of all significantly changing genes are ranked in figures 5.19 and 5.20.

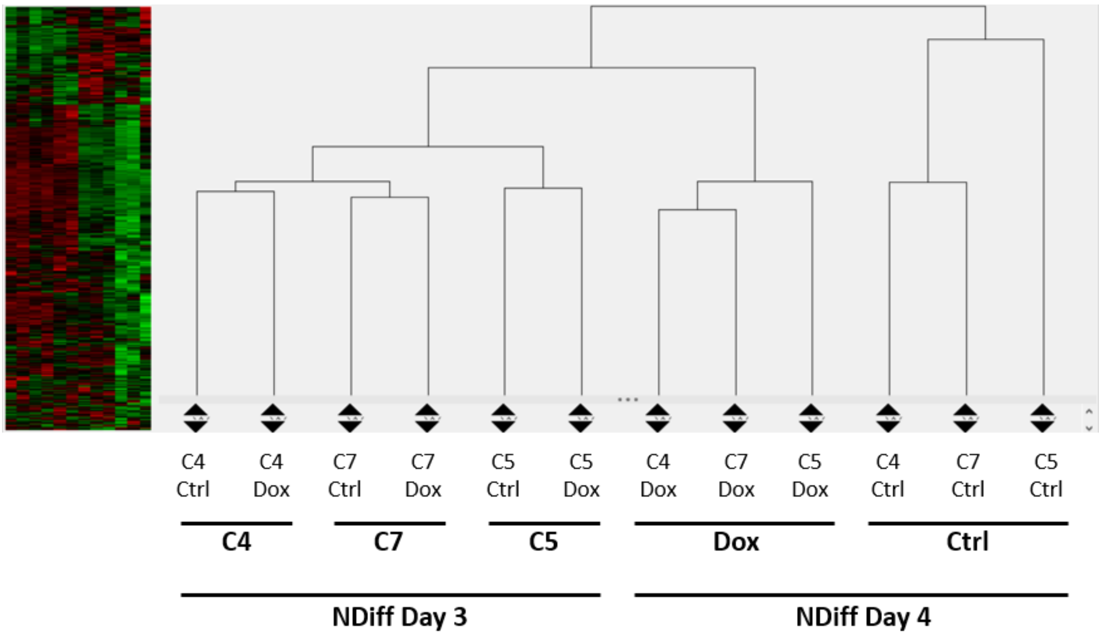

Figure 5.18: Gene expression clustering in A2Lox-Ncad-HA cells during neural differentiation. *A2Lox-Ncad cells were plated into 2i-Lif conditions for 24h before a medium change to NDiff. Dox was added to induce Ncad-HA expression on day two of neural differentiation, and the cells were lysed 24-48h after Dox induction. RNA samples were analysed by Nanostring.*

Relative expression Dox/Ctrl on day 3 of neural differentiation

0.5 0 2

Gene		Gene		Gene	
Cd19	0.22	Map2k2	0.89	E2f1	1.03
Lamc3	0.50	Ifnar1	0.89	Acvr1b	1.04
Fasl	0.51	Kdm5c	0.89	Atr	1.05
Il20ra	0.52	Mcm4	0.89	Eya1	1.08
Hnf1a	0.55	Ezh2	0.89	Pkmyt1	1.10
Id2	0.63	Nf1	0.89	Pten	1.10
Cacnb4	0.69	Mcm2	0.90	Lama5	1.13
Fos	0.69	Eif2b4	0.90	Rel	1.13
Maml2	0.72	Rps6ka5	0.90	Tlx1	1.28
Mmp3	0.72	Polr2h	0.90	Ccna1	1.32
Mapk10	0.73	Tubb5	0.90	Ptprr	1.42
Fst	0.74	Akt1	0.90	Mmp9	1.47
Six1	0.75	Casp9	0.90	Shc3	2.21
Ccnd1	0.75	Tbp	0.90	Npm2	2.59
Cdc6	0.75	Pcna	0.90	Hprt	6.42
Spry4	0.76	Fut8	0.90		
Hspa1a	0.79	E2f5	0.90		
Polr2a	0.80	Rps6ka6	0.90		
Gas1	0.80	Asxl1	0.90		
Dusp6	0.81	Cdk2	0.90		
Cdkn2c	0.82	Tbl1xr1	0.90		
Sos1	0.82	Hsp90b1	0.90		
Mapk8ip1	0.83	Crebbp	0.90		
Jag2	0.83	Fbxw11	0.90		
Pik3r2	0.83	Rac1	0.91		
Fen1	0.83	Ccne2	0.91		
Hmga1	0.84	Pole2	0.91		
Gli3	0.84	Map3k1	0.91		
Spry2	0.84	Ptpn11	0.91		
Polr1b	0.84	Npm1	0.91		
Myc	0.84	Cul1	0.91		
Mllt3	0.84	Tfdp1	0.91		
Plcb4	0.84	Itga6	0.91		
Fzd9	0.85	Gtf2h3	0.91		
Dusp4	0.85	Smc1a	0.92		
Skp2	0.85	Mcm7	0.92		
Abcf1	0.85	Stag2	0.92		
Lig4	0.86	Ctnnb1	0.92		
Atm	0.86	Ttk	0.92		
Cdc25a	0.86	Nf2	0.92		
Sufu	0.87	Rad21	0.93		
Mcm5	0.87	Sin3a	0.93		
Ercc2	0.87	Stk11	0.93		
Ikbkb	0.88	Sf3b1	0.93		
Hdac3	0.88	U2af1	0.93		
Cdk4	0.88	Smarca4	0.93		
Traf7	0.88	Ep300	0.93		
Axin1	0.88	Pbx3	0.93		
Stk4	0.88	Trp53	0.94		
Smo	0.88	Ncor1	0.94		
Hells	0.88	Kras	0.95		
Polr2d	0.88	Msh2	0.95		
Mdm2	0.89	Eef1g	0.95		
Polr2j	0.89	Ppp2r1a	0.95		
Rad51	0.89	Cacna2d3	0.96		

Relative expression Dox/Ctrl on day 4 of neural differentiation

0.5 0 2

Gene		Gene		Gene	
Il6	0.25	Tsc1	0.64	Ppp2r2b	0.83
Il20ra	0.25	Etv4	0.65	Npm1	0.83
Pla2g4e	0.26	Plcb1	0.66	Braf	0.83
Fgf21	0.33	Cacng1	0.66	Cdc14b	0.83
Rasgrp1	0.37	Il3ra	0.67	Kdm6a	0.84
Dusp4	0.37	Figf	0.67	Hdac3	0.84
Lamc3	0.39	Stat3	0.68	Foxo4	0.85
Rasal1	0.39	Mfng	0.68	Eef1g	0.86
Sfrp4	0.39	Nfe2l2	0.68	Ercc3	0.86
Tnfsf10	0.41	Itga9	0.69	Med12	0.87
Gdf6	0.43	Runx1t1	0.70	Sdha	0.87
Cxcl5	0.44	Tlx1	0.70	Stmn1	0.87
Jag2	0.48	Hdac5	0.71	Crebbp	0.88
Pik3cd	0.50	Ubb	0.72	Gsk3b	0.88
Wnt11	0.50	Cacna1h	0.72	Rad21	0.88
Itgb3	0.51	Insr	0.73	Notch1	0.89
Irak2	0.52	Cdh1	0.73	Traf7	0.90
Crlf2	0.53	Fzd8	0.74	Chuk	0.90
Spp1	0.53	Fancl	0.74	Fanca	0.91
Fgf14	0.53	Alas1	0.74	Prkaca	0.91
Map3k12	0.54	Rpl19	0.75	Prkaa2	0.91
Hdac11	0.54	Kit	0.75	Mapk9	0.92
Fosl1	0.54	Ar	0.75	Endog	0.92
Kat2b	0.55	Prkx	0.75	Prkar2a	0.92
Fgf6	0.55	Xrcc4	0.75	Ppp2r1a	0.95
Lep	0.55	Vegfb	0.76	U2af1	1.10
Ntrk1	0.56	Ppp2cb	0.76	Phf6	1.16
Prkcb	0.56	Ppp3ca	0.76	Brca1	1.18
Pla2g4a	0.56	Camk2b	0.76	Ccne1	1.26
Syk	0.56	Dtx3	0.76	Fubp1	1.26
B2m	0.56	Alkbh2	0.76	Fgfr2	1.30
Cblc	0.57	Reln	0.77	Notch3	1.38
Pml	0.57	Fn1	0.77	Jag1	1.49
Nos3	0.57	Bnip3	0.77	Fzd10	1.60
Shc2	0.58	Ep300	0.77	Pitx2	1.62
Nfkbia	0.58	Polr2j	0.78	Pax3	2.29
Efna1	0.58	Fgf13	0.78	Hes5	2.41
Il11ra2	0.58	NEG_B	0.78	Hprt	12.34
Chad	0.59	Hist1h3b	0.79		
Rasgrp2	0.60	Pik3ca	0.79		
Tlr2	0.60	Tspan7	0.79		
Cebpa	0.60	Stag2	0.79		
Birc7	0.60	Acvr1b	0.79		
Pgf	0.60	Shc1	0.79		
Ptch1	0.60	Whsc1l1	0.79		
Dkk4	0.61	Cacna1g	0.79		
Sgk2	0.62	Edc3	0.80		
Birc3	0.62	Bax	0.81		
Pim1	0.62	Uty	0.81		
Hspa2	0.62	Tsc2	0.81		
Efna3	0.63	Mgmt	0.81		
Tet2	0.64	Ercc6	0.83		

Figure 5.19 (page 182): Mean relative expression of significantly changing genes between induced and un-induced A2Lox-Ncad-HA cells on day three of neural differentiation. *Dox was added on day two of the protocol. Gene expression was quantified using Nanostring analysis. Values are a mean of three independent clones from one biological replicate.*

Figure 5.20 (page 183): Mean relative expression of significantly changing genes between induced and un-induced A2Lox-Ncad-HA cells on day four of neural differentiation. *Dox was added on day two of the protocol. Gene expression was quantified using Nanostring analysis. Values are a mean of three independent clones from one biological replicate.*

On both days, the most upregulated gene in the induced cells is *Hprt:* this result is explained by the fact that the *Hprt* locus is the constitutively active site where the overexpression construct is located. Within the set of significantly changing genes, most were found to be downregulated in response to N-cadherin overexpression, and many more genes displayed a significant change in response to N-cadherin overexpression on day four compared to day three of the protocol.

To determine which signalling pathways were most represented in this dataset, the DAVID Functional Annotation Analysis Wizard was used (Huang et al., 2008; Huang et al., 2009). This is an online bioinformatics tool that allows users to input any list of genes and compare them to a custom genetic background. For this analysis, all the significantly changing genes were used as an input gene list, while all 770 genes assayed in the Nanostring panel were input as the background. The output of the analysis is a list of signalling pathways and a corresponding number of input genes involved in that pathway accompanied by a p-value. This approach generates a list of pathways by number of affected genes, but not necessarily by the magnitude or direction of the change in expression of particular genes. The results of the analysis are displayed in Fig. 5.21.

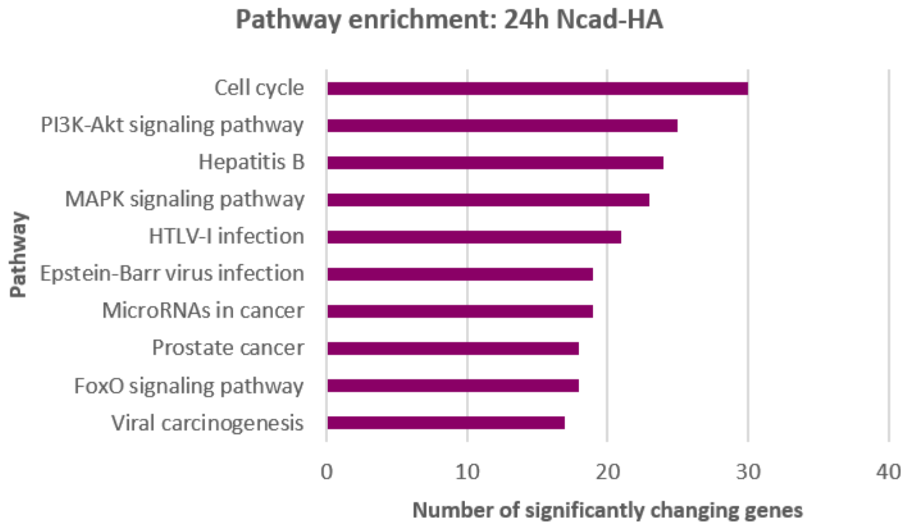

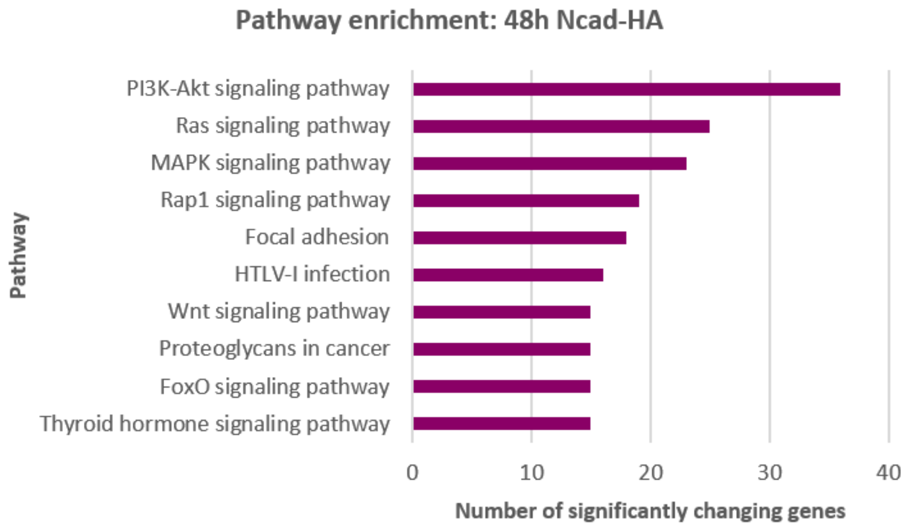

Figure 5.21: Top ten pathways represented by significantly changing genes in response N-cadherin overexpression during neural differentiation. *Significantly changing genes identified by Nanostring RNA analysis were classified by the DAVID functional annotation tool. Significance was calculated by paired T-test on three clonal replicates. Graphs show the number of significantly changing genes (125 genes on day three, 142 genes on day four) compared to all 770 genes assayed.*

The results of the Nanostring and DAVID analyses show that after 24h of N-cadherin overexpression during neural differentiation, genes involved in cell cycle are most affected. Of the top four pathways responding to N-cadherin overexpression at this time-point, two (PI3K-Akt and MAPK) represent components of the FGF pathway. After 48h of N-cadherin overexpression, the top three pathways are components of the FGF pathway. These results imply that FGF signalling is significantly affected by the gain of N-cadherin. In addition, since the majority of significantly changing genes following Dox-induction were downregulated (Figs 5.19, 5.20), the analysis suggests that a gain of N-cadherin during neural differentiation results in the dampening of FGF signalling. To follow up this finding, the mechanism behind this effect was investigated.

5.4.2 Modulating FGF signalling rescues the pro-neural effect of NcKI cells and replicates it in WT cells

To establish how FGF signalling affects gene expression in cadherin mutant cells undergoing neural differentiation, the cells were cultured through a neural differentiation protocol in the presence of an agonist or inhibitor of the FGF signalling pathway. WT, NcKI and A2Lox-Ncad-HA cells were seeded at a density of 5,000 cells per well into 12-well plates in 2i-Lif conditions. After 24h, media were changed to NDiff. On day two of the protocol (48h after media change) 20ng/mL of FGF2, a ligand for the FGF pathway, or 100ng/mL of PD173074 (abbreviated to PD17), a specific inhibitor of FGFR1, was added. Dox was also added to the A2Lox-Ncad-HA cells at this time point. On days three and four, the cells were lysed for qPCR analysis. This experimental protocol is depicted in Figure 5.22. The results of the qPCR analysis are shown in Figures 5.23 and 5.24.

In NcKI cells, *Cdh2* was upregulated compared to WT cells at both time-points and in most conditions, as expected. Addition of FGF2 caused a spike in the FGF target genes *Dusp4* and *Etv4*, while addition of the FGFR1 inhibitor PD17 caused the levels of both of these genes to drop to near-zero levels in all cell lines studied. Interestingly, NcKI cells showed reduced levels of FGF target genes, both when no ligands were added, and when the medium was supplemented with FGF2. This result strongly suggests that forced, premature cadherin switching causes cells to dampen their endogenous FGF output, and to also lose their responsiveness to external FGF signals.

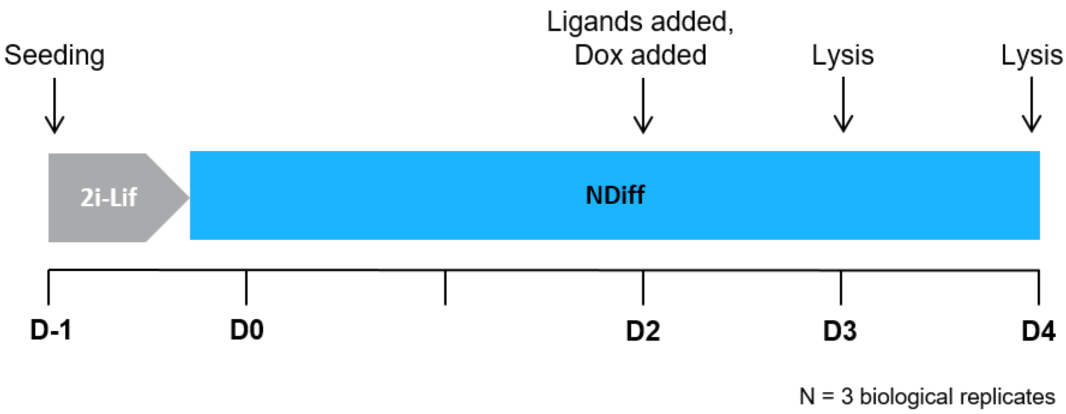

Figure 5.22: Experimental protocol for testing the effect of modulating FGF on neural differentiation during cadherin switching. *WT, NcKI and A2Lox-Ncad-HA cells were seeded at a concentration of 5,000 cells per well into 12-well plates. Ligands added were either FGF2 (at 20ng/mL) or PD17 (at 100ng/mL). Dox added at 1µg/mL as before. Cells were lysed for qPCR analysis on days three and four.*

How does this change in FGF responsiveness affect neural differentiation? Neural marker genes (*Sox1* and *Pax6)* were upregulated in untreated NcKI cells compared to WT cells, as previously shown. Importantly, FGF2 treatment was found to predominantly reduce the expression of these genes, while the FGFR inhibitor generally elevated their levels in both WT and NcKI cells. These results suggest that FGF signalling inhibits neural differentiation. Importantly, promoting FGF signalling reduced the level of *Sox1* to similar levels as those observed in WT cells, while inhibiting FGF signalling in WT cells raised *Sox1* expression to a similar level observed in untreated NcKI cells. The effect was also present but not as pronounced for *Pax6*, where levels of this gene were consistently higher in NcKI cells compared to WT cells in all conditions. This partial rescue suggests that FGF signalling plays a role in the pro-neural effect observed in NcKI cells.

Perhaps surprisingly, a similar rescue was not observed in A2Lox-Ncad-HA cells. As expected, addition of Dox to these cells caused a significant upregulation of *Cdh2*. Interestingly, the addition of PD17 caused a significant spike in the levels of *Cdh2* transcript in both induced and un-induced cells, especially at day four of the protocol, or 48h after the addition of the inhibitor. This result may point towards a role of FGFR1, or FGF signalling as a whole, in the inhibition of *Cdh2* transcription.

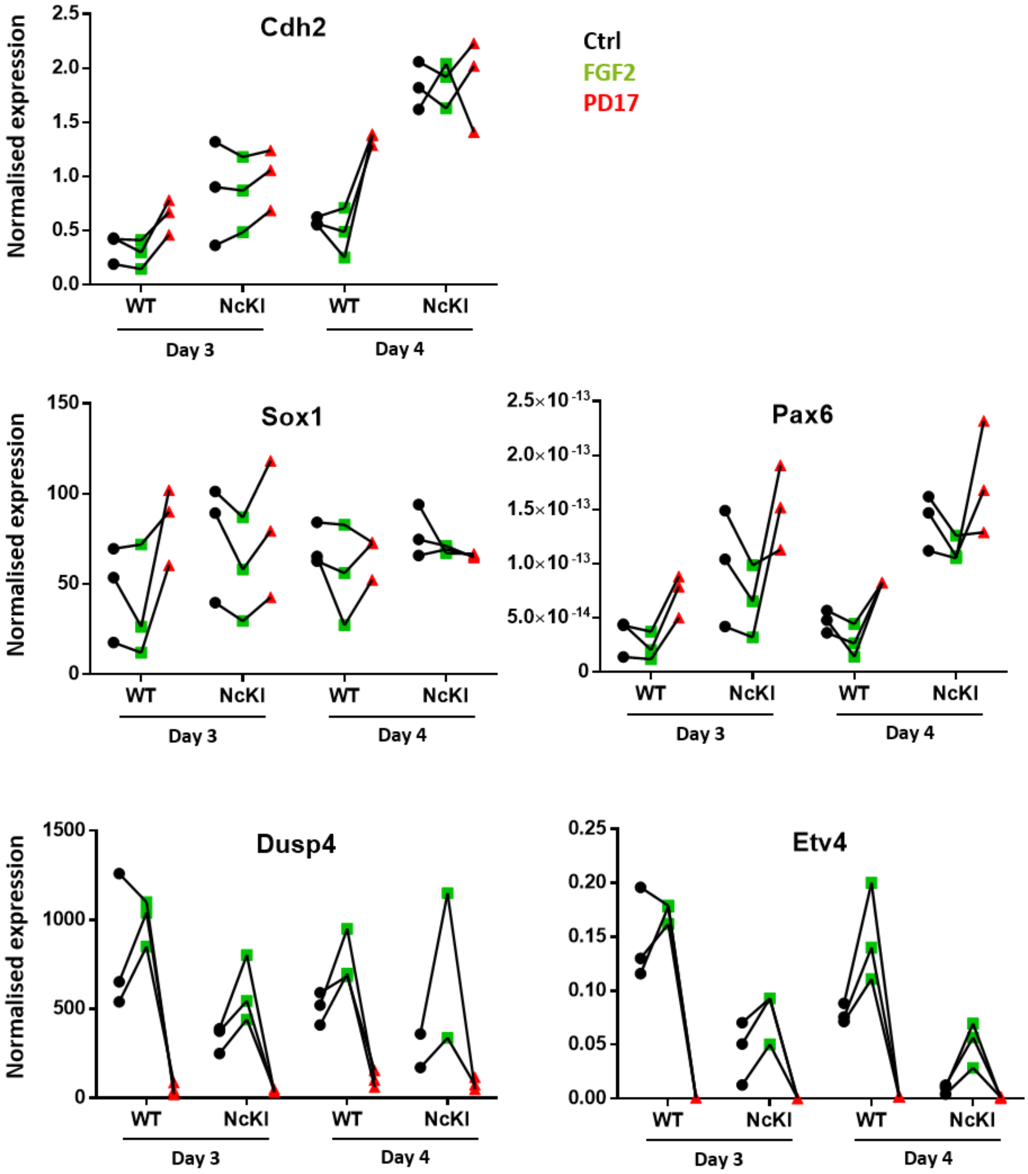

Figure 5.23: Gene expression in WT and NcKI cells on days three and four of neural differentiation with activators and inhibitors of FGF signalling. *Ligands were added on day two of neural differentiation at a concentration of 20ng/mL for FGF2 and 100ng/mL for PD17. N=3 biological replicates, all replicates shown. Lines connect values for each biological replicate.*

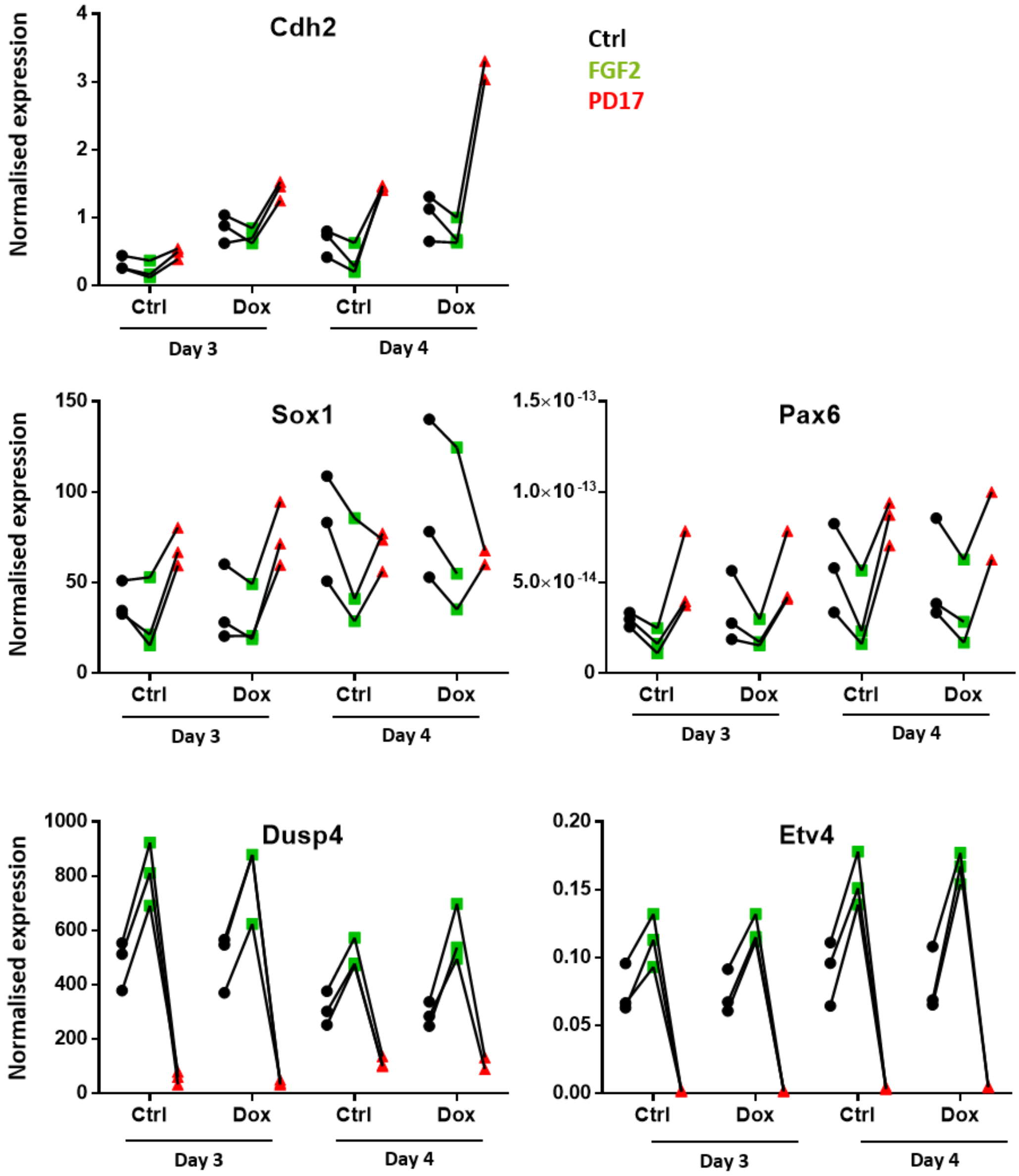

Figure 5.24: Gene expression in A2Lox-Ncad-HA cells on days three and four of neural differentiation with activators and inhibitors of FGF signalling. *Ligands and Dox were added on day two of neural differentiation at a concentration of 20ng/mL for FGF2, 100ng/mL for PD17 and 1µg/mL of Dox. N=3 biological replicates for one clonal cell line, all replicates shown. Lines connect values for each biological replicate.*

As with the NcKI cells, addition of FGF2 and PD17 had a similar effect of reducing or promoting the expression of neural markers, respectively. These results yield further evidence that at this time-point in early neural differentiation, activation of FGF signalling inhibits neural specification.

However, no significant differences were observed in the expression of the two neural markers or the FGF target genes between control and N-cadherin overexpressing cells in any of the conditions tested. This suggests that the gain of N-cadherin was not enough to promote upregulation of neural genes, and did not have a significant effect on the FGF signalling profile of the cells. This result was unexpected, as the large-scale neural differentiation experiment with three independent clones in Chapter 4 showed that overexpression of N-cadherin led to increased expression of neural markers (Fig. 4.15), while the Nanostring experiment implicated the gain of N-cadherin in a dampening of FGF signalling.

Taken together, the results of this study yield a number of conclusions. First, the results clearly indicate that FGF signalling inhibits early neural differentiation, and conversely, inhibition of FGF signalling promotes this process. Second, forced and premature cadherin switching causes a drop in FGF signalling: adding FGF2 to NcKI cells increases *Dusp4* transcript to similar levels as those observed in WT cells, and causes the levels of *Sox1* and *Pax6* to drop in NcKI cells. Conversely, adding an FGFR1 inhibitor to WT cells causes their levels of FGF target transcript to plummet, and increases *Sox1* and *Pax6* transcripts to a similar level as those observed in untreated NcKI cells. Surprisingly, overexpression of N-cadherin alone was unable to produce a similar effect.

These results indicate that cadherin switching promotes early neural differentiation by dampening FGF signalling.

5.5 Discussion

5.5.1 Cell clustering is altered during cadherin switching, but this does not fully explain the pro-neural phenotype of NcKI cells

Since adhesion is a key function of cadherin proteins, it was important to determine whether the pro-neural effect in cadherin mutant cells observed during neural differentiation was caused by changes in adhesion. In order to achieve this, a system for the quantification of nuclear clustering was devised by measuring inter-nuclear distances, as an indirect readout of cellular adhesion.

The analysis of inter-nuclear edge distances in EcKO, NcKI and A2Lox-Ncad-HA cells showed that the loss of E-cadherin resulted in a pronounced clustering defect, where the nuclei were visibly further apart from one another. Moreover, this effect could not be rescued by the knock-in of N-cadherin (Fig. 5.4). This phenotype is similar to that observed *in vivo*, where E-cadherin-null embryos die at pre-implantation stages due to failure in morula compaction due to adhesive defects (Larue et al., 1994). Knocking in N-cadherin can initially rescue morula compaction, but the embryos subsequently die due to a failure in the generation of polarised trophectoderm (Kan et al., 2007). Even when the NcKI mutation is induced after gastrulation, the embryos die at around E8.5 due to gross morphological defects, including massive cell detachment from the ectoderm (Basilicata et al., 2016). These studies identify a specific and critical role for E-cadherin in cell adhesion and highlight its importance at multiple stages of development; the results from the clustering analysis presented here confirm that E-cadherin also plays a specific role in cell-cell adhesion *in vitro*.

The clustering analysis also showed that overexpression of N-cadherin led to a small but significant increase in inter-nuclear edge distance (Fig 5.4). This may be explained by N-cadherin's reduced adhesive capacity compared to E-cadherin: atomic force microscopy studies have shown that E-cadherin has three to four times the adhesive strength of N-cadherin (Chu et al., 2004; Chu et al., 2006). Additionally, levels of *Cdh1* transcript were found to drop in response to Dox in the inducible cells (Fig 4.15), suggesting that the change in adhesion profile from E- to N-cadherin may be promoting looser adhesion in these cells.

Importantly, the changes in clustering were not sufficient to fully explain the pro-neural phenotype observed in cells undergoing cadherin switching. The mean inter-nuclear distance of cells over-expressing N-cadherin, though significantly higher from un-induced cells, was still similar to that of WT cells. The fact that the N-cadherin overexpressing cells display a pro-neural phenotype in contrast to the three control cell lines suggests that an alternative mechanism may be responsible for the effect, which enables the cells to have a neural bias even when they maintain a WT-like clustering profile. Additionally, the analysis found that EcKO and NcKI cells share an almost identical inter-nuclear clustering profile, but these cells behave very differently in neural differentiation conditions, with EcKO cells showing poor long-term survival while NcKI cells show exhibit normal survival and a bias for the neural lineage.

These results showed that while cadherin switching affects cellular clustering, the observed changes in adhesion cannot fully explain the pro-neural phenotype of cells undergoing cadherin switching. This in turn raises the possibility that a signalling effect may be responsible for the neural bias observed in these cells.

5.5.2 Cells lacking E-cadherin lose β-catenin, but retain Wnt responsiveness during early neural differentiation

Since adhesive changes were eliminated as the main mechanism behind the pro-neural effect in cells undergoing cadherin switching, attention was turned to signalling changes in these cells. RPPA protein analysis revealed a significant drop in the level of global β-catenin in cells lacking E-cadherin, an effect previously reported in various E-cadherin-null cell types (Hendriksen et al., 2008; Orsulic et al., 1999; Wetering et al., 2001). However, the levels of two phosphorylated forms of β-catenin were not found to change significantly in the cadherin mutant cells (Figs. 5.5 and 5.6).

Cadherins have traditionally been viewed as negative regulators of WNT signalling, because they sequester newly synthesised cytoplasmic β-catenin to the outer cell membrane, protecting the protein from degradation but also preventing it from being translocated to the nucleus to promote transcription of target genes (discussed in Howard et al 2011). The un-phosphorylated form of β-catenin can be found in three cellular compartments: in an E-cadherin-associated complex at the cytoplasmic membrane, as a newly synthesised form in the cytoplasm, and as the transcriptionally active form in the nucleus; phosphorylation marks the protein for degradation by the cytoplasmic β-catenin destruction complex (Clevers, 2006). The significant drop in the un-phosphorylated form in the cells lacking E-cadherin points towards a global loss of β-catenin. ICC staining of E-cadherin-null cells suggests that all of these compartments are affected (Figs. 5.7 and 5.8) and PickCells analysis additionally confirms a drop in nuclear levels of β-catenin in these cells (Fig. 5.13).

However, the RPPA analysis also showed that there was no change in the levels of two phosphorylated forms of β-catenin after 24h of neural differentiation. This result could indicate that there is no change in the levels of free cytoplasmic β-catenin marked for degradation, perhaps suggesting that the rate of translation of nascent β-catenin is low at this time-point, and stays that way in cells lacking E-cadherin. This idea is supported by the fact that there is an absence of Wnt ligands in the anterior neurectoderm during development (Arnold and Robertson, 2009), implying that this pathway is not involved in neural specification and that WNT signalling is inactive in the cells studied.

While the exact mechanism behind the changes in β-catenin and its subcellular localisation lends itself to further discussion, its relevance to this study hinges on whether this phenotype has an effect on WNT signalling or neural differentiation. Therefore, the WNT signalling response of the cells undergoing cadherin switching was investigated further.

5.5.2.1 Reasons for high variation in nuclear β-catenin in later neural differentiation

At days three and four of the neural differentiation protocol (and in contrast to day one), the levels of nuclear β-catenin and Sox1 quantified by PickCells analysis varied significantly even in identical experimental conditions (Fig. 5.16). There were also notable differences in trends in protein expression observed between control and cadherin mutant cells. There are a number of possible reasons for this high level of variation.

As noted in Chapter 3, the *in vitro* neural differentiation protocol from 2i-Lif used throughout this thesis shows around a day's worth of variation in the timing of Sox1 upregulation and endogenous cadherin switching, and patches of Oct4 and E-cadherin expression remain even after five days of neural differentiation. Since the experiments were performed with related but independent cell lines acting as controls, this variation in the speed of neural differentiation may have contributed to the large differences observed in the behaviour of biological replicates.

The image analysis pipeline for the quantification of nuclear protein signal relies on accurate nuclear segmentation. As mentioned earlier (and illustrated in Fig. 5.1), the later days of the neural differentiation protocol can give rise to areas of high cellular density, leading to poorer-quality nuclear segmentation. This may have contributed to the increased variation observed in the data at days three and four of neural differentiation.

In addition, cells undergoing neural differentiation tend to lift off at the latter stages of this protocol; to try to avoid this, the cells are seeded onto laminin in 2i-Lif conditions for 24h to allow better cell adhesion to the matrix. The cells were found to exhibit weaker adhesion to the glass coverslips than to the underlying tissue culture plastic, and tend to detach during the various media change or washes, even after sample fixation in formaldehyde. The ICC staining protocol also involves a number of wash steps, leading to more cell detachment. As such, the cells that were finally imaged and analysed for nuclear signal intensity may reflect just those cells that were able to survive and adhere to the glass for the duration of the differentiation and staining protocols, and may therefore not be an accurate or reliable representation of all differentiating cells.

5.5.2.2 Cells with depleted β-catenin retain WNT responsiveness

To determine whether the significant changes in levels of β-catenin caused differences in WNT signalling responsiveness, or contributed to the pro-neural phenotype observed during cadherin switching, EcKO and NcKI cells were tested for their WNT responsiveness during neural differentiation. A dose-response effect to the addition of Wnt3a on WNT target genes was observed on day one of the protocol in all cell lines tested (Fig. 5.17). The same effect was also observed to a lesser extent at later time-points, but not for both of the genes tested and not in all conditions. This results showed that within 24h of pathway stimulation, cadherin mutant cells retain WNT responsiveness to comparable levels as those observed in WT cells. This result was confirmed by the behaviour of neural marker genes. Wnt3a was found to significantly inhibit neural differentiation, as previously reported (Faunes et al., 2013), and both control and EcKO cells treated with Wnt3a had significantly lower levels of *Sox1* and *Pax6* on days three and four of the neural differentiation protocol.

The fact that cells lacking E-cadherin have reduced levels of β-catenin, but retain the ability to activate transcriptional targets of this protein, has been previously reported in various cell types (Hendriksen et al., 2008; Wetering et al., 2001), including mES cells (Orsulic et al., 1999). These findings suggest that levels of either global or nuclear β-catenin do not directly correlate with WNT signalling activity. There are several possible explanations for this: first, it is plausible that even low levels of nuclear β-catenin are sufficient to activate WNT target genes. Second, a non-canonical WNT pathway that does not require β-catenin could be responsible for the upregulation of WNT targets. Finally, it is plausible that newly synthesised β-catenin translocates directly to the nucleus, thus bypassing sequestration by E-cadherin at the membrane and resulting in lower global levels of the protein; however this mechanism seems unlikely as nuclear β-catenin levels are also significantly reduced in cells lacking E-cadherin; moreover, it has been reported that the β-catenin/E-cadherin interaction at the membrane "primes" β-catenin for enhanced transcriptional activity (Howard et al., 2011), suggesting that in the absence of E-cadherin at the membrane, β-catenin is less transcriptionally potent.

In addition to showing that cells lacking E-cadherin can retain WNT responsiveness, this experiment also confirmed the pro-neural effect previously observed in NcKI cells. Surprisingly, *Sox1* was also significantly upregulated in some conditions in EcKO cells, perhaps indicating a marginal role for the loss of E-cadherin in promoting neural differentiation. Addition of Wnt3a correlated with a notable improvement in cell survival of EcKO cells, supporting the idea that their instability is the reason that these cells fail to replicate previous reports of improved neural differentiation (Malaguti et al., 2013).

Interestingly, NcKI cells were able to upregulate neural genes even in the presence of high doses of Wnt3a. In particular, the levels of *Sox1* at day four were near-identical irrespective of the Wnt3a concentration that they were exposed to earlier on. This result highlights that NcKI cells exhibit a strong pro-neural phenotype, even in suboptimal differentiation conditions. Since EcKO and NcKI cells have similar adhesion, β-catenin, and WNT responsiveness profiles, yet exhibit markedly different behaviour during neural differentiation, it is likely that the pro-neural phenotype is not primarily caused by the aforementioned factors. It also implies that N-cadherin is an important contributor to this phenotype. This raised the possibility that a signalling pathway other than the WNT pathway is modulated by N-cadherin to promote neural fate.

5.5.3 N-cadherin overexpression dampens FGF signalling during neural differentiation

To determine whether the overexpression of N-cadherin alone could modulate signalling during neural differentiation, Nanostring analysis was used to measure mRNA-level signalling pathway activity in N-cadherin overexpressing cells. Clustering analysis 24h after the addition of Dox to induce N-cadherin overexpression found more differences in gene expression between individual clones than between induced and un-induced samples, while after 48h, the induced samples clustered separately to un-induced samples (Fig. 5.18). This result suggests that major changes in the expression of genes related to cellular signalling occur in response to N-cadherin overexpression within 48h of induction.

A striking feature of the trends in gene expression following N-cadherin overexpression is that the majority of significantly changing genes are downregulated (Figs 5.19 and 5.20). At 48h post-induction, functional annotation analysis shows that the most represented pathways amongst these significantly changing genes are PI3K-Akt, Ras and MAPK, which all represent major branches in the FGF signalling pathway that lie downstream of FGF receptors (Lanner and Rossant, 2010). These results suggest that overexpression of N-cadherin alone is able to cause significant downregulation of the FGF pathway during neural differentiation.

5.5.3.1 Cadherin switching promotes neural differentiation by dampening FGF signalling

In order to determine whether increasing FGF activity could supress the pro-neural effect of N-cadherin, a rescue experiment was designed (Fig 5.22).

First, it was confirmed that N-cadherin knock-in does dampen FGF responsiveness, since NcKI cells displayed significantly lower levels of FGF readouts compared to WT cells (Fig. 5.23). Next, it was confirmed that FGF signalling suppresses neural differentiation: addition of an FGF ligand inhibited the expression of neural genes, while the use of an FGFR1 inhibitor caused the levels of these genes to increase in all cell lines studied. Finally, we asked whether increasing FGF can rescue the pro-neural effect of N-cadherin. Strikingly, addition of the FGF receptor inhibitor to WT cells raised their levels of *Sox1* to similar levels as those seen in untreated NcKI cells, while the addition of an FGF agonist to NcKI cells reduced levels of this gene to similar levels as those observed in untreated WT cells. Similar trends were observed for a second neural marker, *Pax6*. These results strongly suggest that FGF signalling inhibits neural differentiation, and that a dampening of this pathway in NcKI cells allows them to undergo more efficient neural induction compared to WT cells.

However, there is a limitation to this model – RPPA analysis of cells after 24h in neural differentiation conditions showed that NcKI cells displayed higher, not lower levels of most PI3K/Akt and MAPK/ERK components of the FGF pathway (Fig 5.5). In many cases, these increases were statistically significant. This is in contrast to the lowered level of FGF signalling documented in the Nanostring and FGF rescue experiments, which were performed at days 3-4 of neural differentiation. These result suggests that the effect of cadherin switching on

FGF signalling is highly dependent on context and timing. This is discussed in greater detail in Chapter 6.

5.5.3.2 Reasons or a lack neural bias in N-cadherin overexpressing cells in the FGF response study

In contrast to the previous experiment on neural differentiation of N-cadherin overexpressing cells described in this thesis (Fig 4.15), no pro-neural effect was observed in these cells in the final FGF-response experiment (Fig. 5.24). There are several possible reasons for this lack of response. First, the original N-cadherin overexpression experiment in neural differentiation (described in Chapter 4) included three biological replicates of three independent A2Lox-Ncad-HA clonal cell lines, enabling more robust statistical analysis and the detection of smaller significant changes in gene expression due to a larger sample size. Second, perhaps the level of *Cdh2* upregulation in this experiment was not strong enough to have a robust effect on neural differentiation or FGF signalling, or the particular clone chosen may be more recalcitrant to neural differentiation than the two other clones used throughout the rest of the thesis. These limitations may be resolved by repeating the experiment with three independent clonal cell lines and three biological replicates.

It is also unclear why the N-cadherin overexpressing cells do not phenocopy NcKI cells in the FGF response study, with respect to both upregulation of neural markers and downregulation of FGF target genes. One explanation may be that full cadherin switching, or a pronounced drop in the levels of E-cadherin, may be required for the full pro-neural effect.

5.5.4 Summary

In conclusion, the studies described in this chapter have investigated the mechanisms behind the pro-neural effect observed in cells with forced, premature cadherin switching (NcKI cells), and cells with induced N-cadherin overexpression. Cellular clustering was found to be affected by cadherin switching, but these adhesive defects did not correlate with more efficient neural differentiation. Loss of E-cadherin resulted in significant reduction in levels of global and nuclear β-catenin, but this did not affect WNT responsiveness of E-cadherin null cells. Interestingly, NcKI cells displayed efficient neural induction even in suboptimal differentiation conditions with added Wnt3a. Finally, N-cadherin was found to modulate FGF signalling during neural differentiation, and FGF rescue experiments demonstrated that changes in FGF signalling can explain the differences in the rates of neural induction between WT and NcKI cells. Taken together, these results show that cadherin switching promotes neural differentiation by dampening FGF responsiveness.

Chapter VI – General Discussion

6.1 Differences between the timing of cadherin switching *in vitro* and *in vivo*

Cadherin switching is a process occurring at a number of developmental stages, in diverse cell types, and in various tissues. A growing body of evidence implicates the cadherins in playing important roles not only in adhesion, but also in various cellular signalling pathways. The main focus of this project was therefore to assess whether cadherin switching can influence differentiation competence of pluripotent stem cells, and if so, to investigate the molecular mechanisms behind this effect. The anterior neurectoderm was selected since this is a tissue where cadherin switching is observed relatively early in embryogenesis and reproducible protocols for its differentiation have been established *in vitro* (Pollard et al., 2006; Ying et al., 2003a). Additionally, neurectodermal competence has been proposed as the fate that pluripotent cells adopt in the absence of other instructive signals (Muñoz-Sanjuán and Brivanlou, 2002), making it a model system with few external inputs, and that is therefore relatively simple to study.

First, the timing of cadherin switching was investigated: if the switch was found to occur after overt neural specification, it would be unlikely to play a role in the induction of this process. Results presented in this thesis showed that in EpiSCs *in vitro*, cadherin switching is initiated at the transcriptional level in cells that continue to express pluripotency markers (Figs. 3.5, 3.6 & 3.8), and that this switch coincides with the expression of early neural and mesodermal markers, suggesting that it may be tied to priming towards these lineages (Fig. 3.8). Additionally, studies of neural differentiation *in vitro* showed that for a brief time around day three to four of differentiation from 2i-Lif, a subset of cells co-express N-cadherin, Oct4 and Sox1, again suggesting that cadherin switching may coincide with neural priming (Fig. 3.11). These findings showed that *in vitro*, cadherin switching is initiated prior to the loss of pluripotency, prompting the theory that the switch may be occurring early enough to play an instructive role in lineage commitment.

However, *in vivo* gene expression data presented in this thesis and elsewhere have shown that the earliest protein level E- to N-cadherin switch in the developing mouse embryo takes place in nascent mesoderm at around E7.5, followed by ectodermal tissues about a day later (Figs. 3.1, 3.2, and Radice et al., 1997). Other studies have shown that at E7.0, the anterior ectoderm is no longer pluripotent and is primed for epidermal or neurectodermal fate depending on the presence or absence of BMP4, respectively. By E7.5, the ectoderm was shown to be restricted to either neural or epidermal fate depending on its positioning in the embryo (Li et al., 2013).

These studies imply that cadherin switching is initiated at subtly different developmental time-points *in vivo* than in analogous *in vitro* systems, raising questions about the validity of *in vitro* findings if they do not match the events observed during embryonic development. For example, N-cadherin protein has been widely reported to be expressed in EpiSCs (Rugg-Gunn et al., 2012; Takehara et al., 2015), but has not been observed in the primed epiblast *in vivo* – its earliest detection on the transcript level is in the posterior of the E6.5 gastrula (Peng et al., 2016). It is therefore unclear whether the findings on cadherin switching in EpiSCs are directly applicable to *in vivo* development. Further studies are required to determine why some *in vitro* conditions are more permissive to the expression of certain proteins than the analogous stages of embryonic development *in vivo*.

A second population in which cadherin switching is observed are bi-potent NMPs, which can give rise to either neural or mesodermal derivatives. Microarray data from NMPs show that their maturation, occurring between E8.5 and E9.5, is accompanied by an E- to N-cadherin switch (Gouti et al., 2017). Results presented in this thesis showed that N-cadherin overexpression during an *in vitro* NMP maturation protocol biased lineage choice in these cells (Fig. 4.19), suggesting that cadherin switching may play a role in cell fate decisions in this developmental context as well.

For all the developmental contexts in which cadherin switching was studied – EpiSCs, anterior neural differentiation, and NMP maturation – it would be highly informative to test how the *in vitro* findings presented in this thesis hold up when tested in the analogous context *in vivo*. For example, induction of the NcKI mutation *in vivo* has been attempted previously in both the pre- and post-implantation embryo, and in both contexts the mutation resulted in embryonic lethality (Basilicata et al., 2016; Kan et al., 2007). Interestingly, when the mutation was induced post-implantation, it resulted in cell detachment from the E7.5 ectoderm, in addition to several gross embryonic malformations (Basilicata et al., 2016). These findings suggest that forced, premature cadherin switching in this embryonic tissue results in adhesive defects that prohibit normal neurectodermal development, in contrast to the *in vitro* findings presented in this thesis, which found that the mutation promotes neural differentiation despite adhesive defects. As an alternative approach, a less severe mutation could be studied *in vivo* by electroporating the inducible N-cadherin overexpression constructs into the relevant embryonic compartments, and testing their contribution to various lineages.

In conclusion, the results presented in this thesis show that *in vitro*, cadherin switching occurs early enough to play a role in directing pluripotent cells towards certain lineages, and correlates with lineage priming. However, given *in vivo* expression data presented here and prior fate mapping studies (Li et al., 2013), it is not possible to conclude whether cadherin switching may have the same effect during *in vivo* development. We propose that cadherin switching is unlikely to be a critical instructive signal for neurectoderm specification *in vivo*, but may rather be contributing a secondary signal that gives the system additional robustness during embryonic development (discussed in more detail below).

6.2 The role of cadherin switching in neural differentiation

6.2.1 Loss of E-cadherin causes cellular instability during neural differentiation

Previous studies have shown that blocking E-cadherin can lead to faster, more synchronous neural differentiation (Malaguti et al., 2013). It was therefore surprising that populations of EcKO cells did not differ from control cells in their expression of neural marker genes during neural differentiation from 2i-Lif (Fig. 4.4). Instead, the EcKO cells displayed a profound cell death phenotype in the later stages of this process, leading to the necessity of upscaling the experimental protocol just to yield enough sample for qPCR analysis (Fig. 4.3), and suggesting that E-cadherin is necessary to maintain cellular stability during neural differentiation. RPPA analysis also showed that EcKO cells at 24h of differentiation exhibit increased levels of cleaved caspase-3 (Fig. 5.5), a marker of cell death, supporting the notion that these cells have higher levels of apoptosis than parental control cells.

Indeed, E-cadherin has previously been linked to cell survival in other contexts. hESCs do not tolerate single-cell culture, a phenomenon that has been linked to the loss of E-cadherin mediated adhesion. Attenuation of this adhesion by chelation of calcium ions, blocking antibodies or RNAi leads to apoptosis in hESCs, and has been linked to Rho-ROCK signalling (Ohgushi and Sasai, 2011; Ohgushi et al., 2010; Xu et al., 2010). Interestingly, the same effect is observed in dissociated mEpiSCs but not in mESCs, and has been ascribed to pluripotency state-dependent ROCK/myosin hyper-activation (Ohgushi et al., 2010); this may explain why EcKO cells appear healthy in the first 24h of neural differentiation from 2i-Lif conditions, but become increasingly sparse with further culture (Figs. 5.7, 5.14).

However, additional experiments described in this thesis showed that occasionally, surviving EcKO cells could indeed exhibit higher levels of Sox1 mRNA or protein in neural differentiation conditions than control cells, sometimes significantly (Figs. 5.16, 5.17). The evidence is therefore mixed as to whether the loss of E-cadherin can have an effect on neural differentiation- is conceivable that the cell death phenotype of EcKO cells is so extreme that it masks any significant pro-neural effect that this mutation could have. The NcKI mutation was shown to rescue the cell death phenotype, allowing cells to survive the neural differentiation protocol in high numbers. Since NcKI cells have been reported to rescue cadherin-based adhesion during pre-implantation development (Kan et al., 2007), it is possible that the severe and extensive adhesion phenotype of EcKO cells is responsible for their elevated rate of apoptosis.

In subsequent experiments, the NcKI mutation was also found to promote neural differentiation, however it is unclear whether this was due to a pro-neural effect of knocking-in N-cadherin, a synergistic effect of simultaneous loss of E-cadherin and gain of N-cadherin, or even an isolated effect of loss of E-cadherin, with N-cadherin rescuing the cells from apoptosis. The latter effect seems unlikely, as subsequent tests that overexpression of N-cadherin alone could also have a pro-neural effect. In summary, loss of E-cadherin led to significant cell death during neural differentiation, which could be rescued by knocking in N-cadherin; these results, in combination with previously published findings, may implicate a critical role for cadherin-based adhesion during neural differentiation.

6.2.2 E-cadherin is not required for neural lineage commitment in mESCs

A previous report using EcKO cells in embryoid body differentiation culture found that these cells maintain expression of pluripotency genes and fail to upregulate lineage markers even after 30 days in differentiation conditions, and the authors conclude that E-cadherin is required for the lineage commitment of mESCs (Pieters et al., 2016). The results presented here dispute that conclusion, as a small subset of the EcKO cells that survived to the later stages of the neural differentiation protocol were able to upregulate the neural lineage marker *Sox1*, and were not found to differ significantly from control cells in gene expression (Fig. 4.4). Subsequent protein-level analysis confirmed that EcKO cells can upregulate Sox1 protein in permissive conditions (Figs. 5.14, 5.15, 5.17).

In addition, NcKI cells lacking E-cadherin but expressing N-cadherin in its place are also able to robustly upregulate neural lineage markers in permissive conditions, providing further evidence that E-cadherin is not required for lineage commitment. All differentiation experiments presented in this thesis were initiated from a 2i-Lif starting population, corresponding to a state of naïve pluripotency, suggesting that cells lacking E-cadherin are indeed able to pass through all stages of lineage priming, commitment, exit from pluripotency and subsequent differentiation, without the need for this protein. These findings robustly refute the claim proposed by Pieters et al. (2016) that E-cadherin is required for lineage commitment in mESCs.

6.2.3 Gain of N-cadherin biases lineage choice in three *in vitro* contexts

The results summarised in this thesis have shown that *in vitro*, cadherin switching appears to predict or bias lineage choice in three conditions analogous to three different stages of early development: epiblast priming, anterior neuroepithelial differentiation, and maturation of NMPs.

6.2.3.1 Epiblast stem cells (EpiSCs)

In EpiSCs, cadherin switching was found to be initiated prior to the loss of expression of pluripotency markers such as Oct4 (Figs. 3.5, 3.6, and 3.8). This result could indicate that cadherin switching occurs early enough to affect lineage decisions of pluripotent cells. In addition, FACS-sorted EpiSCs with low levels of E-cadherin (and reciprocally high N-cadherin) were also shown to have higher levels of neural and mesodermal markers *Sox1* and *T,* respectively (Fig. 3.8), showing that cadherin switching can predict lineage bias in these cells and may be involved in priming towards these lineages.

In the embryo however, N-cadherin is first detected at the transcript level in the posterior of the gastrula (Peng et al., 2016), perhaps indicating that EpiSC culture is more permissive of cadherin switching than the primed epiblast *in vivo*. This also suggests that the findings summarised here – showing that cadherin switching identifies a bias in neural and mesodermal priming in EpiSCs – may not be directly applicable to *in vivo* development. However, they do highlight that in conditions permissive to N-cadherin expression, this protein identifies a cellular population that appears to be primed for commitment to specific lineages, highlighting that cadherin switching may play a role in differentiation towards these lineages.

A study by Takehara et al. (2015) identified N-cadherin to be the predominantly expressed cadherin species in EpiSCs, and proposed that it stabilises FGFR1 to contribute to primed-state pluripotency in these cells. These results differ from the results obtained during the current study, where E-cadherin was found to be the predominantly expressed cadherin in EpiSCs, with N-cadherin was expressed only by around 13% of EpiSCs (Fig. 3.6). However, Takehara et al. cultured their EpiSCs in a medium without supplemented Activin, in contrast to previously published protocols (Brons et al., 2007; Tesar et al., 2007), making their findings not directly comparable to those presented here.

6.2.3.2 Anterior neural differentiation

In Chapter 4, two independent approaches – gene replacement and inducible protein overexpression – were used to show that a gain of N-cadherin can promote neural differentiation in permissive *in vitro* conditions; both NcKI cells and N-cadherin overexpressing cells displayed a drop in the expression of pluripotency marker *Pou5f1* and an increase in the levels of neural markers *Sox1* and *Pax6* (Figs. 4.5, 4.15). This is in accordance with reports by Larue et al. (1996) who found that E-cadherin-null cells transfected with N-cadherin show a bias for differentiation towards neuroepithelial and cartilage structures.

It should be noted that since NcKI cells lack E-cadherin, and that N-cadherin overexpressing cells displayed significantly lower levels of *Cdh1* within 48h of N-cadherin induction, the possibility exists that an indirect loss of E-cadherin may be contributing to the pro-neural effect observed in these cells. However, this is unlikely since N-cadherin overexpressing cells displayed significantly higher levels of neural markers within 24h of induction (Fig. 4.15), before a significant drop in *Cdh1*, suggesting that N-cadherin alone can play a direct role in promoting neural differentiation.

E-cadherin and N-cadherin share very similar domain architecture, homophilic adhesive function, and binding partners such as β-catenin, but their expression tends to be mutually exclusive in tissues where they are stably expressed (Bedzhov et al., 2013). However, a major difference between the two proteins is in their ability to bind and interact with specific growth factor receptors: E-cadherin is known to bind IGF1R (Bedzhov et al., 2012) and EGF receptors (Hoschuetzky et al., 1994), while N-cadherin has been identified to have specific signalling roles mediated by FGF receptor binding (Nguyen and Mège, 2016; Takehara et al., 2015; Williams et al., 1994). These differential receptor interactions raise the possibility that cadherin switching may be providing a subtle signalling cue, helping to push cells towards the neural lineage.

6.2.3.3 Neuro-mesodermal progenitors (NMPs)

Recently, a single-cell transcriptomics approach was used to analyse changes in gene expression during the maturation of NMPs (Gouti et al., 2017). The dataset revealed that NMP maturation between E8.5 and E9.5 is accompanied by a switch from E- to N-cadherin, presenting a novel context for the study of the effects of cadherin switching. From this point of view, NMPs are an especially interesting progenitor population since they can give rise to both neural and mesodermal progeny cells, and both of these tissues are known to express N-cadherin during development (Radice et al., 1997).

To further study the role of cadherin switching in the context of NMP maturation and lineage choice, N-cadherin overexpression cell line was used in a newly developed protocol that uses 2i-Lif cells as the starting population, and an EpiLSC intermediate (Watson, 2018), to investigate how the overexpression of N-cadherin affects lineage choice in NMPs. The results of these experiments showed that N-cadherin overexpression during NMP maturation caused a significant reduction in the number of single-positive cells expressing the mesoderm marker Brachyury, and a significant increase in cells single-positive for the neural lineage marker Sox2. These populations are taken to be cells committed to either the mesodermal or neural lineages, respectively. There was also a non-significant decrease in the number of cells co-expressing these two markers, and these cells were taken to be a putative bi-potent NMPs (Fig. 4.19).

These results suggested that N-cadherin can have a pro-neural effect even in NMPs. However, due to several technical issues with the *in vitro* protocol used, this result was not pursued further. This finding would benefit from *in vivo* validation, where the inducible N-cadherin cells could for example be electroporated into CLE of developing embryos to check whether N-cadherin could cause also bias lineage choice in this context.

6.3 The effect of cadherin switching on signalling during neural differentiation

6.3.1 Uncoupling the roles of adhesion and signalling in cadherin switching

An important aspect of the project described in this thesis was to assess whether any changes in differentiation patterns caused by cadherins were attributable to the adhesive or to the signalling functions of these proteins. Previous studies investigating the adhesion functions of cadherins have adopted diverse strategies for modulating cadherin-mediated adhesion: from mutating the protein by truncations (Nagafuchi and Takeichi, 1988), deletions (Larue et al., 1994; Radice et al., 1997), domain substitutions (Bedzhov et al., 2012), or point mutagenesis (Tamura et al., 1998), to disturbing cadherin function by blocking antibodies (Malaguti et al., 2013), shRNAs (Onder et al., 2008), or preventing calcium-dependent binding by the addition of chelating agents (Zhang et al., 2010). While these experimental approaches result in changes in adhesion, very few strategies exist to objectively and accurately measure those changes, and many authors have simply relied on observing cells by eye and reporting gross adhesive defects.

In planning the current project, it was hypothesised that using the NcKI cell line would rescue the adhesion defects observed in E-cadherin-null cells, as reported in the pre-implantation embryo (Kan et al., 2007); this would allow for the uncoupling of any signalling effects of cadherin switching from its adhesive effects. In addition, the inter-nuclear edge distance analysis was developed as a strategy to quantitatively monitor differences in cellular adhesion, with the goal of having a more objective method than simply assessing adhesive changes by eye. To our knowledge, this is the first fully quantitative image-analysis technique developed to assess changes in inter-nuclear clustering as an indirect readout of cellular adhesion. The technique could be further strengthened by the development of a cytoplasmic segmentation technique, but this was unavailable at the time of the study.

Surprisingly, the inter-nuclear edge distance analysis found that after 24h in neural differentiation conditions (from a 2i-lif starting population), NcKI cells display a significant clustering defect that is comparable to that seen in EcKO cells (Fig. 5.4). Nevertheless, despite displaying an almost identical clustering profile, these two cell lines exhibited different behaviours during neural differentiation. This suggests that adhesive changes are not the main cause for the pro-neural phenotype observed in NcKI cells, which may instead be better explained by differences in cellular signalling, as described in Chapter 5.

In addition, the inter-nuclear edge distance analysis showed that N-cadherin overexpression contributed to a slight but significant increase in inter-nuclear distances. However, since the cells overexpressing N-cadherin were still found to have comparable clustering profiles to two control cell lines used in the study, it was assumed that any adhesive changes are negligible, and are not likely to be the main cause for the pro-neural effect of N-cadherin overexpression observed in these cells.

In summary, quantifying inter-nuclear edge distances using PickCells software provides an estimate of differences in cellular adhesion between given samples. While it does not allow for the direct uncoupling of adhesion and signalling effects in cells with cadherin mutations, it provides a method to objectively measure and control for changes in cellular clustering, allowing for greater insight on the effects of a particular treatment or condition on cellular adhesion. For the current study, this method proved to be much more useful than subjective estimation of cellular adhesion by eye, and strongly suggested that changes in differentiation were not directly caused by an adhesive effect of cadherin switching. This allowed for the focus of the research to shift from cell-cell adhesion to the interrogation of changes in cellular signalling pathways.

6.3.2 Loss of E-cadherin leads to a significant reduction in levels of β-catenin, but does not perturb WNT signalling

The WNT signalling pathway is involved in pluripotency and development, and the canonical branch of this pathway relies on signal transduction via β-catenin, which is also a key binding partner of cadherins (Clevers, 2006). Both E- and N-cadherin are able to modulate WNT-dependent transcription in certain contexts (Howard et al., 2011), making WNT signalling a possible candidate mechanism for the pro-neural effect observed in response to cadherin switching.

RPPA analysis, ICC and quantitative image analysis all demonstrated a significant loss of β-catenin globally and in the nuclei of cells lacking E-cadherin within 24h of the commencement of neural differentiation (Figs 5.5, 5.13). Similar results have been reported previously upon the loss of E-cadherin in other contexts and in diverse cell types (Hendriksen et al., 2008; Orsulic et al., 1999; Wetering et al., 2001).

The cadherin-catenin interaction has previously been found to act as a positive stimulus for the transcriptional activity of β-catenin, perhaps priming β-catenin for this function (Howard et al., 2011). Others have proposed that the cadherin/catenin complex binds Oct4 at the membrane, titrating the nuclear concentration of this transcription factor to optimal levels for the maintenance of pluripotency (Faunes et al., 2013).

In the experiments presented in this thesis, it was found that both EcKO and NcKI cells maintained nearly identical levels of Oct4 expression in their nuclei compared to control cells at the 24h time-point of neural differentiation, despite the loss of nuclear β-catenin observed in both cell lines. This result suggested that at early stages of differentiation, levels of E-cadherin or β-catenin do not appear to have a significant effect on the nuclear abundance of Oct4 (Fig. 5.13). Levels of nuclear Oct4 were found to increase slightly in response to Wnt3a treatment, an effect that was observed at near identical levels between the cadherin mutant cell lines and their relevant control lines. This result points to two conclusions: that Wnt3a may inhibit either exit from pluripotency or the onset of neural differentiation, as previously reported (Faunes et al., 2013), and that both EcKO and NcKI cells are able to respond to such WNT signals despite their global loss of β-catenin at this time-point, suggesting that neither E-cadherin nor high levels of β-catenin are required for WNT-induced elevation of Oct4.

At later time-points of neural differentiation, Wnt3a treatment was also found to have an inhibitory effect on the expression of neural genes (Fig. 5.17). However, both EcKO and NcKI cell lines upregulated WNT-target genes to comparable levels to those seen control cell lines when cultured with Wnt3a, suggesting that cells lacking E-cadheirn retain WNT-responsiveness even when β-catenin levels are significantly reduced. Similar findings have been reported previously (Hendriksen et al., 2008; Wetering et al., 2001), showing that levels of global or nuclear β-catenin are not an accurate readout of WNT responsiveness or pathway activation.

The Wnt3a experiments also confirmed the pro-neural effect observed in NcKI cells: these cells exhibited significantly higher levels of *Sox1* and *Pax6* compared to WT controls, and were able to upregulate these early neural markers even when exposed to high doses of Wnt3a earlier during the differentiation protocol. These results showed that NcKI cells can promote neural differentiation even in the presence of the anti-neural factor Wnt3a, suggesting that cadherin switching may play a role in ensuring that neural differentiation is a robust and replicable process even in the presence of inhibitory signals. Additionally, the cadherin mutant cells were found to have different FGF signalling profiles during neural differentiation than their control cell lines, raising the possibility that FGF signalling may be behind the pro-neural behaviour observed in the cadherin mutant cells.

In summary, the experiments on Wnt3a supplementation in cadherin mutant cell lines during neural differentiation showed that WNT signalling profiles did not differ significantly between NcKI cells, which were previously shown to exhibit a pro-neural phenotype, and control cells, despite the two lines having different expression profiles of β-catenin. These results suggest that WNT/β-catenin signalling is not the primary cause of the pro-neural effect observed in NcKI cells.

6.3.3 Cadherin switching promotes neural differentiation by dampening FGF responsiveness

Since WNT signalling was eliminated as the primary candidate driving the pro-neural effect observed in NcKI cells, attention was turned to the effects of FGF signalling, following Nanostring mRNA analysis results showing that FGF signalling components were significantly downregulated in induced A2Lox-Ncad-HA cells during neural differentiation (Fig. 5.21).

FGF signalling plays diverse and context-dependent roles in the maintenance of and exit from pluripotency, as well as in subsequent differentiation. Inhibition of FGF signalling promotes self-renewal of ESCs (Guo et al., 2009; Hamilton and Brickman, 2014; Hamilton et al., 2013), while stimulation of the pathway promotes their progression into EpiSCs and the maintenance of that state (Lanner and Rossant, 2010; Sterneckert et al., 2010; Takehara et al., 2015). The role of FGF signalling in neural differentiation is somewhat controversial: some studies show that is it required for and promotes neural differentiation of ES cells cultured in Lif-serum (Lowell et al., 2006; Song et al., 2018; Ying et al., 2003a). However, other studies have shown that FGF signalling inhibits differentiation from the primed EpiSC state to the neural lineage (Greber et al., 2010; Jaeger et al., 2011; Stavridis et al., 2010; Sterneckert et al., 2010). Nevertheless, it is possible to reconcile these conflicting findings by viewing neural specification as a two-step process: the first stage being the conversion from naïve to primed pluripotency, which requires FGF, and the second stage being differentiation, which occurs in the absence of FGF signalling and is inhibited by this pathway.

The results of an FGF rescue experiment performed for this thesis showed that stimulating FGF signalling at day two of neural differentiation (from a 2i-Lif starting population) inhibited neural differentiation, and conversely, FGFR1 inhibition at the same time-point promoted neural marker expression (Fig. 5.23). While the cells used in the study were not EpiSCs, it is likely that after two days of differentiation from 2i-Lif conditions, the cells either resemble or have already passed the stage of primed pluripotency. These results are in accordance with the studies mentioned previously, which showed that FGF signalling inhibits neural differentiation from a primed state.

The FGF rescue experiment confirmed our previous observations that at days three and four of *in vitro* neural differentiation, NcKI cells express lower levels of FGF target genes such as *Dusp4* and *Etv4* than WT cells, and confirmed the pro-neural phenotype observed previously in NcKI cells. Importantly, the high levels of *Sox1* and *Pax6* detected in NcKI cells could be lowered to near-WT levels by the addition of FGF2 to the NcKI cells. Conversely, adding PD17, an FGFR1 inhibitor, to WT cells raised their expression of neural marker genes to similar levels as those observed in untreated NcKI cells, demonstrating that the modulation of FGF signalling could replicate the pro-neural effect observed in NcKI cells (Fig. 5.23).

Surprisingly, the induction of N-cadherin overexpression was not found to have a similar effect on FGF dampening as the NcKI mutation. As discussed in Chapter 5, a larger sample size with three independent clones is recommended to confirm this result with greater confidence. The current data showing that N-cadherin overexpression alone does not have the same weakened FGF signalling profile as NcKI cells suggests that full cadherin switching is required for this phenotype to have a greater effect on FGF dampening. However, since the N-cadherin overexpressing cells in this experiment do not replicate the pro-neural effect observed in the larger-scale study performed in Chapter 4, the effect may be very subtle. Nanostring analysis showed that a decrease in FGF targets was the most significant change in gene expression as a result of N-cadherin overexpression (Fig. 5.21), suggesting that the pro-neural effect of induced A2Lox-Ncad-HA cells may still be ascribable to this pathway. Further studies are needed to confirm this hypothesis.

Taken together, these results provide evidence that forced, premature and complete cadherin switching promotes neural differentiation by dampening FGF responsiveness. However, RPPA data from 24h of neural differentiation showed a contrasting result, where the levels of most phospho-protein species associated with different branches of the FGF pathway were higher in NcKI cells compared to WT cells at this time point (Fig. 5.5). This result suggests that in the first 24h of differentiation from naïve pluripotency, NcKI cells exhibit higher FGF signalling compared to WT cells, perhaps promoting a faster transition towards the primed EpiSC state.

In a model where FGF signalling first promotes priming of ESCs into EpiSCs, and its subsequent inhibition allows cells to differentiate towards the neural lineage, the forced, premature and complete cadherin switching represented by NcKI cells may accelerate the progression of these cells through the early stages of differentiation. The molecular interactions for this effect were not investigated in this project, but a candidate mechanism could be that the prematurely expressed N-cadherin binds and stabilises FGFR1, possibly leading to a faster progression into and out of the EpiSC state (Takehara et al., 2015). However, since the effects of cadherin switching in the context of transitions between early pluripotent states was not studied in this thesis, this hypothesis remains untested.

6.4 Working model

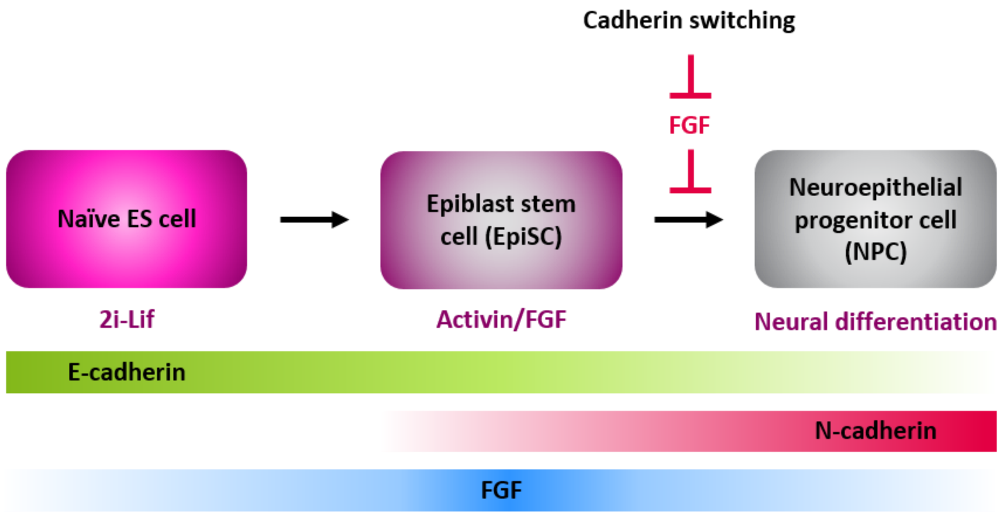

Figure 6.1: Working model. In vitro*, cadherin switching is initiated at the EpiSC stage, prior to the loss of pluripotency, and coincides with lineage priming.* In vivo*, the switch occurs later, at around the time of late gastrulation. FGF signalling peaks at the EpiSC stage, when it is required for the maintenance of the primed pluripotent state. Cadherin switching promotes neural differentiation by dampening FGF signalling during exit from pluripotency and subsequent neural induction. The molecular interactions responsible for this effect remain unknown, but are likely to involve FGFR1.*

The experiments described in this thesis have shown that *in vitro*, cadherin switching occurs prior to the loss of pluripotency and coincides with lineage priming towards the neural and mesodermal fates. *In vitro*, this transition appears to take place earlier than *in vivo,* where its earliest signs are observed at the time of gastrulation (Peng et al., 2016).

During *in vitro* assays from a 2i-Lif starting population, cadherin switching was found to promote neural differentiation, both through forced, premature cadherin switching using the NcKI cell line, and through the induction of N-cadherin alone using an inducible overexpression cell line, A2Lox-Ncad-HA. Cadherin switching at days three and four of neural differentiation was found to correlate with significant dampening of FGF responsiveness. Since FGF signalling is involved in the induction and maintenance of the primed pluripotent state (Lanner and Rossant, 2010; Sterneckert et al., 2010), we propose that cadherin switching dampens FGF responsiveness to allow exit from the pluripotent state and guiding differentiating cells towards the neural lineage, potentially through an interaction with FGFR1.

We do not believe that cadherin switching provides the decisive instructive cue that forces cells to adopt a neural fate. Rather, we propose that cadherin switching makes the process more robust and replicable, allowing cells to resist inappropriate signalling cues, such as Wnt ligands, and allows for replicable neural induction in the anterior embryo even in suboptimal conditions.

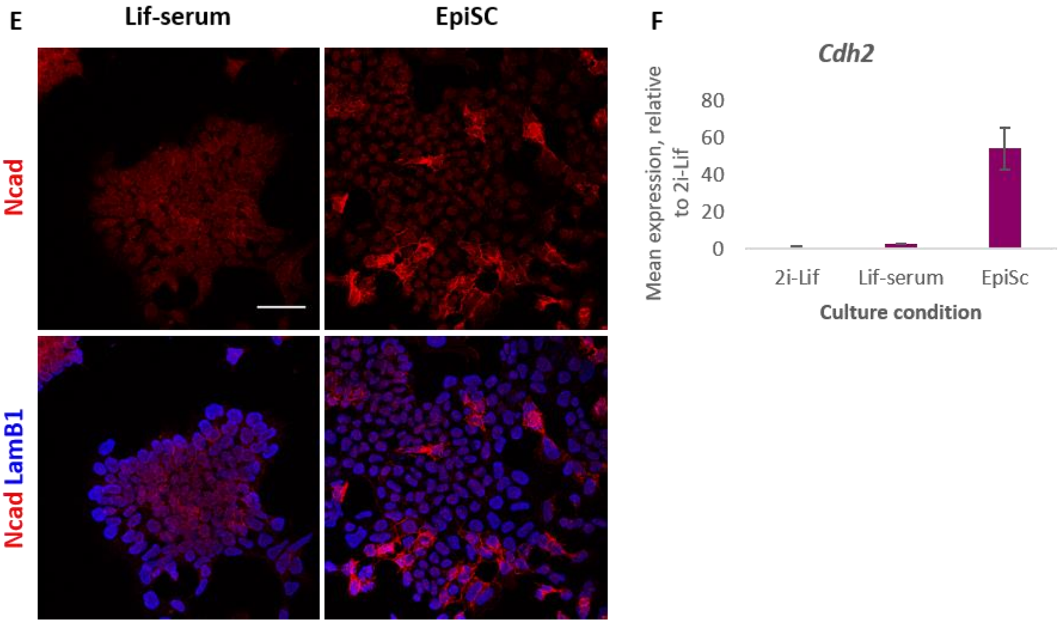

Appendix 1: Non-specific N-cadherin background staining in ICC. A. *Example nuclear background signal from N-cadherin antibody staining in cells negative (Lif-serum) and positive (EpiSC) for N-cadherin. Scale bar=50µm.* ***F.*** *qPCR data for* Cdh2 *(N-cadherin) expression at different stages of pluripotency, showing that cells cultured in Lif-serum are negative for* Cdh2 *mRNA.*

References

Aaku-saraste, E., Hellwig, A. and Huttner, W. B. (1996). Loss of Occludin and Functional Tight Junctions , but Not ZO-1 , during Neural Tube Closure — Remodeling of the Neuroepithelium Prior to Neurogenesis. *Dev. Biol.* **679**, 664–679.

Alexander, N. R., Tran, N. L., Rekapally, H., Summers, C. E., Glackin, C. and Heimark, R. L. (2006). N-cadherin gene expression in prostate carcinoma is modulated by integrin-dependent nuclear translocation of Twist1. *Cancer Res.* **66**, 3365–3369.

Anastasiadis, P. Z. and Reynolds, a B. (2000). The p120 catenin family: complex roles in adhesion, signaling and cancer. *J. Cell Sci.* **113 (Pt 8**, 1319–1334.

Arnold, S. J. and Robertson, E. J. (2009). Making a commitment: cell lineage allocation and axis patterning in the early mouse embryo. *Nat. Rev. Mol. Cell Biol.* **10**, 91–103.

Aubert, J., Stavridis, M. P., Tweedie, S., O'Reilly, M., Vierlinger, K., Li, M., Ghazal, P., Pratt, T., Mason, J. O., Roy, D., et al. (2003). Screening for mammalian neural genes via fluorescence-activated cell sorter purification of neural precursors from Sox1-gfp knock-in mice. *Proc. Natl. Acad. Sci. U. S. A.* **100 Suppl**, 11836–41.

Basilicata, M. F., Frank, M., Solter, D., Brabletz, T. and Stemmler, M. P. (2016). Inappropriate cadherin switching in the mouse epiblast compromises proper signaling between the epiblast and the extraembryonic ectoderm during gastrulation. *Sci. Rep.* **6**, 26562.

Becker, K., Jährling, N., Saghafi, S. and Dodt, H. U. (2013). Immunostaining, dehydration, and clearing of mouse embryos for ultramicroscopy. *Cold Spring Harb. Protoc.* **2013**, 743–744.

Beddington, B. R. S. P. (1981). An autoradiographic analysis of the potency of embryonic ectoderm in the 8th day postimplantation mouse embryo. *J. Embryol. Exp. Morphol.* **64**, 87–104.

Beddington, B. R. S. P. (1982). An autoradio graphic analysis of tissue potency in different regions of the embryonic ectoderm during gastrulation in the mouse. *J. Embryol. Exp. Morphol.* **69**, 265–285.

Bedzhov, I., Liszewska, E., Kanzler, B. and Stemmler, M. P. (2012). Igf1r signaling is indispensable for preimplantation development and is activated via a novel function of E-cadherin. *PLoS Genet.* **8**,.

Bedzhov, I., Alotaibi, H., Basilicata, M. F., Ahlborn, K., Liszewska, E., Brabletz, T. and Stemmler, M. P. (2013). Adhesion, but not a specific cadherin code, is indispensable for ES cell and induced pluripotency. *Stem Cell Res.* **11**, 1250–63.

Boroviak, T., Loos, R., Bertone, P., Smith, A. and Nichols, J. (2014). The ability of inner-cell-mass cells to self-renew as embryonic stem cells is acquired following epiblast specification. *Nat. Cell Biol.* **16**, 516–528.

Boroviak, T., Loos, R., Lombard, P., Okahara, J., Behr, R., Sasaki, E., Nichols, J., Smith, A. and Bertone, P. (2015). Lineage-Specific Profiling Delineates the Emergence and Progression of Naive Pluripotency in Mammalian Embryogenesis. *Dev. Cell* **35**, 366–382.

Boulet, A. M. and Capecchi, M. R. (2012). Signaling by FGF4 and FGF8 is required for axial elongation of the mouse embryo. *Dev. Biol.* **371**, 235–245.

Brons, I. G. M., Smithers, L. E., Trotter, M. W. B., Rugg-Gunn, P., Sun, B., Chuva de Sousa Lopes, S. M., Howlett, S. K., Clarkson, A., Ahrlund-Richter, L., Pedersen, R. a, et al. (2007). Derivation of pluripotent epiblast stem cells from mammalian embryos. *Nature* **448**, 191–195.

Brown, J. M. and Storey, K. G. (2000). A region of the vertebrate neural plate in which neighbouring cells can adopt neural or epidermal fates. *Curr. Biol.* **10**, 869–872.

Burdon, T., Stracey, C., Chambers, I., Nichols, J. and Smith, A. (1999). Suppression of SHP-2 and ERK signalling promotes self-renewal of mouse embryonic stem cells. *Dev. Biol.* **210**, 30–43.

Butz, S. and Larue, L. (1995). Expression of catenins during mouse embryonic development and in adult tissues. *Cell Adhes. Commun.* **3**, 337–352.

Cambray, N. and Wilson, V. (2002). Axial progenitors with extensive potency are localised to the mouse chordoneural hinge. *Development* **129**, 4855–66.

Cambray, N. and Wilson, V. (2007). Two distinct sources for a population of maturing axial progenitors. *Development* **134**, 2829–40.

Campbell, N. A. and Reece, J. B. (2004). *Biology*. 7th ed. San Francisco: Pearson Benjamin Cummings.

Chal, J. and Pourquié, O. (2017). Making muscle: skeletal myogenesis *in vivo* and *in vitro*. *Development* **144**, 2104–2122.

Chalamalasetty, R. B., Garriock, R. J., Dunty, W. C., Kennedy, M. W., Jailwala, P., Si, H. and Yamaguchi, T. P. (2014). Mesogenin 1 is a master regulator of paraxial presomitic mesoderm differentiation. *Development* **141**, 4285–4297.

Chen, H., Guo, R., Zhang, Q., Guo, H., Yang, M., Wu, Z., Gao, S. and Liu, L. (2015a). Erk signaling is indispensable for genomic stability and self-renewal of mouse embryonic stem cells. 1–8.

Chen, D., Wu, Z., Luo, L., Huang, X., Qian, W., Wang, H., Li, S. and Liu, J. (2015b). E-cadherin maintains the activity of neural stem cells and inhibits the migration. **8**, 14247–14251.

Chou, Y. F., Chen, H. H., Eijpe, M., Yabuuchi, A., Chenoweth, J. G., Tesar, P., Lu, J., McKay, R. D. G. and Geijsen, N. (2008). The Growth Factor Environment Defines Distinct Pluripotent Ground States in Novel Blastocyst-Derived Stem Cells. *Cell* **135**, 449–461.

Chu, Y. S., Thomas, W. a., Eder, O., Pincet, F., Perez, E., Thiery, J. P. and Dufour, S. (2004). Force measurements in E-cadherin-mediated cell doublets reveal rapid adhesion strengthened by actin cytoskeleton remodeling through Rac and Cdc42. *J. Cell Biol.* **167**, 1183–1194.

Chu, Y. S., Eder, O., Thomas, W. a., Simcha, I., Pincet, F., Ben-Ze'ev, A., Perez, E., Thiery, J. P. and Dufour, S. (2006). Prototypical type I E-cadherin and type II cadherin-7 mediate very distinct adhesiveness through their extracellular domains. *J. Biol. Chem.* **281**, 2901–2910.

Ciruna, B. and Rossant, J. (2001). FGF Signaling Regulates Mesoderm Cell Fate Specification and Morphogenetic Movement at the Primitive Streak. *Dev. Cell* **1**, 37–49.

Ciruna, B. G., Schwartz, L., Harpal, K., Yamaguchi, T. P. and Rossant, J. (1997). Chimeric analysis of fibroblast growth factor receptor-1 (Fgfr1) function: a role for FGFR1 in morphogenetic movement through the primitive streak. *Development* **124**, 2829–2841.

Clevers, H. (2006). Wnt/B-Catenin Signaling in Development and Disease. *Cell* **127**, 469–480.

Derksen, P. W. B., Liu, X., Saridin, F., Gulden, H. Van Der, Zevenhoven, J., Evers, B., Beijnum, J. R. Van, Griffioen, A. W., Vink, J., Krimpenfort, P., et al. (2006). Somatic inactivation of E-cadherin and p53 in mice leads to metastatic lobular mammary carcinoma through induction of anoikis resistance and angiogenesis. *Cancer Cell* 437–449.

Di-Gregorio, A., Sancho, M., Stuckey, D. W., Crompton, L. a, Godwin, J., Mishina, Y. and Rodriguez, T. a (2007). BMP signalling inhibits premature neural differentiation in the mouse embryo. *Development* **134**, 3359–3369.

Doherty, P., Williams, G. and Williams, E. J. (2000). CAMs and axonal growth: A critical evaluation of the role of calcium and the MAPK cascade. *Mol. Cell. Neurosci.* **16**, 283–295.

Downs, K. M. (2008). Systematic localization of Oct-3/4 to the gastrulating mouse conceptus suggests manifold roles in mammalian development. *Dev. Dyn.* **237**, 464–475.

Dunn, S.-J., Martello, G., Yordanov, B., Emmott, S. and Smith, a G. (2014). Defining an essential transcription factor program for naïve pluripotency. *Science* **344**, 1156–60.

Evans, M. J. and Kaufman, M. H. (1981). Establishment in culture of pluripotential cells from mouse embryos. *Nature* **292**, 154–156.

Faunes, F., Hayward, P., Descalzo, S. M., Chatterjee, S. S., Balayo, T., Trott, J., Christoforou, A., Ferrer-Vaquer, A., Hadjantonakis, A.-K., DasGupta, R., et al. (2013). A membrane-associated β-catenin/Oct4 complex correlates with ground-state pluripotency in mouse embryonic stem cells. *Development* **140**, 1171–1183.

Fedor-Chaiken, M., Hein, P. W., Stewart, J. C., Brackenbury, R. and Kinch, M. S. (2003). E-cadherin binding modulates EGF receptor activation. *Cell Commun. Adhes.* **10**, 105–118.

Fujimori, T., Miyatani, S. and Takeichi, M. (1990). Ectopic expression of N-cadherin perturbs histogenesis in Xenopus embryos. *Development* **110**, 97–104.

Gardner, R. L. (1998). Contributions of blastocyst micromanipulation to the study of mammalian development. *BioEssays* **20**, 168–180.

Garriock, R. J., Chalamalasetty, R. B., Kennedy, M. W., Canizales, L. C., Lewandoski, M. and Yamaguchi, T. P. (2015). Lineage tracing of neuromesodermal progenitors reveals novel Wnt-dependent roles in trunk progenitor cell maintenance and differentiation.

Development **142**, 1628–1638.

Geiss, G. K., Bumgarner, R. E., Birditt, B., Dahl, T., Dowidar, N., Dunaway, D. L., Fell, H. P., Ferree, S., George, R. D., Grogan, T., et al. (2008). Direct multiplexed measurement of gene expression with color-coded probe pairs. *Nat. Biotechnol.* **26**, 317–325.

Goetz, R. and Mohammadi, M. (2013). Exploring mechanisms of FGF signalling through the lens of structural biology. *Nat. Rev. Mol. Cell Biol.* **14**, 166–80.

Goolam, M., Scialdone, A., Graham, S. J. L., MacAulay, I. C., Jedrusik, A., Hupalowska, A., Voet, T., Marioni, J. C. and Zernicka-Goetz, M. (2016). Heterogeneity in Oct4 and Sox2 Targets Biases Cell Fate in 4-Cell Mouse Embryos. *Cell* **165**, 61–74.

Gottardi, C. J. and Gumbiner, B. M. (2004). Distinct molecular forms of ??-catenin are targeted to adhesive or transcriptional complexes. *J. Cell Biol.* **167**, 339–349.

Gottardi, C. J., Wong, E. and Gumbiner, B. M. (2001). E-cadherin suppresses cellular transformation by inhibiting β-catenin signaling in an adhesion-independent manner. *J. Cell Biol.* **153**, 1049–1059.

Gouti, M., Tsakiridis, A., Wymeersch, F. J., Huang, Y., Kleinjung, J., Wilson, V. and Briscoe, J. (2014). In vitro generation of neuromesodermal progenitors reveals distinct roles for wnt signalling in the specification of spinal cord and paraxial mesoderm identity. *PLoS Biol.* **12**,.

Gouti, M., Metzis, V. and Briscoe, J. (2015). The route to spinal cord cell types: A tale of signals and switches. *Trends Genet.* **31**, 282–289.

Gouti, M., Delile, J., Stamataki, D., Wymeersch, F. J., Huang, Y., Kleinjung, J., Wilson, V. and Briscoe, J. (2017). A Gene Regulatory Network Balances Neural and Mesoderm Specification during Vertebrate Trunk Development. *Dev. Cell* **41**, 243–261.e7.

Greber, B., Wu, G., Bernemann, C., Joo, J. Y., Han, D. W., Ko, K., Tapia, N., Sabour, D., Sterneckert, J., Tesar, P., et al. (2010). Conserved and Divergent Roles of FGF Signaling in Mouse Epiblast Stem Cells and Human Embryonic Stem Cells. *Cell Stem Cell* **6**, 215–226.

Guo, G., Yang, J., Nichols, J., Hall, J. S., Eyres, I., Mansfield, W. and Smith, A. (2009). Klf4 reverts developmentally programmed restriction of ground state pluripotency.

Development **136**, 1063–9.

Guo, G., Huss, M., Tong, G. Q., Wang, C., Li Sun, L., Clarke, N. D. and Robson, P. (2010). Resolution of Cell Fate Decisions Revealed by Single-Cell Gene Expression Analysis from Zygote to Blastocyst. *Dev. Cell* **18**, 675–685.

Gurdon, J. B., Elsdale, T. R. and Fischberg, M. (1958). Sexually mature individuals of Xenopus laevis from the transplantation of single somatic nuclei. *Nature* **182**, 64–65.

Haegele, L., Ingold, B., Naumann, H., Tabatabai, G., Ledermann, B. and Brandner, S. (2003). Wnt signalling inhibits neural differentiation of embryonic stem cells by controlling bone morphogenetic protein expression. *Mol. Cell. Neurosci.* **24**, 696–708.

Hamilton, W. B. and Brickman, J. M. (2014). Erk Signaling Suppresses Embryonic Stem Cell Self-Renewal to Specify Endoderm. *Cell Rep.* **9**, 2056–2070.

Hamilton, W. B., Kaji, K. and Kunath, T. (2013). ERK2 Suppresses Self-Renewal Capacity of Embryonic Stem Cells, but Is Not Required for Multi-Lineage Commitment. *PLoS One* **8**,.

Haque, A., Adnan, N., Motazedian, A., Akter, F., Hossain, S., Kutsuzawa, K., Nag, K., Kobatake, E. and Akaike, T. (2015). An Engineered N-Cadherin Substrate for Differentiation, Survival, and Selection of Pluripotent Stem Cell-Derived Neural Progenitors. *PLoS One* **10**, e0135170.

Harrison, O. J. (2005). Cadherin adhesion depends on a salt bridge at the N-terminus. *J. Cell Sci.* **118**, 4123–4130.

Hart, A. H., Hartley, L., Ibrahim, M. and Robb, L. (2004). Identification, Cloning and Expression Analysis of the Pluripotency Promoting Nanog Genes in Mouse and Human. *Dev. Dyn.* **230**, 187–198.

Hawkins, K., Mohamet, L., Ritson, S., Merry, C. L. R. and Ward, C. M. (2012). E-cadherin and, in its absence, N-cadherin promotes Nanog expression in mouse embryonic stem cells via STAT3 phosphorylation. *Stem Cells* **30**, 1842–51.

Hayashi, K., Ohta, H., Kurimoto, K., Aramaki, S. and Saitou, M. (2011). Reconstitution of the mouse germ cell specification pathway in culture by pluripotent stem cells. *Cell* **146**, 519–532.

Hazan, R. B. and Norton, L. (1998). The epidermal growth factor receptor modulates the interaction of E-cadherin with the actin cytoskeleton. *J Biol Chem* **273**, 9078–9084.

Hazan, R. B., Phillips, G. R., Qiao, R. F., Norton, L. and Aaronson, S. A. (2000). Exogenous expression of N-cadherin in breast cancer cells induces cell migration, invasion, and metastasis. *J. Cell Biol.* **148**, 779–90.

Hazan, R. B., Qiao, R., Keren, R., Badano, I. and Suyama, K. (2004). Cadherin switch in tumor progression. *Ann. N. Y. Acad. Sci.* **1014**, 155–163.

Hendriksen, J., Jansen, M., Brown, C. M., van der Velde, H., van Ham, M., Galjart, N., Offerhaus, G. J., Fagotto, F. and Fornerod, M. (2008). Plasma membrane recruitment of dephosphorylated -catenin upon activation of the Wnt pathway. *J. Cell Sci.* **121**, 1793–1802.

Henrique, D., Abranches, E., Verrier, L. and Storey, K. G. (2015). Neuromesodermal progenitors and the making of the spinal cord. *Development* **142**, 2864–2875.

Hillman, N., Sherman, M. I. and Graham, C. (1972). The effect of spatial arrangement on cell determination during mouse development. *Embryol. exp. Morph* **28**, 263–278.

Hooper, M., Hardy, K., Handyside, A., Hunter, S. and Monk, M. (1987). HPRT-deficient (Lesch–Nyhan) mouse embryos derived from germline colonization by cultured cells. *Nature* **326**, 292–295.

Hoschuetzky, H., Aberle, H. and Kemler, R. (1994). Β-Catenin mediates the interaction of the cadherin-catenin complex with epidermal growth factor receptor. *J. Cell Biol.* **127**, 1375–1380.

Howard, S., Deroo, T., Fujita, Y. and Itasaki, N. (2011). A positive role of cadherin in wnt/Β-catenin signalling during epithelial-mesenchymal transition. *PLoS One* **6**,.

Huang, D. W., Sherman, B. T. and Lempicki, R. A. (2008). Systematic and integrative analysis of large gene lists using DAVID bioinformatics resources.

Huang, D. W., Sherman, B. T. and Lempicki, R. A. (2009). Bioinformatics enrichment tools : paths toward the comprehensive functional analysis of large gene lists. **37**, 1–13.

Hulpiau, P. and van Roy, F. (2009). Molecular evolution of the cadherin superfamily. *Int. J. Biochem. Cell Biol.* **41**, 349–369.

Iacovino, M., Hernandez, C., Xu, Z., Bajwa, G., Prather, M. and Kyba, M. (2009). A conserved role for Hox paralog group 4 in regulation of hematopoietic progenitors. *Stem Cells Dev.* **18**, 783–792.

Iacovino, M., Bosnakovski, D., Fey, H., Rux, D., Bajwa, G., Mahen, E., Mitanoska, A., Xu, Z. and Kyba, M. (2011). Inducible cassette exchange: a rapid and efficient system enabling conditional gene expression in embryonic stem and primary cells. *Stem Cells* **29**, 1580–1588.

Iacovino, M., Roth, M. E. and Kyba, M. (2014). Rapid genetic modification of mouse embryonic stem cells by inducible cassette exchange recombination. *Methods Mol. Biol.* **1101**, 339–351.

Islam, S., Carey, T. E., Wolf, G. T., Wheelock, M. J. and Johnson, K. R. (1996). Expression of N-cadherin by human squamous carcinoma cells induces a scattered fibroblastic phenotype with disrupted cell-cell adhesion. *J. Cell Biol.* **135**, 1643–1654.

Jaeger, I., Arber, C., Risner-Janiczek, J. R., Kuechler, J., Pritzsche, D., Chen, I., Naveenan, T., Ungless, M. A. and Li, M. (2011). Temporally controlled modulation of FGF/ERK signaling directs midbrain dopaminergic neural progenitor fate in mouse and human pluripotent stem cells. *Development* **138**, 4363–4374.

Jurberg, A. D., Aires, R., Nóvoa, A., Rowland, J. E. and Mallo, M. (2014). Compartment-dependent activities of Wnt3a/??-catenin signaling during vertebrate axial extension. *Dev. Biol.* **394**, 253–263.

Kadowaki, M., Nakamura, S., Machon, O., Krauss, S., Radice, G. L. and Takeichi, M. (2007). N-cadherin mediates cortical organization in the mouse brain. *Dev. Biol.* **304**, 22–33.

Kalkan, T. and Smith, A. (2014). Mapping the route from naive pluripotency to lineage specification. *Philos. Trans. R. Soc. Lond. B. Biol. Sci.* **369**, 20130540-.

Kam, Y. and Quaranta, V. (2009). Cadherin-bound β-catenin feeds into the Wnt pathway upon adherens junctions dissociation: Evidence for an intersection between β-catenin pools. *PLoS One* **4**,.

Kan, N. G., Stemmler, M. P., Junghans, D., Kanzler, B., de Vries, W. N., Dominis, M. and Kemler, R. (2007). Gene replacement reveals a specific role for E-cadherin in the formation of a functional trophectoderm. *Development* **134**, 31–41.

Kemler, R., Babinet, C., Eisen, H. and Jacob, F. (1977). Surface antigen in early differentiation. *Proc. Natl. Acad. Sci. U. S. A.* **74**, 4449–4452.

Kemler, R., Hierholzer, A., Kanzler, B., Kuppig, S., Hansen, K., Taketo, M. M., de Vries, W. N., Knowles, B. B. and Solter, D. (2004). Stabilization of beta-catenin in the mouse zygote leads to premature epithelial-mesenchymal transition in the epiblast. *Development* **131**, 5817–5824.

Kim, J. B., Islam, S., Kim, Y. J., Prudoff, R. S., Sass, K. M., Wheelock, M. J. and Johnson, K. R. (2000). N-cadherin extracellular repeat 4 mediates epithelial to mesenchymal transition and increased motility. *J. Cell Biol.* **151**, 1193–1205.

Kimura, Y., Matsunami, H., Inoue, T., Shimamura, K., Uchida, N., Ueno, T., Miyazaki, T. and Takeichi, M. (1995). Cadherin-11 expressed in association with mesenchymal morphogenesis in the head, somite, and limb bud of early mouse embryos. *Dev. Biol.* **169**, 347–358.

Kleinsmith, L. J. and Pierce, G. B. (1964). Multipotentiality of Single Embryonal Carcinoma Cells. *Cancer Res.* **24**, 1544–1551.

Koch, A. W., Manzur, K. L. and Shan, W. (2004). Structure-based models of cadherin-mediated cell adhesion: The evolution continues. *Cell. Mol. Life Sci.* **61**, 1884–1895.

Koch, F., Scholze, M., Wittler, L., Schifferl, D., Sudheer, S., Grote, P., Timmermann, B., Macura, K. and Herrmann, B. G. (2017). Antagonistic Activities of Sox2 and Brachyury Control the Fate Choice of Neuro-Mesodermal Progenitors. *Dev. Cell* 1–13.

Kojima, Y., Kaufman-Francis, K., Studdert, J. B., Steiner, K. A., Power, M. D., Loebel, D. A. F., Jones, V., Hor, A., De Alencastro, G., Logan, G. J., et al. (2014). The transcriptional and functional properties of mouse epiblast stem cells resemble the anterior primitive streak. *Cell Stem Cell* **14**, 107–120.

Kotb, A. M., Hierholzer, A. and Kemler, R. (2011). Replacement of E-cadherin by N-cadherin in the mammary gland leads to fibrocystic changes and tumor formation. *Breast Cancer Res.* **13**, R104.

Kunath, T., Saba-El-Leil, M. K., Almousailleakh, M., Wray, J., Meloche, S. and Smith, A. (2007). FGF stimulation of the Erk1/2 signalling cascade triggers transition of pluripotent embryonic stem cells from self-renewal to lineage commitment.

Development **134**, 2895–2902.

Lamouille, S., Xu, J. and Derynck, R. (2014). Molecular mechanisms of epithelial-mesenchymal transition. *Natl. Rev. Mol. Cell Biol.* **15**, 178–196.

Lanner, F. and Rossant, J. (2010). The role of FGF/Erk signaling in pluripotent cells. *Development* **137**, 3351–3360.

Lanza, R. and Atala, A. eds. (2014). *Essentials of Stem Cell Biology*. 3rd ed. London: Elsevier.

Larue, L. and Bellacosa, A. 2005 (2005). Epithelial–mesenchymal transition in development and cancer: role of phosphatidylinositol 3 0 kinase/AKT pathways. *Oncogene* 7443–7454.

Larue, L., Ohsugi, M., Hirchenhain, J. and Kemler, R. (1994). E-cadherin null mutant embryos fail to form a trophectoderm epithelium. *Proc. Natl. Acad. Sci. U. S. A.* **91**, 8263–8267.

Larue, L., Antos, C., Butz, S., Huber, O., Delmas, V., Dominis, M. and Kemler, R. (1996). A role for cadherins in tissue formation. *Development* **122**, 3185–3194.

Lawson, K. A. and Wilson, V. (2016). *3 – A Revised Staging of Mouse Development Before Organogenesis*. Elsevier Inc.

Lawson, K., Meneses, J. and Pedersen, R. (1991). Clonal analysis of epiblast fate during germ layer formation in the mouse embryo. *Development* **911**, 891–911.

Lee, J. D., Silva-Gagliardi, N. F., Tepass, U., McGlade, C. J. and Anderson, K. V (2007). The FERM protein Epb4.1l5 is required for organization of the neural plate and for the epithelial-mesenchymal transition at the primitive streak of the mouse embryo. *Development* **134**, 2007–2016.

Li, L., Liu, C., Biechele, S., Zhu, Q., Song, L., Lanner, F., Jing, N. and Rossant, J. (2013). Location of transient ectodermal progenitor potential in mouse development. *Development* **140**, 4533–43.

Lowell, S., Benchoua, A., Heavey, B. and Smith, A. G. (2006). Notch promotes neural lineage entry by pluripotent embryonic stem cells. *PLoS Biol.* **4**, 805–818.

Luo, Y., Ferreira-Cornwell, M., Baldwin, H., Kostetskii, I., Lenox, J., Lieberman, M. and Radice, G. (2001). Rescuing the N-cadherin knockout by cardiac-specific expression of

N- or E-cadherin. *Development* **128**, 459–469.

Maeda, M. (2005). Cadherin switching: essential for behavioral but not morphological changes during an epithelium-to-mesenchyme transition. *J. Cell Sci.* **118**, 873–887.

Malaguti, M. (2014). The roles of the transcriptional regulator Id1 in pluripotency and differentiation.

Malaguti, M., Nistor, P. a, Blin, G., Pegg, A., Zhou, X. and Lowell, S. (2013). Bone morphogenic protein signalling suppresses differentiation of pluripotent cells by maintaining expression of E-Cadherin. *Elife* **2**, e01197.

Maretto, S., Cordenonsi, M., Dupont, S., Braghetta, P., Broccoli, V., Hassan, A. B., Volpin, D., Bressan, G. M. and Piccolo, S. (2003). Mapping Wnt/beta-catenin signaling during mouse development and in colorectal tumors. *Proc. Natl. Acad. Sci. U. S. A.* **100**, 3299–3304.

Martin, G. (1981). Isolation of a pluripotent cell line from early mouse embryos cultured in medium conditioned by teratocarcinoma stem cells. *Proc. Natl. Acad. Sci.* **78**, 7634–7638.

Martin, B. L. and Kimelman, D. (2012). Canonical Wnt Signaling Dynamically Controls Multiple Stem Cell Fate Decisions during Vertebrate Body Formation. *Dev. Cell* **22**, 223–232.

Martinez-Garay, I., Gil-Sanz, C., Franco, S. J., Espinosa, A., Molnár, Z. and Mueller, U. (2016). Cadherin2/4-signaling via PTP1B and catenins is critical for nucleokinesis during radial neuronal migration in the neocortex. *Development* **44**, dev.132456.

Mathis, L., Kulesa, P. M. and Fraser, S. E. (2001). FGF receptor signalling is required to maintain neural progenitors during Hensen's node progression. *Nat. Cell Biol.* **3**, 559–66.

Megason, S. G. and McMahon, A. P. (2002). A mitogen gradient of dorsal midline Wnts organizes growth in the CNS. *Development* **129**, 2087–2098.

Miyabayashi, T., Teo, J.-L., Yamamoto, M., McMillan, M., Nguyen, C. and Kahn, M. (2007). Wnt/beta-catenin/CBP signaling maintains long-term murine embryonic stem cell pluripotency. *Proc. Natl. Acad. Sci.* **104**, 5668–5673.

Mohamed, O. A., Clarke, H. J. and Dufort, D. (2004). Β-Catenin Signaling Marks the Prospective Site of Primitive Streak Formation in the Mouse Embryo. *Dev. Dyn.* **231**, 416–424.

Moore, R. and Walsh, F. S. (1993). The cell adhesion molecule M-cadherin is specifically expressed in developing and regenerating, but not denervated skeletal muscle. *Development* **117**, 1409–20.

Morgani, S., Nichols, J. and Hadjantonakis, A.-K. (2017). The many faces of Pluripotency: in vitro adaptations of a continuum of in vivo states. *BMC Dev. Biol.* **17**, 7.

Muñoz-Descalzo, S., Hadjantonakis, A.-K. and Arias, A. M. (2015). Wnt/ß-catenin signalling and the dynamics of fate decisions in early mouse embryos and Embryonic Stem (ES) cells. *Semin. Cell Dev. Biol.*

Muñoz-Sanjuán, I. and Brivanlou, A. H. (2002). Neural induction, the default model and embryonic stem cells. *Nat. Rev. Neurosci.* **3**, 271–280.

Murayama, H., Masaki, H., Sato, H., Hayama, T., Yamaguchi, T. and Nakauchi, H. (2014). Successful Reprogramming of Epiblast Stem Cells by Blocking Nuclear Localization of β-Catenin. *Stem Cell Reports* **4**, 103–113.

Nagafuchi, A. and Takeichi, M. (1988). Cell binding function of E-cadherin is regulated by the cytoplasmic domain. *EMBO J.* **7**, 3679–84.

Nguyen, T. and Mège, R. M. (2016). N-cadherin and Fibroblast Growth Factor Receptors crosstalk in the control of developmental and cancer cell migrations. *Eur. J. Cell Biol.*

Nichols, J. and Smith, A. (2009). Naive and primed pluripotent states. *Cell Stem Cell* **4**, 487–92.

Nichols, J., Silva, J., Roode, M. and Smith, A. (2009). Suppression of Erk signalling promotes ground state pluripotency in the mouse embryo. *Development* **136**, 3215–3222.

Nieman, M. T., Prudoff, R. S., Johnson, K. R. and Wheelock, M. J. (1999). N-Cadherin Promotes Motility in Human Breast Cancer Cells Regardless of their E-Cadherin Expression. *J. Cell Biol.* **147**, 631–643.

Nose, A., Tsuji, K. and Takeichi, M. (1990). Localization of specificity determining sites in cadherin cell adhesion molecules. *Cell* **61**, 147–155.

Nusse, R. and Varmus, H. (2012). Three decades of Wnts: a personal perspective on how a scientific field developed. *EMBO J.* **31**, 2670–2684.

Nusse, R., Brown, A., Papkoff, J., Scambler, P., Shackleford, G., McMahon, A., Moon, R. and Varmus, H. (1991). Letters to the editor. *Cell* **64**, 475–476.

Ogawa, K., Nishinakamura, R., Iwamatsu, Y., Shimosato, D. and Niwa, H. (2006). Synergistic action of Wnt and LIF in maintaining pluripotency of mouse ES cells. *Biochem. Biophys. Res. Commun.* **343**, 159–166.

Ohgushi, M. and Sasai, Y. (2011). Lonely death dance of human pluripotent stem cells: ROCKing between metastable cell states. *Trends Cell Biol.* **21**, 274–82.

Ohgushi, M., Matsumura, M., Eiraku, M., Murakami, K., Aramaki, T., Nishiyama, A., Muguruma, K., Nakano, T., Suga, H., Ueno, M., et al. (2010). Molecular pathway and cell state responsible for dissociation-induced apoptosis in human pluripotent stem cells. *Cell Stem Cell* **7**, 225–239.

Ohnishi, Y., Huber, W., Tsumura, A., Kang, M., Xenopoulos, P., Kurimoto, K., Oleå, A. K., Araúzo-Bravo, M. J., Saitou, M., Hadjantonakis, A. K., et al. (2014). Cell-to-cell expression variability followed by signal reinforcement progressively segregates early mouse lineages. *Nat. Cell Biol.* **16**, 27–37.

Ohsugi, M., Larue, L., Schwarz, H. and Kemler, R. (1997). Cell-junctional and cytoskeletal organization in mouse blastocysts lacking E-cadherin. *Dev. Biol.* **185**, 261–271.

Olivera-Martinez, I., Harada, H., Halley, P. A. and Storey, K. G. (2012). Loss of FGF-Dependent Mesoderm Identity and Rise of Endogenous Retinoid Signalling Determine Cessation of Body Axis Elongation. *PLoS Biol.* **10**,.

Olivera-Martinez, I., Schurch, N., Li, R. a, Song, J., Halley, P. a, Das, R. M., Burt, D. W., Barton, G. J. and Storey, K. G. (2014). Major transcriptome re-organisation and abrupt changes in signalling, cell cycle and chromatin regulation at neural differentiation in vivo. *Development* **141**, 3266–76.

Onder, T. T., Gupta, P. B., Mani, S. A., Yang, J., Lander, E. S. and Weinberg, R. A. (2008). Loss of E-cadherin promotes metastasis via multiple downstream transcriptional pathways. *Cancer Res.* **68**, 3645–3654.

Orsulic, S., Huber, O., Aberle, H., Arnold, S. and Kemler, R. (1999). E-cadherin binding prevents beta-catenin nuclear localization and beta-catenin/LEF-1-mediated transactivation. *J. Cell Sci.* **112 (Pt 8**, 1237–1245.

Osorno, R., Tsakiridis, a., Wong, F., Cambray, N., Economou, C., Wilkie, R., Blin, G., Scotting, P. J., Chambers, I. and Wilson, V. (2012). The developmental dismantling of pluripotency is reversed by ectopic Oct4 expression. *J. Cell Sci.* **125**, e1–e1.

Ozawa, M., Hoschutzky, H., Herrenknecht, K. and Kemler, R. (1990). A possible new adhesive site in the cell-adhesion molecule uvomorulin. *Mech. Dev.* **33**, 49–56.

Pages, G., Guerin, S., Grall, D., Bonino, F., Smith, A., Anjuere, F., Auberger, P. and Pouyssegur, J. (1999). Defective thymocyte maturation in p44 MAP kinase (Erk 1) knockout mice. *Sci. (New York, NY)* **286**, 1374–1377.

Papatsenko, D., Darr, H., Kulakovskiy, I. V., Waghray, A., Makeev, V. J., MacArthur, B. D. and Lemischka, I. R. (2015). Single-Cell Analyses of ESCs Reveal Alternative Pluripotent Cell States and Molecular Mechanisms that Control Self-Renewal. *Stem Cell Reports* **5**, 207–220.

Pece, S. and Gutkind, J. S. (2000). Signaling from E-cadherins to the MAPK pathway by the recruitment and activation of epidermal growth factor receptors upon cell-cell contact formation. *J. Biol. Chem.* **275**, 41227–33.

Peng, G., Suo, S., Chen, J., Chen, W., Liu, C., Yu, F., Wang, R., Chen, S., Sun, N., Cui, G., et al. (2016). Spatial Transcriptome for the Molecular Annotation of Lineage Fates and Cell Identity in Mid-gastrula Mouse Embryo. *Dev. Cell* **36**, 681–697.

Pevny, L. H., Sockanathan, S., Placzek, M. and Lovell-Badge, R. (1998). A role for SOX1 in neural determination. *Development* **125**, 1967–78.

Pieters, T., Goossens, S., Haenebalcke, L., Andries, V., Stryjewska, A., De Rycke, R., Lemeire, K., Hochepied, T., Huylebroeck, D., Berx, G., et al. (2016). p120 Catenin-Mediated Stabilization of E-Cadherin Is Essential for Primitive Endoderm Specification. *PLoS Genet.* **12**, 1–28.

Pollard, S. M., Benchoua, A. and Lowell, S. (2006). Neural Stem Cells, Neurons, and Glia. *Methods Enzymol.* **418**, 151–169.

Qian, X., Karpova, T., Sheppard, A. M., McNally, J. and Lowy, D. R. (2004). E-cadherin mediated adhesion inhibits ligand-dependent activation of diverse receptor tyrosine kinases. *EMBO J.* **23**, 1739–1748.

Quinlan, G. a, Williams, E. a, Tan, S. S. and Tam, P. P. (1995). Neuroectodermal fate of epiblast cells in the distal region of the mouse egg cylinder: implication for body plan organization during early embryogenesis. *Development* **121**, 87–98.

R Core Team (2017). R: A language and environment for statistical computing.

Radice, G. L., Rayburn, H., Matsunami, H., Knudsen, K. A., Takeichi, M. and Hynes, R. O. (1997). Developmental defects in mouse embryos lacking N-cadherin. *Dev. Biol.* **181**, 64–78.

Redmer, T., Diecke, S., Grigoryan, T., Quiroga-Negreira, A., Birchmeier, W. and Besser, D. (2011). E-cadherin is crucial for embryonic stem cell pluripotency and can replace OCT4 during somatic cell reprogramming. *EMBO Rep.* **12**, 720–726.

Roux, P. P. and Blenis, J. (2004). ERK and p38 MAPK-Activated Protein Kinases : a Family of Protein Kinases with Diverse Biological Functions ERK and p38 MAPK-Activated Protein Kinases : a Family of Protein Kinases with Diverse Biological Functions. *Microbiol. Mol. Biol. Rev.* **68**, 320–344.

Rugg-Gunn, P. J., Cox, B. J., Lanner, F., Sharma, P., Ignatchenko, V., McDonald, A. C. H., Garner, J., Gramolini, A. O., Rossant, J. and Kislinger, T. (2012). Cell-surface proteomics identifies lineage-specific markers of embryo-derived stem cells. *Dev. Cell* **22**, 887–901.

Saba-El-Leil, M. K., Vella, F. D. J., Vernay, B., Voisin, L., Chen, L., Labrecque, N., Ang, S.-L. and Meloche, S. (2003). An essential function of the mitogen-activated protein kinase Erk2 in mouse trophoblast development. *EMBO Rep.* **4**, 964–968.

Sato, N., Meijer, L., Skaltsounis, L., Greengard, P. and Brivanlou, A. H. (2004). Maintenance of pluripotency in human and mouse embryonic stem cells through activation of Wnt signaling by a pharmacological GSK-3-specific inhibitor. *Nat. Med.* **10**, 55–63.

Schäfer, G., Narasimha, M., Vogelsang, E. and Leptin, M. (2014). Cadherin switching during the formation and differentiation of the Drosophila mesoderm - implications for epithelial-to-mesenchymal transitions. *J. Cell Sci.* **127**, 1511–22.

Schindelin, J., Arganda-Carreras, I., Frise, E., Kaynig, V., Longair, M., Pietzsch, T., Preibisch, S., Rueden, C., Saalfeld, S., Schmid, B., et al. (2012). Fiji: an open-source platform for biological-image analysis. *Nat. Methods* **9**, 676–682.

Seidel, B., Braeg, S., Adler, G., Wedlich, D. and Menke, A. (2004). E- and N-cadherin differ with respect to their associated p120ctn isoforms and their ability to suppress invasive growth in pancreatic cancer cells. *Oncogene* **23**, 5532–5542.

Shan, W. S., Tanaka, H., Phillips, G. R., Arndt, K., Yoshida, M., Colman, D. R. and Shapiro, L. (2000). Functional cis-heterodimers of N- and R-cadherins. *J. Cell Biol.* **148**, 579–590.

Shapiro, L., Fannon, a M., Kwong, P. D., Thompson, a, Lehmann, M. S., Grübel, G., Legrand, J. F., Als-Nielsen, J., Colman, D. R. and Hendrickson, W. a (1995). Structural basis of cell-cell adhesion by cadherins. *Nature* **374**, 327–337.

Smith, A. (2017). Formative pluripotency: the executive phase in a developmental continuum. *Development* **In Press**, 365–373.

Smith, a G., Heath, J. K., Donaldson, D. D., Wong, G. G., Moreau, J., Stahl, M. and Rogers, D. (1988). Inhibition of pluripotential embryonic stem cell differentiation by purified polypeptides. *Nature* **336**, 688–90.

Soncin, F., Mohamet, L., Eckardt, D., Ritson, S., Eastham, A. M., Bobola, N., Russell, A., Davies, S., Kemler, R., Merry, C. L. R., et al. (2009). Abrogation of E-cadherin-mediated cell-cell contact in mouse embryonic stem cells results in reversible LIF-independent self-renewal. *Stem Cells* **27**, 2069–80.

Soncin, F., Mohamet, L., Ritson, S., Hawkins, K., Bobola, N., Zeef, L., Merry, C. L. R. and Ward, C. M. (2011). E-cadherin acts as a regulator of transcripts associated with a wide range of cellular processes in mouse embryonic stem cells. *PLoS One* **6**, e21463.

Song, Y., Lee, S. and Jho, E. hoon (2018). Enhancement of neuronal differentiation by using small molecules modulating Nodal/Smad, Wnt/β-catenin, and FGF signaling. *Biochem. Biophys. Res. Commun.* 1–7.

Spurrier, B., Ramalingam, S. and Nishizuka, S. (2008). Reverse-phase protein lysate microarrays for cell signaling analysis. *Nat. Protoc.* **3**, 1796–1808.

Stamos, J. L. and Weis, W. I. (2013). The β-catenin destruction complex. *Cold Spring Harb.*

Perspect. Biol. **5**, 1–16.

Stavridis, M. P., Lunn, J. S., Collins, B. J. and Storey, K. G. (2007). A discrete period of FGF-induced Erk1/2 signalling is required for vertebrate neural specification. *Development* **134**, 2889–2894.

Stavridis, M. P., Collins, B. J. and Storey, K. G. (2010). Retinoic acid orchestrates fibroblast growth factor signalling to drive embryonic stem cell differentiation. *Development* **137**, 881–890.

Stepniak, E., Radice, G. L. and Vasioukhin, V. (2009). Adhesive and signaling functions of cadherins and catenins in vertebrate development. *Cold Spring Harb. Perspect. Biol.* **1**,.

Sternberg, N. (1981). Bacteriophage P1 site-specific recombination. *J. Mol. Biol.* **150**, 603–608.

Sterneckert, J., Stehling, M., Bernemann, C., Araúzo-Bravo, M. J., Greber, B., Gentile, L., Ortmeier, C., Sinn, M., Wu, G., Ruau, D., et al. (2010). Neural induction intermediates exhibit distinct roles of Fgf signaling. *Stem Cells* **28**, 1772–1781.

Suyama, K., Shapiro, I., Guttman, M. and Hazan, R. B. (2002). A signaling pathway leading to metastasis is controlled by N-cadherin and the FGF receptor. *Cancer Cell* **2**, 301–314.

Takada, S., Stark, K. L., Shea, M. J., Vassileva, G., McMahon, J. A. and McMahon, A. P. (1994). Wnt-3a regulates somites and tailbud formation in the mouse embryo. *Genes Dev.* **8**, 174–189.

Takahashi, K. and Yamanaka, S. (2006). Induction of pluripotent stem cells from mouse embryonic and adult fibroblast cultures by defined factors. *Cell* **126**, 663–76.

Takahashi, K., Tanabe, K., Ohnuki, M., Narita, M., Ichisaka, T., Tomoda, K. and Yamanaka, S. (2007). Induction of pluripotent stem cells from adult human fibroblasts by defined factors. *Cell* **131**, 861–72.

Takehara, T., Teramura, T., Onodera, Y., Frampton, J. and Fukuda, K. (2015). Cdh2 stabilizes FGFR1 and contributes to primed-state pluripotency in mouse epiblast stem cells. *Sci. Rep.* **5**, 14722.

Tam, P. P. (1989). Regionalisation of the mouse embryonic ectoderm: allocation of prospective ectodermal tissues during gastrulation. *Development* **107**, 55–67.

Tam, P. P. L. and Loebel, D. a F. (2007). Gene function in mouse embryogenesis: get set for gastrulation. *Nat. Rev. Genet.* **8**, 368–381.

Tam, P. P. L. and Quinlan, G. A. (1996). Mapping vertebrate embryos. *Curr. Biol.* **6**, 104–106.

Tamura, K., Shan, W. S., Hendrickson, W. a, Colman, D. R. and Shapiro, L. (1998). Structure-function analysis of cell adhesion by neural (N-)cadherin. *Neuron* **20**, 1153–1163.

ten Berge, D., Kurek, D., Blauwkamp, T., Koole, W., Maas, A., Siu, R. K. and Nusse, R. (2011). Embryonic stem cells require Wnt proteins to prevent differentiatino to epiblast stem cells. **13**, 1070–1075.

Tesar, P. J., Chenoweth, J. G., Brook, F. a, Davies, T. J., Evans, E. P., Mack, D. L., Gardner, R. L. and McKay, R. D. G. (2007). New cell lines from mouse epiblast share defining features with human embryonic stem cells. *Nature* **448**, 196–199.

Thomson, J. A., Itskovitz-Eldor, J., Shapiro, S. S., Waknitz, M. A., Swiergiel, J. J., Marshall, V. S. and Jones, J. M. (1998). Embryonic Stem Cell Lines Derived from Human Blastocysts. *Science (80-.).* **282**, 1145–1147.

Tomschy, a, Fauser, C., Landwehr, R. and Engel, J. (1996). Homophilic adhesion of E-cadherin occurs by a co-operative two-step interaction of N-terminal domains. *EMBO J.* **15**, 3507–14.

Torres, M., Stoykova, a, Huber, O., Chowdhury, K., Bonaldo, P., Mansouri, a, Butz, S., Kemler, R. and Gruss, P. (1997). An alpha-E-catenin gene trap mutation defines its function in preimplantation development. *Proc. Natl. Acad. Sci. U. S. A.* **94**, 901–6.

Tsakiridis, A. and Wilson, V. (2015). Assessing the bipotency of in vitro-derived neuromesodermal progenitors. *F1000Research* **4**, 100.

Tsakiridis, A., Huang, Y., Blin, G., Skylaki, S., Wymeersch, F., Osorno, R., Economou, C., Karagianni, E., Zhao, S., Lowell, S., et al. (2014). Distinct Wnt-driven primitive streak-like populations reflect in vivo lineage precursors. *Development* **141**, 1209–21.

Turner, D. a, Hayward, P. C., Baillie-Johnson, P., Rué, P., Broome, R., Faunes, F. and Martinez Arias, A. (2014). Wnt/β-catenin and FGF signalling direct the specification and maintenance of a neuromesodermal axial progenitor in ensembles of mouse embryonic stem cells. *Development* **141**, 4243–53.

Tzouanacou, E., Wegener, A., Wymeersch, F. J., Wilson, V. and Nicolas, J. F. (2009). Redefining the Progression of Lineage Segregations during Mammalian Embryogenesis by Clonal Analysis. *Dev. Cell* **17**, 365–376.

Utton, M. a, Eickholt, B., Howell, F. V, Wallis, J. and Doherty, P. (2001). Soluble N-cadherin stmulates fibroblast growth factor receptor dependent neurite outgrowth and N-cadherin and the fibroblast growth factor receptor co-cluster in cells. *J Neurochem* **76**, 1421–1430.

van de Ven, C., Bialecka, M., Neijts, R., Young, T., Rowland, J. E., Stringer, E. J., Van Rooijen, C., Meijlink, F., Novoa, A., Freund, J. N., et al. (2011). Concerted involvement of Cdx/Hox genes and Wnt signaling in morphogenesis of the caudal neural tube and cloacal derivatives from the posterior growth zone. *Development* **138**, 3451–3462.

van Raamsdonk, C. D. and Tilghman, S. M. (2000). Dosage requirement and allelic expression of PAX6 during lens placode formation. *Development* **127**, 5439–5448.

van Roy, F. and Berx, G. (2008). The cell-cell adhesion molecule E-cadherin. *Cell. Mol. Life Sci.* **65**, 3756–88.

Walters, J., Pop, C., Scott, F. L., Drag, M., Swartz, P., Mattos, C., Salvesen, G. S. and Clark, A. C. (2009). A constitutively active and uninhibitable caspase-3 zymogen efficiently induces apoptosis. *Biochem. J.* **424**, 335–345.

Watson, J. (2018). Investigating the Role of Wnt / Planar Cell Polarity (PCP) in Neuromesodermal Progenitors (NMPs).

Wennekamp, S., Mesecke, S., Nédélec, F. and Hiiragi, T. (2013). A self-organization framework for symmetry breaking in the mammalian embryo. *Nat. Rev. Mol. Cell Biol.* **14**, 452–9.

Wetering, M. Van De, Barker, N., Harkes, I. C., Wetering, M. Van De, Barker, N., Harkes, I. C., Heyden, M. Van Der, Dijk, N. J., Hollestelle, A., Klijn, J. G. M., et al. (2001). Mutant E-cadherin Breast Cancer Cells Do Not Display Constitutive Wnt Signaling Mutant E-cadherin Breast Cancer Cells Do Not Display Constitutive Wnt Signaling. 278–284.

Wheelock, M. J., Shintani, Y., Maeda, M., Fukumoto, Y. and Johnson, K. R. (2008). Cadherin switching. *J. Cell Sci.* **121**, 727–735.

Williams, E. J., Furness, J., Walsh, F. S. and Doherty, P. (1994). Activation of the FGF receptor underlies neurite outgrowth stimulated by L1, N-CAM, and N-cadherin. *Neuron* **13**, 583–594.

Williams, E. J., Williams, G., Howell, F. V., Skaper, S. D., Walsh, F. S. and Doherty, P. (2001). Identification of an N-cadherin Motif that Can Interact with the Fibroblast Growth Factor Receptor and Is Required for Axonal Growth. *J. Biol. Chem.* **276**, 43879–43886.

Wilmut, I., Schnieke, A. E., McWhir, J., Kind, A. J. and Campbell, K. H. S. (1997). Viable offspring derived from fetal and adult mammalian cells. *Nature* **385**, 810–813.

Wilson, V., Olivera-Martínez, I. and Storey, K. G. (2009). Stem cells, signals and vertebrate body axis extension. *Development* **136**, 2133–2133.

Wymeersch, F. J., Huang, Y., Blin, G., Cambray, N., Wilkie, R., Wong, F. C. K. and Wilson, V. (2016). Position-dependent plasticity of distinct progenitor types in the primitive streak. *Elife* **5**,.

Xu, Y., Zhu, X., Hahm, H. S., Wei, W., Hao, E., Hayek, A. and Ding, S. (2010). Revealing a core signaling regulatory mechanism for pluripotent stem cell survival and self-renewal by small molecules. *Proc. Natl. Acad. Sci. U. S. A.* **107**, 8129–34.

Yamanaka, Y., Lanner, F. and Rossant, J. (2010). FGF signal-dependent segregation of primitive endoderm and epiblast in the mouse blastocyst. *Development* **137**, 715–724.

Yang, J. and Weinberg, R. a (2008). Epithelial-mesenchymal transition: at the crossroads of development and tumor metastasis. *Dev. Cell* **14**, 818–29.

Ying, Q.-L., Stavridis, M., Griffiths, D., Li, M. and Smith, A. (2003a). Conversion of embryonic stem cells into neuroectodermal precursors in adherent monoculture. *Nat. Biotechnol.* **21**, 183–186.

Ying, Q. L., Nichols, J., Chambers, I. and Smith, A. (2003b). BMP induction of Id proteins suppresses differentiation and sustains embryonic stem cell self-renewal in collaboration with STAT3. *Cell* **115**, 281–292.

Ying, Q.-L., Wray, J., Nichols, J., Batlle-Morera, L., Doble, B., Woodgett, J., Cohen, P. and Smith, A. (2008). The ground state of embryonic stem cell self-renewal. *Nature* **453**, 519–23.

Yoshikawa, Y., Fujimori, T., McMahon, a P. and Takada, S. (1997). Evidence that absence of Wnt-3a signaling promotes neuralization instead of paraxial mesoderm development in the mouse. *Dev. Biol.* **183**, 234–242.

Yu, J., Vodyanik, M. a, Smuga-Otto, K., Antosiewicz-Bourget, J., Frane, J. L., Tian, S., Nie, J., Jonsdottir, G. a, Ruotti, V., Stewart, R., et al. (2007). Induced pluripotent stem cell lines derived from human somatic cells. *Science (80-.).* **318**, 1917–20.

Yu, Y., Wang, X., Zhang, X., Zhai, Y., Lu, X., Ma, H., Zhu, K., Zhao, T., Jiao, J., Zhao, Z.-A., et al. (2018). ERK inhibition promotes neuroectodermal precursor commitment by blocking self-renewal and primitive streak formation of the epiblast. *Stem Cell Res. Ther.* **9**, 2.

Zhang, J., Woodhead, G. J., Swaminathan, S. K., Noles, S. R., McQuinn, E. R., Pisarek, A. J., Stocker, A. M., Mutch, C. a, Funatsu, N. and Chenn, A. (2010). Cortical neural precursors inhibit their own differentiation via N-cadherin maintenance of beta-catenin signaling. *Dev. Cell* **18**, 472–9.

Zhu, Q., Song, L., Peng, G., Sun, N., Chen, J., Zhang, T., Sheng, N., Tang, W., Qian, C., Qiao, Y., et al. (2014). The transcription factor Pou3f1 promotes neural fate commitment via activation of neural lineage genes and inhibition of external signaling pathways. *Elife* **2014**, 1–21.